

DOC.20031223.0004

OCRWM	MODEL COVER SHEET	1. QA: QA Page 1 of 188
--------------	--------------------------	----------------------------

2. Type of Mathematical Model
 Process Model Abstraction Model System Model
 Describe Intended Use of Model
 The purpose of this Model Report is to provide a methodology for evaluating the near-field host rock water and gas-phase compositions that can be used in the TSPA Model. This abstraction model inherits the conceptual basis from the drift-scale coupled processes models (i.e., THC Seepage Model), but is an independently developed model.

3. Title
 Abstraction of Drift-Scale Coupled Processes

4. DI (including Rev. No. and Change No., if applicable):
 MDL-NBS-HS-000018 REV00

5. Total Attachments 3	6. Attachment Numbers - No. of Pages in Each I-4, II-2, III-4
---------------------------	--

	Printed Name	Signature	Date
7. Originator	N. Spycher	SIGNATURE ON FILE	12/19/03
8. GEO	B. Kirstein	SIGNATURE ON FILE	12/19/03
9. Checker	P. Persoff	SIGNATURE ON FILE	12/19/2003
10. QER	S. Harris	SIGNATURE ON FILE	12/19/2003
11. Responsible Manager/Lead	J.S.Y. Wang/ Y. Tsang	SIGNATURE ON FILE	12/19/2003
12. Responsible Manager	P. Dixon	SIGNATURE ON FILE	12/19/03

13. Remarks
 Block 7. Additional contributors: J. Apps (Sections 4.1.3, 5.3, 6.4, 7.3, 8.3, Attachment I.3) and E.L. Sonnenthal (Section 6.3 and the development of the process model).
 Block 9. Additional check performed by G. Lu.
 NOTE: The following references will be tracked with TBVs (listed by DIRS Reference Number):
 DIRS 165052: TBV-5645
 DIRS 165087: TBV-5639
 DIRS 165228: TBV-5643
Technical Error Report (TER) log numbers addressed in this model report
 N/A

OFFICE OF CIVILIAN RADIOACTIVE WASTE MANAGEMENT
MODEL REVISION RECORD

1. Page: 2 of 188

2. Model Title:
Abstraction of Drift-Scale Coupled Processes

3. DI (including Rev. No. and Change No., if applicable):
MDL-NBS-HS-000018 REV00

4. Revision/Change No.	5. Description of Revision/Change
REV 00	<p>This report is a revision of an Analysis/Model Report by the same title--Document Identifier ANL-NBS-HS-000029 REV00 (CRWMS M&O 2000 [123916]).</p> <p>In this new model report, the entire documentation was revised. Side bars are not used because the changes were too extensive to use Step 5.8d)1) per AP-SIII.10Q Rev. 2/ICN 1.</p>

TABLE OF CONTENTS

1.	PURPOSE	13
1.1	BACKGROUND	13
1.2	OBJECTIVE	16
1.3	MODEL LIMITATIONS.....	16
2.	QUALITY ASSURANCE	19
3.	USE OF SOFTWARE.....	21
4.	INPUTS	23
4.1	DIRECT INPUT	23
4.1.1	DSCPA Model Inputs.....	23
4.1.2	Degraded-Drift THC Simulation Inputs.....	24
4.1.3	Inputs for Radionuclide Sorption Evaluation.....	24
4.2	CRITERIA	24
4.3	CODES AND STANDARDS.....	30
5.	ASSUMPTIONS	31
5.1	DSCPA MODEL	31
5.2	THC SIMULATIONS CONSIDERING DRIFT DEGRADATION.....	31
5.3	ASSESSMENT OF RADIONUCLIDE SORPTION DEPENDENCE ON TEMPERATURE	31
6.	MODEL DISCUSSION	33
6.1	RELEVANT FEATURES, EVENTS, AND PROCESSES	33
6.1.1	FEPs Included for TSPA-LA	33
6.1.2	Other FEPs Relevant to this Model Report.....	44
6.2	THC SEEPAGE MODEL ABSTRACTION.....	46
6.2.1	Conceptual Model	46
6.2.2	Alternative Conceptual Models.....	55
6.2.3	Mathematical Model.....	56
6.2.4	Abstraction of Aqueous Species and CO ₂ Predicted Concentrations.....	56
6.3	THC SIMULATIONS CONSIDERING DRIFT DEGRADATION.....	97
6.3.1	Conceptual Model	97
6.3.2	Alternative Conceptual Model	98
6.3.3	Mathematical Model.....	98
6.3.4	Model Setup	98
6.3.5	Simulation Results.....	101
6.4	TEMPERATURE EFFECT ON RADIONUCLIDE SORPTION	126
6.4.1	Conceptual Model	126
6.4.2	Alternative Conceptual Models.....	127
6.4.3	Mathematical Model.....	130
6.4.4	Evaluation of the Temperature Dependence of Selected K _d Data.....	137

TABLE OF CONTENTS (Continued)

7.	VALIDATION	173
7.1	DRIFT-SCALE COUPLED PROCESSES ABSTRACTION MODEL	173
	7.1.1 Confidence Building During Model Development	173
	7.1.2 Post-Development Validation Activities	173
7.2	THC SIMULATIONS CONSIDERING DRIFT DEGRADATION	174
7.3	TEMPERATURE EFFECT ON RADIONUCLIDE SORPTION	174
8.	CONCLUSIONS	175
8.1	DSCPA MODEL	175
8.2	THC SIMULATIONS CONSIDERING DRIFT DEGRADATION	176
8.3	TEMPERATURE EFFECT ON RADIONUCLIDE SORPTION	177
9.	INPUTS AND REFERENCES	179
9.1	DOCUMENTS CITED	179
9.2	CODES, STANDARDS, REGULATIONS, AND PROCEDURES	186
9.3	SOURCE DATA, LISTED BY DATA TRACKING NUMBER	186
9.4	OUTPUT DATA, LISTED BY DATA TRACKING NUMBER	188
	ATTACHMENT I—LIST OF MODEL INPUT AND OUTPUT FILES	I-1
	ATTACHMENT II—ABSTRACTED DATA STATISTICAL CALCULATIONS	II-1
	ATTACHMENT III—INPUT WATER COMPOSITIONS	III-1

LIST OF FIGURES

6.2-1.	THC Seepage Model Mesh (Tptpll REV02 Model, No Drift Degradation).....	47
6.2-2.	Quadrant Designations for Abstraction of Data from the THC Seepage Model.....	50
6.2-3.	Conceptual Model for Abstraction of In-Drift Seepage Water Chemistry	53
6.2-4.	Abstraction of Model Results around the Modeled Drift as a Function of Time: pH.....	71
6.2-5.	Abstraction of Model Results around the Modeled Drift as a Function of Time: Concentration of Carbon Dioxide Gas.....	72
6.2-6.	Abstraction of Model Results around the Modeled Drift as a Function of Time: Total Aqueous Carbonate Concentration.....	73
6.2-7.	Abstraction of Model Results around the Modeled Drift as a Function of Time: Total Aqueous Chloride Concentration	74
6.2-8.	Abstraction of Model Results around the Modeled Drift as a Function of Time: Total Aqueous Nitrate Concentration	75
6.2-9.	Abstraction of Model Results around the Modeled Drift as a Function of Time: Ratio of Total Aqueous Nitrate to Total Aqueous Chloride Concentrations.....	76
6.2-10.	Abstraction of Model Results around the Modeled Drift as a Function of Time: Total Aqueous Sulfate Concentration.....	77
6.2-11.	Abstraction of Model Results around the Modeled Drift as a Function of Time: Ratio of Total Aqueous Sulfate to Total Aqueous Chloride Concentrations.....	78
6.2-12.	Abstraction of Model Results around the Modeled Drift as a Function of Time: Total Aqueous Fluoride Concentration.....	79
6.2-13.	Abstraction of Model Results around the Modeled Drift as a Function of Time: Total Aqueous Calcium Concentration.....	80
6.2-14.	Abstraction of Model Results around the Modeled Drift as a Function of Time: Ratio of Total Aqueous Calcium to Total Aqueous Chloride Concentrations.....	81
6.2-15.	Abstraction of Model Results around the Modeled Drift as a Function of Time: Ratio of Total Aqueous Calcium to Total Aqueous Carbonate Concentrations.....	82
6.2-16.	Abstraction of Model Results around the Modeled Drift as a Function of Time: Total Aqueous Magnesium Concentration	83
6.2-17.	Abstraction of Model Results around the Modeled Drift as a Function of Time: Total Aqueous Sodium Concentration.....	84
6.2-18.	Abstraction of Model Results around the Modeled Drift as a Function of Time: Ration of Total Aqueous Sodium to Total Aqueous Chloride Concentrations.....	85
6.2-19.	Abstraction of Model Results around the Modeled Drift as a Function of Time: Total Aqueous Potassium Concentration.....	86
6.2-20.	Abstraction of Model Results around the Modeled Drift as a Function of Time: Total Aqueous Silica Concentration.....	87
6.2-21.	Abstraction of Model Results around the Modeled Drift as a Function of Drift- Wall Temperature: pH.....	89

LIST OF FIGURES (Continued)

6.2-22.	Abstraction of Model Results around the Modeled Drift as a Function of Drift-Wall Temperature: Concentration of Carbon Dioxide Gas	90
6.2-23.	Abstraction of Model Results around the Modeled Drift as a Function of Drift-Wall Temperature: Total Aqueous Chloride Concentration	91
6.2-24.	Abstraction of Model Results around the Modeled Drift as a Function of Drift-Wall Temperature: Ratio of Total Aqueous Calcium to Total Aqueous Carbonate Concentrations	92
6.2-25.	Abstraction of Model Results around the Modeled Drift as a Function of Liquid Saturation: pH	93
6.2-26.	Abstraction of Model Results around the Modeled Drift as a Function of Liquid Saturation: Concentration of Carbon Dioxide Gas	94
6.2-27.	Abstraction of Model Results around the Modeled Drift as a Function of Liquid Saturation: Total Aqueous Chloride Concentration	95
6.2-28.	Abstraction of Model Results around the Modeled Drift as a Function of Liquid Saturation: Ratio of Total Aqueous Calcium to Total Aqueous Carbonate Concentrations	96
6.3-1.	Numerical Mesh for Simulations Considering Drift Degradation. The rubble zone is outlined by a thick solid line, depicting an approximately circular shape (dashed line)	99
6.3-2.	TH Simulation (Degraded vs. Intact Drift): Time Profiles of Modeled Waste Package Temperatures	103
6.3-3.	TH Simulation (Degraded vs. Intact Drift): Time Profiles of Modeled Temperatures in Fractures at Three Drift-Wall Locations	104
6.3-4.	TH Simulation (Degraded Drift): Contour Plot of Modeled Temperatures (solid contour lines, in°C) and Liquid Saturations in the Matrix and Fractures at 600 Years (color scale) Near the Time of Maximum Dryout in Fractures	105
6.3-5.	TH Simulation (Degraded vs. Intact Drift): Time Profiles of Modeled Liquid Saturations in Fractures at Three Drift-Wall Locations	106
6.3-6.	TH Simulation (Degraded vs. Intact Drift): Time Profiles of Modeled Liquid Saturations in Matrix at Three Drift-Wall Locations	107
6.3-7.	TH Simulation (Degraded vs. Intact Drift): Time Profiles of Modeled Air Mass Fractions in Fractures at Three Drift-Wall Locations	108
6.3-8.	TH Simulation (Degraded vs. Intact Drift): Time Profiles of Modeled Vertical Water Flux in Fractures at the Drift Crown	109
6.3-9.	THC Simulation (Degraded vs. Intact Drift): Abstraction around the Modeled Drift as a Function of Time—Distance between Drift Center and Gridblocks Picked Up by the Abstraction Procedure	112
6.3-10.	THC Simulation (Degraded vs. Intact Drift): Abstraction around the Modeled Drift as a Function of Time—Profiles of Modeled Temperatures	113
6.3-11.	THC Simulation (Degraded vs. Intact Drift): Abstraction around the Modeled Drift as a Function of Time—Profiles of Modeled Liquid Saturations	114
6.3-12.	THC Simulation (Degraded vs. Intact Drift): Abstraction around the Modeled Drift as a Function of Time—Profiles of Modeled pH	115

LIST OF FIGURES (Continued)

6.3-13.	THC Simulation (Degraded vs. Intact Drift): Abstraction around the Modeled Drift as a Function of Time—Profiles of Modeled Carbon Dioxide Gas Concentrations.....	116
6.3-14.	THC Simulation (Degraded vs. Intact Drift): Abstraction around the Modeled Drift as a Function of Time—Profiles of Total Aqueous Carbonate Concentrations.....	117
6.3-15.	THC Simulation (Degraded vs. Intact Drift): Abstraction around the Modeled Drift as a Function of Time—Profiles of Total Aqueous Chloride Concentrations.....	118
6.3-16.	THC Simulation (Degraded vs. Intact Drift): Abstraction around the Modeled Drift as a Function of Time—Profiles of Total Aqueous Fluoride Concentrations.....	119
6.3-17.	THC Simulation (Degraded vs. Intact Drift): Abstraction around the Modeled Drift as a Function of Time—Profiles of Total Aqueous Calcium Concentrations.....	120
6.3-18.	THC Simulation (Degraded vs. Intact Drift): Abstraction around the Modeled Drift as a Function of Time—Profiles of Total Aqueous Calcium and Total Aqueous Carbonate Concentrations.....	121
6.3-19.	THC Simulation (Degraded vs. Intact Drift): Abstraction around the Modeled Drift as a Function of Time—Profiles of Total Aqueous Sodium Concentrations.....	122
6.3-20.	THC Simulation (Degraded vs. Intact Drift): Abstraction around the Modeled Drift as a Function of Time—Profiles of Total Aqueous Sodium and Total Aqueous Chloride Concentrations.....	123
6.3-21.	THC Simulation (Degraded Drift): Contour Plot of Modeled Temperatures (solid lines in °C) and Liquid Saturations (color scale) in Fractures at 2,400 Years.....	124
6.3-22.	THC Simulation (Degraded Drift): Contour Plot of Modeled Fracture Permeability Change at 2,400 Years.....	125
6.4-1.	Calculated Values of $\log K_d$ as a Function of Reciprocal Absolute Temperature, Based on Batch Sorption of Specified Radioelements on Crushed Yucca Mountain Tuff and Mineral Samples.....	146
6.4-2.	Calculated Values of $\log K_d$ as a Function of Reciprocal Absolute Temperature, Based on Both Sorption and Desorption Radioelements on Crushed Yucca Mountain Tuff.....	154
6.4-3a–b.	Calculated Value of $\log K_d$ as a Function of Reciprocal Absolute Temperature, Based on Both Sorption and Desorption of Specified Radioelements on Tuff Core Samples from Yucca Mountain.....	158
6.4-4a–c.	Log K_d Values as a Function of the Reciprocal Absolute Temperature for Specified Elements on Various Sorbents.....	167
6.4-5.	Range of ΔH_r° for the Sorption of Radioelements on Natural Substrates.....	170

INTENTIONALLY LEFT BLANK

LIST OF TABLES

3.1.	Qualified Software Used in This Report	21
4.1-1.	Direct Inputs	23
4.1-2.	Drift-Degradation Simulation Inputs.....	24
4.1-3.	Radionuclide Sorption Inputs	24
4.2-1.	Project Requirements and YMRP Acceptance Criteria Applicable to This Model Report.....	25
6-1.	Scientific Notebooks	33
6.1-1.	Features, Events, and Processes Addressed in This Model Report.....	34
6.2-1.	Tptpll THC Model REV02 Runs Used for Abstraction Analyses	58
6.2-2.	Standard Deviations in Water and Gas Compositions Predicted in Zones of High Liquid Saturation above the Drift Crown (HISAT – TOP, Fractures).....	59
6.2-3.	Standard Deviations in Water and Gas Compositions Predicted at the Boiling/Wetting Front in Fractures above the Drift Crown (FRONT–TOP, Fractures).....	63
6.3-1.	Boundary Conditions.....	100
6.3-2.	Infiltration Rates.....	100
6.3-3.	Drift-Scale Simulations Considering Drift Degradation	101
6.4-1.	Factors Influencing K_d for an Adsorbent, Based on Conditions Expected in the Subsurface	131
6.4-2.	Rock Samples Used for Radioelement Sorption and Radioelements Sorbed	137
6.4-3.	Mineralogical Composition of Rock Samples, by X-Ray Analysis	138
6.4-4.	Batch Sorption Ratios for Pulverized Tuff and Mineral Samples* from Sorption Experiments at Room Temperature ($20 \pm 4^\circ\text{C}$), 60°C , and 80 or 90°C with J-13 Well Water	139
6.4-5.	Calculation of the Enthalpy of Sorption of Aqueous Species on Various Sorbents.....	148
6.4-6.	Average Sorption and Desorption Ratios for Pulverized Tuff ^a from Sorption and Desorption Experiments at Room Temperature ($20 \pm 4^\circ\text{C}$) and at 70°C with J-13 Well Water	149
6.4-7.	Sorption and Desorption Ratios for Plutonium and Americium on Tuffaceous Core from Sorption and Desorption Experiments at Room Temperature ($20 \pm$ 4°C) and at 85°C with J-13 Well Water	151
6.4-8.	Calculation of the Enthalpy of Sorption of Aqueous Species on Various Sorbents.....	159
6.4-9.	Sorption Coefficients, K_d , for Various Metal Species, Reported in the Literature (Unqualified Data).....	161
6.4-10.	Enthalpy, Entropy and Gibbs Free Energy of Adsorption of Aqueous Species on Various Sorbents (Unqualified Data from the Published Literature).....	163
6.4-11.	Calculated Enthalpy of Sorption of Aqueous Species on Various Sorbents (from the literature)	168
6.4-12.	Radioelement Enthalpies of Sorption, ΔH_r , based on Qualified and Unqualified Data from LANL	171

INTENTIONALLY LEFT BLANK

ACRONYMS

2-D	two-dimensional
AP	Administrative Procedure (DOE)
B.E.T.	Brunauer-Emmett-Teller
BSC	Bechtel SAIC Company, LLC
BWIP	Basalt Water Isolation Project
CRWMS	Civilian Radioactive Waste Management System
DIRS	Document Input Reference System
DOE	Department of Energy
DSCPA	Drift Scale Coupled Processes Abstraction
DST	Drift Scale Test
DTN	Data Tracking Number
EOS	equation of state
EDL	electrical double layer
FEP	Features, Events and Processes
IEP	Isoelectric Point
LBNL	Lawrence Berkeley National Laboratory
LA	License Application
LAM	Linear Adsorptivity Model
LANL	Los Alamos National Laboratory
M&O	Management and Operating Contractor
NRC	Nuclear Regulatory Commission
NTS	Nevada Test Site
OCRWM	Office of Civilian Radioactive Waste Management
PA	Performance Assessment
P&CE	Physical and Chemical Environment
PZNPC	point of zero net proton charge
Q	Qualified
QA	Quality Assurance

ACRONYMS (Continued)

SCM	Software Configuration Management
SD	standard deviation
SN	Scientific Notebook
STN	Software Tracking Number
TDMS	Technical Data Management System
TH	thermal-hydrological
THC	thermal-hydrological-chemical
TSPA	Total System Performance Assessment
TSPA-MAD	Total System Performance Assessment-License Application Methods and Approach
TWP	technical work plan
UZ	unsaturated zone
YMP	Yucca Mountain Project
YMPO	Yucca Mountain Project Office
YMRP	<i>Yucca Mountain Review Plan, Final Report</i>
WP	waste package

1. PURPOSE

1.1 BACKGROUND

This Model Report describes the abstraction for the Total System Performance Assessment (TSPA) Model, of results from the Thermal-Hydrological-Chemical (THC) Seepage Model documented in *Drift-Scale Coupled Processes (DST and THC Seepage) Models*, MDL-NBS-HS-000001, REV02 (BSC 2003 [162050]). This Model Report (REV00) was previously issued as ANL-NBS-HS-000029 REV00 (CRWMS M&O 2000 [123916]). It has been developed in accordance with *Technical Work Plan for: Performance Assessment Unsaturated Zone* (Bechtel SAIC Company, LLC (BSC) 2002 [160819]). This technical work plan (TWP) describes planning information pertaining to the technical scope, content, and management of this Model Report in Section 1.12, Work Package AUZM08, Drift-Scale Coupled Processes Abstraction Model. The plan for validation of the abstraction model documented in this report is given in Attachment I, Model Validation Plans, Section I-3-5, of the TWP.

In addition to abstraction analyses, this report includes an assessment of the effect of temperature on radionuclide sorption. This study is presented as part of the activities planned in the TWP for this model report (BSC 2002 [160819], Section 1.12.4).

The scope of work defined in the TWP was increased by also including in the present report an evaluation of the THC Seepage Model's sensitivity to drift degradation. This evaluation was conducted as a result of recent drift degradation studies (BSC 2003 [162711]) to assess the effects of drift degradation on predicted seepage chemistry. This added scope of work is documented in Trend No. 1PA-2003-096, *Seepage Evaluation for Degraded Drifts under Thermal Conditions*.

A few other minor changes were made to the work scope defined in the TWP. The general abstraction procedure implemented in this report was modified (Section 6.2.1.1) from that outlined in the TWP (BSC 2002 [160819], Section I-3-5-1). Also, somewhat different Acceptance Criteria (Section 4.2) were identified from those in the TWP (BSC 2002 [160819], Section 3) because the *Yucca Mountain Review Plan, Final Report* (YMRP, NRC 2003 [163274]) was revised after completion of the TWP. Finally, the list of Features, Events and Processes (FEPs) has changed somewhat from that used in the TWP (BSC 2002 [160819], Section 2.4), because the FEPs provided in the LA FEP list (DTN: MO0307SEPFEPS4.000 [164527]) superseded those provided in the TWP. Differences are described in Section 6.1. No other changes were made from the TWP.

The Drift-Scale Coupled Processes Abstraction (DSCPA) model documented in this report provides a methodology for evaluating the near-field composition of water and gases around a typical waste emplacement drift as these relate to the chemistry of seepage, if any, into the drift. The DSCPA Model inherits the conceptual basis of the THC Seepage Model, but is an independently developed model. The relationship between the DSCPA and other closely related models, together with their main functions in providing seepage chemistry information for TSPA-LA, are illustrated in Figure 1-1. The DSCPA Model does not provide direct input to the

TSPA Model. However, it plays an important role in the sequence of activities required to evaluate seepage chemistry histories used in TSPA-LA (Figure 1-1).

The purpose of the DSCPA Model is further discussed in Section 1.2. The abstraction methodology of the DSCPA Model (Section 6.2.1) was initially applied to results of the THC Seepage Model as presented in BSC (2003 [162050], Section 6.8.5.3.2). Other outputs of the THC Seepage Model (DTN: LB0302DSCPTHCS.002 [161976]) fed to the Physical and Chemical Environment (P&CE) Model (BSC 2003 [161963], Section 6.6) were also subjected to the same initial abstraction. The present report serves as a full documentation of this abstraction and also provides additional analyses in support of the choice of waters selected for further abstraction in the P&CE Model Report (BSC 2003 [161963], Section 6.6).

The work scope for studies presented in this Model Report is presented in the TWP and other documents cited above and can be summarized as follows: (1) revise the abstraction model used to estimate water and gas compositions near waste emplacement drifts; (2) perform additional THC simulations for one or more degraded-drift cases to evaluate the effects of drift collapse on results of the THC Seepage Model; and (3) evaluate the effect of temperature on the distribution (sorption) coefficients (K_d 's) of radionuclides. Results presented in this report were submitted to the Technical Data Management System (TDMS) under specific Data Tracking Numbers (DTNs) as listed in Attachment I.

The major change since previous abstractions of results from the THC Seepage Model is that the DSCPA Model now considers abstraction in space around the modeled waste emplacement drift, tracking the evolution of pore water and gas-phase composition at the edge of the dryout zone around the drift. The breakdown of predicted water/gas composition histories into specific broad representative time periods (as was done in previous abstractions) is not done here. Such abstraction through time is treated by a second abstraction implemented in the *Engineered Barrier System: Physical and Chemical Environment Model, Review Copy* (BSC 2003 [161963]) (Figure 1-1).

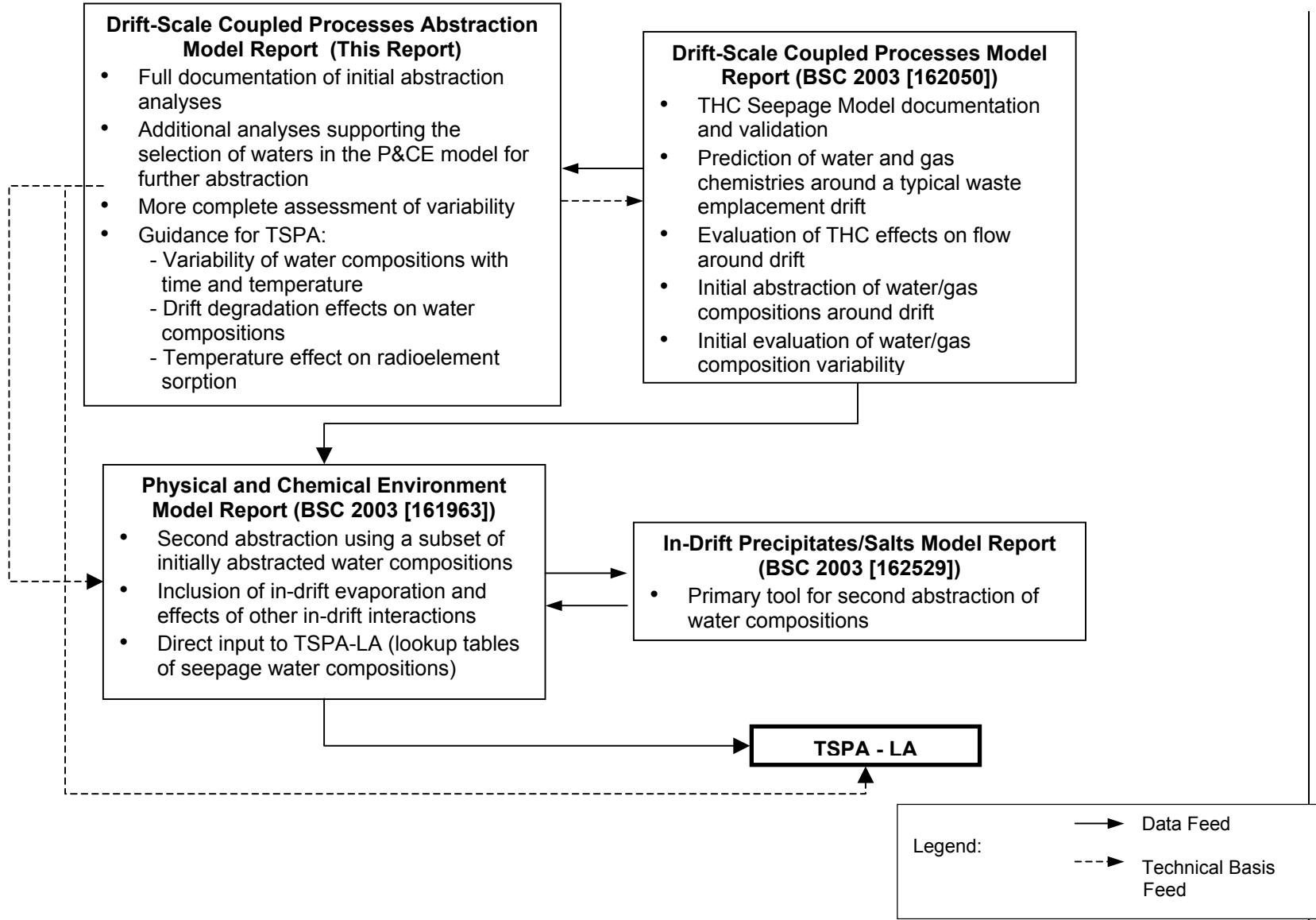


Figure 1-1. Relationships between the DSCPA and Other Closely Related Models and Their Functions in Providing Seepage Chemistry Information for TSPA-LA

1.2 OBJECTIVE

The purpose of the DSCPA Model is to provide a methodology for computing the near-field host rock water and gas-phase compositions that can be used in the TSPA model or other models feeding TSPA. This abstraction model inherits the conceptual basis from the drift-scale coupled processes models (i.e., THC Seepage Model), but is an independently developed model (Figure 1-1).

The DSCPA model is intended to be used only with the TSPA model, or those models directly feeding TSPA, for the estimation of water and gas compositions in the near-field around potential waste emplacement drifts. It is postulated that water and gases around waste emplacement drifts could enter the drifts at any time. The heating period includes both the preclosure, in which the repository drifts are ventilated, and the postclosure periods. The use of this model is strictly limited to TSPA-LA.

The purpose of the THC simulations considering drift degradation is to evaluate the sensitivity of the THC Seepage Model results to drift degradation, for use in FEPs screening and abstraction analyses. Radionuclide sorption studies are also presented in this report to evaluate the effect of temperature on the retardation of radionuclide transport, to assess whether temperature effects, if there are any, should be considered in TSPA-LA.

The THC Seepage Model (BSC 2003 [162050]) focuses on the seepage chemistry, while the Drift-Scale Thermal-Hydrological (TH) Seepage Model (BSC 2003 [161530]) evaluates the seepage quantity during the thermal period. For boiling conditions, both models corroborate each other and show that the vaporization barrier at the boiling front (i.e., dryout from the complete boiling of *in situ* and percolation water) is effective in reducing seepage. The Drift-Scale TH Seepage Model Report (BSC 2003 [161530]) further discusses the transition from thermal seepage to ambient seepage, taking into account the interaction between thermal and capillary processes.

1.3 MODEL LIMITATIONS

In the THC Seepage Model (BSC 2003 [162050]), no water is predicted to enter emplacement drifts. Therefore, for abstraction of model results, a set of criteria must be applied to determine which model area must be abstracted to obtain water and gas compositions most representative of water that could seep into drifts (Section 6.2.1). These criteria are the only limitation of the DSCPA Model itself.

There are many other limitations regarding the predicted compositions of water and gas abstracted in this report. These limitations, however, relate to the THC Seepage Model and not to the DSCPA Model. The reader should refer to *Drift-Scale Coupled Processes (DST and THC Seepage) Models* (BSC 2003 [162050]) to evaluate model limitations and uncertainties before using any data from this report.

Results of simulations considering drift degradation include all the limitations of the THC Seepage Model, with added limitations regarding the conceptualization of the degraded drift. This conceptualization considers one size (two drift diameters) and one shape (more or less circular) for the degraded zone, together with a given proportion of void space within the

collapse zone (23%) (Section 6.3.1). In reality, degraded zones of a variety of sizes and shapes, and with various degrees of rubble material compaction, would be expected to occur along a collapsed drift. Also, the degradation case evaluated in this report considers immediate degradation after waste emplacement (i.e., from time = 0) and does not account for potentially ineffective ventilation in the collapsed drift during the ventilated preclosure period.

Limitations regarding the evaluation of radionuclide sorption as a function of temperature are primarily those resulting from the simplified treatment of sorption processes in this study. Sorption is treated by using distribution coefficient (K_d) values measured in the laboratory and fitted to simple sorption isotherms (linear in this case). Potentially very large variations in K_d values could result from natural variations in geochemical and hydrological conditions in the subsurface. This is because laboratory determinations of K_d values do not discriminate as to the mechanism of sorption, which vary and can be quite sensitive to actual field conditions (Section 6.4.3.1).

INTENTIONALLY LEFT BLANK

2. QUALITY ASSURANCE

Development of this Model Report and the supporting modeling activities are subject to the Office of Civilian Radioactive Waste Management (OCRWM) quality assurance (QA) program as indicated in *Technical Work Plan for: Performance Assessment Unsaturated Zone*, TWP-NBS-HS-000003 REV 02 (BSC 2002 [160819], Section 8.2, Work Package (WP) AUZM08). Approved QA procedures identified in the TWP (BSC 2002 [160819], Section 4) have been used to conduct and document the activities described in this model report. The TWP also identifies the methods used to control the electronic management of data (BSC 2002 [160819], Section 8.4, WP AUZM08) during modeling and documentation activities.

This Model Report provides abstraction of drift-scale coupled processes in the unsaturated zone rocks above the repository. These rocks are a natural barrier and are classified in the *Q-List* (BSC 2003 [165179]) as “Safety Category” because they are important to waste isolation, as defined in AP-2.22Q, *Classification Analyses and Maintenance of the Q-List*. The results of this report are important to the demonstration of compliance with the postclosure performance objectives prescribed in 10 CFR 63.113 (66 FR 55732 [156671]). The report contributes to the analysis and modeling data used to support postclosure performance assessment; the conclusions do not directly impact engineered features important to preclosure safety, as defined in AP-2.22Q.

INTENTIONALLY LEFT BLANK

3. USE OF SOFTWARE

A list of qualified software used in this study is shown in Table 3.1. These software packages have been baselined in accordance with AP-SI.1Q, *Software Management*, is appropriate for the intended use, has been used strictly within the range of validation, and was obtained from the Software Configuration Management (SCM).

Microsoft Excel was obtained as acquired off-the-shelf software and used for the DSCPA Model analyses (Section 6.2.3) (Excel 97) and to fit sorption coefficient data (Section 6.4.4) (Excel 98).

Table 3.1. Qualified Software Used in This Report

Software Name and Version	Software Tracking Number (STN)	DIRS Reference Number
CUTCHEM V1.0	10898-1.0-00	161127
TOUGHREACT V3.0	10396-3.0-00	161256

INTENTIONALLY LEFT BLANK

4. INPUTS

4.1 DIRECT INPUT

This section summarizes inputs to the DSCPA model (Section 4.1.1), to the thermal-hydrological-chemical (THC) simulations considering drift degradation (Section 4.1.2), and to the analyses of radionuclide sorption (Section 4.1.3).

4.1.1 DSCPA Model Inputs

The inputs to the DSCPA Model are outputs from the THC Seepage Model described in Section 6.8 of *Drift-Scale Coupled Processes (DST and THC Seepage) Models* (BSC 2003 [162050]). These inputs and descriptions are summarized in Table 4.1-1. It is re-emphasized that the DSCPA Model consists of abstracting model results. Therefore, the inputs are typically few, because they are limited to the results of the corresponding process-level model (in this case, the THC Seepage Model). There are numerous inputs to the THC Seepage Model, and these inputs are listed in Section 4.1 of the above-mentioned report.

Table 4.1-1. Direct Inputs

DTN	Description of Input Parameters
<p>DTN: LB0302DSCPTHCS.002 [161976]</p> <p>The following files were used: thc6_w0_r.xls thc6_w4_r.xls thc6_w5_r.xls thc6_w6_r.xls thc6_w7_r.xls</p> <p>thc6_w0_drift_r.xls thc6_w4_drift_r.xls thc6_w5_drift_r.xls thc6_w6_drift_r.xls thc6_w7_drift_r.xls</p>	<p>Simulations referred to as "Group 1" in this report (Section 6.2.4)</p> <p>Modeled concentrations of aqueous species and CO₂(gas), temperature, and liquid saturation at various locations around the emplacement drift (non-zero liquid saturation areas only). These are results of THC Seepage Model simulations using five different input water compositions (W0, W4, W5, W6, and W7; see Attachment III).</p> <p>Drift crown and base temperatures (at drift wall), and waste package temperature for the same simulations as above.</p>
<p>DTN: LB0307DSTTHCR2.002 [165541]</p> <p>The following files were used: thc25_w0 thc6_w0e3 thc6_w0a thc6_w0b</p> <p>thc25_w0_drift thc6_w0e3_drift thc6_w0a_drift thc6_w0b_drift</p>	<p>Simulations referred to as "Group 2" in this report (Section 6.2.4)</p> <p>Modeled concentrations of aqueous species and CO₂(gas), temperature, and liquid saturation at various locations around the emplacement drift (non-zero liquid saturation areas only). These are results of sensitivity studies using the THC Seepage Model and one input water composition (W0; see Attachment III).</p> <p>Drift crown and base temperatures (at drift wall), and waste package temperature for the same simulations as above.</p>

4.1.2 Degraded-Drift THC Simulation Inputs

THC simulations considering drift degradation were run using the input data shown in Table 4.1-2. The drift configuration and properties were altered to represent degradation, using a conceptualization and model approximations discussed in Sections 6.3.1 and 6.3.4, respectively.

Table 4.1-2. Drift-Degradation Simulation Inputs

DTN	Description of Input Parameters
LB0307DSTTHCR2.001 [166054]	All model inputs (Tptpl THC Model REV02 as discussed in BSC 2003 [162050], Section 6.8) except for mesh configuration (below) and other changes in conceptualization and model approximations discussed in Section 6.3.1 and 6.3.4, respectively.
LB0303DSCPTHSM.001 [163688]	Model mesh configuration around the drift (Tptpl Submodel as discussed in BSC 2003 [161530], Section 6.2.1.2)

4.1.3 Inputs for Radionuclide Sorption Evaluation

Radionuclide sorption data are reported in the form of distribution coefficient (“ K_d ”) values. Sources of K_d values for cesium, strontium, barium, and neptunium are listed in Table 4.1-3. These data are further discussed in Section 6.4.4, together with data from other sources used as corroborative information. Note that data for other radionuclides were not considered because they did not include K_d measurements as a function of temperature.

Table 4.1-3. Radionuclide Sorption Inputs

DTN	Description of Input Parameters
LA0010JC831341.001 [162476]	Distribution coefficient (K_d) for barium
LA0010JC831341.002 [153321]	Distribution coefficient (K_d) for cesium
LA0010JC831341.003 [153322]	Distribution coefficient (K_d) for strontium
LA0010JC831341.007 [153319]	Distribution coefficient (K_d) for neptunium

4.2 CRITERIA

Technical requirements to be satisfied by Total System Performance Assessment (TSPA) are based on 10 CFR 63.114 (66 FR 55732 [156671]) (*Requirements for Performance Assessment*). These technical requirements are also identified in the *Yucca Mountain Project Requirements Document* (Canori and Leitner 2003 [161770], Section 3). The acceptance criteria that will be used by the Nuclear Regulatory Commission (NRC) to determine whether the technical requirements have been met are identified in the *Yucca Mountain Review Plan, Final Report* (YMRP; NRC 2003 [163274]). The pertinent requirements and acceptance criteria for this Model Report are summarized in Table 4.2-1. Note that different Acceptance Criteria were identified in the TWP (BSC 2002 [160819], Section 3) because the *Review Plan* has been revised since completion of the TWP.

Table 4.2-1. Project Requirements and YMRP Acceptance Criteria Applicable to This Model Report

Requirement Number ^a	Requirement Title ^a	10 CFR 63 Link	YMRP Acceptance Criteria
PRD-002/T-015	Requirements for Performance Assessment	10 CFR 63.114(a-c) [156671]	Criteria 1 to 4 for <i>Quantity and Chemistry of Water Contacting Engineered barriers and Waste Forms</i> ^b
PRD-002/T-016	Requirements for Multiple Barriers	10 CFR 63.115(c) [156671]	Criterion 3 for <i>System Description and Demonstration of Multiple Barriers</i> . ^c

NOTES: ^a from Canori and Leitner (2003 [161770], Section 3)

^b from NRC (2003 [163274], Section 2.2.1.3.3.3)

^c from NRC (2003 [163274], Section 2.2.1.1.3)

The acceptance criteria identified in Sections 2.2.1.3.3.3 of the YMRP (NRC 2003 [163274]) are given below, followed by pointers to sections in the upstream report describing the process model (BSC 2003 [162050]) and the present report where these are addressed:

- Acceptance Criterion 1, *System Description and Model Integration Are Adequate*:

The applicable subcriteria are:

Subcriterion 1. This subcriterion requires that the TSPA adequately incorporates important design features, physical phenomena, and couplings, and uses consistent and appropriate assumptions throughout the quantity and chemistry of water contacting engineered barriers and the waste-form abstraction process. This subcriterion is addressed in BSC (2003 [162050], Sections 6.2, 6.3, and 6.4) and Section 6.2.1.

Subcriterion 2. This subcriterion requires that the abstraction of the quantity and chemistry of water contacting engineered barriers and waste forms uses assumptions, technical bases, data, and models that are appropriate and consistent with other related U.S. Department of Energy (DOE) abstractions. BSC (2003 [162050], Sections 5, 6, and 7) and Sections 5, 6.2, and 7.1 address this subcriterion regarding water chemistry.

Subcriterion 4. This subcriterion requires that spatial and temporal abstractions appropriately address physical couplings (thermal-hydrological-mechanical-chemical). BSC (2003 [162050], Sections 6.8.5.3 and 6.8.5.4) and Section 6.2.1 address this subcriterion.

Subcriterion 5. This subcriterion requires that sufficient technical bases and justification are provided for TSPA assumptions and approximations for modeling coupled thermal-hydrological-mechanical-chemical effects on seepage and flow, the waste package chemical environment, and the chemical environment for radionuclide release. This subcriterion also requires that the effects of distribution of flow on the amount of water contacting the engineered barriers and waste forms are consistently addressed, in all relevant abstractions. The upstream report documenting the process model addresses coupled THC effects on water chemistry and flow in the unsaturated zone (UZ) up to the drift wall (BSC 2003 [162050], Section 6). It therefore addresses parts of this

subcriterion. An evaluation of temperature effects on radionuclide sorption, which affects transport, is presented in Section 6.4.

Subcriterion 8. This subcriterion requires that adequate technical bases are provided, including activities such as independent modeling, laboratory or field data, or sensitivity studies, for inclusion of any thermal-hydrological-mechanical-chemical couplings and features, events, and processes (FEPS). FEPS are addressed in Section 6.1, technical bases in BSC (2003 [162050], Sections 6.2–6.4) and Section 6.2.1, modeling and sensitivity studies in BSC (2003 [162050], Sections 6.5–6.8) and Section 6.2.4, and modeling of field and laboratory experiments in BSC (2003 [162050], Section 7.0), thus addressing this subcriterion.

Subcriterion 9. This subcriterion requires that performance-affecting processes that have been observed in thermal-hydrological tests and experiments are included in the performance assessment. Simulations presented in the upstream report documenting the process model reproduce coupled THC effects observed in thermal test BSC (2003 [162050], Section 7.1) and laboratory experiments BSC (2003 [162050], Sections 7.2 and 7.3), and therefore address this subcriterion.

Subcriteria 3, 6, 7, 10, 11, and 12 are not applicable.

- Acceptance Criterion 2, *Data Are Sufficient for Model Justification*:

The applicable subcriteria are:

Subcriterion 1. This subcriterion requires that geological, hydrological, and geochemical values used in the safety case are adequately justified, and that adequate descriptions of how data were used, interpreted, and appropriately synthesized into the parameters are provided. This subcriterion is addressed in BSC (2003 [162050], Sections 4.1, 6.2, 6.3, and 6.4).

Subcriterion 2. This subcriterion requires that sufficient data were collected on the characteristics of the natural system and engineered materials to establish initial and boundary conditions for conceptual models of thermal-hydrological-chemical coupled processes that affect seepage, flow, and the waste package chemical environment. The process model report addresses parts of this subcriterion by considering variations in pore-water compositions (BSC 2003 [162050], Sections 6.2.2 and 6.8.5) and rock properties (BSC 2003 [162050], Sections 6.5–6.8) representative of the natural system.

Subcriterion 3. This subcriterion requires that thermal-hydrological tests were designed and conducted with the explicit objectives of observing thermal-hydrological processes in the temperature ranges expected for repository conditions and making measurements for mathematical models. This subcriterion also requires that data are sufficient to verify that thermal-hydrological conceptual models address important thermal-hydrological phenomena. BSC (2003 [162050], Section 7.1), which presents details on results of the Drift Scale Test and simulations reproducing results of this test, addresses this subcriteria.

Subcriteria 4 and 5 are not applicable.

- Acceptance Criterion 3, *Data Uncertainty Is Characterized and Propagated Through the Model Abstraction*

The applicable subcriteria are:

Subcriterion 1. This subcriterion requires that models use parameter values, assumed ranges, probability distributions, and/or bounding assumptions that are technically defensible and reasonably account for uncertainties and variabilities. This subcriterion is addressed in the process model by using ranges of input data and alternative conceptualizations of the modeled systems BSC (2003 [162050], Sections 6.2.2 and 6.3). Uncertainty is also discussed in BSC (2003 [162050], Section 6.9) and further evaluated in Section 6.2.4.

Subcriterion 2. This subcriterion requires that parameter values, assumed ranges, probability distributions, and bounding assumptions used in the calculations of quantity and chemistry of water contacting engineered barriers and waste forms are technically defensible and reasonable, based on data from the Yucca Mountain region (i.e., Drift Scale Test [DST]), and a combination of techniques that include laboratory experiments, field measurements, and process-level modeling studies. The process model report addresses the parts of this subcriterion that relate to the uncertainty of the chemistry of water that could potentially enter drifts, with inputs and results discussed in BSC (2003 [162050], Sections 6.2.2, 6.8.5, 6.9), and validation including the results of the DST and laboratory experiments presented in BSC (2003 [162050], Section 7). Model results are further evaluated in Section 6.2.4.

Subcriterion 3. This subcriterion requires that input values used in the TSPA calculations of quantity and chemistry of water contacting engineered barriers (e.g., drip shield and waste package) are consistent with the initial and boundary conditions and the assumptions of the conceptual models and design concepts for the Yucca Mountain site. This criterion also requires that correlations between input values are appropriately established in the DOE TSPA; that parameters used to define initial conditions, boundary conditions, and the computational domain of sensitivity analyses—involving coupled thermal-hydrological-mechanical-chemical effects on seepage and flow, the waste package chemical environment, and the chemical environment for radionuclide release—are consistent with available data; and that reasonable or conservative ranges of parameters or function relations are established. This subcriterion is addressed in the upstream report documenting the process model, with respect to the chemistry of water that could potentially enter drifts, with the conceptual models described in BSC (2003 [162050], Sections 6.3–6.4), initial and boundary conditions discussed in BSC (2003 [162050], Sections 6.5.2, 6.7.2 and 6.8.2), and ranges of input parameters presented in BSC (2003 [162050], Sections 6.5.3, 6.6.1, 6.7.3 and 6.8.3).

Subcriterion 4. This subcriterion requires that adequate representation of uncertainties in the characteristics of the natural system and engineered materials is provided in parameter development for conceptual models, process-level models, and alternative conceptual models. This subcriterion also states that the DOE may constrain these uncertainties using sensitivity analyses or conservative limits. This subcriterion is

addressed by considering ranges of input parameters and alternative conceptualizations (e.g., BSC 2003 [162050], Table 6-1, Sections 6.2.2 and 6.3), as well as evaluations of the spread of model results (Section 6.2.4).

Subcriterion 5 is not applicable.

- Acceptance Criterion 4, *Model Uncertainty Is Characterized and Propagated through the Model Abstraction*:

The applicable subcriteria are:

Subcriterion 1. This subcriterion requires that alternative modeling approaches of features, events, and processes (FEPs) consistent with available data and current scientific understanding are investigated. This subcriterion also requires that the results and limitations are appropriately considered in the abstraction. This subcriterion is addressed by reviewing FEPS (Section 6.1), using alternative conceptual models (Section 6.3), and evaluating model limitation and uncertainty (BSC 2003 [162050], Sections 1.3, 6.9 and 8.4) (Section 6.2.4).

Subcriterion 2. This subcriterion requires that alternative modeling approaches are considered, that the selected modeling approach is consistent with available data and current scientific understanding, and that the results, limitations, and uncertainties of the chosen model are provided. This subcriterion is addressed by considering various model conceptualizations (BSC 2003 [162050], Section 6.3), evaluating spread in model results (Sections 6.2.4), and reporting on limitations and uncertainties (BSC 2003 [162050], Section 1.3, 6.9 and 8.4) (Section 1.3).

Subcriterion 3. This subcriterion requires that consideration of conceptual model uncertainty is consistent with available site characterization data, laboratory experiments, field measurements, natural analog information and process-level modeling studies; and that the treatment of conceptual model uncertainty does not result in an under-representation of the risk estimate. This subcriterion is addressed by using site-specific data (BSC 2003 [162050], Section 4.1) as well as data from field and laboratory experiments (BSC 2003 [162050], Section 7), considering ranges of key input parameters (e.g., BSC 2003 [162050], Section 6.2.2) and alternative conceptualizations (BSC 2003 [162050], Section 6.3), and spread in model results (BSC 2003 [162050], Section 6.9).

Subcriterion 4. This subcriterion requires that adequate consideration is given to effects of thermal-hydrological-mechanical-chemical coupled processes in the assessment of alternative conceptual models. These effects may include: (1) thermal-hydrological effects on gas, water, and mineral chemistry; (2) effects of microbial processes on the waste package chemical environment for radionuclide release; (3) changes in water chemistry that may result from the release of corrosion products from the waste package and interactions between engineered materials and groundwater; and (4) changes in boundary conditions (e.g., drift shape and size) and hydrological properties, relating to the response of the geomechanical system to thermal loading. The upstream report documenting the process model addresses part (i) of this subcriterion through conceptual

and mathematical models described in BSC (2003 [162050], Sections 6.2 and 6.4), and model results presented in BSC (2003 [162050], Sections 6.5.5, 6.6.2, 6.7.5, and 6.8.5). The effect of drift degradation (related to geomechanical effects) on water chemistry is evaluated in Section 6.3.

Subcriterion 5 is not applicable.

- Acceptance Criterion 5, *Model Abstraction Output Is Supported by Objective Comparisons*:

The applicable subcriteria are:

Subcriterion 1. This subcriterion requires that the models implemented in this TSPA abstraction provide results consistent with output from detailed process-level models and/or empirical observations (laboratory and field testing and/or natural analogs). This subcriterion is addressed in Sections 6.2.4 and 7.1.

Subcriterion 2. This subcriterion requires that abstracted models for coupled thermal-hydrological-chemical effects on seepage and flow and the waste package chemical environment are based on the same assumptions and approximations demonstrated to be appropriate for process-level models. Abstractions of processes, such as thermo-chemically induced changes in hydrological properties, must be adequately justified by comparison to results of process-level modeling that are consistent with direct observations and field studies. This subcriterion is addressed in Sections 6.2.4 and 7.1.

Subcriterion 3. This subcriterion requires that accepted and well-documented procedures are used to construct and test the numerical models that simulate coupled thermal-hydrological-chemical effects on seepage and flow and waste package chemical environment. Analytical and numerical models must be appropriately supported, and abstracted model results must be compared with different mathematical models, to judge the robustness of results. This subcriterion is addressed in the upstream report documenting the process model (BSC 2003 [162050], Sections 6.4) as well as in Section 6.2.4.

The acceptance criterion identified in Sections 2.2.1.1.3 of the YMRP (NRC 2003 [163274]) is given below, followed by a short description of its applicability to this Model Report.

- Acceptance Criterion 6, *Technical Basis for Barrier Capability Is Adequately Presented*:

This Model Report documents the abstraction of results from the THC Seepage Model (the process model), providing input to downstream users for predicting the chemistry of water potentially contacting engineered barriers and waste forms. The technical bases for the process model are consistent with the technical basis for the performance assessment, including consideration of the natural barrier created by host rocks, and the capillary pressure barrier at the drift wall (BSC 2003 [162050], Sections 6.8.1, 6.8.5.2, and 6.8.5.4) and around a potentially degraded drift (Sections 6.3.1, 6.3.5.1 and 6.3.5.2). The effect of a potential barrier created by mineral precipitation around the drift is also evaluated in BSC (2003 [162050], Section 6.8.5.4).

4.3 CODES AND STANDARDS

No specific formally established standards have been identified as applying to this modeling activity.

5. ASSUMPTIONS

The development of methodologies used for the abstraction of drift-scale coupled processes, for the consideration of drift degradation and for the assessment of radionuclide sorption dependence on temperature, are discussed in Section 6. Many simplifications and approximations underlie these methodologies. Yet other simplifications and approximations are inherent in data that describe repository designs and associated parameters on which model simulations rely. Assumptions are used when there is an absence of data or information for a parameter or concept. In this report there are no such assumptions. Approximations and simplifications relating to the methodologies developed in this report are presented in Section 6. In addition, assumptions, approximations, and simplifications relating to the development and implementation of the process model applied to simulate drift-scale coupled processes are documented in BSC (2003 [162050], Sections 5 and 6.4.6).

5.1 DSCPA MODEL

There are no assumptions specific to the DSCPA model, because there are none that meet the definition given above. Approximations are presented in Section 6.2.1.

5.2 THC SIMULATIONS CONSIDERING DRIFT DEGRADATION

There are no assumptions specific to the conceptualization of a degraded drift, because there are none that meet the definition given above. Approximations are presented in Sections 6.3.1 and 6.3.4.

5.3 ASSESSMENT OF RADIONUCLIDE SORPTION DEPENDENCE ON TEMPERATURE

There are no assumptions specific to the assessment of radionuclide sorption dependence on temperature, because there are none that meet the definition given above. Approximations are presented in Sections 6.4.3.1 and 6.4.3.3.

INTENTIONALLY LEFT BLANK

6. MODEL DISCUSSION

This section presents the conceptual and mathematical models implemented in this study, and their results. Relevant features, events, and processes (FEPs) are discussed in Section 6.1. Section 6.2 reports on the abstraction of results from the THC Seepage Model, Section 6.3 on the effect of drift degradation on these results, and Section 6.4 on the effect of temperature on radionuclide sorption. Sections 6.2, 6.3, and 6.4 are further divided to each address, as applicable, conceptual and mathematical models, alternative conceptualizations, and model results. Model validation is discussed in Section 7.

The model development, data, and results are documented in the scientific notebooks (SNs) listed in Table 6-1. The intended use of output data from this Model Report is discussed in Section 1.1. Applicable acceptance criteria from the *Yucca Mountain Review Plan, Final Report* (YMRP) are discussed in Section 4.2, with pointers referring to sections addressing these criteria here and in the upstream report documenting the process model (BSC 2003 [162050]). The barrier capability of the host rocks, the capillary barrier at the drift wall or at the edge of a rubble zone caused by potential collapse of the drift wall, and the potential barrier resulting from mineral precipitation around the drift are given consideration in the process model simulations presented in BSC (2003 [162050], Section 6.8) and in Section 6.3.

Output data from analyses presented in this section were submitted to the TDMS under DTNs as shown in Attachment I (and in tables and figures as appropriate).

Table 6-1. Scientific Notebooks

LBNL Scientific Notebook ID	M&O Scientific Notebook ID	Relevant Pages	Citation
YMP-LBNL-YWT-JA-1A	SN-LBNL-SCI-005-V1	249–285	Wang 2003 [165562]
YMP-LBNL-DSM-ELS-1	SN-LBNL-SCI-142-V2	124, 126–129	Wang 2003 [165562]
YMP-LBNL-DSM-NS-2	SN-LBNL-SCI-141-V2	151–153, 200–219	Wang 2003 [165562]

6.1 RELEVANT FEATURES, EVENTS, AND PROCESSES

The following tables (Tables 6.1-1 and 6.1-2) of FEPs were taken from the LA FEP List (DTN: MO0307SEPFEPS4.000 [164527]). The list of FEPs given in the *Technical Work Plan for Performance Assessment Unsaturated Zone* (BSC 2002 [160819], Section 2.4) is now superseded by the FEP list given in the LA FEP List (DTN: MO0307SEPFEPS4.000 [164527]).

6.1.1 FEPs Included for TSPA-LA

The results of the THC Seepage Model (BSC 2003 [162050]) and analyses presented in the present report are part of the basis for the treatment of FEPs as discussed in the Total System Performance Assessment-License Application Methods and Approach (TSPA-MAD) (BSC 2002 [160146], Section 3.2.2). As already mentioned in Section 1.1, these results do not feed TSPA-LA directly. These results first feed another model (BSC 2003 [161963]) as discussed in Section 1.1 and shown in Figure 1-1. Lookup tables generated in BSC (2003 [161963]) are then used in the TSPA Model, which directly supports LA.

The results of the present report, of the upstream process model (BSC 2003 [162050]), and/or other relevant model reports are used to fully document the technical basis for the include/exclude status of these FEPs for TSPA-LA. The included FEPs are listed in Table 6.1-1 and can be found in the model abstraction reports as described in Section 2.4 of the TWP (BSC 2002 [160819]) and the FEP report as described in Section 1.12.10 of the TWP (BSC 2002 [160819]). Excluded FEPs are to be documented in the FEP report as described in Section 1.12.10 of the TWP (BSC 2002 [160819]).

Table 6.1-1. Features, Events, and Processes Addressed in This Model Report

LA FEP Number	FEP Name	YMP Description	Other Upstream Reports Used for FEP Disposition
1.1.02.02.0A	Preclosure ventilation	<p>The duration of preclosure ventilation acts together with waste package spacing (as per design) to control the extent of the boiling front (zone of reduced water content).</p> <p><i>TSPA Disposition: Included</i></p> <p><i>Preclosure ventilation in drifts will remove a considerable amount of the heat output from the waste canisters. The preclosure period is 50 years, during which the major fraction of the thermal load is removed from the drifts. This effect of preclosure ventilation on the thermal load provided to the rock is explicitly simulated with the THC Seepage Model that feeds into the DSCPA model, by using time-dependent boundary conditions for the thermal load (BSC 2003 [162050], Section 4.1.7). These boundary conditions reflect the current emplacement design (waste package spacing, average heat output of waste canisters, etc.), as provided in design drawing 800-IED-EBS0-00201-000-00A (BSC 2003 [164069]).</i></p> <p><i>Thus, the results from the THC Seepage Model and their abstraction (Section 6.2 of the present report; summary tables of concentrations through time submitted under DTNs LB0302DSCPTHCS.002 [161976], LB0307DSTTHCR2.002 [165541], and LB0311ABSTHCR2.003 [Output]; and tables of concentrations and summary statistics through time submitted under DTN LB0311ABSTHCR2.001 [Output]) explicitly account for the impact of preclosure ventilation and waste package spacing on the THC conditions in the near-drift rock. DTNs LB0302DSCPTHCS.002 [161976] and LB0311ABSTHCR2.001 [Output] are used to feed and/or provide technical basis for another model (BSC 2003 [161963]) that generates lookup tables that are used in the TSPA Model.</i></p> <p><i>Note that pre-closure ventilation also causes initial rock drying in the drift vicinity as a result of evaporation effects. The reduced relative humidity in the emplacement drifts leads to evaporation of water at the drift surfaces and the development of a small zone of reduced saturation in the drift vicinity. This early dryout as a result of evaporation is neglected in the THC Seepage Model, because seepage into ventilated drifts is highly unlikely (BSC 2003 [165564], Section 6.5.2.1).</i></p>	<p>BSC 2003 [161530] BSC 2003 [165564] BSC 2003 [162050]</p>

Table 6.1-1. Features, Events, and Processes Addressed in This Model Report (Continued)

LA FEP Number	FEP Name	YMP Description	Other Upstream Reports Used for FEP Disposition
1.2.02.01.OA	Fractures	<p>Groundwater flow in the Yucca Mountain region and transport of any released radionuclides may take place along fractures. The rate of flow and the extent of transport in fractures are influenced by characteristics such as orientation, aperture, asperity, fracture length, connectivity, and the nature of any linings or infills.</p> <p><i>TSPA Disposition: Included</i></p> <p><i>Flow processes in fractures or other channels affect modeled THC coupled processes because of 1) their strong effect on TH behavior (BSC 2003 [165564], Sections 6.4.4.1 and 6.4.4.2), and 2) their strong effect on water and gas chemistry (BSC 2003 [162050], Section 6.2.1). The latter is primarily due to volatilization of steam and CO₂ from the rock matrix-water and subsequent transport and condensation in fractures. The amount of mobilized CO₂ with steam directly affects the pH of the condensate, which in turn affects the degree of water-rock interaction and water chemistry. These THC processes are influenced by the fracture characteristics, such as orientation, aperture, asperity, length, connectivity, and fillings. The THC Seepage Model that feeds into the DSPCA model explicitly simulate the flow processes in fractures using appropriate continuum properties that represent these characteristics (BSC 2003 [162050], Sections 6.4.3, 6.4.4, and 6.4.7).</i></p> <p><i>Thus, the results from the THC Seepage Model and their abstraction (Section 6.2 of the present report; summary tables of concentrations through time submitted under DTNs LB0302DSCPTHCS.002 [161976], LB0307DSTTHCR2.002 [165541], and LB0311ABSTHCR2.003 [Output]; and tables of concentrations and summary statistics through time submitted under DTN LB0311ABSTHCR2.001 [Output]) explicitly account for the effect of fractures on predicted water and gas chemistry. DTNs LB0302DSCPTHCS.002 [161976] and LB0311ABSTHCR2.001 [Output] are used to feed and/or provide technical basis for another model (BSC 2003 [161963]) that generates lookup tables that are used in the TSPA Model.</i></p>	<p>BSC 2003 [163045] BSC 2003 [160240] BSC 2003 [161773] BSC 2003 [163933] BSC 2003 [165564] BSC 2003 [164889] BSC 2003 [162050]</p>
1.3.01.00.OA	Climate change	<p>Climate change may affect the long-term performance of the repository. This includes the effects of long-term change in global climate (e.g., glacial/interglacial cycles) and shorter-term change in regional and local climate. Climate is typically characterized by temporal variations in precipitation and temperature.</p> <p><i>TSPA Disposition: Included</i></p> <p><i>Potential effects of climate change on the amount of infiltration and percolation at Yucca Mountain are taken implicitly into account in the THC Seepage Model by considering different climate stages and climate scenarios when setting infiltration rates at the top model boundary (BSC 2003 [162050], Section 6.2.1.3 and 6.8.2).</i></p> <p><i>Thus, the results from the THC Seepage Model and their abstraction (Section 6.2 of the present report; summary tables of concentrations through time submitted under DTNs LB0302DSCPTHCS.002 [161976], LB0307DSTTHCR2.002 [165541], and LB0311ABSTHCR2.003 [Output]; and tables of concentrations and summary statistics through time submitted under DTN LB0311ABSTHCR2.001 [Output]) implicitly account for the effect of climate change on THC processes. DTNs LB0302DSCPTHCS.002 [161976] and LB0311ABSTHCR2.001 [Output] are used to feed and/or provide technical basis for another model (BSC 2003 [161963]) that generates lookup tables that are used in the TSPA Model.</i></p> <p><i>Note that seepage is calculated in the TSPA-LA using percolation flux distributions derived in Abstraction of Drift Seepage (BSC 2003 [165564], Section 6.6.4.1), which are based on results from the UZ Flow and Transport Model (BSC 2003 [163045]) that are given in DTNs LB0302PTNTSW91.001 [162277] and LB0305PTNTSW91.001 [163690]. These flux distributions are based on the same varying climate stages and scenarios as identified and used in the THC Seepage Model.</i></p>	<p>BSC 2003 [163045] USGS 2001 [158378] USGS 2001 [160355] BSC 2003 [162050] BSC 2003 [165564] BSC 2003 [163933]</p>

Table 6.1-1. Features, Events, and Processes Addressed in This Model Report (Continued)

LA FEP Number	FEP Name	YMP Description	Other Upstream Reports Used for FEP Disposition
1.4.01.01.0A	Climate modification increases recharge	<p>Climate modification causes an increase in recharge in the Yucca Mountain region. Increased recharge might lead to increased flux through the repository, perched water, or water table rise.</p> <p><i>TSPA Disposition: Included</i></p> <p><i>Potential effects of climate change on the amount of infiltration and percolation at Yucca Mountain are taken into account in the THC Seepage Model by implicitly considering different climate stages and climate scenarios when setting infiltration rates at the top model boundary (BSC 2003 [162050], Sections 6.2.1.3 and 6.8.2).</i></p> <p><i>Thus, the results from the THC Seepage Model and their abstraction (Section 6.2 of the present report; summary tables of concentrations through time submitted under DTNs LB0302DSCPTHCS.002 [161976], LB0307DSTTHCR2.002 [165541], and LB0311ABSTHCR2.003 [Output]; and tables of concentrations and summary statistics through time submitted under DTN LB0311ABSTHCR2.001 [Output]) implicitly account for the effect of climate change on predicted water and gas chemistry. DTNs LB0302DSCPTHCS.002 [161976] and LB0311ABSTHCR2.001 [Output] are used to feed and/or provide technical basis for another model (BSC 2003 [161963]) that generates lookup tables that are used in the TSPA Model.</i></p> <p><i>Note that seepage is calculated in the TSPA-LA using percolation flux distributions derived in Abstraction of Drift Seepage (BSC 2003 [165564], Section 6.6.4.1), which are based on results from the UZ Flow and Transport Model (BSC 2003 [163045]) that are given in DTNs LB0302PTNTSW91.001 [162277] and LB0305PTNTSW91.001 [163690]. These flux distributions are based on the same varying climate stages and scenarios as identified and used in the THC Seepage Model.</i></p>	<p>BSC 2003 [163045] BSC 2003 [163933] BSC 2003 [162050] BSC 2003 [165564] BSC 2003 [164889]</p>
2.1.08.01.0A	Water influx at the repository	<p>An increase in the unsaturated water flux at the repository affects thermal, hydrologic, chemical, and mechanical behavior of the system. Increases in flux could result from climate change, but the cause of the increase is not an essential part of the FEP.</p> <p><i>TSPA Disposition: Included</i></p> <p><i>The potential increase in the magnitude of percolation flux at the repository, as a result of climate changes is accounted for in the THC Seepage Model by implicitly considering different climate stages, and climate scenarios when setting infiltration rates at the top model boundary (BSC 2003 [162050], Sections 6.2.1.3 and 6.8.2). Also, flux increases caused by reflux of water upon boiling are explicitly accounted for by the modeling of coupled THC processes (BSC 2003 [162050], Sections 6.2.1 and 6.8.5.2).</i></p> <p><i>Therefore, these effects are directly accounted for in results from the THC Seepage Model and their abstraction (Section 6.2 of the present report; summary tables of concentrations through time submitted under DTNs LB0302DSCPTHCS.002 [161976], LB0307DSTTHCR2.002 [165541], and LB0311ABSTHCR2.003 [Output]; and tables of concentrations and summary statistics through time submitted under DTN LB0311ABSTHCR2.001 [Output]). DTNs LB0302DSCPTHCS.002 [161976] and LB0311ABSTHCR2.001 [Output] are used to feed and/or provide technical basis for another model (BSC 2003 [161963]) that generates lookup tables that are used in the TSPA Model.</i></p> <p><i>Note that seepage is calculated in the TSPA-LA using percolation flux distributions derived in Abstraction of Drift Seepage (BSC 2003 [165564], Section 6.6.4.1), which are based on results from the UZ Flow and Transport Model (BSC 2003 [163045]) that are given in DTNs LB0302PTNTSW91.001 [162277] and LB0305PTNTSW91.001 [163690]. These flux distributions are based on the same varying climate stages and scenarios as identified and used in the THC Seepage Model.</i></p>	<p>BSC 2003 [163045] BSC 2003 [165692] BSC 2003 [162050] BSC 2003 [164889]</p>

Table 6.1-1. Features, Events, and Processes Addressed in This Model Report (Continued)

LA FEP Number	FEP Name	YMP Description	Other Upstream Reports Used for FEP Disposition
2.2.03.01.0A	Stratigraphy	<p>Stratigraphic information is necessary information for the performance assessment. This information should include identification of the relevant rock units, soils and alluvium, and their thickness, lateral extents, and relationships to each other. Major discontinuities should be identified.</p> <p><i>TSPA Disposition: Included</i></p> <p><i>The overall distribution of percolation flux at the repository horizon is influenced by stratigraphic layering and by major discontinuities. For example, the PTn- unit overlying the Topopah Spring welded tuff units can divert a fraction of percolating water to intercepting faults and fault zones, thereby changing the spatial distribution of fluxes (BSC 2003 [165564], Section 6.4.1.1), which could affect water-rock interaction and seepage water chemistry. Also, the mineralogy of stratigraphic intervals affects seepage water chemistry. For example, the presence of fluorite in the Tptpl hydrogeologic unit may affect fluoride concentrations in pore waters in this unit (BSC 2003 [162050], Sections 6.7.5.2). Finally, the thermal perturbation of the unsaturated rock extends far into the geologic units overlying and underlying the emplacement drifts. For these reasons, the THC seepage model includes explicitly the Yucca Mountain stratigraphy (BSC 2003 [162050], Sections 4.1.2, 6.5.1, 6.7.1, and 6.8.1), using stratigraphic information from DTN LB990501233129.004 [111475] and mineralogical information from DTN LB0101DSTTHCR1.002 [161277].</i></p> <p><i>Therefore, the results from the THC Seepage Model and their abstraction (Section 6.2 of the present report; summary tables of concentrations through time submitted under DTNs LB0302DSCPTHCS.002 [161976], LB0307DSTTHCR2.002 [165541], and LB0311ABSTHCR2.003 [Output]; and tables of concentrations and summary statistics through time submitted under DTN LB0311ABSTHCR2.001 [Output]) explicitly account for the effect of stratigraphy on predicted water and gas chemistry. DTNs LB0302DSCPTHCS.002 [161976] and LB0311ABSTHCR2.001 [Output] are used to feed and/or provide technical basis for another model (BSC 2003 [161963]) that generates lookup tables that are used in the TSPA Model.</i></p>	<p>BSC 2003 [161530] BSC 2003 [162050] BSC 2003 [163045] BSC 2003 [160109] BSC 2003 [163933] BSC 2003 [165564] BSC 2003 [164889]</p>

Table 6.1-1. Features, Events, and Processes Addressed in This Model Report (Continued)

LA FEP Number	FEP Name	YMP Description	Other Upstream Reports Used for FEP Disposition
2.2.03.02.0A	Rock properties of host rock and other units	<p>Physical properties such as porosity and permeability of the relevant rock units, soils, and alluvium are necessary for the performance assessment. Possible heterogeneities in these properties should be considered. Questions concerning events and processes that may cause these physical properties to change over time are considered in other FEPs.</p> <p><i>TSPA Disposition: Included</i></p> <p><i>The THC Seepage Model feeding into the DSCPA model explicitly represents the physical properties of the unsaturated rock (BSC 2003 [162050], Section 6.4.7).</i></p> <p><i>Therefore, these effects are explicitly accounted for in results from the THC Seepage Model and their abstraction (Section 6.2 of the present report; summary tables of concentrations through time submitted under DTNs LB0302DSCPTHCS.002 [161976], LB0307DSTTHCR2.002 [165541], and LB0311ABSTHCR2.003 [Output]; and tables of concentrations and summary statistics through time submitted under DTN LB0311ABSTHCR2.001 [Output]). DTNs LB0302DSCPTHCS.002 [161976] and LB0311ABSTHCR2.001 [Output] are used to feed and/or provide technical basis for another model (BSC 2003 [161963]) that generates lookup tables that are used in the TSPA Model.</i></p> <p><i>Small-scale fracture permeability heterogeneity was also investigated and deemed not to significantly affect seepage water chemistry (BSC 2003 [162050], Section 6.6.2.3). The THC Seepage Model includes rock properties from DTNs LB991091233129.006 [111480], LB0205REVUZPRP.001 [159525], LB0208UZDSCPMI.002 [161243], LB0207REVUZPRP.002 [159672] and LB0210THRMLPRP.001 [160799]).</i></p> <p><i>Potential alterations of these properties as a result of THC processes are explicitly accounted for by the modeling of coupled THC processes, and result in reducing fracture permeability (BSC 2003 [162050], Section 6.8.5.4). These potential alterations are neglected in the TSPA-LA, because they would reduce seepage (BSC 2003 [165564], Section 6.5.1.4) (i.e., the model is more conservative if these effects are ignored).</i></p>	<p>BSC 2003 [162050] BSC 2003 [163045] BSC 2003 [165564] BSC 2003 [163933] BSC 2003 [164889]</p>
2.2.07.02.0A	Unsaturated groundwater flow in the geosphere	<p>Groundwater flow occurs in unsaturated rocks in most locations above the water table at Yucca Mountain, including at the location of the repository. See other FEPs for discussions of specific issues related to unsaturated flow.</p> <p><i>TSPA Disposition: Included</i></p> <p><i>The THC Seepage Model that feeds into the DSCPA Model simulates groundwater flow and water-gas-rock interactions in unsaturated rock and explicitly accounts for various relevant aspects of unsaturated groundwater flow (BSC 2003 [162050], Section 6.2.1).</i></p> <p><i>Therefore, the results from the THC Seepage Model and their abstraction (Section 6.2 of the present report; summary tables of concentrations through time submitted under DTNs LB0302DSCPTHCS.002 [161976], LB0307DSTTHCR2.002 [165541], and LB0311ABSTHCR2.003 [Output]; and tables of concentrations and summary statistics through time submitted under DTN LB0311ABSTHCR2.001 [Output]) explicitly account for the effect of unsaturated groundwater flow on predicted water and gas chemistry. DTNs LB0302DSCPTHCS.002 [161976] and LB0311ABSTHCR2.001 [Output] are used to feed and/or provide technical basis for another model (BSC 2003 [161963]) that generates lookup tables that are used in the TSPA Model.</i></p>	<p>BSC 2003 [162050] BSC 2003 [163045] BSC 2003 [163933] BSC 2003 [165564] USGS 2001 [160355] BSC 2003 [165564] BSC 2003 [164889]</p>

Table 6.1-1. Features, Events, and Processes Addressed in This Model Report (Continued)

LA FEP Number	FEP Name	YMP Description	Other Upstream Reports Used for FEP Disposition
2.2.07.04.OA	Focusing of unsaturated flow (fingers, weeps)	<p>Unsaturated flow can differentiate into zones of greater and lower saturation (fingers) that may persist as preferential flow paths. Heterogeneities in rock properties, including fractures and faults, may contribute to focusing. Focused flow may become locally saturated.</p> <p><i>TSPA Disposition: Included</i></p> <p><i>Intermediate-scale focusing of flow from the site scale to the drift scale is implicitly accounted for in the TH seepage abstraction by using appropriate flow focusing factors (BSC 2003 [165564], Section 6.6.4.2). Such flow focusing is not taken into account in the THC Seepage Model results and their abstraction (Section 6.2 of the present report; summary tables of concentrations through time submitted under DTNs LB0302DSCPTHCS.002 [161976], LB0307DSTTHCR2.002 [165541], and LB0311ABSTHCR2.003 [Output]; and tables of concentrations and summary statistics through time submitted under DTN LB0311ABSTHCR2.001 [Output]). This is because fracture permeability heterogeneity was deemed not to significantly affect seepage water chemistry (BSC 2003 [162050], Section 6.6.2.3). DTNs LB0302DSCPTHCS.002 [161976] and LB0311ABSTHCR2.001 [Output] are used to feed and/or provide technical basis for another model (BSC 2003 [161963]) that generates lookup tables that are used in the TSPA Model.</i></p>	<p>BSC 2003 [163045] BSC 2003 [165564] BSC 2003 [164889] BSC 2003 [163933] BSC 2003 [162050]</p>
2.2.07.08.OA	Fracture flow in the UZ	<p>Fractures or other analogous channels act as conduits for fluids to move into the subsurface to interact with the repository and as conduits for fluids to leave the vicinity of the repository and be conducted to the SZ. Water may flow through only a portion of the fracture network, including flow through a restricted portion of a given fracture plane.</p> <p><i>TSPA Disposition: Included</i></p> <p><i>Flow processes in fractures or other channels affect modeled THC coupled processes because of 1) their strong effect on TH behavior (BSC 2003 [165564], Sections 6.4.4.1 and 6.4.4.2), and 2) their strong effect on water and gas chemistry (BSC 2003 [162050], Section 6.2.1). The latter is primarily due to volatilization of steam and CO₂ from the rock matrix-water and subsequent transport and condensation in fractures. The amount of mobilized CO₂ with steam directly affects the pH of the condensate, which in turn affects the degree of water-rock interaction and water chemistry. These THC processes are influenced by the fracture characteristics, such as orientation, aperture, asperity, length, connectivity, and fillings. The THC Seepage Model that feeds into the DSPCA model explicitly simulate the flow processes in fractures using appropriate continuum properties that represent these characteristics (BSC 2003 [162050], Sections 6.4.3, 6.4.4, and 6.4.7).</i></p> <p><i>Thus, the results from the THC Seepage Model and their abstraction (Section 6.2 of the present report; summary tables of concentrations through time submitted under DTNs LB0302DSCPTHCS.002 [161976], LB0307DSTTHCR2.002 [165541], and LB0311ABSTHCR2.003 [Output]; and tables of concentrations and summary statistics through time submitted under DTN LB0311ABSTHCR2.001 [Output]) explicitly account for the effect of fractures on predicted water and gas chemistry. DTNs LB0302DSCPTHCS.002 [161976] and LB0311ABSTHCR2.001 [Output] are used to feed and/or provide technical basis for another model (BSC 2003 [161963]) that generates lookup tables that are used in the TSPA Model.</i></p>	<p>BSC 2003 [162050] BSC 2003 [163045] BSC 2003 [160240] BSC 2003 [161773] BSC 2003 [163933] BSC 2003 [165564] BSC 2003 [164889]</p>

Table 6.1-1. Features, Events, and Processes Addressed in This Model Report (Continued)

LA FEP Number	FEP Name	YMP Description	Other Upstream Reports Used for FEP Disposition
2.2.07.09.0A	Matrix imbibition in the UZ	<p>Water flowing in fractures or other channels in the unsaturated zone is imbibed into the surrounding rock matrix. This may occur during steady flow, episodic flow, or into matrix pores that have been dried out during the thermal period.</p> <p><i>TSPA Disposition: Included</i> <i>The THC Seepage Model explicitly accounts for matrix imbibition using appropriate dual-permeability modeling concepts (BSC 2003 [162050], Section 6.2.1). This is needed because the thermal perturbation of the unsaturated rock results in significant transfer of liquid and gas from the matrix into the fractures and vice versa (e.g., BSC 2003 [162050], Figure 6.2-2). Therefore, these effects are directly accounted for in results from the THC Seepage Model and their abstraction (Section 6.2 of the present report; summary tables of concentrations through time submitted under DTNs LB0302DSCPTHCS.002 [161976], LB0307DSTTHCR2.002 [165541], and LB0311ABSTHCR2.003 [Output]; and tables of concentrations and summary statistics through time submitted under DTN LB0311ABSTHCR2.001 [Output]). DTNs LB0302DSCPTHCS.002 [161976] and LB0311ABSTHCR2.001 [Output] are used to feed and/or provide technical basis for another model (BSC 2003 [161963]) that generates lookup tables that are used in the TSPA Model.</i></p>	<p>BSC 2003 [162050] BSC 2003 [163045] BSC 2003 [163933] BSC 2003 [165564]</p>
2.2.07.10.0A	Condensation zone forms around drifts	<p>Condensation of the two-phase flow generated by repository heat forms in the rock where the temperature drops below the local vaporization temperature. Waste package emplacement geometry and thermal loading will affect the scale at which condensation caps form (over waste packages, over panels, or over the entire repository), and to the extent to which "shedding" will occur as water flows from the region above one drift to the region above another drift or into the rock between drifts.</p> <p><i>TSPA Disposition: Included</i> <i>The coupled processes of vapor condensation forming a condensation cap above the drifts and occurrence of "shedding" between drifts are explicitly simulated with the THC Seepage Model (BSC 2003 [162050], Sections 6.2.1, 6.5.5.1, 6.6.2.1 and 6.8.5.4). Using this model, the impact of condensation and drainage on seepage water chemistry is assessed for various simulation cases (BSC 2003 [162050], Sections 6.5, 6.6, 6.7, and 6.8) (also see Section 6.3). Therefore, the results from the THC Seepage Model and their abstraction (Section 6.2 of the present report; summary tables of concentrations through time submitted under DTNs LB0302DSCPTHCS.002 [161976], LB0307DSTTHCR2.002 [165541], and LB0311ABSTHCR2.003 [Output]; and tables of concentrations and summary statistics through time submitted under DTN LB0311ABSTHCR2.001 [Output]) explicitly include these effects. DTNs LB0302DSCPTHCS.002 [161976] and LB0311ABSTHCR2.001 [Output] are used to feed and/or provide technical basis for another model (BSC 2003 [161963]) that generates lookup tables that are used in the TSPA Model.</i></p>	<p>BSC 2003 [161530] BSC 2003 [165564] BSC 2003 [162050]</p>

Table 6.1-1. Features, Events, and Processes Addressed in This Model Report (Continued)

LA FEP Number	FEP Name	YMP Description	Other Upstream Reports Used for FEP Disposition
2.2.07.11.OA	Resaturation of geosphere dryout zone	<p>Following the peak thermal period, water in the condensation cap may flow downward into the drifts. Influx of cooler water from above, such as might occur from episodic flow, may accelerate return flow from the condensation cap by lowering temperatures below the condensation point. Percolating groundwater will also contribute to resaturation of the dry-out zone. Vapor flow, as distinct from liquid flow by capillary processes, may also contribute.</p> <p><i>TSPA Disposition: Included</i> <i>Resaturation of the dryout zone around drifts, and the potential of return flow from the condensation zone back to the drifts, are explicitly simulated with the THC Seepage Model (BSC 2003 [162050], Sections 6.2.1, 6.5.5, 6.6.2, 6.7.5, 6.8.5). Using this model, the impact of resaturation on reflux chemistry is assessed as part of the abstraction methodology (i.e., the compositions of abstracted "FRONT" waters reflect concentration increases due to the dissolution of salts precipitated during dryout; see Section 6.2.4.1.2). Therefore, the results from the THC Seepage Model and their abstraction (Section 6.2 of the present report; summary tables of concentrations through time submitted under DTNs LB0302DSCPTHCS.002 [161976], LB0307DSTTHCR2.002 [165541], and LB0311ABSTHCR2.003 [Output]; and tables of concentrations and summary statistics through time submitted under DTN LB0311ABSTHCR2.001 [Output]) explicitly include these effects. DTNs LB0302DSCPTHCS.002 [161976] and LB0311ABSTHCR2.001 [Output] are used to feed and/or provide technical basis for another model (BSC 2003 [161963]) that generates lookup tables that are used in the TSPA Model.</i></p>	BSC 2003 [161530] BSC 2003 [165564] BSC 2003 [162050]
2.2.08.01.OB	Chemical characteristics of groundwater in the UZ	<p>Chemistry and other characteristics of groundwater in the unsaturated zone may affect groundwater flow and radionuclide transport of dissolved and colloidal species. Groundwater chemistry and other characteristics, including temperature, pH, Eh, ionic strength, and major ionic concentrations, may vary spatially throughout the system as a result of different rock mineralogy.</p> <p><i>TSPA Disposition: Included</i> <i>THC Seepage Model simulations feeding this abstraction report were run explicitly using five different input water compositions spanning the range of compositions at Yucca Mountain (Attachment III) (see also BSC 2003 [162050] Sections 6.2.2 and 6.8.5). This variability of pore-water compositions in repository host units implicitly reflects spatial variations in rock mineralogy and infiltration rates. Therefore, the results of the THC Seepage Model and their abstraction (Section 6.2 of the present report; summary tables of concentrations through time submitted under DTNs LB0302DSCPTHCS.002 [161976], LB0307DSTTHCR2.002 [165541], and LB0311ABSTHCR2.003 [Output]; and tables of concentrations and summary statistics through time submitted under DTN LB0311ABSTHCR2.001 [Output]) explicitly reflect the natural variability of pore-water compositions and implicitly reflect the natural variability of rock mineralogy. DTNs LB0302DSCPTHCS.002 [161976] and LB0311ABSTHCR2.001 [Output] are used to feed and/or provide technical basis for another model (BSC 2003 [161963]) that generates lookup tables that are used in the TSPA Model.</i> <i>The temperature effect on radionuclide transport is investigated in Section 6.3 with effects reported in DTN LB0311ABSTHCR2.004 [Output]. The conclusion is made that this effect can be ignored, either because the uncertainty in measured K_d values is larger than temperature-induced K_d variations, or because ignoring the effect provide conservatively less retardation (Section 8.3). Colloidal transport is addressed in the reports cited in column 4.</i></p>	BSC 2003 [163228] BSC 2003 [162050]

Table 6.1-1. Features, Events, and Processes Addressed in This Model Report (Continued)

LA FEP Number	FEP Name	YMP Description	Other Upstream Reports Used for FEP Disposition
2.2.08.04.0A	Redissolution of precipitates directs more corrosive fluids to containers	<p>Redissolution of precipitates that have plugged pores as a result of evaporation of groundwater in the dry-out zone, produces a pulse of fluid reaching the waste packages when gravity-driven flow resumes, which is more corrosive than the original fluid in the rock.</p> <p><i>TSPA Disposition: Included</i></p> <p><i>The THC Seepage Model simulations feeding this abstraction report explicitly consider the formation of salt precipitates upon dryout (BSC 2003 [162050], Section 6.4.5) and their dissolution during re-wetting around drifts (BSC 2003 [162050], Section 6.8.5.3) and the resulting effect on percolation water chemistry (Section 6.2.4.1.2) (see also BSC 2003 [162050], Section 6.8.5.4, p. 240).</i></p> <p><i>Therefore, the results of the THC Seepage Model and their abstraction (Section 6.2 of the present report; summary tables of concentrations through time submitted under DTNs LB0302DSCPTHCS.002 [161976], LB0307DSTTHCR2.002 [165541], and LB0311ABSTHCR2.003 [Output]; and tables of concentrations and summary statistics through time submitted under DTN LB0311ABSTHCR2.001 [Output]) explicitly reflect the effect of salt redissolution upon rewetting. The effect results in an increase in both salinity and variability (Section 6.2.4.1.2). DTNs LB0302DSCPTHCS.002 [161976] and LB0311ABSTHCR2.001 [Output] are used to feed and/or provide technical basis for another model (BSC 2003 [161963]) that generates lookup tables that are used in the TSPA Model.</i></p>	BSC 2003 [162050]
2.2.08.12.0A	Chemistry of water flowing into the drift	<p>Inflowing water chemistry may be used in analysis or modeling that requires initial water chemistry in the drift. Chemistry of water flowing into the drift is affected by initial water chemistry in the rock, mineral and gas composition in the rock, and thermal-hydrological-chemical processes in the rock.</p> <p><i>TSPA Disposition: Included</i></p> <p><i>The THC Seepage Model was designed specifically to investigate the effect of thermal-hydrological-chemical processes in the host rock (BSC 2003 [162050] Section 6.2.1.2), including the effects of initial water chemistry (BSC 2003 [162050], Section 6.2.2.1), and mineral and gas compositions in the rock (BSC 2003 [162050], Section 6.2.2.2).</i></p> <p><i>Therefore, these effects are explicitly taken into account in the results of the THC Seepage Model and their abstraction (Section 6.2 of the present report; summary tables of concentrations through time submitted under DTNs LB0302DSCPTHCS.002 [161976], LB0307DSTTHCR2.002 [165541], and LB0311ABSTHCR2.003 [Output]; and tables of concentrations and summary statistics through time submitted under DTN LB0311ABSTHCR2.001 [Output]). DTNs LB0302DSCPTHCS.002 [161976] and LB0311ABSTHCR2.001 [Output] are used to feed and/or provide technical basis for another model (BSC 2003 [161963]) that generates lookup tables that are used in the TSPA Model.</i></p> <p><i>Because no water is predicted to actually seep into the modeled drift, the abstraction method was specifically designed to consider waters deemed most representative of potential in-drift seepage (Section 6.2.1, Figures 6.2-2 and 6.2-3) (DTN LB0311ABSTHCR2.001 [Output]).</i></p>	BSC 2003 [162050]

Table 6.1-1. Features, Events, and Processes Addressed in This Model Report (Continued)

LA FEP Number	FEP Name	YMP Description	Other Upstream Reports Used for FEP Disposition
2.2.10.03.0B	Natural geothermal effects on flow in the UZ	<p>The existing geothermal gradient, and spatial or temporal variability in that gradient, may affect groundwater flow in the UZ.</p> <p><i>TSPA Disposition: Included</i></p> <p><i>The natural geothermal gradient at Yucca Mountain is explicitly included in starting conditions of the THC Seepage Model by setting the ground surface temperature (top model boundary) and the temperature at the water table (bottom boundary) to measured values (BSC 2003 [162050], Section 6.8.2). The effect of this temperature gradient on flow is explicitly accounted for by the coupled heat/flow transport algorithms implemented into the THC simulator (TOUGHREACT V3.0; LBNL 2002 [161256]). Therefore, this effect is explicitly taken into account in the results of the THC Seepage Model and their abstraction (Section 6.2 of the present report; summary tables of concentrations through time submitted under DTNs LB0302DSCPTHCS.002 [161976], LB0307DSTTHCR2.002 [165541], and LB0311ABSTHCR2.003 [Output]; and tables of concentrations and summary statistics through time submitted under DTN LB0311ABSTHCR2.001 [Output]). DTNs LB0302DSCPTHCS.002 [161976] and LB0311ABSTHCR2.001 [Output] are used to feed and/or provide technical basis for another model (BSC 2003 [161963]) that generates lookup tables that are used in the TSPA Model.</i></p>	BSC 2003 [162050] BSC 2003 [165692] BSC 2003 [163045]
2.2.10.10.0A	Two-phase buoyant flow/ heat pipes	<p>Heat from waste generates two-phase buoyant flow. The vapor phase (water vapor) escapes from the mountain. A heat pipe consists of a system for transferring energy between a hot and a cold region (source and sink respectively) using the heat of vaporization and movement of the vapor as the transfer mechanism. Two-phase circulation continues until the heat source is too weak to provide the thermal gradients required to drive it. Alteration of the rock adjacent to the drift may include dissolution which maintains the permeability necessary to support the circulation (as inferred for some geothermal systems).</p> <p><i>TSPA Disposition: Included</i></p> <p><i>The coupled processes causing heat-pipe behavior are explicitly simulated with the THC Seepage Model (BSC 2003 [162050], Section 6.2.1.1). The continuous boiling and refluxing of water in this zone affects water-rock interactions (BSC 2003 [162050], Section 6.2.1.2). The resulting water chemistry in the heat pipe is captured by the HISAT waters (Section 6.2.4.1.1) (see also BSC 2003 [162050], Section 6.8.5.3.2). Therefore, the effect of heat pipes on predicted water and gas chemistries is explicitly taken into account in the results of the THC Seepage Model and their abstraction (Section 6.2 of the present report; summary tables of concentrations through time submitted under DTNs LB0302DSCPTHCS.002 [161976], LB0307DSTTHCR2.002 [165541], and LB0311ABSTHCR2.003 [Output]; and tables of concentrations and summary statistics through time submitted under DTN LB0311ABSTHCR2.001 [Output]). DTNs LB0302DSCPTHCS.002 [161976] and LB0311ABSTHCR2.001 [Output] are used to feed and/or provide technical basis for another model (BSC 2003 [161963]) that generates lookup tables that are used in the TSPA Model.</i></p>	BSC 2003 [161530] BSC 2003 [165564] BSC 2003 [162050]

Table 6.1-1. Features, Events, and Processes Addressed in This Model Report (Continued)

LA FEP Number	FEP Name	YMP Description	Other Upstream Reports Used for FEP Disposition
2.2.10.12.0A	Geosphere dry-out due to waste heat	<p>Repository heat evaporates water from the UZ rocks near the drifts as the temperature exceeds the vaporization temperature. This zone of reduced water content (reduced saturation) migrates outward during the heating phase (about the first 1,000 years) and then migrates back to the containers as heat diffuses throughout the mountain and the radioactive sources decay. This FEP addresses the effects of dry-out within the rocks.</p> <p><i>TSPA Disposition: Included</i></p> <p><i>The coupled processes of vaporization, dryout, and resaturation are explicitly simulated with the THC Seepage Model, including the formation of a dry (or nearly dry) zone around drifts, expanding and then receding through time following the pulse of heat released from the waste packages (BSC 2003 [162050], Sections 6.2.1 and 6.8.5.2).</i></p> <p><i>Therefore, these effects are explicitly taken into account in the results of the THC Seepage Model and their abstraction (Section 6.2 of the present report; summary tables of concentrations through time submitted under DTNs LB0302DSCPTHCS.002 [161976], LB0307DSTTHCR2.002 [165541], and LB0311ABSTHCR2.003 [Output]; and tables of concentrations and summary statistics through time submitted under DTN LB0311ABSTHCR2.001 [Output]). DTNs LB0302DSCPTHCS.002 [161976] and LB0311ABSTHCR2.001 [Output] are used to feed and/or provide technical basis for another model (BSC 2003 [161963]) that generates lookup tables that are used in the TSPA Model.</i></p>	BSC 2003 [165564] BSC 2003 [161530] BSC 2003 [162050]

6.1.2 Other FEPs Relevant to this Model Report

The FEPs listed in Table 6.1-2 are other FEPs taken from the LA FEP list that are associated with the subject matter of this report, regardless of the anticipated status for exclusion or inclusion in TSPA-LA as represented in BSC 2002 [160819]. The results of this report and upstream process models are part of the basis for the treatment of FEPs as discussed in TSPA-MAD (BSC 2002 [160146], Section 3.2.2). Cross-references for each FEP to the relevant sections of this report, to the upstream report documenting the process model (BSC 2003 [162050]), and/or to other relevant model reports are also given in Table 6.1-2.

Table 6.1-2. Other FEPs Relevant to This Model Report

LA FEP Number	FEP Name	YMP Description	Relevant Upstream Reports and/or Sections where Discussed in this Report
2.1.09.12.0A	Rind (chemically altered zone) forms in the nearfield	Thermal-chemical processes involving precipitation, condensation, and re-dissolution alter the properties of the adjacent rock. These alterations may form a rind, or altered zone, in the rock, with hydrological, thermal, and mineralogical properties different from the initial conditions.	BSC (2003 [162050], Sections 6.2.1, 6.4.4, 6.5.5.2, 6.6.2.3.1, 6.7.5.2, 6.8.5.4) BSC (2003 [165564], Sections 6.4.4.2 and 6.5.1.4)
2.2.01.05.0A	Radionuclide transport in the excavation disturbed zone	Radionuclide transport through the excavation disturbed zone may differ from transport in the EBS and the undisturbed host rock. Transport processes such as dissolution and precipitation, sorption, and colloid filtration should be considered.	BSC (2003 [163228]) CRWMS M&O (2000 [122799]) Section 6.3 of the present abstraction report discusses the effects of temperature on radionuclide sorption.
2.2.07.20.0A	Flow diversion around repository drifts	Flow in unsaturated rock tends to be diverted by openings such as waste emplacement drifts due to the effects of capillary forces. The resulting diversion of flow could have an effect on seepage into the repository. Flow diversion around the drift openings could also lead to the development of a zone of lower flow rates and low saturation beneath the drift, known as the drift shadow.	BSC (2003 [162050], Sections 6.2.1, 6.5.5.1, 6.6.2.1, 6.8.5.4) BSC (2003 [165564])
2.2.08.03.0B	Geochemical interactions and evolution in the UZ	Groundwater chemistry and other characteristics, including temperature, pH, Eh, ionic strength, and major ionic concentrations, may change through time, as a result of the evolution of the disposal system or from mixing with other waters. Geochemical interactions may lead to dissolution and precipitation of minerals along the groundwater flow path, affecting groundwater flow, rock properties, and sorption of contaminants. Effects on hydrological flow properties of the rock, radionuclide solubilities, sorption processes, and colloidal transport are relevant. Kinetics of chemical reactions should be considered in the context of the time scale of concern.	BSC (2003 [162050], Sections 6.2.2, 6.5.5.2, 6.6.2.3, 6.7.5.2, 6.8.5.3) (BSC 2001 [154826])

Table 6.1-2. Other Features, Events, and Processes Relevant to This Model Report (Continued)

LA FEP Number	FEP Name	YMP Description	Relevant Upstream Reports and/or Sections where Discussed in this Report
2.2.10.06.0A	Thermal-chemical alteration in the UZ (solubility, speciation, phase changes, precipitation/dissolution)	Thermal effects may affect radionuclide transport directly by causing changes in radionuclide speciation and solubility in the UZ or indirectly, by causing changes in the host rock mineralogy that affect the flow path. Relevant processes include volume effects associated with silica phase changes, precipitation and dissolution of fracture-filling minerals (including silica and calcite), and alteration of zeolites and other minerals to clays.	BSC 2001 [154826] Note: Section 6.3 of the present abstraction report discusses the effects of temperature on radionuclide sorption.

6.2 THC SEEPAGE MODEL ABSTRACTION

6.2.1 Conceptual Model

The conceptualization of drift-scale coupled processes underlying the THC Seepage Model is presented in BSC (2003 [162050], Section 6.2). Here, only the conceptualization of the abstraction itself is examined.

The intention of the THC Seepage Model is to analyze the effect of THC processes in the rock around waste emplacement drifts (BSC 2003 [162050]), including:

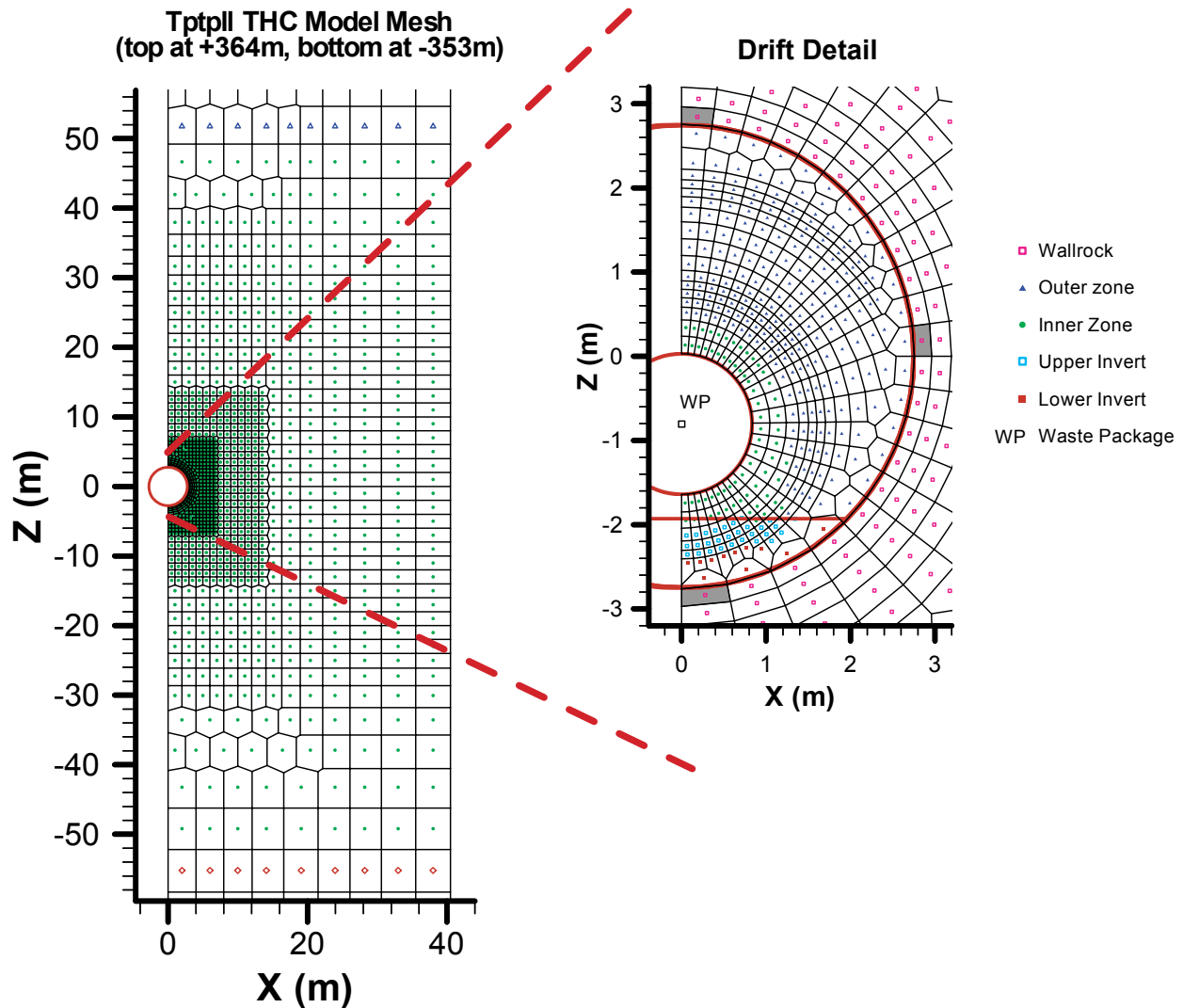
- Predicting the composition of waters and gases that could enter the drifts
- Evaluating the effect of THC processes on seepage into drifts

However, the THC Seepage Model does not simulate actual seepage of water into drifts because the range of simulated infiltration rates (including rates for future climate conditions of high infiltration) remains well below the theoretical seepage threshold for rocks around the drift (e.g., BSC 2003 [161530], Section 6.2.2.1.2). Instead, the model is used to compute the compositions of pore water and gas in the repository host-rock (matrix and fractures) around a typical drift (Figure 6.2-1). Predicted water and gas compositions are then obtained from locations (around the modeled drift) that are deemed the most likely to yield fluids that could seep into the drift. Water and gas compositions predicted at the drift wall are also considered, although, as discussed later, water composition data at the drift wall are not available during the time that the drift wall remains dry.

Whether to use predicted concentrations from the fracture or matrix continuum is also part of the abstraction conceptual model. The permeability of fractures around the drift is several orders of magnitude higher than the permeability of the matrix. Also, fractures have much lower capillarity than the matrix. Therefore, any water potentially seeping into the drift by gravity is likely to be fracture water, and the composition of that water is used for all areas above the drift.

In contrast, both fracture and matrix water could potentially contribute to in-drift seepage in areas where the drift invert contacts wallrock (by imbibition into the porous invert). For this reason, both fracture and matrix waters are considered in areas below the drift.

Predicted concentration gradients near the drift are steep, resulting from steep temperature and liquid saturation gradients. Therefore, abstracted water compositions depend strongly on the location (around the drift) chosen for abstraction. Because of the transient nature of the thermal pulse, predicted water compositions also change significantly through time. Therefore, abstractions in both space and time need to be considered, as further examined below.



Grid source DTN: LB0011DSTTHCR1.002 [161282]

NOTE: Shaded gridblocks around the drift are those previously selected for abstraction of data at the drift wall.

Figure 6.2-1. THC Seepage Model Mesh (Tptpl REV02 Model, No Drift Degradation)

6.2.1.1 Spatial Abstraction of Water and Gas Compositions

The THC Seepage Model consists of a two-dimensional, half-drift (symmetric) chimney model extending vertically from near the ground surface down to the water table, and horizontally from drift center to the midpoint between drifts (BSC 2003 [162050], Sections 6.5–6.8) (Figure 6.2-1). The most recent revision of this model (BSC 2003 [162050], Section 6.8) considers a geographic location near the center of the repository block (at approximately Nevada State Plane coordinates E170572, N233195), with a drift located in the Tptpl hydrogeologic unit. This location pertains to all model results discussed in this report, although the results are applicable to other locations as described below.

Simulations considering a significantly different location (using the stratigraphy at the location of borehole SD-9) and a drift in the Tptpmn hydrogeologic unit were also run (BSC 2003 [162050], Section 6.5). These simulations indicate that, in terms of predicted water and gas compositions, differences in model results caused by changes in geographic location and repository host rock unit are not as significant (BSC 2003 [162050], Section 6.7.5.2) as differences resulting from the variability in input water compositions and spatial location around the modeled drift (BSC 2003 [162050], Section 6.8.5.3.2). This variability could be reasonably regarded as encompassing a range of potential geographic locations, implicitly representing changes in stratigraphy, rock properties, and/or infiltration rates throughout the repository. For these reasons, results of the THC Seepage Model as examined here, for one geographic location but including the variability introduced by using different water compositions and locations around the modeled drift, are deemed to be reasonably applicable to other locations within the proposed repository footprint.

Previous abstractions of water compositions from this model (CRWMS M&O 2000 [123916]) considered single points (model gridblocks) each at the crown, side, and base of the drift. However, points at these three locations provide only limited information on the chemistry of waters that could seep into drifts. These locations do not capture the spatial variability of model results around the drift and, more importantly, cannot provide water compositions during the dryout period when all water is boiled off at these locations. To circumvent these limitations, the abstraction model was developed such that results could be extracted from the model grid from wider areas above, to the side and below the drift, and then also following the expanding-then-receding boiling (or wetting) front, as described below.

First, two “types” of water are considered to be the best candidates for potentially seeping into a modeled drift (and thus the best candidates for abstraction):

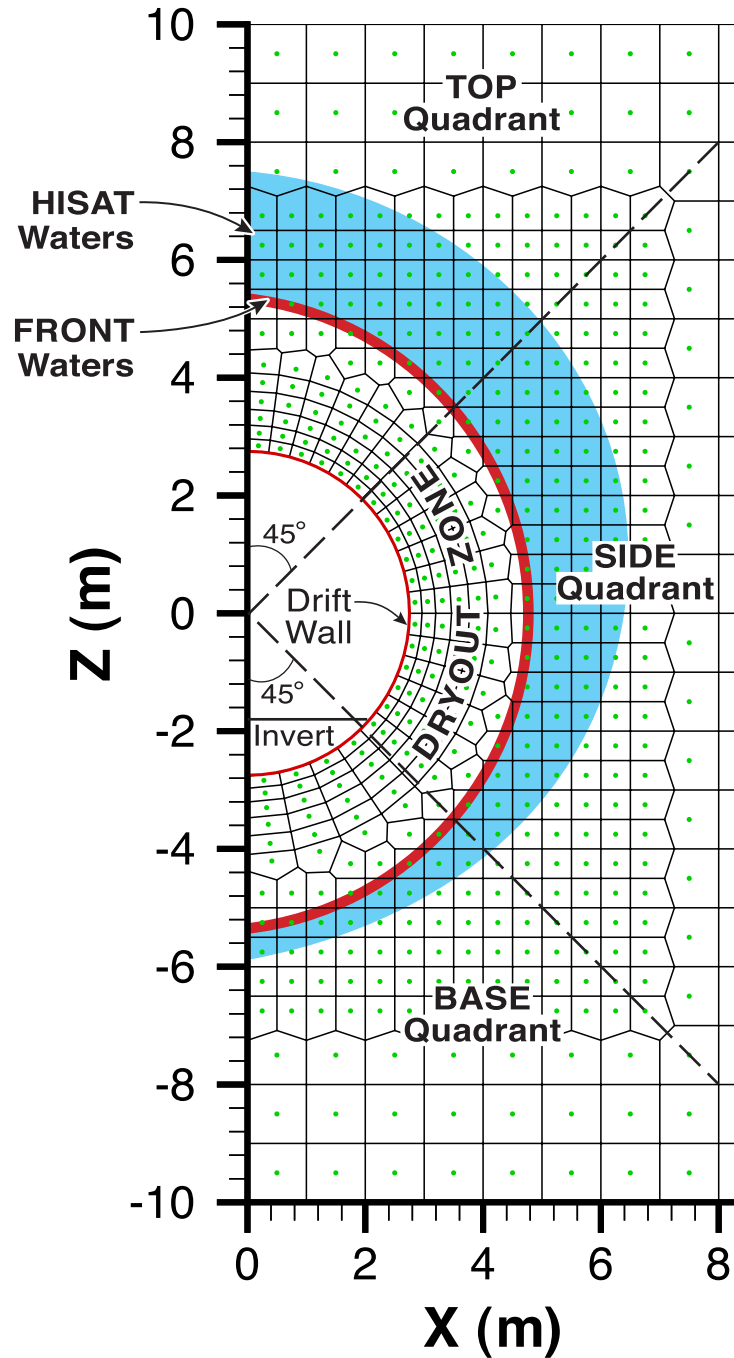
- Waters in zones around the drift where liquid saturations are higher than in surrounding host rock (e.g., condensation zones): this water is given the attribute “HISAT”.
- Waters from zones closest to the drift (i.e., where non-zero liquid saturations occur closest to the drift wall): this water is given the attribute “FRONT”.

The cross-sectional area around the modeled half-drift is then divided into three quadrants with the following spatial characteristics and assigned attributes (Figure 6.2-2):

- A first quadrant encompassing the area above the drift, defined by model gridblocks

having a ratio of their vertical (Z) to their horizontal (X) coordinate greater or equal to 1 (45° arc from crown): this quadrant is given the attribute “TOP”.

- A second quadrant encompassing the area to the side of the drift, defined by model grid blocks having their Z/X ratio ranging from -1 to $+1$ (45° arc above and 45° below the drift spring line): this quadrant is given the attribute “SIDE”.
- A third quadrant encompassing the area below the drift, defined by model gridblocks having their Z/X ratio less than -1 (45° arc from base): this quadrant is given the attribute “BASE”.



Grid source DTN: LB0011DSTTHCR1.002 [161282]

NOTE: The areas delineating HISAT and FRONT waters are for illustrative purposes only. The extent of these areas varies through time and is different for fracture and matrix waters.

Figure 6.2-2. Quadrant Designations for Abstraction of Data from the THC Seepage Model

Model results for gridblocks from these quadrants are then extracted for each water type (FRONT and HISAT) as described below.

FRONT waters (boiling/wetting front)—At each printout interval, model results are extracted for gridblocks according to the following criteria (in order of preference):

1. Search-radius of 25 m from drift center, then,
2. Non-zero liquid saturation (in matrix or fractures depending on the selected medium) then,
3. First six gridblocks with smallest radial distance from drift center—these are ranked with attribute INDX=1 through 6 from the closest to the farthest from the drift center. However, if ties occur (same radial distance), the gridblocks and corresponding indexes INDX are selected and ranked in order of decreasing liquid saturation, then decreasing absolute values of Z coordinates (equivalent to increasing X coordinates).

HISAT waters (zone of increased liquid saturation)—At each printout interval, model results are extracted for gridblocks according to the following criteria (in order of preference):

1. Search-radius of 25 m from drift center, then,
2. First six gridblocks with highest liquid saturation (in matrix or fractures depending on the selected medium)—these are ranked with attribute INDX=1 through 6 from most to least liquid saturated. However, if ties occur (same liquid saturation), then gridblocks and corresponding indexes INDX are selected and ranked in order of increasing radial distance from drift center, then decreasing absolute values of Z coordinates (equivalent to increasing X coordinates).

Thus, for FRONT waters, priority is given to gridblocks that are wet and closest to the drift wall. If two or more selected wet gridblocks occur at the same distance from drift center, then the wettest ones are selected. If two or more of them have the same liquid saturation (and are located at the same distance from the drift), then the gridblocks most directly above or below the drift are selected.

In contrast, for HISAT waters, priority is given to gridblocks that are the wettest within a given distance (25 m) from drift center. If two or more selected wet gridblocks have the same liquid saturation, then the one closest to drift center is selected. If two or more gridblocks are located at the same distance from the drift (and have the same liquid saturation), then those most directly above or below the drift are selected.

The selection of no more than six gridblocks for each water at each time step stems from the configuration of the numerical grid. In this grid, each successive radially distributed row of gridblocks in the TOP quadrant, from the drift wall outwards, contains approximately six gridblocks (Figure 6.2-2). By limiting the number of selected gridblocks, extraction of data over too wide an area is avoided, so that the potential for overlapping HISAT and FRONT waters is limited. Note that because the selection of gridblocks relies on the liquid saturation in a particular

medium (fractures or matrix), abstracted fracture and matrix data following the procedure described above do not necessarily correspond to the same gridblocks.

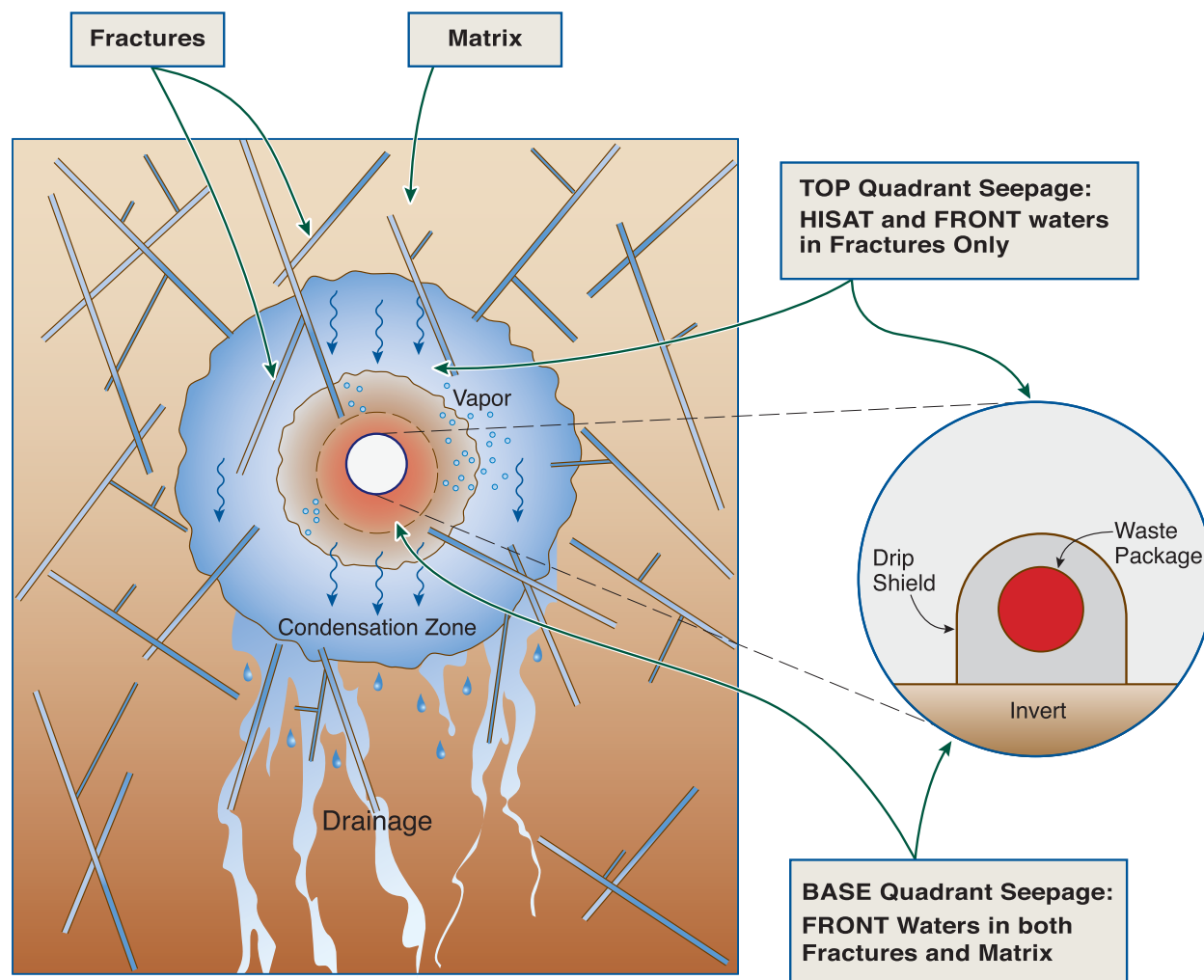
The described abstraction method is used to extract simulated water and CO₂ concentrations for six points (gridblocks) per time interval for each run, for each extracted type of water (FRONT or HISAT) in each quadrant (TOP, SIDE, and BASE). In this way, the method captures the spatial variability of model results around the drift for each given model run. It also captures the predicted compositions of waters closest to the drift during and after the dryout period. The method is used with both fracture and matrix waters. The large quantity of data extracted in this way is then narrowed down to consider only waters deemed most susceptible to seep into drifts, namely:

- HISAT waters for the fracture medium in the TOP quadrant
- FRONT waters for the fracture medium in the TOP and BASE quadrants
- FRONT waters for the matrix medium in the BASE quadrant.

This constitutes the main conceptualization for abstraction (Figure 6.2-3). The data from the SIDE quadrant are not considered further in this report, because most in-drift seepage is expected to occur by gravity drainage above the drift, while a small fraction may occur by imbibition into the invert at the base of the drift (BSC 2003 [165692]).

It can be argued that HISAT waters (from zones with increased liquid saturation) would evolve towards the composition of FRONT waters (boiling/wetting front) as they migrate towards the drift. Thus, the FRONT waters could be considered more representative of potential in-drift seepage than HISAT waters. As discussed later, the compositions of FRONT waters display more variability than HISAT waters because they have been boiled (evaporated) to a more variable degree than HISAT waters, depending on their exact location near the boiling (wetting) front. They may also be more subject to uncertainties associated with modeling chemical processes under degrees of high evaporation.

Finally, note that during the dryout period, when model data are extracted from gridblocks away from the drift wall, this abstraction method does not capture in-drift gas composition. However, these gas compositions can be obtained from data extracted for gridblocks directly adjacent to the drift crown, springline (side), and base reported in BSC (2003 [162050], Section 6.8.5.3.1). These in-drift gas compositions, at any given time, are much more homogenous than pore-water compositions around the drift, and therefore do not need further abstraction in space.



NOTE: Arrows show drainage

Figure 6.2-3. Conceptual Model for Abstraction of In-Drift Seepage Water Chemistry

6.2.1.2 Time Abstraction of Water and Gas Compositions

Abstraction of THC Seepage Model results through time for TSPA-LA is carried out in another Model Report (*Engineered Barrier System: Physical and Chemical Environment Model* (BSC 2003 [161963])). For this reason, no abstraction in time is implemented here.

Time profiles of pore-water compositions reported in BSC (2003 [162050], Section 6.8.5.3.2) for the zone of increased liquid saturation above the drift (HISAT waters) show that the following successive stages in the evolution of water composition in this zone can be distinguished:

1. A dilution stage occurs when the dryout zone is expanding, roughly from 50 to around 100–150 years. It is caused by steam originating from water boiling in the rock matrix then migrating and condensing into fractures (BSC 2003 [162050], Section 6.2.1.1).

2. An evaporative concentration stage takes place while the zone of increased liquid saturation remains essentially stationary. The water in fractures is concentrated by boiling the percolating water, with little or no additional influx of condensation water derived from boiling matrix water. This stage lasts approximately from 150 years to 600 years for most waters, but is shorter by several hundred years under the higher infiltration rate (as shown by chloride profiles in BSC (2003 [162050], Figure 6.8-28).
3. A “back-to-ambient” stage starts while boiling is still occurring, after approximately 600 years (and earlier at higher infiltration rates), then continuing after the collapse of the boiling front. During this stage, the dilution by percolating waters overcomes the effect of evaporative concentration and brings concentrations back to their ambient values.

These three stages could be used to further define abstraction time-periods for predicted concentrations of pore waters in the zone of increased liquid saturation above the drift. The first and second stage could bound minimum and maximum concentrations, respectively, while the third stage would be representative of long-term ambient conditions.

Note that the temperature histories and lengths of the boiling period are expected to vary over the repository footprint, because of spatial differences in infiltration rates and host-rock geologic units, and heat loss at the edge of the proposed repository. These effects are captured by the Multiscale Thermohydrological (MSTH) Model (BSC 2003 [165692], Section 6.3.1.1). For a mean infiltration case similar to that used in the THC Seepage Model, the MSTH Model predicts the time (after closure) when boiling ceases at the drift wall to be a maximum of 1,356 years, and around 1,000 years for 90% of investigated locations (BSC 2003 [165692], Table 6.3-5). This time is defined in the MSTH model as the time when the average drift wall temperature drops below 96°C. With the THC Seepage Model, when chemistry effects are disabled (TH only), the rewetting of fractures at the modeled drift crown is predicted to occur between 1,150 and 1,350 years after closure (BSC 2003 [162050], Section 6.8.5.2). This time window is constrained by a 200-year printout interval used in the model. Within this time window, predicted temperatures around the drift also drop below 96°C. Therefore, when water-rock interactions are not considered, the THC Seepage Model predicts temperatures similar to those predicted with the MSTH model at hottest locations. This is mostly because the THC Seepage Model does not account for heat loss at the edge of the repository (BSC 2003 [162050], Section 1.3) or 3-D heat transfer effects in the host rock. In-drift heat transfer (from the waste package to the drift wall) is also treated somewhat differently in the MSTH Model compared to the THC Seepage Models. However, this does not result in significant differences between these models in predicted drift-wall temperatures for given waste package temperatures. For example, the maximum waste package and drift wall temperatures from the THC Seepage Model are around 164°C and 141°C, respectively (BSC 2003 [162050], Figure 6.8-4). With the MSTH model for a similar mean infiltration case, the same waste package temperature (around 164°C) corresponds to a drift-wall temperature around 139°C (BSC 2003 [165692], Figure 6.3-2).

When mineral precipitation is taken into effect, the THC Seepage Model predicts that fractures at the drift crown rewet several hundred years later (1,750 to 2,150 years after closure, depending on the initial water composition). This is because mineral precipitation above the drift causes a reduction in fracture permeability and subsequent partial diversion of percolation waters around

the drift (BSC 2003 [162050], Section 6.8.5.4). For these THC simulations, the temperature drop below 96°C at the drift wall occurs between 1,350 and 1,550 years after closure, which is approximately 200 years more than for the case when the effect of water-rock interaction is ignored (with all other input parameters kept identical).

Because boiling and temperature affect water-rock interactions, and thus predicted water and gas compositions, the abstraction of the THC Seepage Model results in time would need to take into account the variability of temperature histories and boiling lengths throughout the repository. Because the THC Seepage Model results apply to hottest locations within the repository, where boiling would prevail for the longest time, water compositions using this model are expected to yield more concentrated waters than in cooler areas.

As noted earlier, differences in water and gas chemistries related to geographic location but not to temperature (i.e., stratigraphy and infiltration rates,) are likely encompassed in the variability of model results. This is because the THC Seepage Model considers a range of input water compositions (Attachment III) that can be reasonably regarded as implicitly representing changes in mineralogy, rock properties, and infiltration rates throughout the proposed repository.

6.2.2 Alternative Conceptual Models

Alternative conceptualizations of the THC Seepage Model are discussed in BSC (2003 [162050], Section 6.3). Here, only alternative abstraction models are examined.

As discussed in Section 6.2.1, the main difficulty in abstracting water compositions from the THC Seepage Model is that the model does not predict in-drift seepage to occur, even under conditions of increased infiltration from climate change. Therefore, the decision as to which water compositions to extract from the model forms the most important basis for abstraction. In this regard, the method described in Section 6.2.1.1 can be viewed as addressing two alternative conceptualizations:

- Abstraction of compositions from zones of increased liquid saturation above the drift (HISAT-TOP waters in fractures)
- Abstraction of compositions from the boiling/wetting front (FRONT-TOP and FRONT-BASE waters in fractures and matrix)

As discussed in BSC (2003 [162050], Section 6.8.5.3.2), examining the variability of predicted water compositions in zones of highest liquid saturation provides a better means of evaluating the model sensitivity to various input data or model conceptualizations than would examination of predicted water compositions directly at the boiling front. This is because waters at the boiling front show more variable compositions, resulting from a large range in their degree of evaporative concentration (i.e., large variations among small liquid saturation values). However, when evaluating the compositional variability of waters that could seep into a drift during the boiling period (by somehow penetrating the dryout zone), the predicted water composition at the boiling front should also be considered. For this reason, both water types (HISAT and FRONT) are given consideration here, and thus both alternatives are covered (Section 6.2.4.1 below).

The abstraction concept and method described in Section 6.2.1.1 address spatial abstraction for given times. An alternative is to use the same data (extracted as described in Section 6.2.1.1), but reformatted for examination as a function of drift wall temperature (which relates more directly to the potential for in-drift seepage) and of liquid saturation (which also relates more directly to mobility). These two alternatives are also considered (Section 6.2.4.2).

Alternative methods for abstraction of specific time periods are not considered in this report. As discussed in Section 6.2.1.2, the abstraction of the THC Seepage Model through time for TSPA-LA is examined in another model report by BSC (2003 [161963]).

6.2.3 Mathematical Model

The mathematical formulations that underlie the THC Seepage Model are described in detail in BSC (2003 [162050], Section 6.4). The spatial abstraction methodology described in Section 6.2.1.1 was implemented using CUTCHEM V1.0 (LBNL 2002 [161127]), with further information on point selection provided in Section 6.2.1.1 and in the qualification documentation for this software (LBNL 2002 [161127]). Data manipulation was implemented using MS Excel97, using standard functions to calculate summary statistics and sort, filter, and plot the extracted data (Attachment II).

The following summary statistics were computed with the data: average, minimum, maximum, and standard deviation. These statistics were computed on log-transformed data, except for pH, because predicted concentrations (and concentration ratios) vary over several orders of magnitude. Also, the chemical potential that drives reactions is a logarithmic function of concentration. As a result, distributions of these concentrations are closer to log-normal than normal. Because pH is itself a function of the logarithm of the hydrogen ion (more precisely activity), this model output variable was not log-transformed.

6.2.4 Abstraction of Aqueous Species and CO₂ Predicted Concentrations

In this section, abstraction methods discussed in Sections 6.2.1 and 6.2.2 are applied to results of the THC Seepage Model simulations reported in BSC (2003 [162050], Section 6.8.5). These simulations cover a range of input data and alternative conceptualizations, as follows:

- Five different input initial water compositions (BSC 2003 [162050], Section 6.2.2.1): W0, the base-case composition, and alternative compositions W4 through W7 (Attachment III).
- Three different infiltration scenarios (using water W0): stepwise increase from 6 to 25 mm/yr, fixed 6 mm/yr, and fixed 25 mm/yr (BSC 2003 [162050], Table 6.8-2)
- Two different water vapor-pressure models implemented in TOUGHREACT V3.0 (LBNL 2002 [161256], modules EOS4 and EOS3): respectively with and without vapor-pressure lowering due to capillary pressure (simulations using water W0).
- Two values of CO₂ diffusion coefficient (using water W0) resulting in a difference in the CO₂ gas diffusion coefficient by a factor of six.

For abstraction analyses, these simulations were consolidated into two different groups: Group 1, including the simulations using the five different input water compositions (W0, W4, W5, W6, and W7), and Group 2, including only runs making use of water composition W0 (also a total of five simulations) (Table 6.2-1). Thus, Group-1 simulations reflect the spread of model results caused by the natural variability of water compositions in the repository units, whereas Group-2 simulations reflect the sensitivity of model results to other important input parameters and model conceptualizations (as listed above). The relative spread in model results is then evaluated as a function of time separately for Group 1 and Group 2 (Section 6.2.4.1). As discussed in Section 6.2.4.1, this spread is generally larger for Group 1 than for Group 2. For this reason, further spread analyses were carried out using only Group 1. These additional analyses include evaluating some of the model results as a function of drift-wall temperature and liquid saturation (Section 6.2.4.2).

Table 6.2-1. Tptpl THC Model REV02 Runs Used for Abstraction Analyses

Group Assignment (for summary statistics)	Input Water ^(a)	Infiltration Rate ^(b) (mm/yr)	Vapor Pressure Lowering ^(c)	CO ₂ Diffusion ^(d)	Run ID ^(e)	Source Data ^(f)
1 and 2	W0	Stepped 6/16/25	Yes	Higher	thc6_w0	LB0302DSCPTHCS.002 [161976]
1	W4	Stepped 6/16/25	Yes	Higher	thc6_w4	LB0302DSCPTHCS.002 [161976]
1	W5	Stepped 6/16/25	Yes	Higher	thc6_w5	LB0302DSCPTHCS.002 [161976]
1	W6	Stepped 6/16/25	Yes	Higher	thc6_w6	LB0302DSCPTHCS.002 [161976]
1	W7	Stepped 6/16/25	Yes	Higher	thc6_w7	LB0302DSCPTHCS.002 [161976]
2	W0	Stepped 6/16/25	No	Higher	thc6_w0e3	LB0307DSTTHCR2.002 [165541]
2	W0	Constant 6	Yes	Higher	thc6_w0a	LB0307DSTTHCR2.002 [165541]
2	W0	Constant 25	Yes	Higher	thc25_w0	LB0307DSTTHCR2.002 [165541]
2	W0	Stepped 6/16/25	Yes	Lower	thc6_w0b	LB0307DSTTHCR2.002 [165541]

NOTE: ^a Attachment III.

^b BSC (2003 [162050], Table 6.8-2)

^c TOUGHREACT V3.0 (LBNL 2002 [161256]) flow modules: EOS3 neglects vapor pressure lowering due to capillary pressure; EOS4 takes this effect into account.

^d Six-fold increase between runs labeled "Higher" and "Lower" due to input CO₂ molecular diameter of 1×10^{-10} m versus 2.5×10^{-10} m, respectively (see BSC 2003 [162050], Section 6.8.3).

^e THC Seepage Model simulations from BSC (2003 [162050], Section 6.8).

^f See Table 4.1-1 for source data files.

6.2.4.1 Spatial Abstraction as a Function of Time

Summary statistics (minimum, maximum, mean, and standard deviation) of extracted data were calculated (Sections 6.2.3) at each specific time for Group 1 and Group 2 simulation results. These data reflect 30 observations at each point in time (i.e., 5 runs \times 6 extracted data points indexed INDX=1–6). The standard deviations for Group 1 and Group 2 results are summarized in Tables 6.2-2 and 6.2-3.

The summary statistics for Group 1 are shown in Figures 6.2-4 through 6.2-20 in the form of "whisker" plots defining concentration profiles through time. In these figures, "whiskers" show minimum and maximum values tied with a vertical line, superposed with a wide bar representing two standard deviations centered on the mean. The mean is itself represented by a symbol (filled circle). These "whiskers" are superposed with lines representing minimum, maximum, and mean concentrations for waters assigned to the same specific INDX value (INDX=5 for HISAT waters, and INDX=4 for FRONT waters, as determined further below). FRONT and HISAT waters with these INDX values constitute subsets of the complete data sets (i.e., those including INDX 1 through 6) most representative of the complete set.

Note that, for convenience, Figures 6.2-4 through 6.2-20 do not display data for all simulated points in time. These data are displayed for the times shown on Tables 6.2-2 and 6.2-3, with points omitted at 150 years. The figures capture the general character of the data, although in some instances data for times not shown in these figures may display a somewhat larger scatter (mostly in the period between 50 and 100 years). Profiles as functions of temperature and liquid saturation discussed later (and excluding summary statistics) include data for all points in time (Section 6.2.4.2).

Table 6.2-2. Standard Deviations in Water and Gas Compositions Predicted in Zones of High Liquid Saturation above the Drift Crown (HISAT – TOP, Fractures)

Time (yr)	pH			Calcium			Magnesium			Sodium			Chloride		
	Grp 1	Grp 2	Grp 1+2	Grp 1	Grp 2	Grp 1+2	Grp 1	Grp 2	Grp 1+2	Grp 1	Grp 2	Grp 1+2	Grp 1	Grp 2	Grp 1+2
0	0.11	0.00	0.11	0.11	0.00	0.11	0.52	0.00	0.52	0.18	0.00	0.18	0.29	0.00	0.29
53	0.14	0.17	0.22	0.15	0.09	0.17	0.82	0.30	0.87	0.25	0.20	0.32	0.37	0.20	0.42
100	0.13	0.18	0.23	0.04	0.04	0.06	0.23	0.27	0.36	0.11	0.12	0.17	0.31	0.12	0.33
150	0.15	0.23	0.27	0.07	0.37	0.38	0.20	0.84	0.86	0.08	0.42	0.43	0.31	0.49	0.58
200	0.09	0.21	0.23	0.23	0.29	0.37	0.38	0.62	0.73	0.16	0.30	0.34	0.40	0.36	0.54
300	0.10	0.14	0.17	0.40	0.31	0.51	0.35	0.40	0.53	0.26	0.29	0.39	0.46	0.33	0.57
400	0.11	0.12	0.16	0.35	0.31	0.47	0.38	0.40	0.55	0.24	0.27	0.36	0.40	0.31	0.51
500	0.15	0.14	0.21	0.41	0.35	0.54	0.49	0.47	0.68	0.29	0.28	0.41	0.44	0.34	0.56
600	0.17	0.14	0.22	0.42	0.36	0.55	0.47	0.48	0.67	0.26	0.28	0.38	0.40	0.33	0.52
800	0.10	0.15	0.18	0.20	0.32	0.38	0.28	0.27	0.39	0.12	0.14	0.19	0.30	0.17	0.34
1,000	0.09	0.09	0.12	0.16	0.08	0.18	0.23	0.12	0.26	0.10	0.06	0.11	0.29	0.07	0.30
1,200	0.09	0.08	0.12	0.15	0.05	0.16	0.22	0.09	0.24	0.09	0.03	0.09	0.29	0.04	0.29
1,400	0.08	0.06	0.10	0.17	0.03	0.17	0.19	0.06	0.20	0.08	0.01	0.08	0.29	0.02	0.29
1,600	0.07	0.05	0.09	0.16	0.03	0.16	0.18	0.05	0.19	0.08	0.01	0.08	0.29	0.01	0.29
1,800	0.06	0.04	0.07	0.13	0.07	0.15	0.15	0.07	0.16	0.06	0.01	0.06	0.23	0.00	0.23
2,000	0.08	0.04	0.08	0.18	0.02	0.18	0.19	0.04	0.20	0.08	0.02	0.09	0.32	0.04	0.32
2,200	0.06	0.07	0.09	0.18	0.09	0.20	0.17	0.12	0.21	0.06	0.03	0.07	0.29	0.05	0.29
2,400	0.06	0.07	0.09	0.18	0.12	0.22	0.17	0.11	0.20	0.06	0.02	0.06	0.29	0.05	0.29
5,000	0.05	0.06	0.08	0.14	0.08	0.16	0.14	0.07	0.16	0.06	0.02	0.06	0.29	0.01	0.29
7,000	0.05	0.04	0.06	0.14	0.07	0.15	0.12	0.10	0.16	0.06	0.02	0.06	0.29	0.00	0.29
10,000	0.03	0.03	0.05	0.14	0.09	0.16	0.10	0.12	0.16	0.06	0.03	0.06	0.29	0.00	0.29
20,000	0.04	0.04	0.06	0.14	0.05	0.15	0.11	0.10	0.15	0.06	0.02	0.06	0.29	0.00	0.29
50,000	0.05	0.09	0.10	0.14	0.02	0.14	0.09	0.12	0.15	0.05	0.03	0.06	0.29	0.00	0.29
100,000	0.03	0.13	0.14	0.13	0.01	0.13	0.08	0.18	0.20	0.05	0.04	0.06	0.29	0.00	0.29
Interval (yr)	Grp 1	Grp 2	Grp 1+2	Grp 1	Grp 2	Grp 1+2	Grp 1	Grp 2	Grp 1+2	Grp 1	Grp 2	Grp 1+2	Grp 1	Grp 2	Grp 1+2
0 – 100,000	0.09	0.10	0.14	0.19	0.14	0.24	0.26	0.23	0.37	0.12	0.11	0.17	0.32	0.12	0.36
150 – 600	0.13	0.16	0.21	0.31	0.33	0.47	0.38	0.53	0.67	0.22	0.31	0.39	0.40	0.36	0.54
600 – 2,000	0.09	0.08	0.12	0.20	0.12	0.24	0.24	0.15	0.29	0.11	0.07	0.13	0.30	0.09	0.32
2,000 – 100,000	0.05	0.06	0.08	0.15	0.06	0.17	0.13	0.11	0.18	0.06	0.03	0.07	0.29	0.02	0.29
Maximum	0.17	0.23	0.27	0.42	0.37	0.55	0.82	0.84	0.87	0.29	0.42	0.43	0.46	0.49	0.58

Table 6.2-2. Standard Deviations in Water and Gas Compositions Predicted in Zones of High Liquid Saturation above the Drift Crown (HISAT – TOP, Fractures) (Continued)

Time (yr)	Silica			Carbonate			Sulfate			Potassium			Fluoride		
	Grp 1	Grp 2	Grp 1+2	Grp 1	Grp 2	Grp 1+2	Grp 1	Grp 2	Grp 1+2	Grp 1	Grp 2	Grp 1+2	Grp 1	Grp 2	Grp 1+2
0	0.08	0.00	0.08	0.14	0.00	0.14	0.37	0.00	0.37	0.06	0.00	0.06	0.30	0.00	0.30
53	0.20	0.18	0.27	0.22	0.15	0.26	0.44	0.20	0.49	0.24	0.19	0.31	0.25	0.19	0.31
100	0.06	0.05	0.08	0.16	0.20	0.26	0.39	0.12	0.40	0.11	0.12	0.17	0.08	0.05	0.10
150	0.05	0.21	0.22	0.20	0.23	0.31	0.38	0.48	0.62	0.08	0.43	0.44	0.07	0.11	0.13
200	0.14	0.16	0.21	0.23	0.23	0.32	0.46	0.36	0.58	0.16	0.31	0.35	0.12	0.10	0.16
300	0.19	0.20	0.28	0.30	0.11	0.32	0.51	0.33	0.61	0.27	0.30	0.40	0.18	0.07	0.19
400	0.16	0.18	0.24	0.22	0.09	0.24	0.44	0.30	0.54	0.24	0.28	0.37	0.13	0.08	0.15
500	0.17	0.15	0.23	0.13	0.07	0.15	0.51	0.35	0.62	0.29	0.29	0.41	0.12	0.06	0.13
600	0.16	0.14	0.21	0.13	0.11	0.17	0.45	0.35	0.57	0.27	0.29	0.39	0.13	0.06	0.14
800	0.04	0.10	0.10	0.07	0.12	0.14	0.37	0.24	0.45	0.12	0.15	0.19	0.07	0.10	0.12
1,000	0.02	0.05	0.06	0.06	0.11	0.12	0.37	0.08	0.38	0.10	0.06	0.12	0.05	0.05	0.07
1,200	0.02	0.04	0.05	0.08	0.09	0.12	0.37	0.04	0.37	0.09	0.03	0.09	0.04	0.05	0.06
1,400	0.02	0.04	0.04	0.07	0.08	0.11	0.37	0.02	0.37	0.08	0.02	0.08	0.05	0.04	0.06
1,600	0.01	0.04	0.04	0.07	0.06	0.09	0.37	0.01	0.37	0.08	0.01	0.08	0.06	0.03	0.06
1,800	0.01	0.03	0.03	0.06	0.04	0.07	0.28	0.05	0.28	0.06	0.01	0.06	0.05	0.06	0.08
2,000	0.01	0.03	0.03	0.07	0.04	0.08	0.38	0.02	0.38	0.08	0.02	0.09	0.07	0.04	0.08
2,200	0.02	0.07	0.07	0.08	0.07	0.10	0.37	0.05	0.38	0.07	0.04	0.08	0.07	0.05	0.09
2,400	0.02	0.06	0.07	0.07	0.06	0.09	0.37	0.05	0.37	0.07	0.02	0.07	0.07	0.06	0.09
5,000	0.01	0.02	0.02	0.07	0.04	0.08	0.37	0.01	0.37	0.07	0.02	0.07	0.06	0.04	0.07
7,000	0.01	0.02	0.02	0.08	0.08	0.11	0.37	0.00	0.37	0.06	0.02	0.07	0.05	0.03	0.06
10,000	0.01	0.02	0.02	0.08	0.13	0.15	0.37	0.00	0.37	0.06	0.01	0.06	0.05	0.04	0.07
20,000	0.01	0.02	0.02	0.09	0.07	0.12	0.37	0.00	0.37	0.06	0.02	0.06	0.06	0.02	0.06
50,000	0.02	0.04	0.04	0.10	0.07	0.12	0.37	0.00	0.37	0.05	0.05	0.07	0.06	0.01	0.06
100,000	0.02	0.05	0.06	0.10	0.08	0.13	0.37	0.00	0.37	0.05	0.05	0.07	0.05	0.01	0.05
Interval (yr)	Grp 1	Grp 2	Grp 1+2	Grp 1	Grp 2	Grp 1+2	Grp 1	Grp 2	Grp 1+2	Grp 1	Grp 2	Grp 1+2	Grp 1	Grp 2	Grp 1+2
0 – 100,000	0.06	0.08	0.10	0.12	0.10	0.16	0.39	0.13	0.43	0.12	0.11	0.17	0.09	0.06	0.11
150 – 600	0.15	0.18	0.23	0.20	0.14	0.25	0.46	0.36	0.59	0.22	0.32	0.39	0.13	0.08	0.15
600 – 2,000	0.04	0.06	0.07	0.08	0.08	0.11	0.37	0.10	0.40	0.11	0.07	0.14	0.06	0.05	0.09
2,000 – 100,000	0.01	0.04	0.04	0.08	0.07	0.11	0.37	0.02	0.37	0.06	0.03	0.07	0.06	0.03	0.07
Maximum	0.20	0.21	0.28	0.30	0.23	0.32	0.51	0.48	0.62	0.29	0.43	0.44	0.30	0.19	0.31

Table 6.2-2. Standard Deviations in Water and Gas Compositions Predicted in Zones of High Liquid Saturation above the Drift Crown (HISAT – TOP, Fractures) (Continued)

Time (yr)	Nitrate			CO ₂ (gas)			Ca/Na			NO ₃ /Cl			HCO ₃ /Cl		
	Grp 1	Grp 2	Grp 1+2	Grp 1	Grp 2	Grp 1+2	Grp 1	Grp 2	Grp 1+2	Grp 1	Grp 2	Grp 1+2	Grp 1	Grp 2	Grp 1+2
0	0.27	0.00	0.27	0.23	0.00	0.23	0.25	0.00	0.25	0.38	0.00	0.38	0.40	0.00	0.40
53	0.35	0.20	0.41	0.32	0.30	0.44	0.30	0.12	0.32	0.38	0.00	0.38	0.44	0.15	0.46
100	0.30	0.12	0.32	0.29	0.39	0.49	0.11	0.12	0.16	0.38	0.00	0.38	0.43	0.21	0.48
150	0.28	0.49	0.57	0.35	0.42	0.55	0.11	0.13	0.17	0.38	0.00	0.38	0.48	0.57	0.75
200	0.33	0.36	0.49	0.32	0.42	0.53	0.23	0.09	0.24	0.38	0.00	0.38	0.58	0.45	0.74
300	0.42	0.33	0.54	0.34	0.19	0.39	0.31	0.10	0.33	0.37	0.01	0.37	0.70	0.39	0.80
400	0.40	0.31	0.51	0.25	0.14	0.29	0.18	0.16	0.24	0.37	0.01	0.37	0.58	0.36	0.68
500	0.39	0.34	0.52	0.13	0.11	0.17	0.18	0.12	0.21	0.37	0.01	0.37	0.54	0.39	0.67
600	0.41	0.33	0.52	0.08	0.13	0.15	0.25	0.10	0.27	0.38	0.01	0.38	0.50	0.41	0.65
800	0.28	0.18	0.33	0.07	0.16	0.17	0.12	0.24	0.27	0.38	0.00	0.38	0.35	0.26	0.44
1,000	0.27	0.08	0.29	0.03	0.18	0.18	0.08	0.06	0.10	0.38	0.00	0.38	0.35	0.13	0.37
1,200	0.27	0.04	0.28	0.01	0.16	0.16	0.07	0.04	0.08	0.38	0.00	0.38	0.37	0.10	0.38
1,400	0.27	0.02	0.27	0.01	0.13	0.13	0.09	0.03	0.10	0.38	0.00	0.38	0.36	0.08	0.37
1,600	0.27	0.01	0.27	0.01	0.10	0.10	0.08	0.03	0.09	0.38	0.00	0.38	0.35	0.06	0.36
1,800	0.33	0.00	0.33	0.01	0.07	0.07	0.08	0.07	0.10	0.38	0.00	0.38	0.28	0.04	0.28
2,000	0.28	0.05	0.28	0.01	0.06	0.06	0.09	0.04	0.10	0.38	0.00	0.38	0.39	0.06	0.39
2,200	0.27	0.05	0.28	0.03	0.11	0.12	0.12	0.07	0.14	0.38	0.00	0.38	0.36	0.09	0.38
2,400	0.27	0.05	0.28	0.02	0.09	0.09	0.12	0.11	0.16	0.38	0.00	0.38	0.36	0.09	0.37
5,000	0.27	0.01	0.27	0.04	0.05	0.06	0.08	0.10	0.12	0.38	0.00	0.38	0.36	0.04	0.36
7,000	0.27	0.00	0.27	0.06	0.08	0.10	0.08	0.06	0.10	0.38	0.00	0.38	0.36	0.08	0.37
10,000	0.27	0.00	0.27	0.08	0.15	0.17	0.08	0.06	0.10	0.38	0.00	0.38	0.35	0.13	0.37
20,000	0.27	0.00	0.27	0.12	0.10	0.15	0.08	0.03	0.09	0.38	0.00	0.38	0.35	0.07	0.36
50,000	0.27	0.00	0.27	0.12	0.16	0.20	0.09	0.04	0.10	0.38	0.00	0.38	0.36	0.07	0.37
100,000	0.27	0.00	0.27	0.11	0.22	0.24	0.08	0.04	0.09	0.38	0.00	0.38	0.37	0.08	0.37
Interval (yr)	Grp 1	Grp 2	Grp 1+2	Grp 1	Grp 2	Grp 1+2	Grp 1	Grp 2	Grp 1+2	Grp 1	Grp 2	Grp 1+2	Grp 1	Grp 2	Grp 1+2
0 – 100,000	0.31	0.12	0.35	0.13	0.16	0.22	0.14	0.08	0.16	0.38	0.00	0.38	0.42	0.18	0.47
150 – 600	0.37	0.36	0.52	0.24	0.24	0.35	0.21	0.12	0.24	0.37	0.01	0.37	0.56	0.43	0.71
600 – 2,000	0.30	0.09	0.32	0.03	0.12	0.13	0.11	0.08	0.14	0.38	0.00	0.38	0.37	0.14	0.41
2,000 – 100,000	0.27	0.02	0.28	0.07	0.11	0.13	0.09	0.06	0.11	0.38	0.00	0.38	0.36	0.08	0.37
Maximum	0.42	0.49	0.57	0.35	0.42	0.55	0.31	0.24	0.33	0.38	0.01	0.38	0.70	0.57	0.80

Table 6.2-2. Standard Deviations in Water and Gas Compositions Predicted in Zones of High Liquid Saturation above the Drift Crown (HISAT – TOP, Fractures) (Continued)

Time (yr)	SO4/Cl			Na/Cl			Ca/CO3			Ca/Cl		
	Grp 1	Grp 2	Grp 1+2	Grp 1	Grp 2	Grp 1+2	Grp 1	Grp 2	Grp 1+2	Grp 1	Grp 2	Grp 1+2
0	0.22	0.00	0.22	0.36	0.00	0.36	0.19	0.00	0.19	0.24	0.00	0.24
53	0.22	0.00	0.22	0.27	0.01	0.27	0.33	0.08	0.34	0.31	0.12	0.33
100	0.22	0.02	0.22	0.29	0.03	0.29	0.19	0.23	0.30	0.27	0.11	0.29
150	0.22	0.01	0.22	0.30	0.09	0.32	0.27	0.49	0.56	0.24	0.15	0.28
200	0.22	0.01	0.22	0.32	0.08	0.33	0.45	0.41	0.60	0.21	0.10	0.23
300	0.22	0.00	0.22	0.28	0.07	0.29	0.68	0.36	0.77	0.19	0.06	0.20
400	0.22	0.03	0.22	0.19	0.08	0.21	0.53	0.36	0.64	0.12	0.09	0.15
500	0.22	0.03	0.22	0.17	0.07	0.19	0.51	0.41	0.65	0.11	0.07	0.13
600	0.22	0.06	0.22	0.16	0.06	0.17	0.54	0.45	0.70	0.17	0.05	0.18
800	0.22	0.13	0.25	0.18	0.04	0.18	0.27	0.41	0.49	0.14	0.22	0.26
1,000	0.22	0.01	0.22	0.20	0.02	0.20	0.22	0.11	0.25	0.15	0.06	0.16
1,200	0.22	0.01	0.22	0.21	0.01	0.21	0.23	0.10	0.25	0.15	0.04	0.15
1,400	0.22	0.00	0.22	0.21	0.01	0.21	0.24	0.09	0.26	0.13	0.02	0.13
1,600	0.22	0.00	0.22	0.22	0.01	0.22	0.23	0.08	0.24	0.13	0.03	0.14
1,800	0.22	0.04	0.22	0.17	0.01	0.17	0.19	0.09	0.21	0.11	0.07	0.13
2,000	0.22	0.03	0.22	0.23	0.02	0.24	0.25	0.04	0.25	0.15	0.05	0.16
2,200	0.22	0.01	0.22	0.23	0.03	0.23	0.26	0.14	0.29	0.12	0.05	0.13
2,400	0.22	0.00	0.22	0.23	0.04	0.23	0.25	0.16	0.30	0.12	0.08	0.15
5,000	0.22	0.00	0.22	0.23	0.02	0.23	0.21	0.10	0.23	0.15	0.08	0.17
7,000	0.22	0.00	0.22	0.24	0.02	0.24	0.19	0.05	0.20	0.18	0.07	0.19
10,000	0.22	0.00	0.22	0.25	0.03	0.25	0.17	0.05	0.17	0.20	0.09	0.22
20,000	0.22	0.00	0.22	0.26	0.02	0.26	0.15	0.03	0.15	0.22	0.05	0.23
50,000	0.22	0.00	0.22	0.26	0.03	0.27	0.15	0.07	0.17	0.24	0.02	0.24
100,000	0.22	0.00	0.22	0.26	0.04	0.27	0.15	0.08	0.17	0.24	0.01	0.24
Interval (yr)	Grp 1	Grp 2	Grp 1+2	Grp 1	Grp 2	Grp 1+2	Grp 1	Grp 2	Grp 1+2	Grp 1	Grp 2	Grp 1+2
0 – 100,000	0.22	0.02	0.22	0.24	0.03	0.24	0.28	0.18	0.35	0.18	0.07	0.20
150 – 600	0.22	0.02	0.22	0.24	0.08	0.25	0.49	0.41	0.65	0.17	0.09	0.19
600 – 2,000	0.22	0.03	0.23	0.20	0.02	0.20	0.27	0.17	0.33	0.14	0.07	0.16
2,000 – 100,000	0.22	0.01	0.22	0.24	0.03	0.25	0.20	0.08	0.21	0.18	0.05	0.19
Maximum	0.22	0.13	0.25	0.36	0.09	0.36	0.68	0.49	0.77	0.31	0.22	0.33

Input DTN: LB0302DSCPTHCS.002 [161976]

LB0307DSTTHCR2.002 [165541]

Output-DTN: LB0311ABSTHCR2.001

NOTES: Standard deviation values are shown for two sets of simulation results (Grp 1 and Grp 2) and their combined effect (Grp 1+2):

- Runs using input water compositions W0, W4, W5, W6, and W7 (Grp 1 column)
- Runs using input water composition (W0) and different conceptualization and ranges of input data (Grp 2 column) (stepped up infiltration rate 6-16-25 mm/yr, constant 6 mm/year, constant 25 mm/yr, with and without vapor pressure lowering, and with 6-times difference in CO₂ diffusion coefficient – see BSC 2003 [162050] Section 6.8).
- Combined standard deviation (SD) as $SD_{(Grp\ 1+2)} = (SD_{(Grp\ 1)}^2 + SD_{(Grp\ 2)}^2)^{0.5}$ (Grp 1+2 column)

Standard deviation values and units are as follows:

- For pH, standard deviation in (+) pH units
- For other data, standard deviation of logarithmic values of total molality for aqueous species, volume fraction for CO₂, and unitless molal ratios, thus representing a (+) change in log₁₀ values of concentrations and concentration ratios around the mean of log₁₀ values (e.g., 0.5 corresponds to total spread of one order of magnitude)

The bottom of the table shows averages of individual standard deviations over the time intervals shown.

See Attachment II for analyses.

Table 6.2-3. Standard Deviations in Water and Gas Compositions Predicted at the Boiling/Wetting Front in Fractures above the Drift Crown (FRONT-TOP, Fractures)

Time (yr)	pH			Calcium			Magnesium			Sodium			Chloride		
	Grp 1	Grp 2	Grp 1+2	Grp 1	Grp 2	Grp 1+2	Grp 1	Grp 2	Grp 1+2	Grp 1	Grp 2	Grp 1+2	Grp 1	Grp 2	Grp 1+2
0	0.11	0.00	0.11	0.11	0.00	0.11	0.52	0.00	0.52	0.18	0.00	0.18	0.29	0.00	0.29
53	0.34	0.19	0.39	0.72	0.48	0.86	0.70	0.51	0.87	0.88	0.76	1.16	0.92	0.76	1.20
100	0.06	0.14	0.15	0.22	0.26	0.34	0.25	0.36	0.44	0.24	0.34	0.42	0.37	0.36	0.52
150	0.08	0.26	0.27	0.26	0.43	0.50	0.34	0.90	0.96	0.33	0.49	0.59	0.48	0.54	0.73
200	0.06	0.20	0.21	0.27	0.22	0.35	0.26	0.50	0.56	0.12	0.25	0.27	0.37	0.28	0.46
300	0.10	0.12	0.16	0.46	0.33	0.56	0.37	0.38	0.52	0.26	0.31	0.41	0.45	0.34	0.57
400	0.14	0.14	0.19	0.44	0.40	0.60	0.49	0.49	0.70	0.32	0.39	0.51	0.46	0.42	0.62
500	0.17	0.16	0.24	0.44	0.46	0.63	0.54	0.53	0.76	0.35	0.44	0.56	0.45	0.48	0.66
600	0.20	0.19	0.27	0.48	0.50	0.70	0.55	0.59	0.81	0.35	0.45	0.57	0.45	0.51	0.68
800	0.10	0.16	0.19	0.20	0.34	0.40	0.28	0.33	0.43	0.12	0.17	0.21	0.30	0.21	0.36
1,000	0.08	0.08	0.12	0.16	0.08	0.18	0.22	0.12	0.26	0.10	0.06	0.11	0.29	0.07	0.30
1,200	0.09	0.08	0.12	0.15	0.05	0.16	0.21	0.09	0.23	0.08	0.03	0.09	0.29	0.03	0.29
1,400	0.08	0.06	0.10	0.17	0.03	0.17	0.19	0.06	0.20	0.08	0.01	0.08	0.29	0.02	0.29
1,600	0.07	0.12	0.14	0.16	0.36	0.39	0.18	0.05	0.19	0.08	0.30	0.31	0.29	0.36	0.46
1,800	0.17	0.04	0.17	0.56	0.07	0.57	0.44	0.07	0.44	0.53	0.01	0.53	0.62	0.01	0.62
2,000	0.24	0.28	0.37	0.63	0.80	1.02	0.49	0.68	0.84	0.43	0.51	0.67	0.48	0.61	0.78
2,200	0.06	0.08	0.10	0.13	0.09	0.16	0.15	0.14	0.20	0.06	0.04	0.07	0.23	0.06	0.24
2,400	0.06	0.13	0.14	0.15	0.34	0.37	0.17	0.12	0.20	0.07	0.27	0.28	0.28	0.32	0.42
5,000	0.06	0.06	0.08	0.15	0.08	0.17	0.15	0.07	0.17	0.07	0.02	0.07	0.29	0.01	0.29
7,000	0.04	0.10	0.11	0.14	0.07	0.16	0.15	0.10	0.18	0.07	0.02	0.07	0.30	0.00	0.30
10,000	0.03	0.11	0.11	0.14	0.09	0.16	0.14	0.13	0.19	0.06	0.03	0.07	0.30	0.00	0.30
20,000	0.04	0.24	0.24	0.14	0.05	0.15	0.13	0.11	0.17	0.06	0.02	0.06	0.30	0.00	0.30
50,000	0.04	0.21	0.21	0.14	0.02	0.15	0.09	0.12	0.15	0.05	0.03	0.06	0.29	0.00	0.29
100,000	0.02	0.21	0.21	0.13	0.01	0.13	0.08	0.18	0.20	0.05	0.04	0.06	0.29	0.00	0.29
Interval (yr)	Grp 1	Grp 2	Grp 1+2	Grp 1	Grp 2	Grp 1+2	Grp 1	Grp 2	Grp 1+2	Grp 1	Grp 2	Grp 1+2	Grp 1	Grp 2	Grp 1+2
0 – 100,000	0.10	0.14	0.18	0.27	0.23	0.37	0.30	0.28	0.42	0.21	0.21	0.31	0.38	0.23	0.47
150 – 600	0.12	0.18	0.22	0.39	0.39	0.56	0.42	0.56	0.72	0.29	0.39	0.48	0.44	0.43	0.62
600 – 2,000	0.13	0.13	0.19	0.31	0.28	0.45	0.32	0.25	0.43	0.22	0.19	0.32	0.38	0.23	0.47
2,000 – 100,000	0.07	0.16	0.18	0.20	0.17	0.27	0.17	0.18	0.26	0.10	0.11	0.16	0.31	0.11	0.36
Maximum	0.34	0.28	0.39	0.72	0.80	1.02	0.70	0.90	0.96	0.88	0.76	1.16	0.92	0.76	1.20

Table 6.2-3. Standard Deviations in Water and Gas Compositions Predicted at the Boiling/Wetting Front in Fractures above the Drift Crown (FRONT-TOP, Fractures) (Continued)

Time (yr)	Silica			Carbonate			Sulfate			Potassium			Fluoride		
	Grp 1	Grp 2	Grp 1+2	Grp 1	Grp 2	Grp 1+2	Grp 1	Grp 2	Grp 1+2	Grp 1	Grp 2	Grp 1+2	Grp 1	Grp 2	Grp 1+2
0	0.08	0.00	0.08	0.14	0.00	0.14	0.37	0.00	0.37	0.06	0.00	0.06	0.30	0.00	0.30
53	0.88	0.76	1.16	0.58	0.09	0.59	0.95	0.76	1.22	0.88	0.77	1.17	0.87	0.62	1.07
100	0.26	0.32	0.42	0.25	0.18	0.31	0.45	0.36	0.57	0.24	0.35	0.42	0.23	0.20	0.30
150	0.27	0.27	0.38	0.26	0.24	0.35	0.51	0.51	0.72	0.39	0.50	0.63	0.26	0.15	0.30
200	0.10	0.15	0.18	0.25	0.21	0.33	0.42	0.28	0.50	0.12	0.25	0.28	0.11	0.11	0.16
300	0.18	0.24	0.30	0.32	0.13	0.34	0.49	0.35	0.60	0.26	0.32	0.41	0.19	0.08	0.21
400	0.20	0.27	0.34	0.23	0.12	0.26	0.49	0.40	0.63	0.33	0.40	0.52	0.15	0.06	0.16
500	0.21	0.31	0.37	0.12	0.09	0.16	0.49	0.44	0.66	0.35	0.45	0.57	0.15	0.06	0.17
600	0.20	0.31	0.37	0.14	0.11	0.18	0.48	0.46	0.67	0.35	0.46	0.58	0.16	0.05	0.17
800	0.04	0.11	0.12	0.07	0.12	0.14	0.37	0.27	0.46	0.12	0.18	0.22	0.07	0.10	0.12
1,000	0.02	0.05	0.06	0.06	0.11	0.12	0.37	0.08	0.38	0.10	0.06	0.12	0.05	0.05	0.07
1,200	0.02	0.04	0.05	0.08	0.09	0.12	0.37	0.04	0.37	0.08	0.03	0.09	0.04	0.05	0.06
1,400	0.02	0.04	0.04	0.07	0.08	0.11	0.37	0.02	0.37	0.08	0.02	0.08	0.05	0.04	0.06
1,600	0.01	0.04	0.04	0.07	0.08	0.11	0.37	0.28	0.46	0.08	0.27	0.28	0.06	0.05	0.07
1,800	0.12	0.03	0.12	0.15	0.04	0.16	0.67	0.04	0.67	0.58	0.01	0.58	0.14	0.06	0.16
2,000	0.07	0.29	0.30	0.19	0.26	0.32	0.58	0.65	0.87	0.45	0.50	0.67	0.16	0.22	0.27
2,200	0.02	0.07	0.08	0.06	0.07	0.09	0.29	0.06	0.29	0.06	0.04	0.07	0.05	0.05	0.07
2,400	0.02	0.06	0.06	0.06	0.08	0.10	0.36	0.28	0.45	0.07	0.26	0.27	0.06	0.06	0.08
5,000	0.01	0.02	0.02	0.06	0.04	0.07	0.37	0.00	0.37	0.07	0.02	0.07	0.06	0.04	0.07
7,000	0.00	0.02	0.02	0.07	0.08	0.11	0.38	0.00	0.38	0.07	0.02	0.07	0.06	0.03	0.07
10,000	0.01	0.02	0.02	0.07	0.13	0.15	0.38	0.00	0.38	0.06	0.01	0.07	0.05	0.04	0.07
20,000	0.01	0.02	0.02	0.09	0.07	0.11	0.38	0.00	0.38	0.06	0.02	0.06	0.05	0.03	0.06
50,000	0.02	0.03	0.04	0.10	0.07	0.12	0.37	0.00	0.37	0.05	0.05	0.07	0.06	0.01	0.06
100,000	0.02	0.05	0.06	0.10	0.08	0.13	0.37	0.00	0.37	0.05	0.05	0.07	0.05	0.01	0.05
Interval (yr)	Grp 1	Grp 2	Grp 1+2	Grp 1	Grp 2	Grp 1+2	Grp 1	Grp 2	Grp 1+2	Grp 1	Grp 2	Grp 1+2	Grp 1	Grp 2	Grp 1+2
0 – 100,000	0.12	0.15	0.19	0.15	0.11	0.19	0.44	0.22	0.52	0.21	0.21	0.31	0.14	0.09	0.17
150 – 600	0.19	0.26	0.32	0.22	0.15	0.27	0.48	0.41	0.63	0.30	0.40	0.50	0.17	0.08	0.19
600 – 2,000	0.06	0.11	0.14	0.10	0.11	0.16	0.45	0.23	0.53	0.23	0.19	0.33	0.09	0.08	0.12
2,000 – 100,000	0.02	0.06	0.07	0.09	0.10	0.13	0.39	0.11	0.43	0.10	0.11	0.16	0.07	0.05	0.09
Maximum	0.88	0.76	1.16	0.58	0.26	0.59	0.95	0.76	1.22	0.88	0.77	1.17	0.87	0.62	1.07

Table 6.2-3. Standard Deviations in Water and Gas Compositions Predicted at the Boiling/Wetting Front in Fractures above the Drift Crown (FRONT-TOP, Fractures) (Continued)

Time (yr)	Nitrate			CO ₂ (gas)			Ca/Na			NO ₃ /Cl			HCO ₃ /Cl		
	Grp 1	Grp 2	Grp 1+2	Grp 1	Grp 2	Grp 1+2	Grp 1	Grp 2	Grp 1+2	Grp 1	Grp 2	Grp 1+2	Grp 1	Grp 2	Grp 1+2
0	0.27	0.00	0.27	0.23	0.00	0.23	0.25	0.00	0.25	0.38	0.00	0.38	0.40	0.00	0.40
53	0.92	0.76	1.19	0.28	0.19	0.34	1.28	0.29	1.31	0.38	0.00	0.38	0.90	0.78	1.20
100	0.35	0.36	0.50	0.30	0.28	0.41	0.26	0.14	0.30	0.38	0.00	0.38	0.58	0.44	0.73
150	0.57	0.54	0.79	0.32	0.46	0.56	0.38	0.17	0.42	0.39	0.00	0.39	0.64	0.61	0.88
200	0.33	0.28	0.43	0.31	0.41	0.51	0.26	0.10	0.28	0.37	0.01	0.37	0.59	0.35	0.69
300	0.43	0.35	0.55	0.34	0.18	0.38	0.37	0.10	0.38	0.37	0.01	0.37	0.71	0.44	0.84
400	0.46	0.43	0.62	0.25	0.16	0.29	0.24	0.14	0.28	0.37	0.01	0.37	0.63	0.51	0.81
500	0.46	0.48	0.67	0.12	0.11	0.16	0.22	0.09	0.24	0.37	0.01	0.37	0.55	0.56	0.79
600	0.46	0.51	0.69	0.09	0.12	0.15	0.28	0.10	0.30	0.38	0.01	0.38	0.54	0.60	0.81
800	0.28	0.21	0.35	0.07	0.15	0.17	0.12	0.24	0.27	0.38	0.00	0.38	0.35	0.29	0.46
1,000	0.28	0.08	0.29	0.03	0.18	0.18	0.08	0.06	0.10	0.38	0.00	0.38	0.35	0.13	0.37
1,200	0.27	0.04	0.28	0.01	0.16	0.16	0.07	0.04	0.08	0.38	0.00	0.38	0.37	0.10	0.38
1,400	0.27	0.02	0.27	0.01	0.13	0.13	0.09	0.03	0.10	0.38	0.00	0.38	0.36	0.08	0.37
1,600	0.27	0.38	0.47	0.01	0.10	0.10	0.08	0.07	0.11	0.38	0.03	0.38	0.35	0.42	0.55
1,800	0.88	0.01	0.88	0.02	0.07	0.07	0.31	0.07	0.32	0.36	0.00	0.36	0.72	0.04	0.72
2,000	0.63	0.61	0.88	0.01	0.18	0.18	0.54	0.52	0.75	0.36	0.03	0.36	0.58	0.80	0.99
2,200	0.33	0.06	0.33	0.01	0.12	0.12	0.07	0.06	0.09	0.38	0.00	0.38	0.29	0.09	0.31
2,400	0.28	0.35	0.45	0.01	0.10	0.10	0.08	0.12	0.14	0.38	0.03	0.38	0.33	0.39	0.51
5,000	0.27	0.00	0.27	0.04	0.05	0.06	0.08	0.10	0.13	0.38	0.00	0.38	0.35	0.04	0.35
7,000	0.27	0.00	0.27	0.06	0.08	0.10	0.08	0.07	0.10	0.38	0.00	0.38	0.35	0.08	0.36
10,000	0.27	0.00	0.27	0.08	0.15	0.17	0.07	0.07	0.10	0.38	0.00	0.38	0.35	0.13	0.37
20,000	0.27	0.00	0.27	0.12	0.10	0.16	0.08	0.04	0.09	0.38	0.00	0.38	0.35	0.07	0.36
50,000	0.27	0.00	0.27	0.12	0.16	0.19	0.09	0.04	0.10	0.38	0.00	0.38	0.37	0.07	0.37
100,000	0.27	0.00	0.27	0.12	0.22	0.25	0.08	0.04	0.09	0.38	0.00	0.38	0.37	0.08	0.38
Interval (yr)	Grp 1	Grp 2	Grp 1+2	Grp 1	Grp 2	Grp 1+2	Grp 1	Grp 2	Grp 1+2	Grp 1	Grp 2	Grp 1+2	Grp 1	Grp 2	Grp 1+2
0 – 100,000	0.39	0.23	0.48	0.12	0.16	0.22	0.23	0.11	0.26	0.38	0.01	0.38	0.47	0.30	0.58
150 – 600	0.45	0.43	0.63	0.24	0.24	0.34	0.29	0.12	0.32	0.38	0.01	0.38	0.61	0.51	0.80
600 – 2,000	0.42	0.23	0.51	0.03	0.14	0.14	0.20	0.14	0.25	0.37	0.01	0.37	0.45	0.31	0.58
2,000 – 100,000	0.32	0.12	0.37	0.06	0.13	0.15	0.13	0.11	0.18	0.38	0.01	0.38	0.37	0.19	0.44
Maximum	0.92	0.76	1.19	0.34	0.46	0.56	1.28	0.52	1.31	0.39	0.03	0.39	0.90	0.80	1.20

Table 6.2-3. Standard Deviations in Water and Gas Compositions Predicted at the Boiling/Wetting Front in Fractures Above the Drift Crown (FRONT-TOP, Fractures) (Continued)

Time (yr)	SO ₄ /Cl			Na/Cl			Ca/CO ₃			Ca/Cl		
	Grp 1	Grp 2	Grp 1+2	Grp 1	Grp 2	Grp 1+2	Grp 1	Grp 2	Grp 1+2	Grp 1	Grp 2	Grp 1+2
0	0.22	0.00	0.22	0.36	0.00	0.36	0.19	0.00	0.19	0.24	0.00	0.24
53	0.22	0.00	0.22	0.27	0.01	0.27	1.28	0.50	1.37	1.19	0.29	1.22
100	0.22	0.01	0.22	0.30	0.04	0.30	0.46	0.38	0.59	0.21	0.14	0.25
150	0.21	0.04	0.21	0.31	0.11	0.32	0.51	0.54	0.74	0.36	0.15	0.39
200	0.22	0.01	0.22	0.32	0.07	0.32	0.51	0.33	0.61	0.15	0.08	0.17
300	0.22	0.00	0.22	0.27	0.06	0.28	0.76	0.42	0.86	0.21	0.05	0.22
400	0.22	0.06	0.23	0.18	0.08	0.20	0.63	0.50	0.80	0.15	0.08	0.17
500	0.22	0.10	0.24	0.14	0.07	0.16	0.54	0.54	0.76	0.16	0.06	0.17
600	0.22	0.11	0.24	0.14	0.07	0.16	0.60	0.60	0.85	0.21	0.07	0.22
800	0.22	0.13	0.25	0.18	0.04	0.19	0.26	0.43	0.51	0.14	0.22	0.26
1,000	0.22	0.01	0.22	0.20	0.02	0.20	0.22	0.11	0.25	0.14	0.06	0.16
1,200	0.22	0.01	0.22	0.21	0.01	0.21	0.23	0.10	0.25	0.15	0.04	0.15
1,400	0.22	0.00	0.22	0.21	0.01	0.21	0.24	0.09	0.26	0.13	0.02	0.13
1,600	0.22	0.08	0.23	0.22	0.06	0.22	0.22	0.43	0.48	0.13	0.03	0.14
1,800	0.34	0.04	0.34	0.16	0.01	0.16	0.69	0.09	0.70	0.31	0.07	0.31
2,000	0.39	0.20	0.44	0.12	0.14	0.19	0.81	1.05	1.32	0.50	0.42	0.65
2,200	0.22	0.01	0.22	0.17	0.03	0.17	0.19	0.12	0.23	0.11	0.04	0.12
2,400	0.22	0.04	0.22	0.21	0.06	0.21	0.20	0.41	0.45	0.13	0.07	0.15
5,000	0.22	0.00	0.22	0.22	0.02	0.23	0.20	0.11	0.23	0.15	0.08	0.17
7,000	0.22	0.00	0.22	0.24	0.02	0.24	0.19	0.06	0.20	0.17	0.07	0.19
10,000	0.22	0.00	0.22	0.25	0.03	0.25	0.16	0.06	0.17	0.20	0.09	0.22
20,000	0.22	0.00	0.22	0.26	0.02	0.26	0.15	0.02	0.15	0.22	0.05	0.23
50,000	0.22	0.00	0.22	0.27	0.03	0.27	0.16	0.06	0.17	0.23	0.02	0.23
100,000	0.22	0.00	0.22	0.27	0.04	0.27	0.16	0.08	0.18	0.23	0.01	0.23
Interval (yr)	Grp 1	Grp 2	Grp 1+2	Grp 1	Grp 2	Grp 1+2	Grp 1	Grp 2	Grp 1+2	Grp 1	Grp 2	Grp 1+2
0 – 100,000	0.23	0.04	0.24	0.23	0.04	0.23	0.40	0.29	0.51	0.24	0.09	0.27
150 – 600	0.22	0.05	0.23	0.23	0.08	0.24	0.59	0.49	0.77	0.21	0.08	0.22
600 – 2,000	0.26	0.07	0.27	0.18	0.05	0.19	0.41	0.36	0.58	0.21	0.11	0.25
2,000 – 100,000	0.24	0.03	0.24	0.22	0.04	0.23	0.25	0.22	0.34	0.22	0.09	0.24
Maximum	0.39	0.20	0.44	0.36	0.14	0.36	1.28	1.05	1.37	1.19	0.42	1.22

Input DTN: LB0302DSCPTHCS.002 [161976]
 LB0307DSTTHCR2.002 [165541]
 Output-DTN: LB0311ABSTHCR2.001

NOTE: Standard deviation values are shown for two sets of simulation results (Grp 1 and Grp 2) and their combined effect (Grp 1+2):

- Runs using input water compositions W0, W4, W5, W6, and W7 (Grp 1 column)
- Runs using input water composition (W0) and different conceptualization and ranges of input data (Grp 2 column) (stepped up infiltration rate 6-16-25 mm/yr, constant 6 mm/year, constant 25 mm/yr, with and without vapor pressure lowering, and with 6-times difference in CO₂ diffusion coefficient – see BSC 2003 [162050] Section 6.8).
- Combined standard deviation (SD) as $SD_{(Grp\ 1+2)} = (SD_{(Grp\ 1)}^2 + SD_{(Grp\ 2)}^2)^{0.5}$ (Grp 1+2 column)

Standard deviation values and units are given as follow:

- For pH, standard deviation in (+) pH units
- For other data, standard deviation of logarithmic values of total molality for aqueous species, volume fraction for CO₂, and unitless molal ratios; thus (+) change in log10 values of concentrations and concentration ratios around mean of log10 values (e.g., 0.5 corresponds to total spread of one order of magnitude)

The bottom of the table shows averages of individual standard deviations over the time intervals shown. See Attachment II for analyses.

6.2.4.1.1 Zone of Increased Liquid Saturation Above the Drift

Waters from this zone are those extracted with attributes HISAT and TOP from the fracture medium (Section 6.2.1.1). These waters represent the condensation zone above the drift during the time period when temperatures around the drift exceed the boiling point of water (boiling period). After the boiling period, these waters represent the zone of increased liquid saturation above the drift resulting from the diversion of percolating water by the drift opening and/or zones of lower permeability created by mineral precipitation during the boiling period (e.g., BSC 2003 [162050], Section 6.8.5.4).

The predicted compositions of HISAT-TOP waters in fractures, and associated CO₂ partial pressures, were analyzed in BSC (2003 [162050], Section 6.8.5.3). This preliminary analysis indicated that:

1. Runs using five different input water compositions (i.e., natural variability) (Group 1 runs) produced a spread in predicted water and gas compositions generally larger than the spread resulting from sensitivity analyses (Group 2 runs) using the same input water composition.
2. At any one point in time, the relative spread (expressed as two standard deviations) of predicted concentrations for Group 1 and Group 2 (separately) generally did not exceed an order of magnitude and was often much less.
3. Finally, for all analyzed simulations, the predicted general concentration trends were quite similar.

Standard deviations in concentrations of aqueous species and CO₂ gas in fractures predicted from Group 1 simulations are given in BSC (2003 [162050], Section 6.9.2). These deviations are more thoroughly compared here with those predicted for Group 2 runs (Table 6.2-2). The Group 2 standard deviations are generally less than for Group 1, although during the period when the spread is largest (typically during the evaporative concentration stage from approximately 150 to 600 years), the Group 2 standard deviations are commonly larger than for Group 1, although typically not by much (Table 6.2-2). On average, however, the standard deviations calculated for Group 1 are close to or larger than the deviations calculated for Group 2. For this reason, further analyses of Group 2 results are not presented here.

The two-standard-deviation spread in predicted concentrations and concentration ratios for either Group 1 or Group 2 runs generally does not exceed one order of magnitude (Tables 6.2-2 and 6.2-3, Columns Grp 1 and Grp 2). If each run from Group 1 (runs using water compositions W0, W4, W5, W6, and W7 representing natural variability) individually showed the same spread in results as the spread for Group 2 (runs using only W0 but representing uncertainties other than water composition), then the combined standard deviation could be approximated by simply adding together the variances of both groups, then taking the square root of this sum to obtain the standard deviation (Tables 6.2-2 and 6.2-3, Column Grp 1+2). The resulting combined spread also remains mostly within one order of magnitude.

The whisker plots for all HISAT-TOP waters in fractures (including points assigned to INDX=1 through 6) (Figures 6.2-4c – 6.2-20c) were visually compared to the minimum, maximum, and

mean concentrations for subsets of these waters assigned to a single INDX value. In doing so, waters assigned to INDX=5 were found to provide the most reasonably representative subset of the full data. The time profiles of the minimum, maximum, and mean concentrations for these waters (INDX=5) are shown superposed on the whiskers in Figures 6.2-4c–6.2-20c. These figures show that these waters have mean concentrations (dashed lines) close to the mean of the complete data set (filled circles) at most points in time. Also, the minimum and maximum concentrations (solid lines) of these waters most commonly encompass the two standard deviations (wide bars) calculated from the full data set.

The shapes, through time, of predicted concentration profiles for HISAT-TOP waters in fractures, and the reasons behind these shapes, are discussed in BSC (2003 [162050], Section 6.8.5.3.2). Here, the focus is given to variations in relative spread through time for these model results. By examining Figures 6.2-4c through 6.2-20c, it can be seen that the concentrations of most aqueous species show a larger spread during the evaporative concentration period (from ~150 to 600 years) than at later times. Good examples are calcium, magnesium, sodium, and potassium (Figures 6.2-13a, 6.2-16a, 6.2-17a, and 6.2-19a). During this time period, spatial variations in the degree of evaporative concentration above the drift are expected to add variability to predicted concentrations. This tends to be supported by the plots of concentration ratios to chloride (e.g., Figures 6.2-9c, 6.2-14c, 6.2-18c), which do not show as great a difference in spread between the ~150–600-year period and later time periods as do the plots of individual concentrations (e.g., Figures 6.2-8c, 6.2-13c, and 6.2-17c).

In general, it can be seen in Figures 6.2-4 through 6.2-20 (and in Tables 6.2-2 and 6.2-3) that the two-standard-deviation spread in predicted concentrations and concentration ratios for Group 1 mostly remains below one order of magnitude. The decreased spread at later times is caused by incoming waters that have somewhat homogenized from reaction with the wallrock (same mineral assemblage in all runs) and evolved following very similar temperature paths (e.g., BSC 2003 [162050], Figure 6.8-23). The most visible examples of such homogenization are concentration profiles for aqueous species constrained by near-saturation with respect to fast reacting minerals, such as fluoride constrained by fluorite (Figure 6.2-12c) and aqueous silica constrained by amorphous silica (Figure 6.2-20c). The spread in predicted CO₂ concentrations for some time after the evaporative concentration stage (Figure 6.2-5c) is also sharply reduced. This reduction in spread is attributed to incoming waters impacted (in each run) to a similar extent with CO₂ exsolved from matrix water and mobilized into fractures (i.e., impact by CO₂-enriched condensate) (BSC 2003 [162050], Section 6.8.5.3.2).

6.2.4.1.2 Boiling/Wetting Front

Waters from the boiling/wetting front are those with attributes FRONT-TOP and FRONT-BASE in fractures, and FRONT-BASE in matrix (Section 6.2.1.1). As mentioned earlier, these waters could be considered more representative of potential in-drift seepage than HISAT waters because the latter would likely evolve towards the composition of FRONT waters as they percolate towards the drift. However, because FRONT waters are more evaporated than HISAT waters, they are subject to greater uncertainty, because modeled chemical processes under high evaporation are less precise.

Summary statistics for FRONT waters were calculated and displayed in the same manner as done previously with HISAT waters. Standard deviations calculated for Group 1 and Group 2 simulation results are in general somewhat larger for FRONT waters (Table 6.2-3) than for HISAT waters (Table 6.2-2). The spread for FRONT waters is expected to be somewhat larger than for HISAT waters, because wet model gridblocks closest to the boiling/wetting front display liquid saturations that are smaller and more variable than in zones of higher liquid saturation. The increase in the variability of liquid saturation translates into an increase in the variability of evaporative concentration effects, thus affecting the variability of predicted concentrations. Note that standard deviations in Tables 6.2-2 and 6.2-3 represent only the TOP quadrant data. Standard deviations for FRONT-BASE waters (fractures and matrix) are included in data files accompanying this report (Attachment II) and are generally also larger than for HISAT waters. These data are also shown in Figures 6.2-4–6.2-20 for Group-1 model results.

As noted with HISAT waters, the standard deviations for Group 1 on the average exceed those for Group 2 (Table 6.2-3). For this reason, further analyses using FRONT waters from Group 2 runs are not presented here. It should be noted, though, that when standard deviation values are large, they are commonly larger for Group 2 than Group 1, although generally not by very much (Table 6.2-3).

Summary statistics for FRONT waters from Group 1 were plotted as done previously for other waters (Figures 6.2-4a, b, d through 6.2-20a, b, d). FRONT waters assigned to INDX=4 were deemed the most representative subset of the complete data (i.e., including INDX values 1 through 6).

FRONT-TOP waters show an increased spread in predicted concentrations for many constituents during the evaporative concentration period (~150–600 years), most noticeably for calcium, magnesium, sodium and potassium (Figures 6.2-13a, 6.2-16a, 6.2-17a, and 6.2-19a). A similar increase was noted with HISAT-TOP waters, although to a somewhat lesser extent (e.g., Figures 6.2-13c, 6.2-16c, 6.2-17c, and 6.2-19c). For FRONT-TOP waters, however, the spread also increases sharply at around 2,000 years. This pattern is not observed with the other waters (HISAT-TOP or FRONT-BASE) and results from the dissolution of salts when the boiling front recedes towards the drift wall at around 2,000 years. These salts were deposited as the result of dryout in fractures around the drift (see BSC 2003 [162050], Sections 6.4.5 and 6.8.5.4).

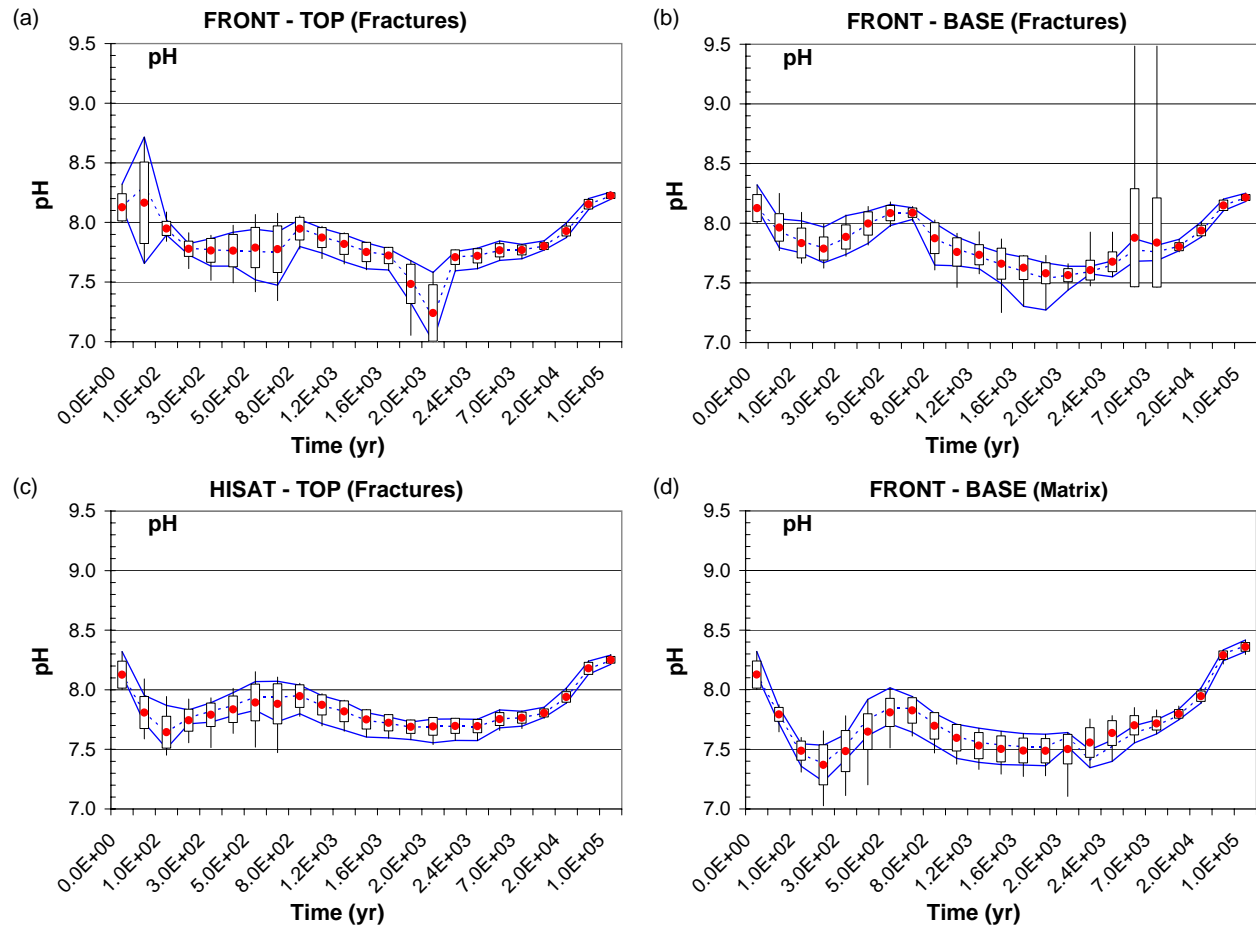
This effect is not noticeable in HISAT waters because the zone of high liquid saturation does not collapse back to the drift wall when the boiling front recedes. This is because percolation waters are partly diverted by, and accumulate above (and within) a thin low-permeability zone formed above the drift at the edge of the dryout zone during the boiling period, primarily as the result of silica precipitation by evaporative concentration. This low-permeability zone persists after boiling ends (BSC 2003 [162050], Section 6.8.5.4) and keeps the area with higher liquid saturation stationary above the drift.

The matrix rewets sooner (at ~200–300 years) than fractures (at ~2,000 years), and matrix dryout is not as extensive as in fractures. As a result, profiles for FRONT-BASE matrix waters (Figures 6.2-7d, 6.2-13d, 6.2-17d) mostly do not show an increase in spread around 2,000 years (as do FRONT-BASE fracture waters: e.g., 6.2-7b, 6.2-13b, 6.2-17b). Instead, some increase in spread

is noticeable at around 200–400 years, mainly for magnesium, sodium, and potassium (Figures 6.2-16d, 6.2-17d, and 6.2-19d).

Note that the larger spread of pH values at 5,000 and 7,000 years for FRONT-BASE waters (Figure 6.2-4b) is an artifact. It is caused by pH values near 8.8 and 9.5 in a single model gridblock that escaped rewetting until this time period, and for which water was not fully chemically speciated, because of constraints on ionic strength during speciation computations (BSC 2003 [162050], Section 6.4.6.1, Approx. no. 13). This also explains the lack of a similar spread increase in the CO₂ concentration profile during the same time period (Figure 6.2-5b).

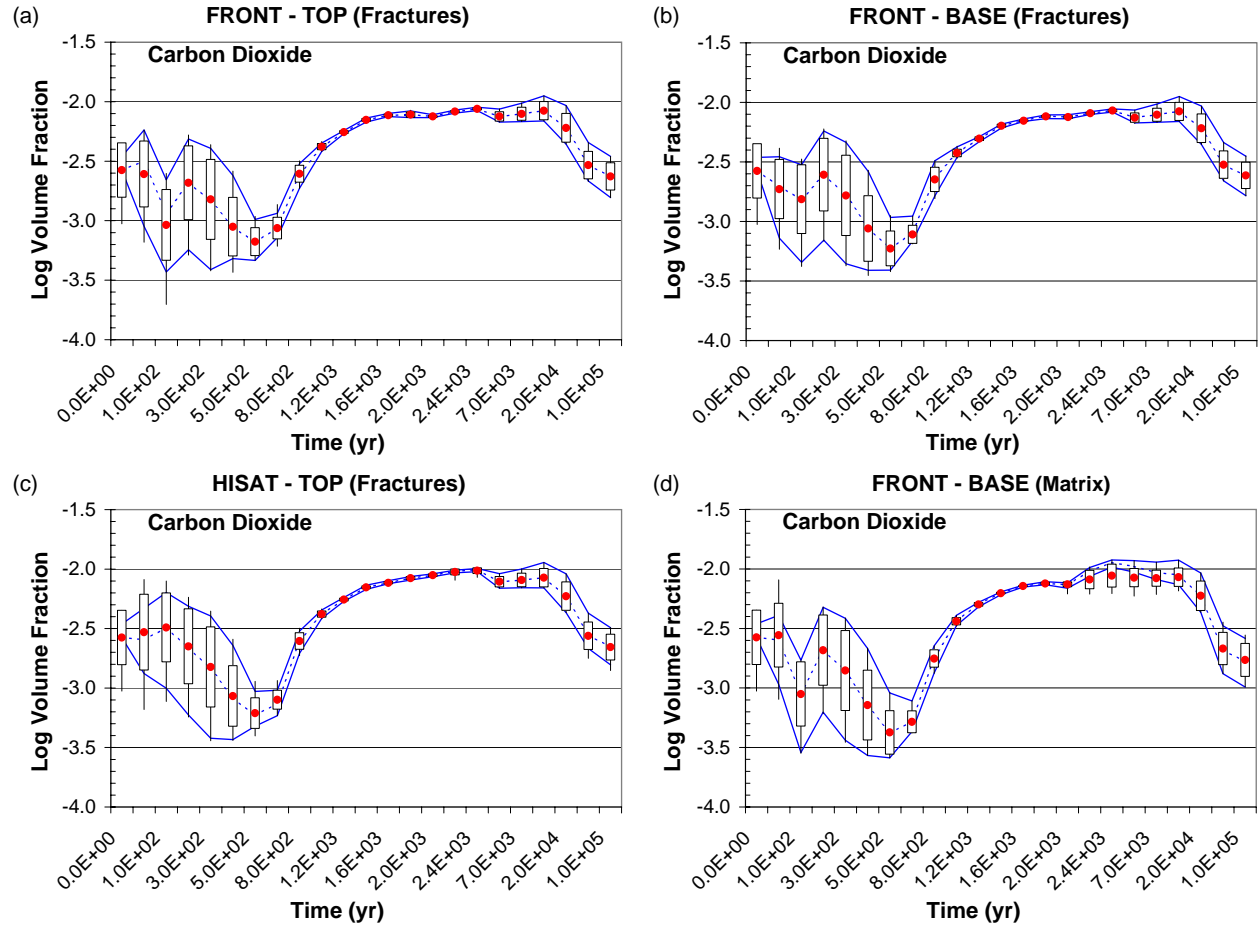
Similar to HISAT waters, the two-standard-deviation spread in predicted concentrations for FRONT waters typically remains within one order of magnitude (Figures 6.2-4 through 6.2-20 and Table 6.2-3). As observed with HISAT waters, the spread is often smaller at later times, particularly for aqueous species constrained by near-saturation with respect to fast-reacting minerals such as fluoride and aqueous silica (Figures 6.2-12 and 6.2-20). The spread of CO₂ after the evaporative concentration stage (after ~600 years) (Figure 6.2-5) also decreases, for the same reasons discussed earlier for HISAT waters.



Input-DTNs: LB0302DCSPHCS.002 [161976]; LB0307DSTTHCR2.002 [165541]
Output-DTN: LB0311ABSTHCR2.001

NOTE: Results for Group 1 simulations. Vertical lines define the spread between minimum and maximum values. Wide vertical bars define two times the standard deviation, centered around the mean (solid circles). Line profiles represent minimum and maximum values (solid lines) and mean (dashed lines) for subsets of data represented by INDX=4 for FRONT waters and INDX=5 for HISAT waters. See text (Section 6.2.4.1). The spacing of time values on the horizontal axis is not to scale.

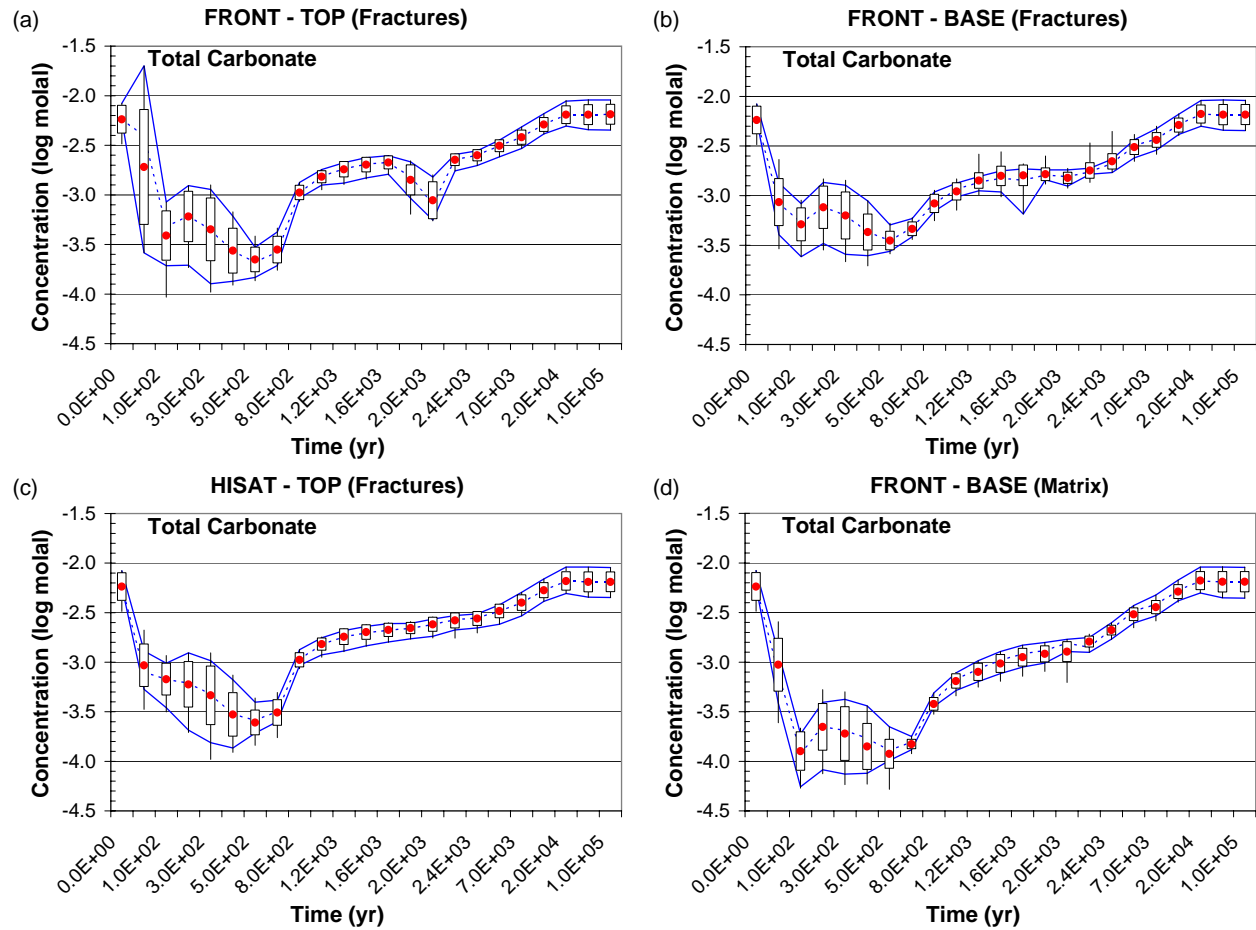
Figure 6.2-4. Abstraction of Model Results around the Modeled Drift as a Function of Time: pH



Input-DTNs: LB0302DCSPHCS.002 [161976]; LB0307DSTTHCR2.002 [165541]
 Output-DTN: LB0311ABSTHCR2.001

NOTE: Results for Group 1 simulations, log-transform data. Vertical lines define the spread between minimum and maximum values. Wide vertical bars define two times the standard deviation, centered around the mean (solid circles). Line profiles represent minimum and maximum values (solid lines) and mean (dashed lines) for subsets of data represented by INDX=4 for FRONT waters and INDX=5 for HISAT waters. See text (Section 6.2.4.1). The spacing of time values on the horizontal axis is not to scale.

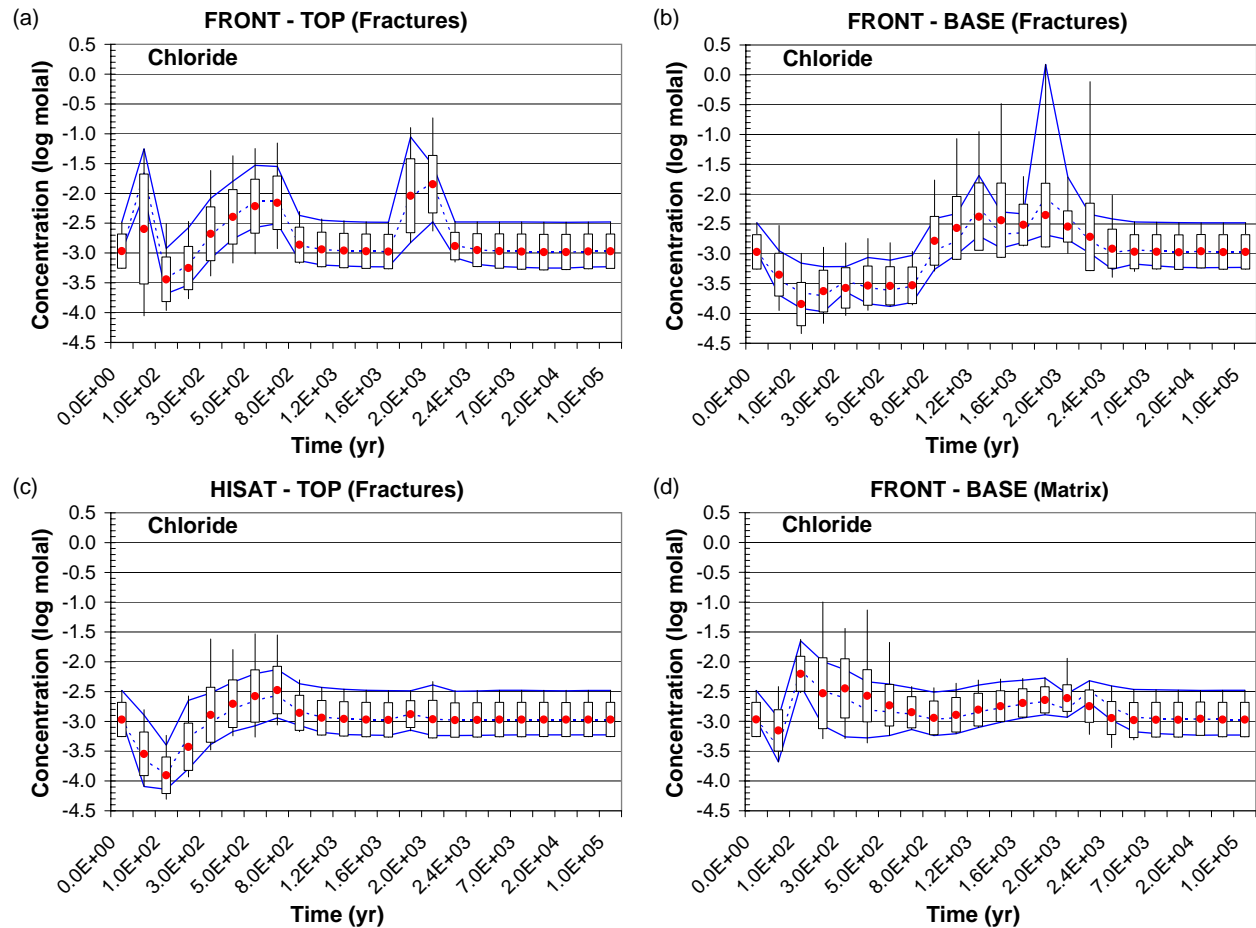
Figure 6.2-5. Abstraction of Model Results around the Modeled Drift as a Function of Time: Concentration of Carbon Dioxide Gas



Input-DTNs: LB0302DCSPHCS.002 [161976]; LB0307DSTTHCR2.002 [165541]
 Output-DTN: LB0311ABSTHCR2.001

NOTE: Results for Group 1 simulations, log-transform data. Vertical lines define the spread between minimum and maximum values. Wide vertical bars define two times the standard deviation, centered around the mean (solid circles). Line profiles represent minimum and maximum values (solid lines) and mean (dashed lines) for subsets of data represented by INDX=4 for FRONT waters and INDX=5 for HISAT waters. See text (Section 6.2.4.1). The spacing of time values on the horizontal axis is not to scale.

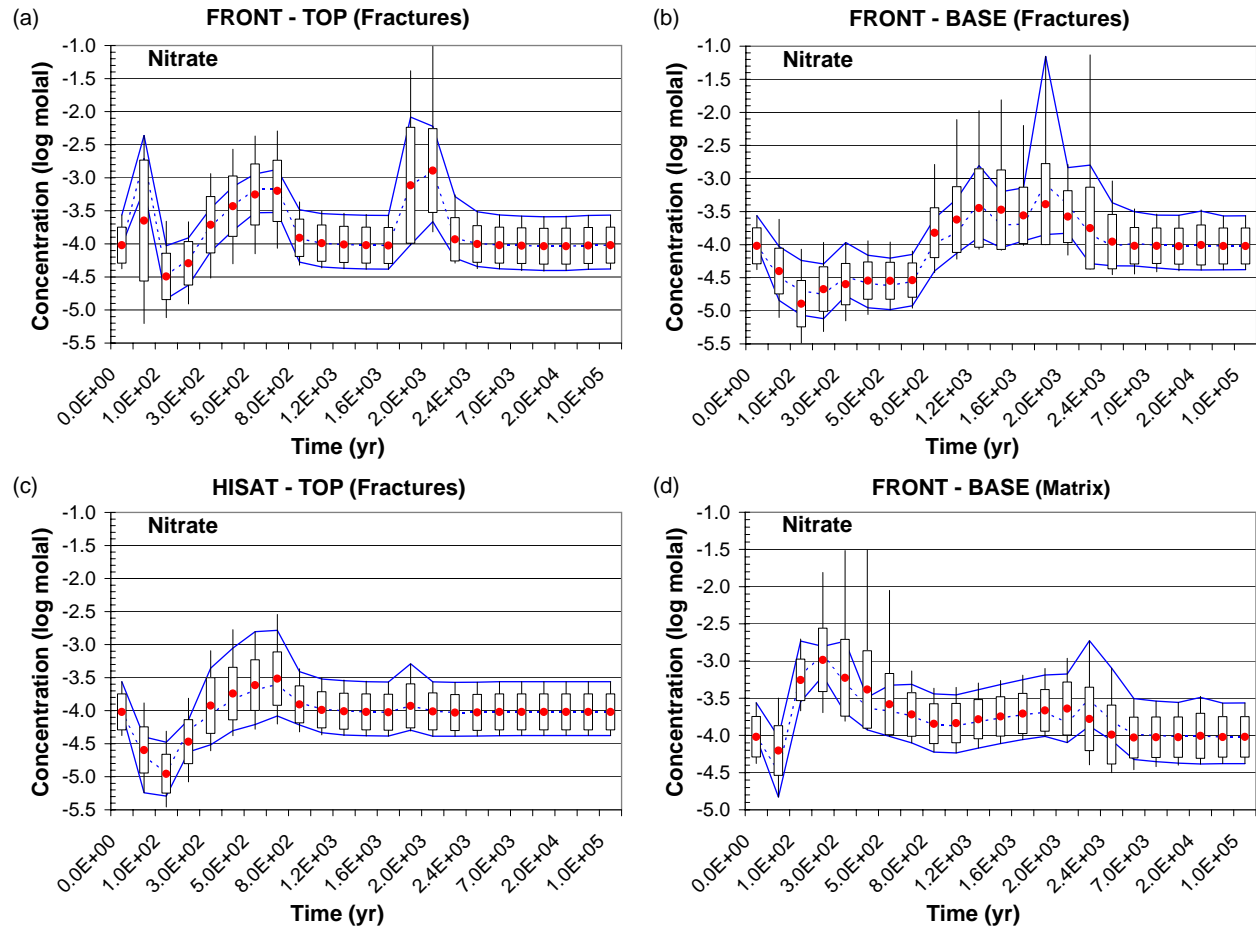
Figure 6.2-6. Abstraction of Model Results around the Modeled Drift as a Function of Time: Total Aqueous Carbonate Concentration



Input-DTNs: LB0302DCSPHCS.002 [161976]; LB0307DSTTHCR2.002 [165541]
 Output-DTN: LB0311ABSTHCR2.001

NOTE: Results for Group 1 simulations, log-transform data. Vertical lines define the spread between minimum and maximum values. Wide vertical bars define two times the standard deviation, centered around the mean (solid circles). Line profiles represent minimum and maximum values (solid lines) and mean (dashed lines) for subsets of data represented by INDX=4 for FRONT waters and INDX=5 for HISAT waters. See text (Section 6.2.4.1). The spacing of time values on the horizontal axis is not to scale.

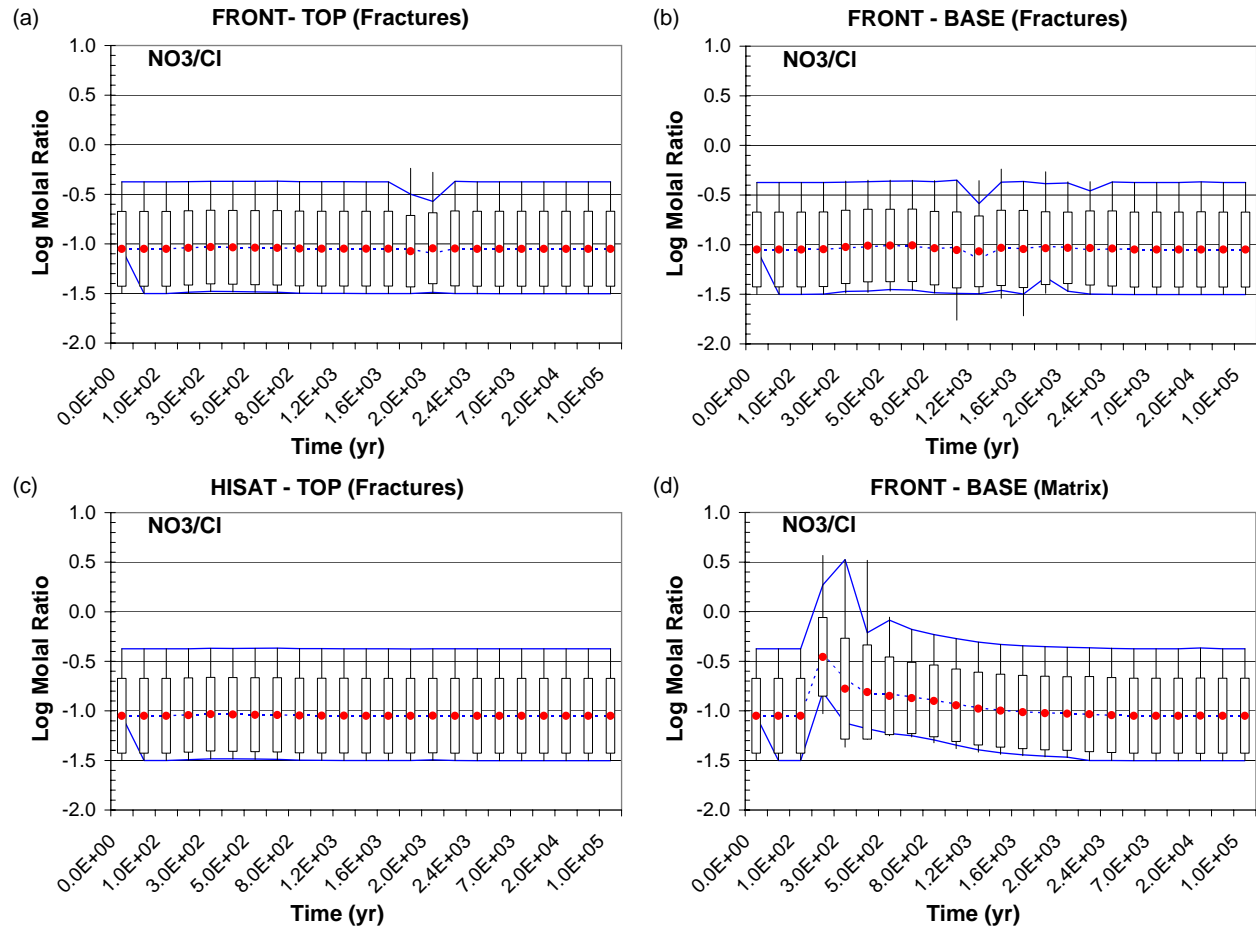
Figure 6.2-7. Abstraction of Model Results around the Modeled Drift as a Function of Time: Total Aqueous Chloride Concentration



Input-DTNs: LB0302DCSPHCS.002 [161976]; LB0307DSTTHCR2.002 [165541]
 Output-DTN: LB0311ABSTHCR2.001

NOTE: Results for Group 1 simulations, log-transform data. Vertical lines define the spread between minimum and maximum values. Wide vertical bars define two times the standard deviation, centered around the mean (solid circles). Line profiles represent minimum and maximum values (solid lines) and mean (dashed lines) for subsets of data represented by INDX=4 for FRONT waters and INDX=5 for HISAT waters. See text (Section 6.2.4.1). The spacing of time values on the horizontal axis is not to scale.

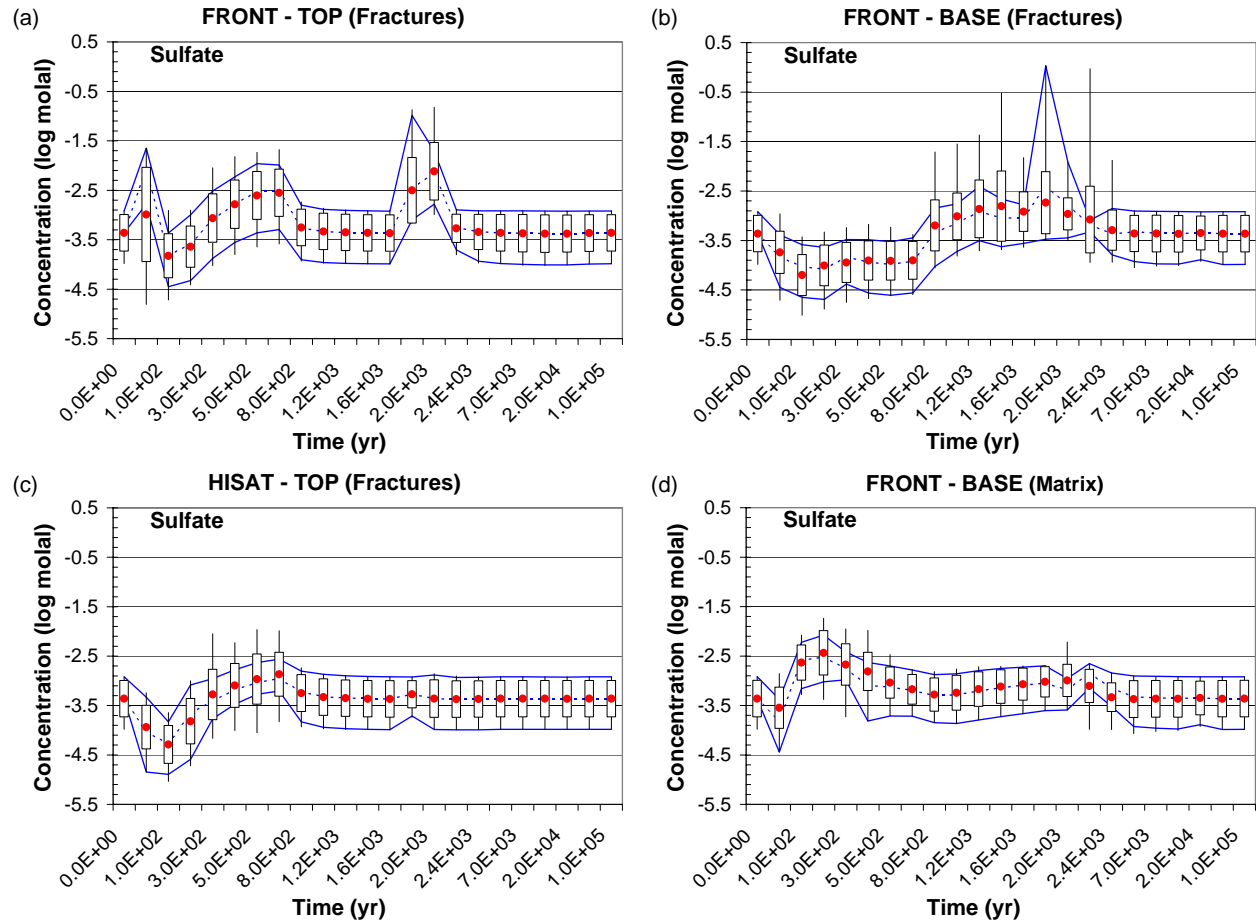
Figure 6.2-8. Abstraction of Model Results around the Modeled Drift as a Function of Time: Total Aqueous Nitrate Concentration



Input-DTNs: LB0302DCSPHCS.002 [161976]; LB0307DSTTHCR2.002 [165541]
 Output-DTN: LB0311ABSTHCR2.001

NOTE: Results for Group 1 simulations, log-transform data. Vertical lines define the spread between minimum and maximum values. Wide vertical bars define two times the standard deviation, centered around the mean (solid circles). Line profiles represent minimum and maximum values (solid lines) and mean (dashed lines) for subsets of data represented by INDX=4 for FRONT waters and INDX=5 for HISAT waters. See text (Section 6.2.4.1). The spacing of time values on the horizontal axis is not to scale.

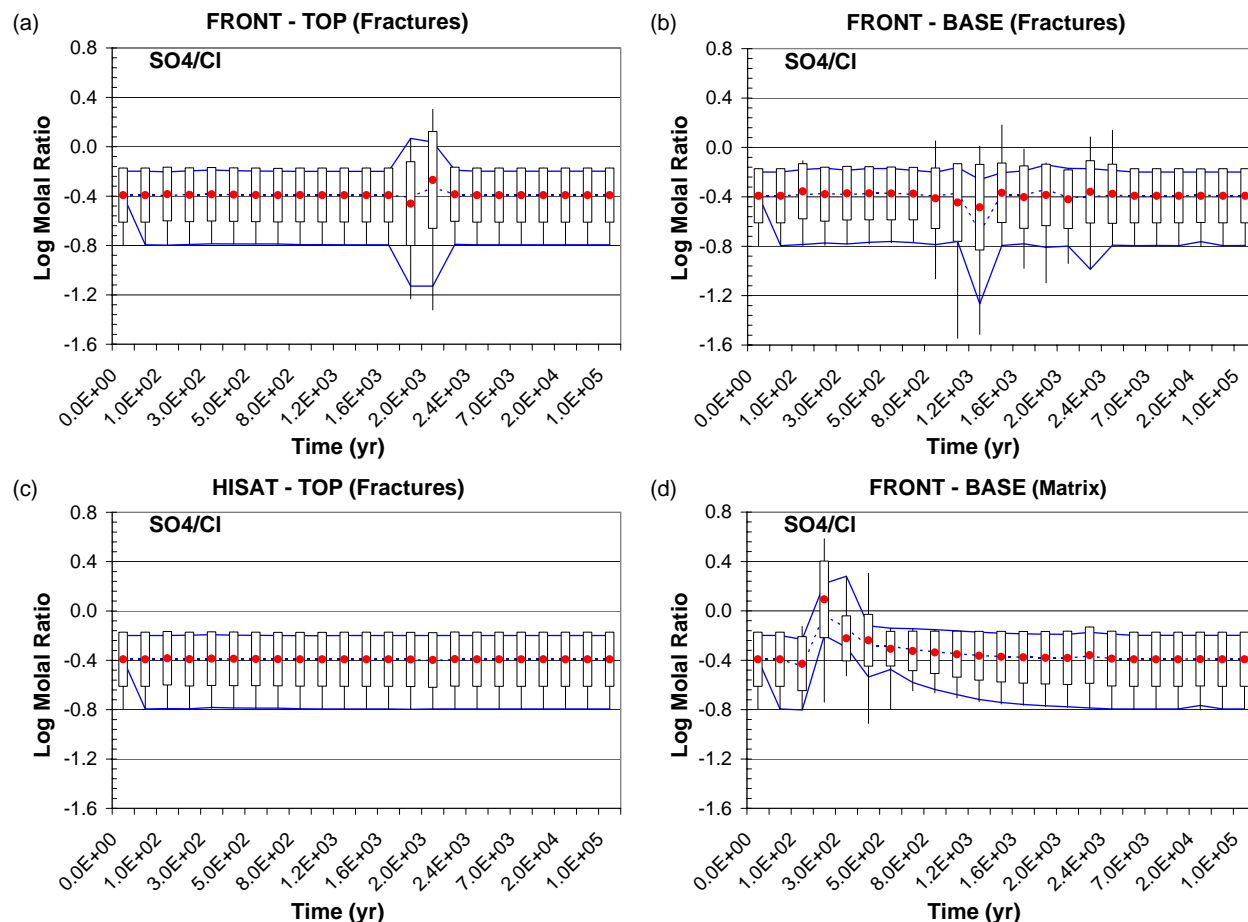
Figure 6.2-9. Abstraction of Model Results around the Modeled Drift as a Function of Time: Ratio of Total Aqueous Nitrate to Total Aqueous Chloride Concentrations



Input-DTNs: LB0302DCSPHCS.002 [161976]; LB0307DSTTHCR2.002 [165541]
Output-DTN: LB0311ABSTHCR2.001

NOTE: Results for Group 1 simulations, log-transform data. Vertical lines define the spread between minimum and maximum values. Wide vertical bars define two times the standard deviation, centered around the mean (solid circles). Line profiles represent minimum and maximum values (solid lines) and mean (dashed lines) for subsets of data represented by INDX=4 for FRONT waters and INDX=5 for HISAT waters. See text (Section 6.2.4.1). The spacing of time values on the horizontal axis is not to scale.

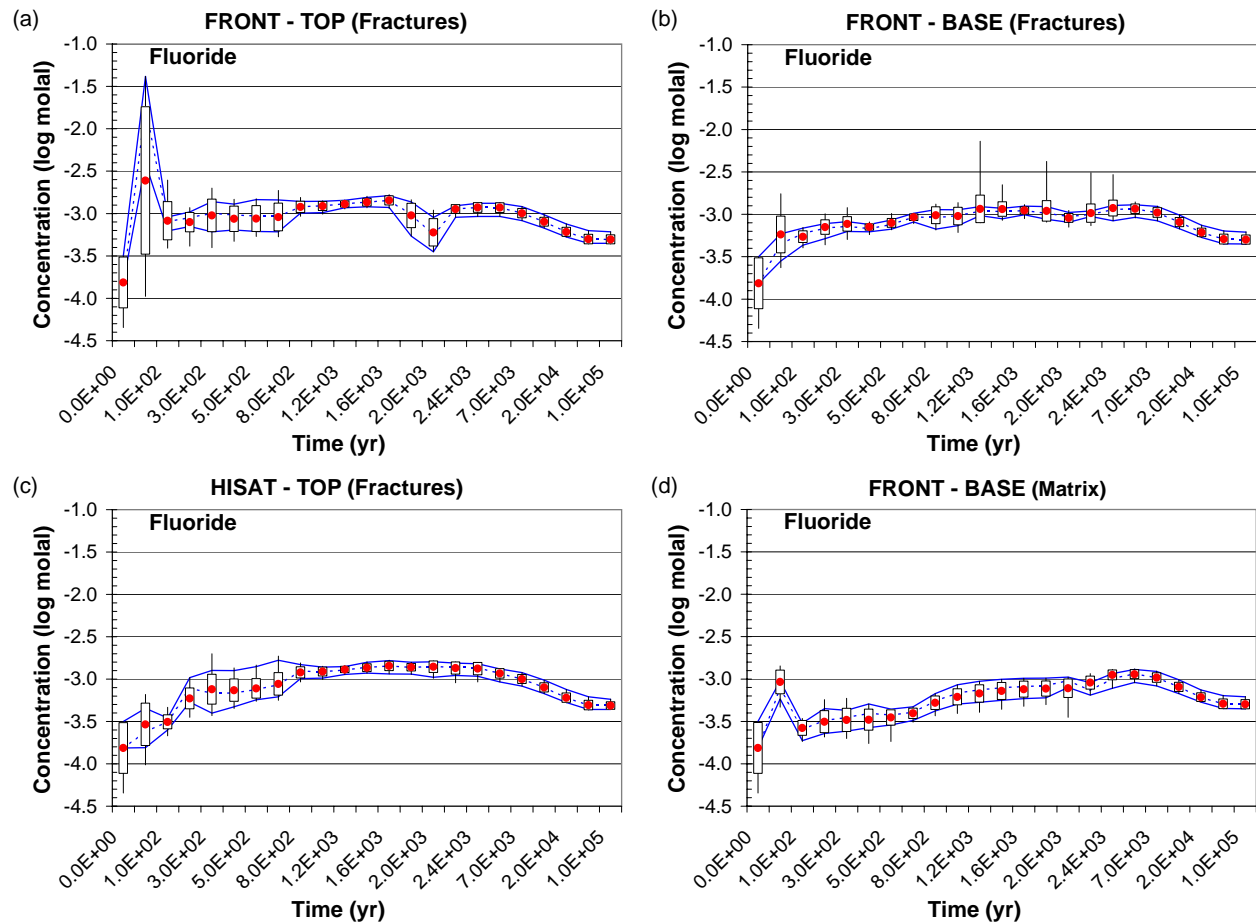
Figure 6.2-10. Abstraction of Model Results around the Modeled Drift as a Function of Time: Total Aqueous Sulfate Concentration



Input-DTNs: LB0302DCSPTHCS.002 [161976]; LB0307DSTTHCR2.002 [165541]
Output-DTN: LB0311ABSTHCR2.001

NOTE: Results for Group 1 simulations, log-transform data. Vertical lines define the spread between minimum and maximum values. Wide vertical bars define two times the standard deviation, centered around the mean (solid circles). Line profiles represent minimum and maximum values (solid lines) and mean (dashed lines) for subsets of data represented by INDX=4 for FRONT waters and INDX=5 for HISAT waters. See text (Section 6.2.4.1). The spacing of time values on the horizontal axis is not to scale.

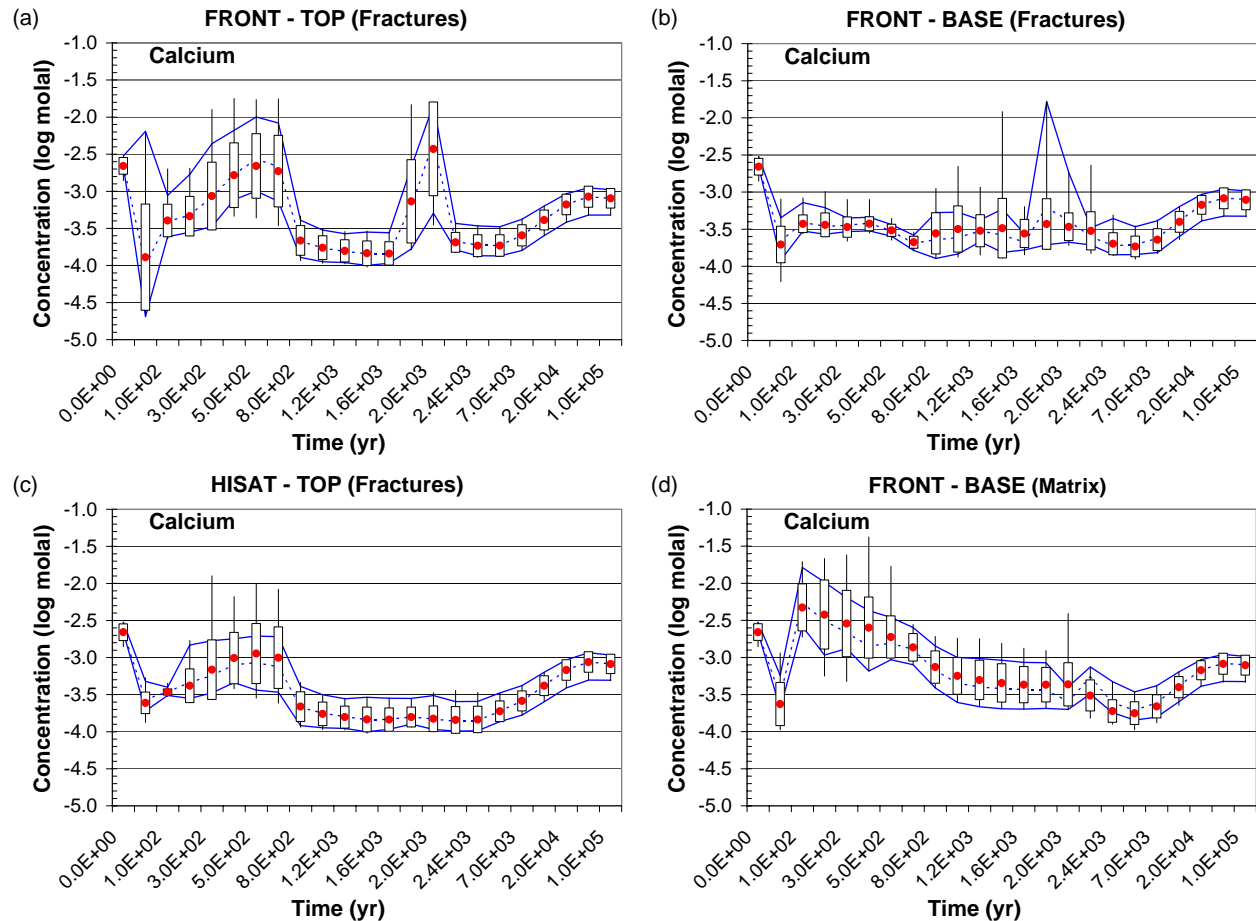
Figure 6.2-11. Abstraction of Model Results around the Modeled Drift as a Function of Time: Ratio of Total Aqueous Sulfate to Total Aqueous Chloride Concentrations



Input-DTNs: LB0302DCSPTHCS.002 [161976]; LB0307DSTTHCR2.002 [165541]
 Output-DTN: LB0311ABSTHCR2.001

NOTE: Results for Group 1 simulations, log-transform data. Vertical lines define the spread between minimum and maximum values. Wide vertical bars define two times the standard deviation, centered around the mean (solid circles). Line profiles represent minimum and maximum values (solid lines) and mean (dashed lines) for subsets of data represented by INDX=4 for FRONT waters and INDX=5 for HISAT waters. See text (Section 6.2.4.1). The spacing of time values on the horizontal axis is not to scale.

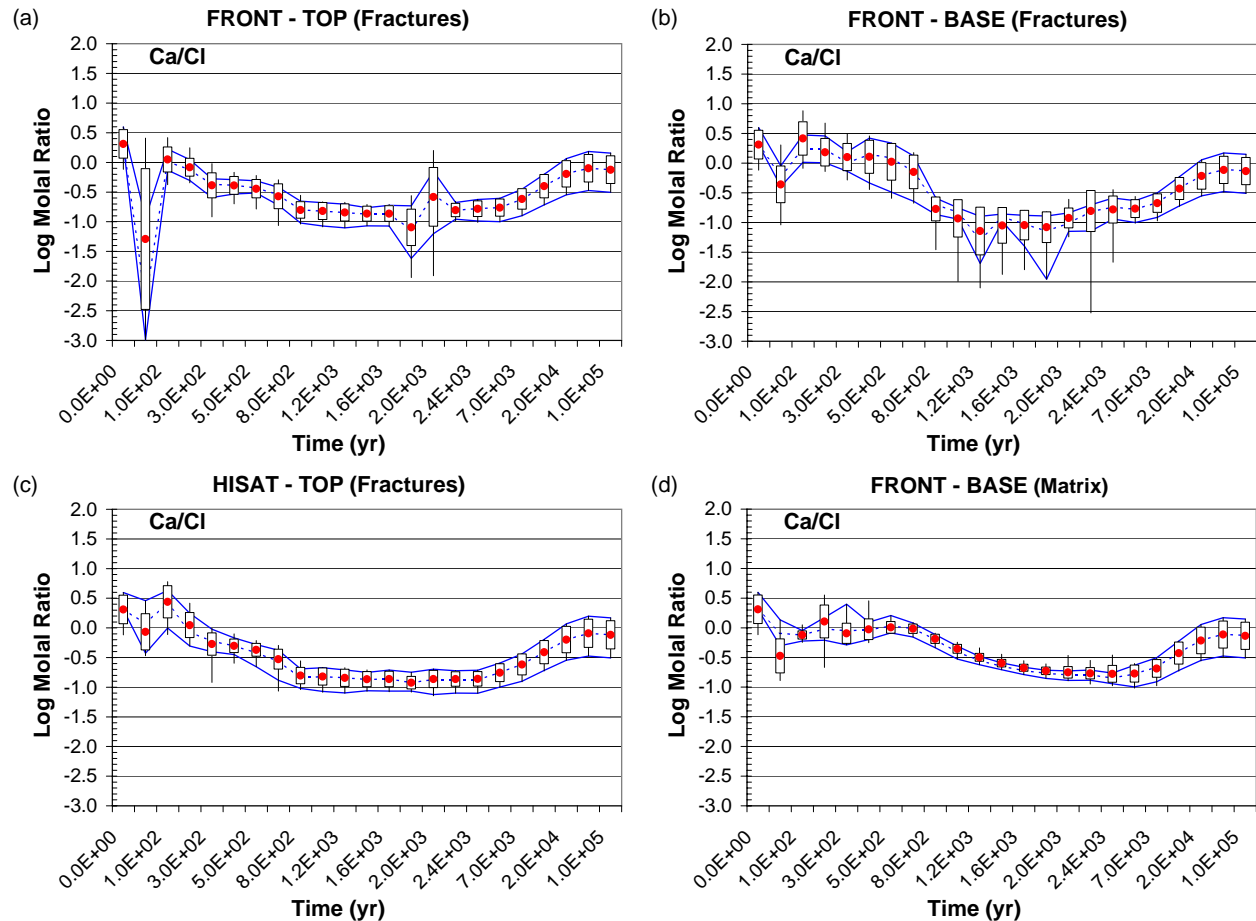
Figure 6.2-12. Abstraction of Model Results around the Modeled Drift as a Function of Time: Total Aqueous Fluoride Concentration



Input-DTNs: LB0302DCSPHCS.002 [161976]; LB0307DSTTHCR2.002 [165541]
 Output-DTN: LB0311ABSTHCR2.001

NOTE: Results for Group 1 simulations, log-transform data. Vertical lines define the spread between minimum and maximum values. Wide vertical bars define two times the standard deviation, centered around the mean (solid circles). Line profiles represent minimum and maximum values (solid lines) and mean (dashed lines) for subsets of data represented by INDX=4 for FRONT waters and INDX=5 for HISAT waters. See text (Section 6.2.4.1). The spacing of time values on the horizontal axis is not to scale.

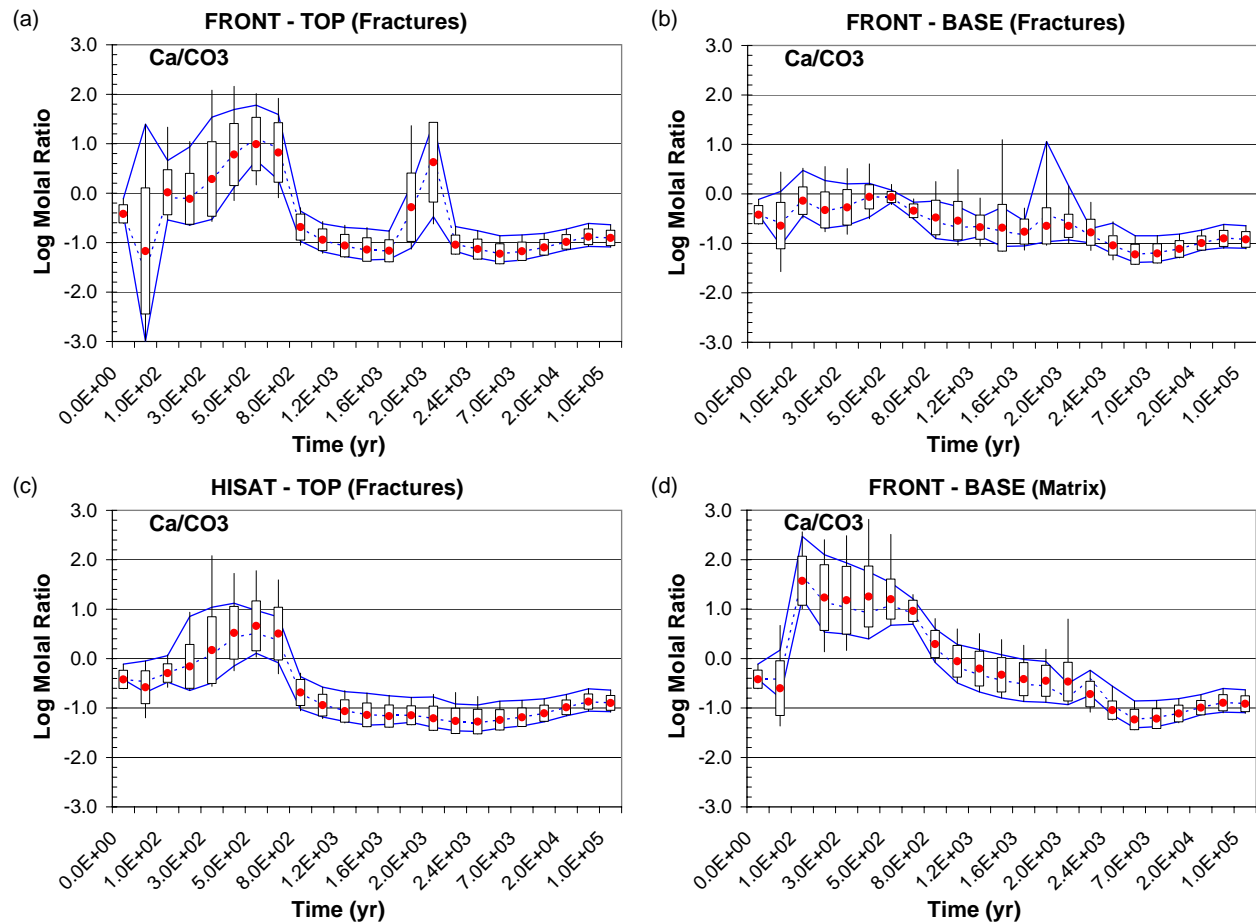
Figure 6.2-13. Abstraction of Model Results around the Modeled Drift as a Function of Time: Total Aqueous Calcium Concentration



Input-DTNs: LB0302DCSPHCS.002 [161976]; LB0307DSTTHCR2.002 [165541]
 Output-DTN: LB0311ABSTHCR2.001

NOTE: Results for Group 1 simulations, log-transform data. Vertical lines define the spread between minimum and maximum values. Wide vertical bars define two times the standard deviation, centered around the mean (solid circles). Line profiles represent minimum and maximum values (solid lines) and mean (dashed lines) for subsets of data represented by INDX=4 for FRONT waters and INDX=5 for HISAT waters. See text (Section 6.2.4.1). The spacing of time values on the horizontal axis is not to scale.

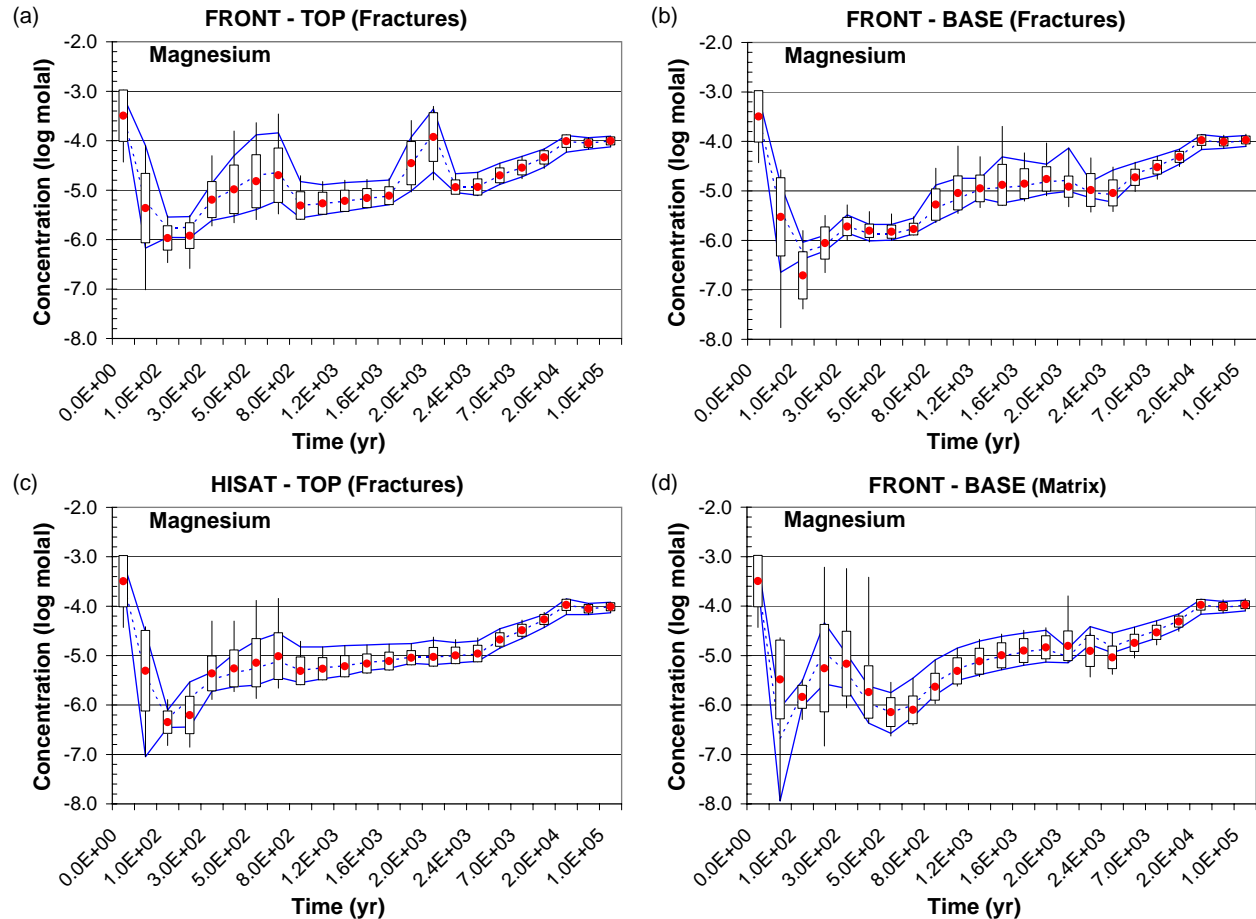
Figure 6.2-14. Abstraction of Model Results around the Modeled Drift as a Function of Time: Ratio of Total Aqueous Calcium to Total Aqueous Chloride Concentrations



Input-DTNs: LB0302DCSPTHCS.002 [161976]; LB0307DSTTHCR2.002 [165541]
 Output-DTN: LB0311ABSTHCR2.001

NOTE: Results for Group 1 simulations, log-transform data. Vertical lines define the spread between minimum and maximum values. Wide vertical bars define two times the standard deviation, centered around the mean (solid circles). Line profiles represent minimum and maximum values (solid lines) and mean (dashed lines) for subsets of data represented by INDX=4 for FRONT waters and INDX=5 for HISAT waters. See text (Section 6.2.4.1). The spacing of time values on the horizontal axis is not to scale.

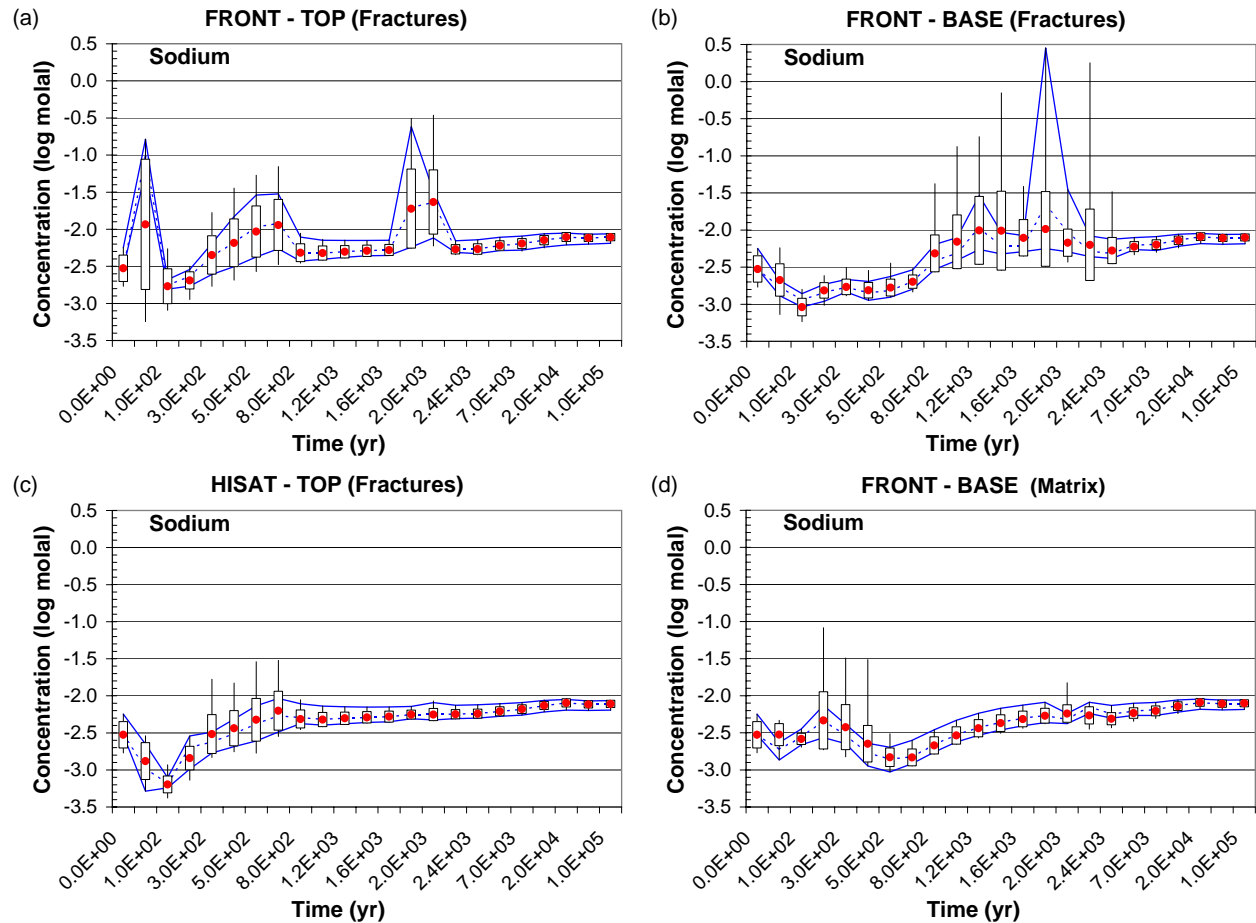
Figure 6.2-15. Abstraction of Model Results around the Modeled Drift as a Function of Time: Ratio of Total Aqueous Calcium to Total Aqueous Carbonate Concentrations



Input-DTNs: LB0302DCSPTHCS.002 [161976]; LB0307DSTTHCR2.002 [165541]
 Output-DTN: LB0311ABSTHCR2.001

NOTE: Results for Group 1 simulations, log-transform data. Vertical lines define the spread between minimum and maximum values. Wide vertical bars define two times the standard deviation, centered around the mean (solid circles). Line profiles represent minimum and maximum values (solid lines) and mean (dashed lines) for subsets of data represented by INDX=4 for FRONT waters and INDX=5 for HISAT waters. See text (Section 6.2.4.1). The spacing of time values on the horizontal axis is not to scale.

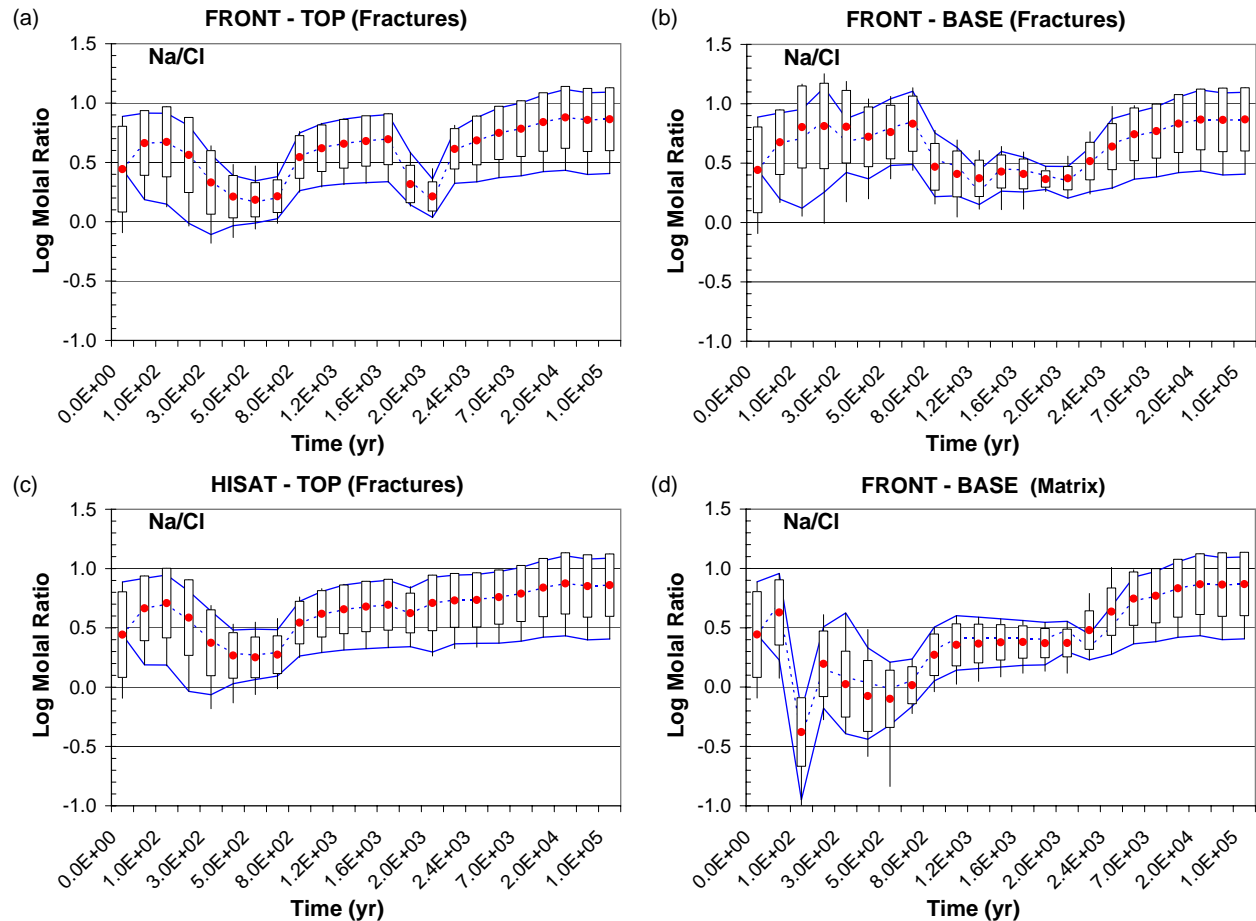
Figure 6.2-16. Abstraction of Model Results around the Modeled Drift as a Function of Time: Total Aqueous Magnesium Concentration



Input-DTNs: LB0302DCSPHCS.002 [161976]; LB0307DSTTHCR2.002 [165541]
 Output-DTN: LB0311ABSTHCR2.001

NOTE: Results for Group 1 simulations, log-transform data. Vertical lines define the spread between minimum and maximum values. Wide vertical bars define two times the standard deviation, centered around the mean (solid circles). Line profiles represent minimum and maximum values (solid lines) and mean (dashed lines) for subsets of data represented by INDX=4 for FRONT waters and INDX=5 for HISAT waters. See text (Section 6.2.4.1). The spacing of time values on the horizontal axis is not to scale.

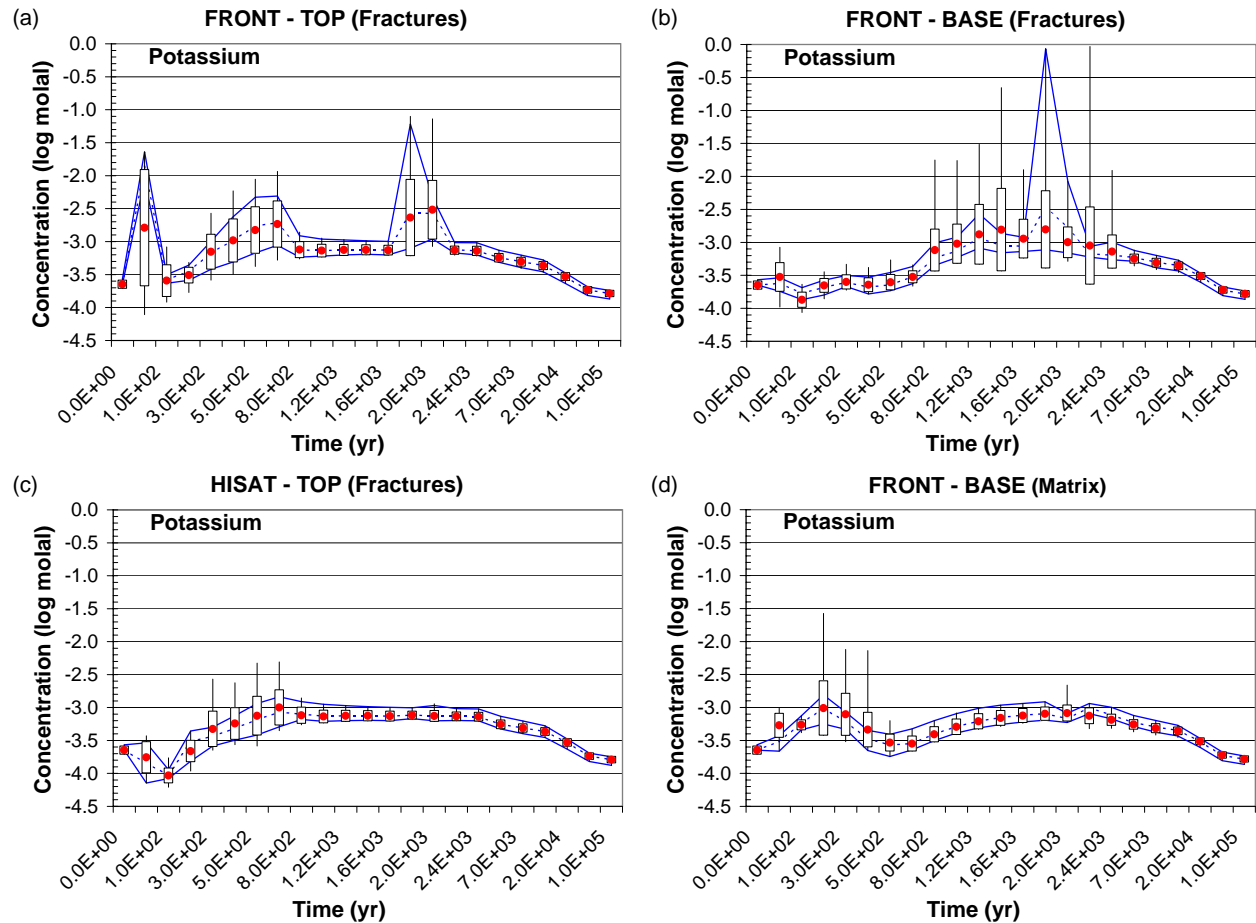
Figure 6.2-17. Abstraction of Model Results around the Modeled Drift as a Function of Time: Total Aqueous Sodium Concentration



Input-DTNs: LB0302DCSPHCS.002 [161976]; LB0307DSTTHCR2.002 [165541]
 Output-DTN: LB0311ABSTHCR2.001

NOTE: Results for Group 1 simulations, log-transform data. Vertical lines define the spread between minimum and maximum values. Wide vertical bars define two times the standard deviation, centered around the mean (solid circles). Line profiles represent minimum and maximum values (solid lines) and mean (dashed lines) for subsets of data represented by INDX=4 for FRONT waters and INDX=5 for HISAT waters. See text (Section 6.2.4.1). The spacing of time values on the horizontal axis is not to scale.

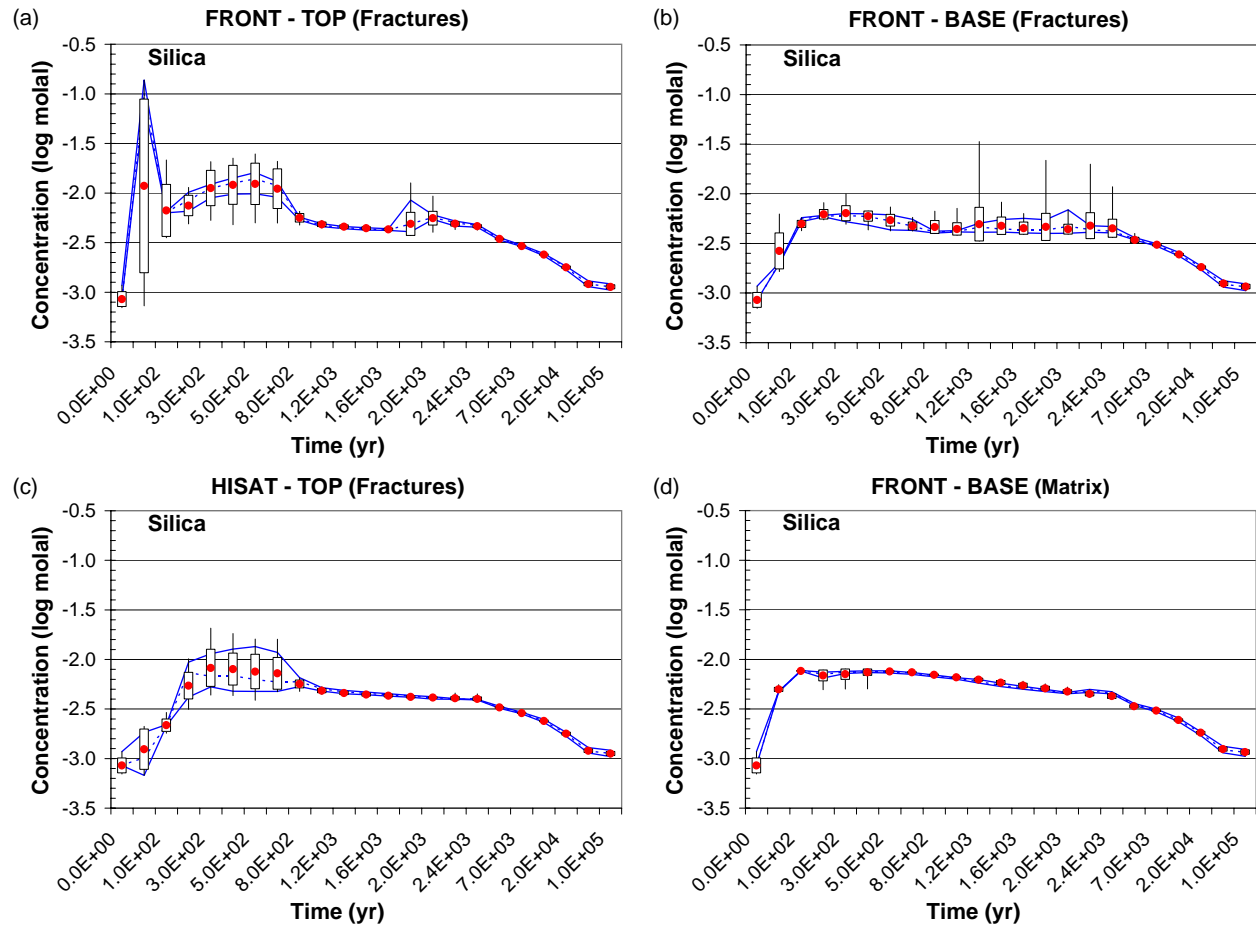
Figure 6.2-18. Abstraction of Model Results around the Modeled Drift as a Function of Time: Ratio of Total Aqueous Sodium to Total Aqueous Chloride Concentrations



Input-DTNs: LB0302DCSPHCS.002 [161976]; LB0307DSTTHCR2.002 [165541]
 Output-DTN: LB0311ABSTHCR2.001

NOTE: Results for Group 1 simulations, log-transform data. Vertical lines define the spread between minimum and maximum values. Wide vertical bars define two times the standard deviation, centered around the mean (solid circles). Line profiles represent minimum and maximum values (solid lines) and mean (dashed lines) for subsets of data represented by INDX=4 for FRONT waters and INDX=5 for HISAT waters. See text (Section 6.2.4.1). The spacing of time values on the horizontal axis is not to scale.

Figure 6.2-19. Abstraction of Model Results around the Modeled Drift as a Function of Time: Total Aqueous Potassium Concentration



Input-DTNs: LB0302DCSPHCS.002 [161976]; LB0307DSTTHCR2.002 [165541]
 Output-DTN: LB0311ABSTHCR2.001

NOTE: Results for Group 1 simulations, log-transform data. Vertical lines define the spread between minimum and maximum values. Wide vertical bars define two times the standard deviation, centered around the mean (solid circles). Line profiles represent minimum and maximum values (solid lines) and mean (dashed lines) for subsets of data represented by INDX=4 for FRONT waters and INDX=5 for HISAT waters. See text (Section 6.2.4.1). The spacing of time values on the horizontal axis is not to scale.

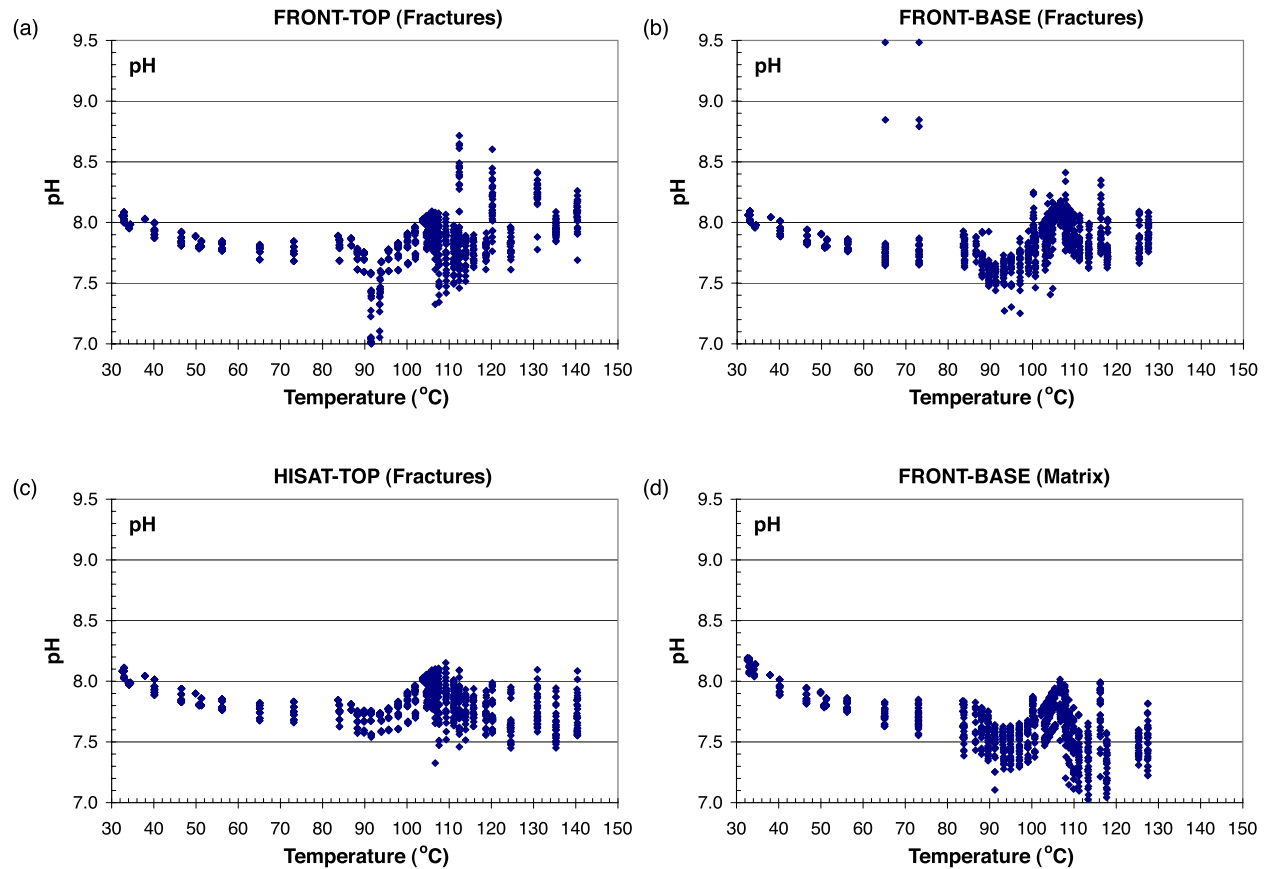
Figure 6.2-20. Abstraction of Model Results around the Modeled Drift as a Function of Time: Total Aqueous Silica Concentration

6.2.4.2 Abstraction as a Function of Temperature and Liquid Saturation

Scatter plots of predicted concentrations (pH, CO₂ gas, and chloride) and concentration ratios (calcium over total aqueous carbonate) were generated for Group 1 results as a function of temperature, using the drift crown and base temperatures for waters from the TOP and BASE quadrants, respectively (Figures 6.2-21 through 6.2-24). Similar plots as a function of liquid saturation were also generated (Figures 6.2-25 through 6.2-28). Compared to figures discussed earlier, these plots have the advantage of showing all data points. Because predicted temperatures are the same for all runs considered here (i.e., almost identical temperatures predicted for each run at each point in time), summary statistics presented earlier as a function of time essentially also apply to the data represented as a function of temperature. Therefore, the temperature plots can be viewed as a general rearrangement of the time-profile data (Figures 6.2-4 through 6.2-20), sorted in order of increasing temperature. This is not the case, however, for profiles as a function of liquid saturation.

As would be expected, the spread in model results typically increases with temperature, showing trend deviations related to the same processes as those discussed earlier for the time profiles. Values of pH above 8.5 in Figure 6.2-21b are artifacts and correspond to the points mentioned earlier for the time profiles at 5,000 and 7,000 years (Figure 6.2-4b). The increased spread of dissolved constituent concentrations after the collapse of the boiling front (FRONT waters) is visible in fractures when the drift crown has reached rewetting (below boiling) temperatures around 90–95°C (e.g., Figures 6.2-21a, 23a, and 24a). The effect is less visible in the matrix at the base of the drift, which is fully rewetted below drift-base temperatures around 105–110°C (e.g., Figure 6.2-24d). The higher rewetting temperatures in matrix than in fractures results from higher capillary pressure in the matrix, causing more vapor pressure lowering than in fractures. The likelihood of in-drift seepage is essentially nil above these temperatures, because of the resulting vaporization barrier around the drift (BSC 2003 [161530], Section 6.2.1.1.2). Therefore, in terms of abstracting in-drift seepage water compositions, the data above these temperatures can be justifiably discarded, leaving for consideration (for the most part) the results showing the least spread in predicted concentrations.

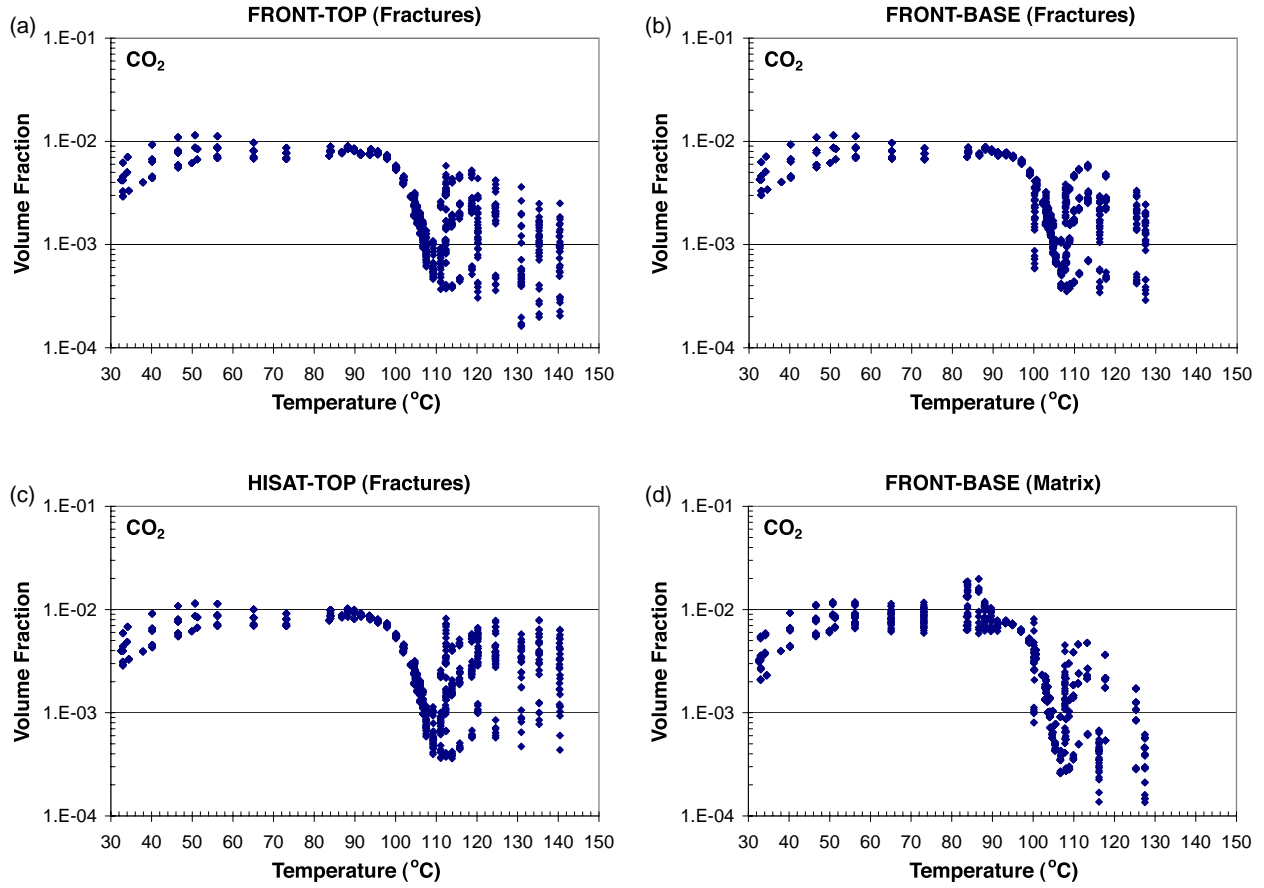
For dissolved constituents, profiles in terms of liquid saturation are expected to show a general trend of increasing concentration, as well as spread, with decreasing liquid saturation, because of evaporative concentration. This is observed for chloride (Figure 6.2-27), a nonreactive species, but as much for pH (Figure 6.2-25). This inverse correlation is also evident for the profile of Ca/CO₃ ratios (Figure 6.2-28), because aqueous carbonate is being volatilized as CO₂ gas together with water when liquid saturations fall. Points below residual liquid saturation (typically around 0.1 for matrix and 0.01 for fractures) could not contribute to in-drift seepage because the movement of water at liquid saturation below the residual value is prevented by capillary forces. Therefore, excluding data points below residual liquid saturation would be justifiable, to the extent that values of residual saturation themselves can be defended. Doing so would thus further narrow the spread and magnitude of the data that should be considered representative of potential in-drift seepage.



Input-DTNs: LB0302DCSPTHCS.002 [161976]; LB0307DSTTHCR2.002 [165541]
 Output-DTN: LB0311ABSTHCR2.001

NOTE: Results for Group-1 simulations. Horizontal axis represents predicted temperatures at the drift crown for data in the TOP quadrant, and at the drift base for data in the BASE quadrant. See text (Section 6.2.4.2).

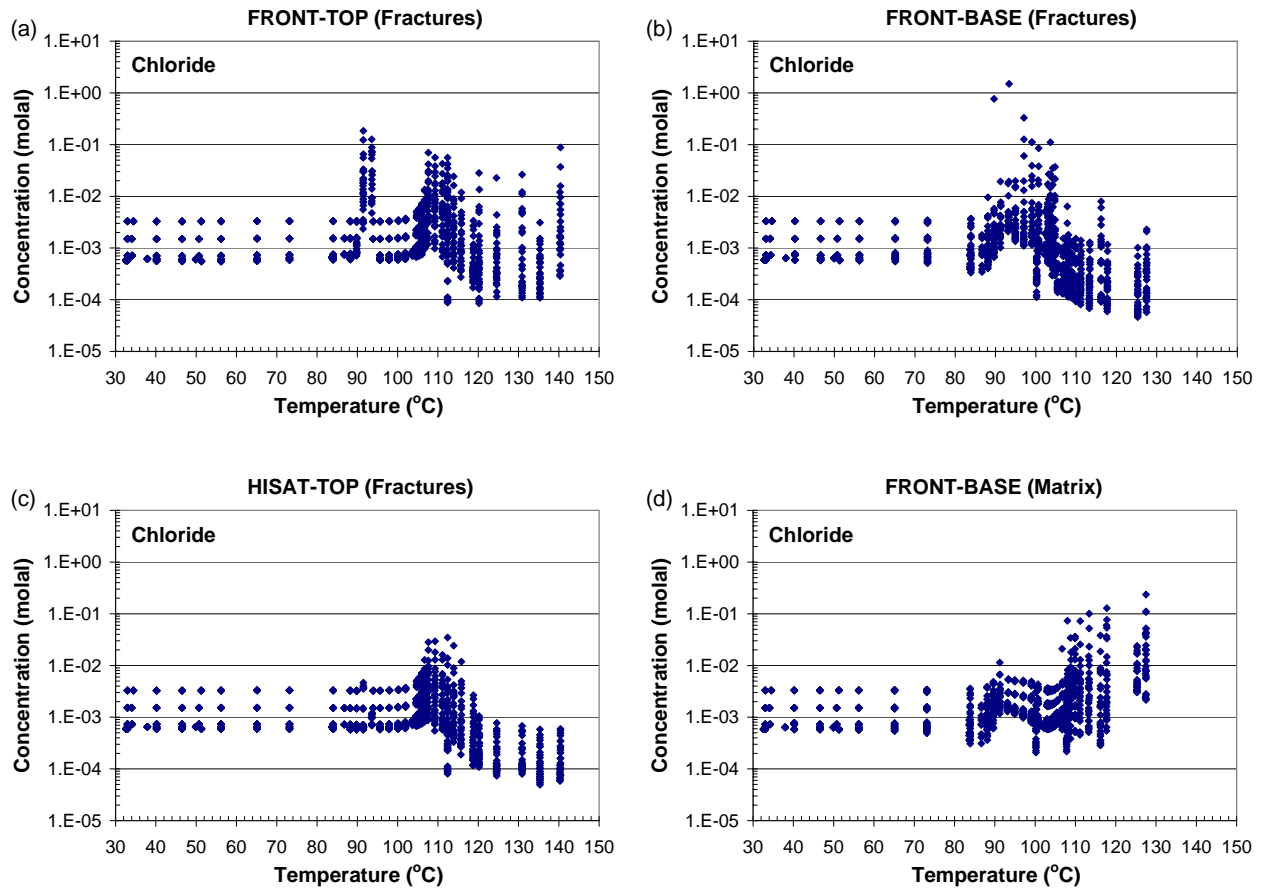
Figure 6.2-21. Abstraction of Model Results around the Modeled Drift as a Function of Drift-Wall Temperature: pH



Input-DTNs: LB0302DCSPTHCS.002 [161976]; LB0307DSTTHCR2.002 [165541]
 Output-DTN: LB0311ABSTHCR2.001

NOTE: Results for Group-1 simulations. Horizontal axis represents predicted temperatures at the drift crown for data in the TOP quadrant, and at the drift base for data in the BASE quadrant. See text (Section 6.2.4.2).

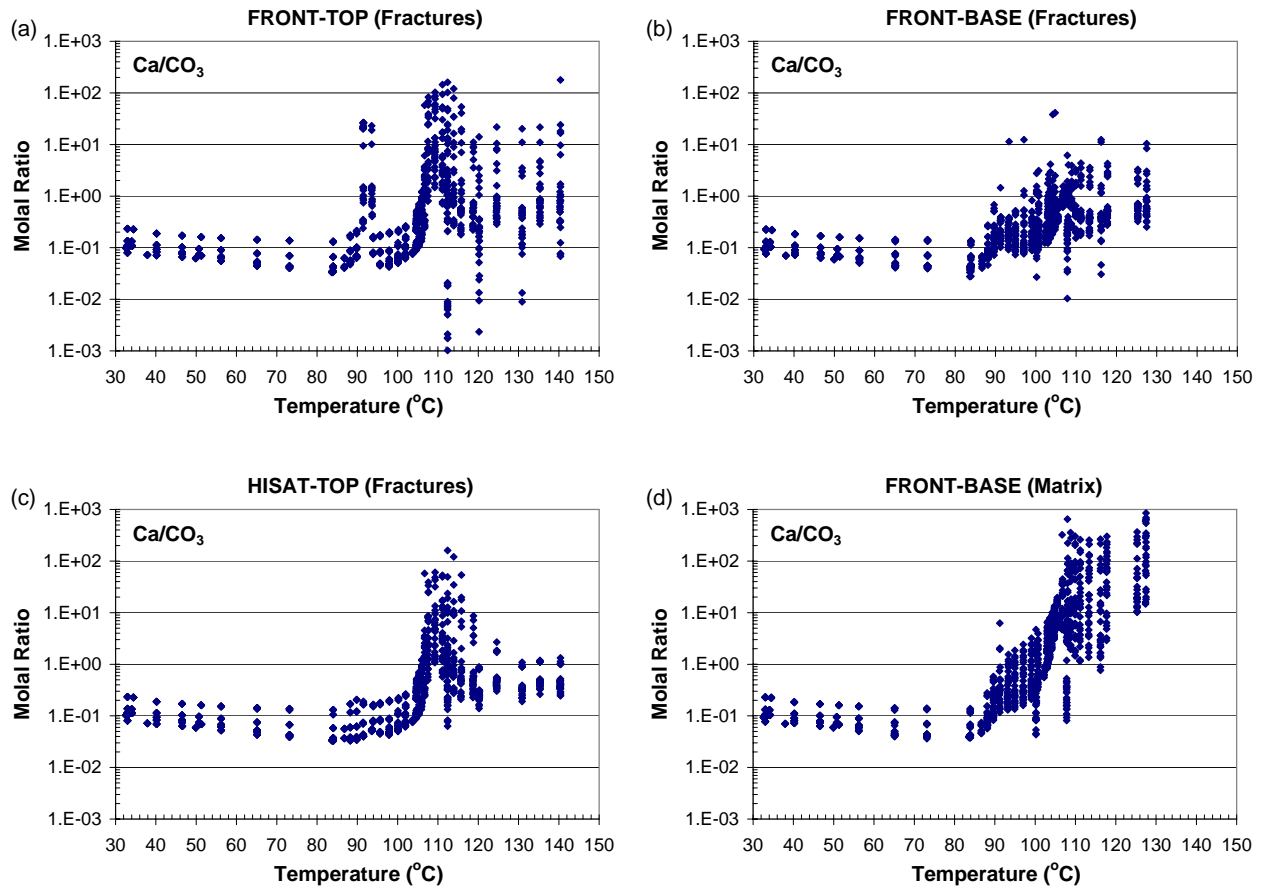
Figure 6.2-22. Abstraction of Model Results around the Modeled Drift as a Function of Drift-Wall Temperature: Concentration of Carbon Dioxide Gas



Input-DTNs: LB0302DCSPTHCS.002 [161976]; LB0307DSTTHCR2.002 [165541]
 Output-DTN: LB0311ABSTHCR2.001

NOTE: Results for Group-1 simulations. Horizontal axis represents predicted temperatures at the drift crown for data in the TOP quadrant, and at the drift base for data in the BASE quadrant. See text (Section 6.2.4.2).

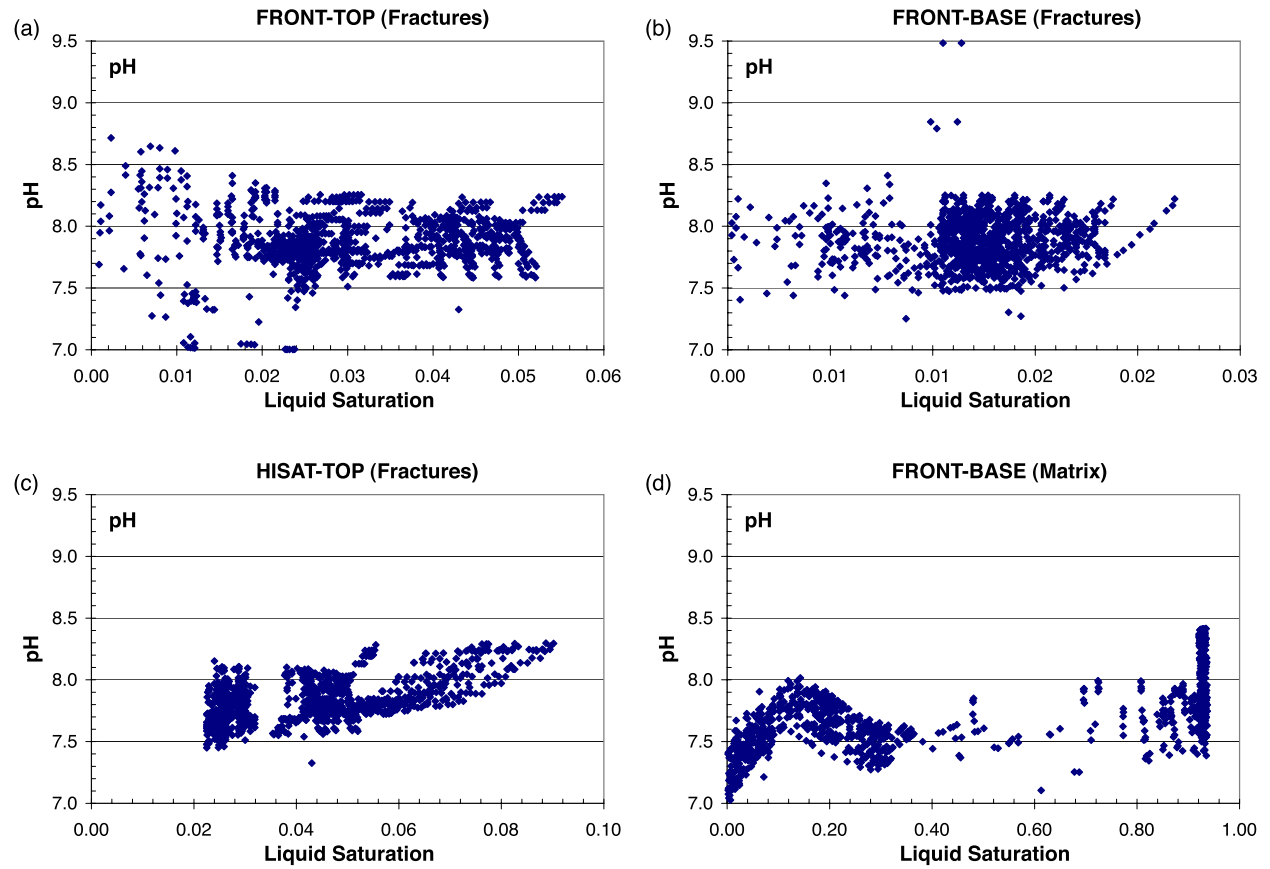
Figure 6.2-23. Abstraction of Model Results around the Modeled Drift as a Function of Drift-Wall Temperature: Total Aqueous Chloride Concentration



Input-DTNs: LB0302DCSPTHCS.002 [161976]; LB0307DSTTHCR2.002 [165541]
 Output-DTN: LB0311ABSTHCR2.001

NOTE: Results for Group-1 simulations. Horizontal axis represents predicted temperatures at the drift crown for data in the TOP quadrant, and at the drift base for data in the BASE quadrant. See text (Section 6.2.4.2).

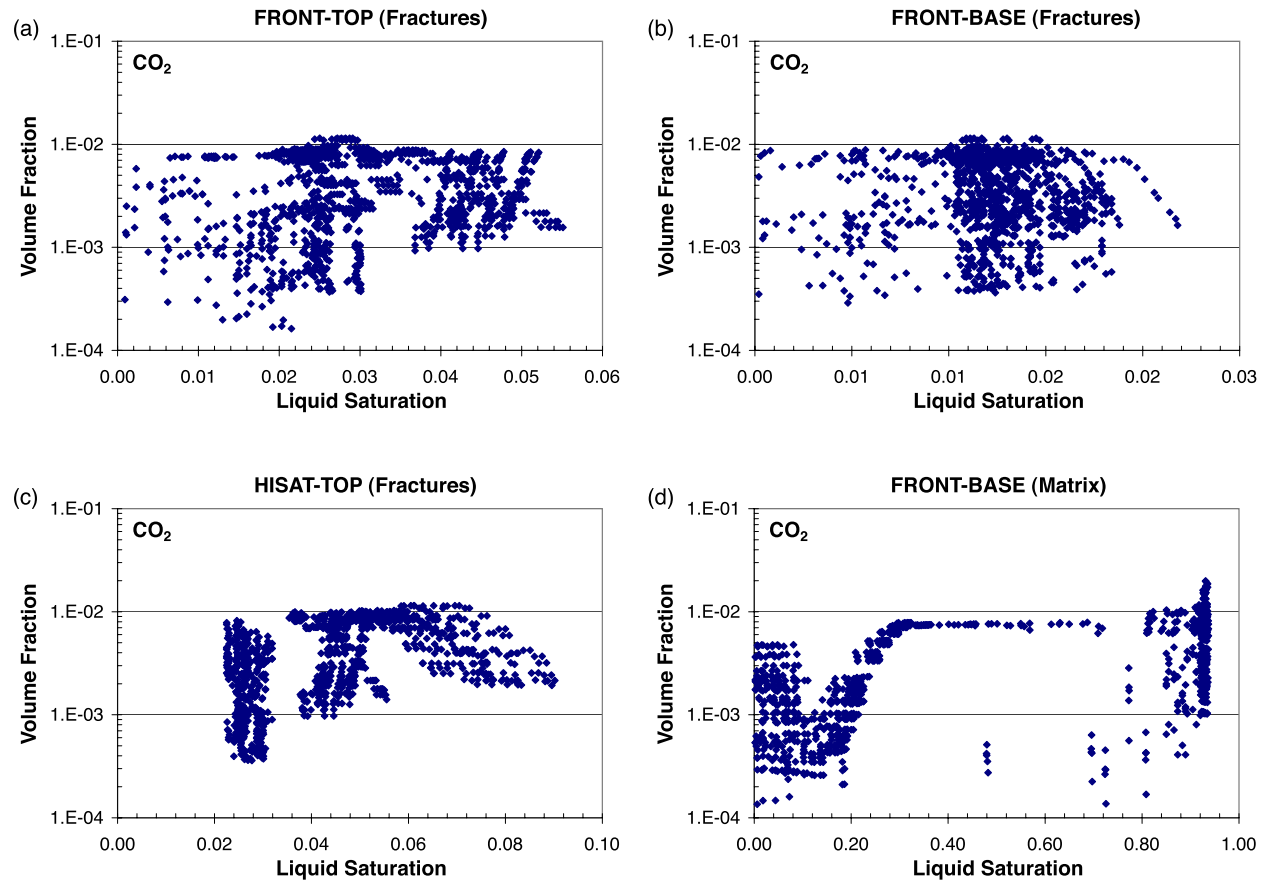
Figure 6.2-24. Abstraction of Model Results around the Modeled Drift as a Function of Drift-Wall Temperature: Ratio of Total Aqueous Calcium to Total Aqueous Carbonate Concentrations



Input-DTNs: LB0302DCSPHCS.002 [161976]; LB0307DSTTHCR2.002 [165541]
 Output-DTN: LB0311ABSTHCR2.001

NOTE: Results for Group-1 simulations. See text (Section 6.2.4.2).

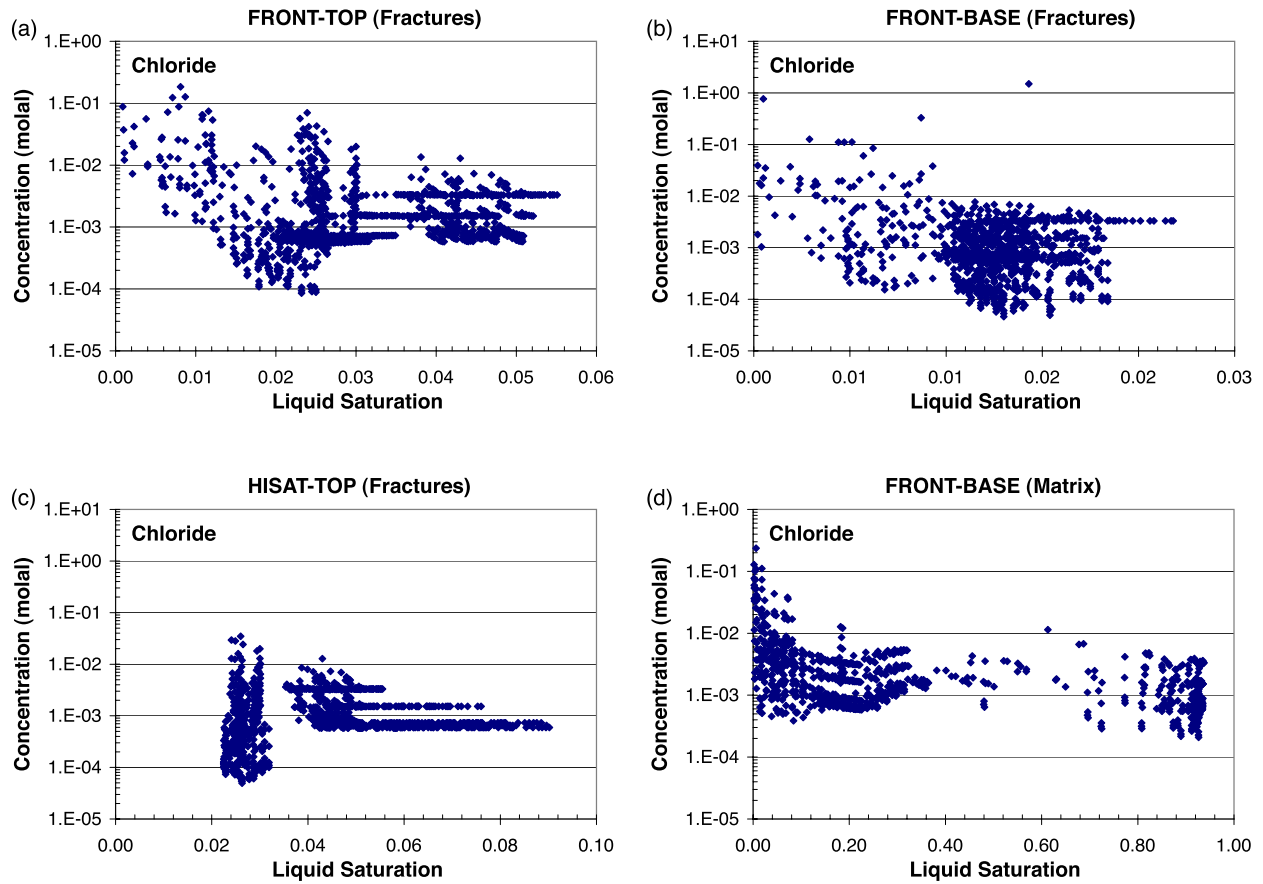
Figure 6.2-25. Abstraction of Model Results around the Modeled Drift as a Function of Liquid Saturation: pH



Input-DTNs: LB0302DCSPHCS.002 [161976]; LB0307DSTTHCR2.002 [165541]
 Output-DTN: LB0311ABSTHCR2.001

NOTE: Results for Group-1 simulations. See text (Section 6.2.4.2).

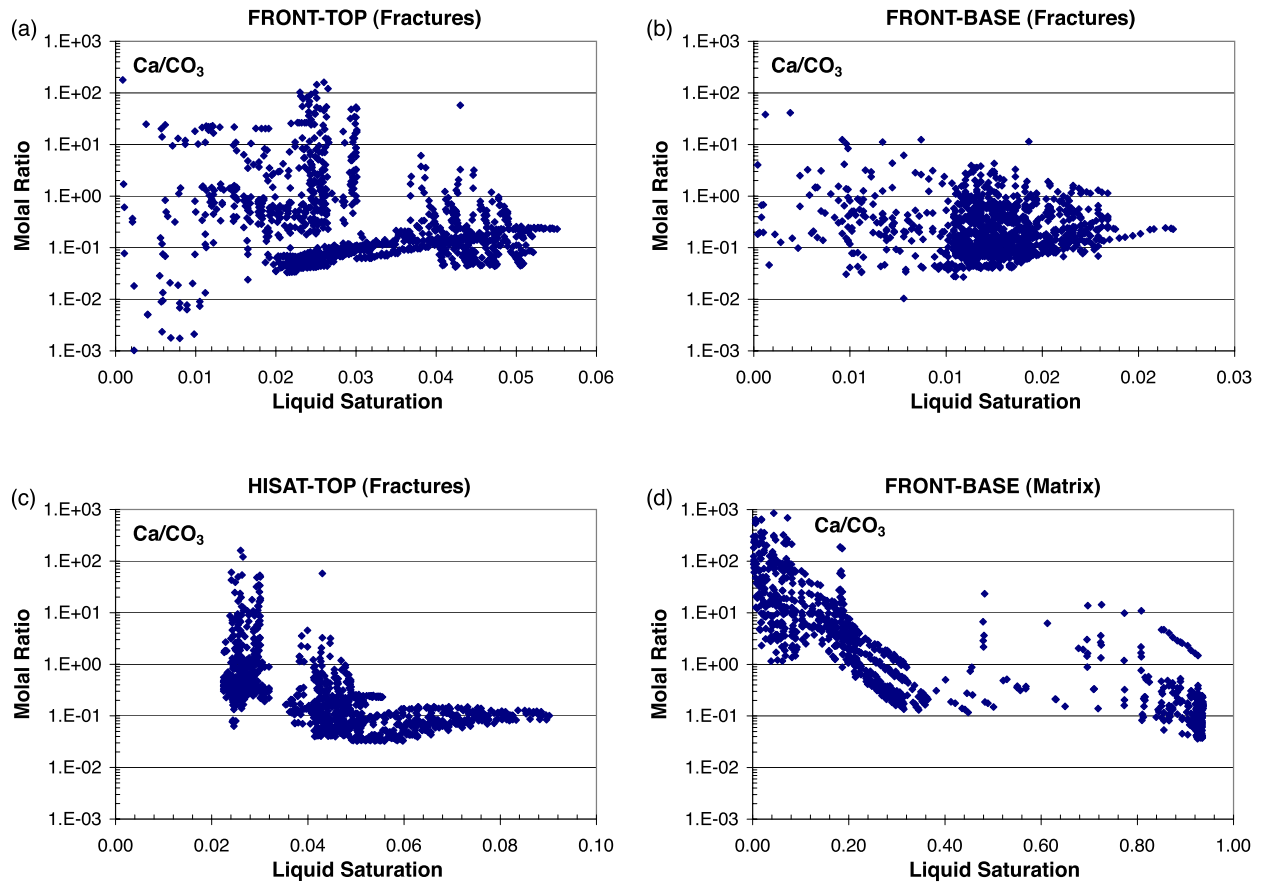
Figure 6.2-26. Abstraction of Model Results around the Modeled Drift as a Function of Liquid Saturation: Concentration of Carbon Dioxide Gas



Input-DTNs: LB0302DCSPHCS.002 [161976]; LB0307DSTTHCR2.002 [165541]
 Output-DTN: LB0311ABSTHCR2.001

NOTE: Results for Group-1 simulations. See text (Section 6.2.4.2).

Figure 6.2-27. Abstraction of Model Results around the Modeled Drift as a Function of Liquid Saturation: Total Aqueous Chloride Concentration



Input-DTNs: LB0302DCSPTHCS.002 [161976]; LB0307DSTTHCR2.002 [165541]
 Output-DTN: LB0311ABSTHCR2.001

NOTE: Results for Group-1 simulations. See text (Section 6.2.4.2).

Figure 6.2-28. Abstraction of Model Results around the Modeled Drift as a Function of Liquid Saturation: Ratio of Total Aqueous Calcium to Total Aqueous Carbonate Concentrations

6.3 THC SIMULATIONS CONSIDERING DRIFT DEGRADATION

Results of the THC Seepage Model are presented in this section for a case considering drift degradation. These results complement those presented in BSC 2003 ([162050], Section 6.8) for the case of an intact drift, and analyzed above in Section 6.2.

The drift degradation case was run using the Tptpll THC Model REV02 as presented in BSC 2003 ([162050], Section 6.8), with modifications to include a drift with collapsed wallrock on top of the drip shield. The simulations use the same stratigraphic column, rock thermal and hydrological properties, and thermal load as for previous Tptpll THC Model REV02 simulations. Unless specifically mentioned elsewhere in this section, other input data remain unchanged from previous work. Key elements of these simulations include:

- Drift in the Tptpll unit
- Stratigraphy at a location near the center of the repository (at approximately Nevada State Plane coordinates E170572, N233195)
- Initial heat load of 1.45 kW/m, with an initial 50-year period of 86.3% heat removal by ventilation
- Collapsed wallrock material on top of the drip shield, forming a rubble zone extending vertically to a distance equal to twice the diameter of the original drift ($2 \times 5.5 = 11$ m) from the base of the original drift.

The model conceptualization is briefly discussed below (Sections 6.3.1–6.3.4) and is followed by a discussion of the model results (Section 6.3.5) with comparisons to a parallel intact-drift case.

6.3.1 Conceptual Model

The general conceptualization of the THC Seepage Model, including the conceptualization of the simulated coupled processes, chemical system, and model domain, have not changed from previous work (BSC 2003 [162050], Section 6.2). Details concerning this conceptualization are not repeated here.

The conceptualization of the drift degradation zone around the waste package was taken directly from BSC 2003 ([165564], Section 6.4.3.4). The drift is modeled as a collapsed rubble zone above the drip shield (Figure 6.3-1). The drip shield itself is not explicitly modeled, but its effect is taken into account in the effective thermal conductivity input into the model for the space between the waste package and drip shield during postclosure (see BSC 2003 [162050], Section 4.1.7). For simplicity and parallelism with the intact-drift case, this space and the presence of rubble above it, is maintained during the initial 50-year preclosure period, essentially assuming collapse to have occurred immediately after waste emplacement. The space between the waste package and the rubble is kept open, thus conceptually representing an intact drip shield during the post closure period (BSC 2003 [162711], Section 6). The heat load is unchanged from the intact-drift case, also to ensure parallelism between the two cases and thus facilitate comparison of model results. Therefore, as already mentioned in Section 1.3, this conceptualization does not

account for potentially ineffective ventilation in the collapsed drift during preclosure. The loss in ventilation could potentially lead to much higher temperatures. However, it can be assumed that collapse during preclosure would either be unlikely or remediated, such that this eventuality need not be considered further.

The rubble material in the collapsed zone is conceptualized by two continua: (1) rock with Tptpl matrix properties, and (2) void space totaling 23.1% of the rubble zone by volume. The representation assumes rubble to consist of centimeter- to decimeter-wide rock fragments. The void volume fraction was estimated in BSC 2003 ([165564], Section 6.4.3.4) from bulking factors in BSC (2003 [162711] Section 6.4.2.1). The contact area between intact rock and rock fragments in the rubble zone is taken here as the full interface area (between rock and rubble zone) times 76.9% (1 minus rubble zone porosity).

To enable simulations of water-gas-rock interactions in the void continuum, this continuum was assigned an arbitrary solid content of 20% by volume. The total continuum volume (as opposed to true void volume) was adjusted to keep the proportion of true void space at 23.1% of the rubble zone volume. The rubble zone was modeled with a diameter equal to twice the original drift diameter ($2 \times 5.5 = 11\text{m}$) BSC (2003 [162711], Attachment XVIII) and an approximately circular shape (Figure 6.3-1). The corresponding numerical grid and collapsed zone properties are presented in Section 6.3.4.

6.3.2 Alternative Conceptual Model

The drift degradation case discussed here can be considered, by itself, an alternative conceptualization of the THC Seepage Model, complementing the cases with intact drift documented in BSC 2003 ([162050], Section 6.3). Alternative conceptualizations of the collapsed drift itself were not evaluated because such an evaluation was not within the scope of this abstraction report. BSC 2003 ([165564], Section 6.4.3.4) considers two cases of contact area between intact rock and the rubble zone (full area as considered here, and half the full area) for TH simulations (no THC). These two cases can be regarded as alternative TH conceptualizations.

6.3.3 Mathematical Model

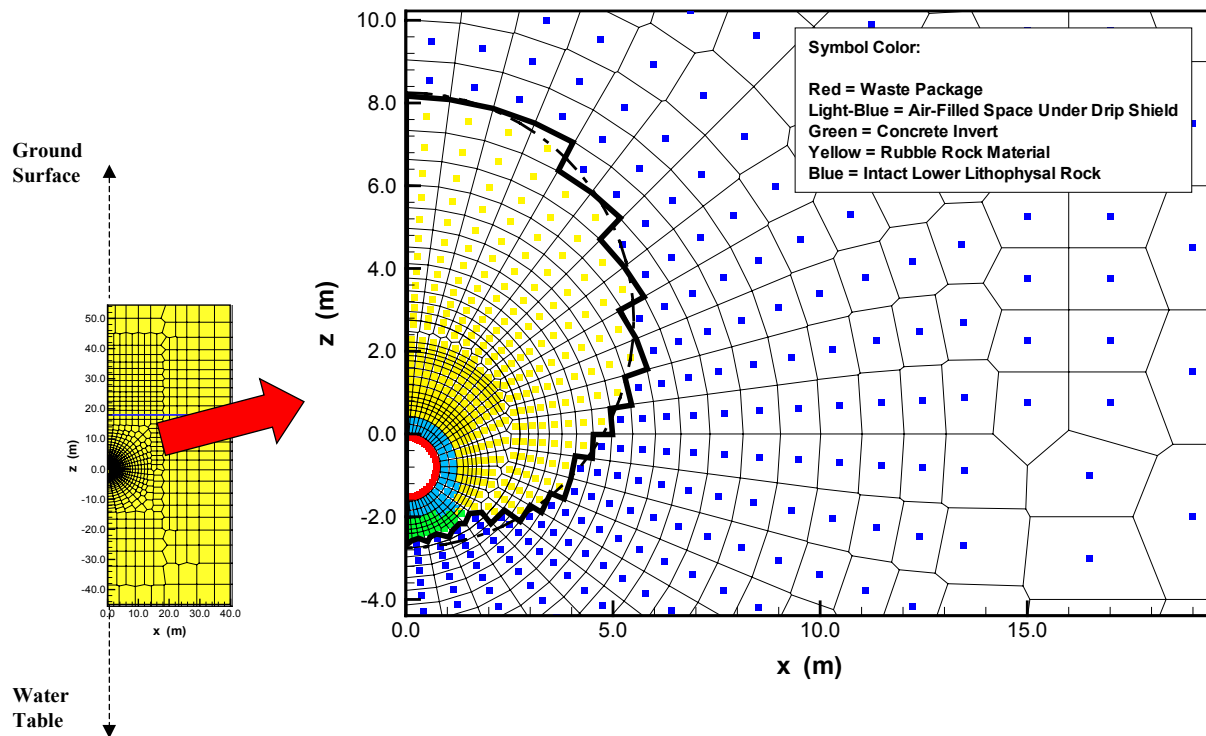
The computer code (TOUGHREACT V3.0, LBNL 2002 [161256]), the mathematical model, and the approximations used for simulations presented in this report are unchanged from BSC 2003 ([162050], Section 6.4). Model setup and specific parameters relating to the collapsed zone are discussed in Section 6.3.4.

6.3.4 Model Setup

The model mesh, boundary conditions, input parameters and other general model setup specifications are summarized below. Except for some important changes made to account for drift degradation, the basic setup and most input parameters remain the same as in BSC 2003 ([162050], Section 6.8).

6.3.4.1 Numerical Mesh

Simulations were performed on a vertical two-dimensional (2-D) mesh taken from BSC 2003 ([165564], Section 6.4.3.4) (Figure 6.3-1). This mesh is similar (but not identical) to the mesh used for the Tptpll THC Model REV01 and REV02 described in BSC 2003 ([162050], Sections 6.7.1 and 6.8.1). It is, however, identical to that used for the drift-scale TH simulations presented in BSC (2003 [161530]). This mesh is an adaptation of the Tptpmn THC Model REV01 mesh (BSC 2003 [162050], Section 6.5.1, Figure 6.5-1) to the stratigraphic column used for the Tptpll model (BSC 2003 [162050], Table 6.7-1). The mesh incorporates a radial grid extending further from the drift wall than the mesh of the Tptpll model. The advantage of this expanded radial grid is that it was already available and could be easily adapted to the case of a degraded drift, without the need for redesign (Figure 6.3-1).



Source: BSC 2003 ([165564], Figure 6.4-23)

Figure 6.3-1. Numerical Mesh for Simulations Considering Drift Degradation. The rubble zone is outlined by a thick solid line, depicting an approximately circular shape (dashed line).

6.3.4.2 Boundary Conditions

Boundary conditions were set as in the Tptpll THC Model REV02 (BSC 2003 [162050], Section 6.8.2) (Table 6.3-1), but considering a degraded rather than intact drift. The same infiltration rates at the top model boundary were used as previously (Table 6.3-2), increasing step-wise to take into account future climatic variations.

Table 6.3-1. Boundary Conditions

Boundary	Boundary Condition
Top (bottom of alluvium near ground surface)	T = 16.13°C S _g = 0.99 P = 84725 Pa Time-varying infiltration rate (mean infiltration regime only) Constant composition of infiltration and PCO ₂
Bottom (water table)	T = 32.62°C S _L = 0.99999 P = 92000 Pa Constant water composition and PCO ₂
Sides	No flux for water, gas, heat, and chemical species
Drift Wall	The wall itself is absent. The drift is collapsed to the drip shield (see Figure 6.3-1), and no liquid or gas fluxes are allowed through the drip shield. The contact area between the rubble zone and intact rock is taken as ~76.9% of the full interface area (Section 6.3.1).
Waste Package	Initial full heat load of 1.45 kW/m decreasing with time (due to radioactive decay), and reduced by 86.3% during the first 50 years (due to heat removal by ventilation)

Data References: BSC (2003 [162050], Table 6.8-1)

NOTES: T = Temperature

S_g = Gas saturation

S_L = Liquid saturation

P = Total system pressure

Table 6.3-2. Infiltration Rates

Case	Infiltration Rate (mm/y)	Time Period (years)
Mean Infiltration (increasing stepwise)	6	0 to 600 (present day)
	16	600 to 2,000 (monsoon)
	25	2,000 to 100,000 (glacial transition)

Data References: BSC (2003 [162050], Table 6.8-2)

6.3.4.3 General Setup, Inputs, and Modeling Procedure

Simulations were run using TOUGHREACT V3.0 (LBNL 2002 [161256]). Simulations were carried out in the same manner and using mostly the same input data as described in BSC (2003 [162050], Section 6.8.5). Differences from previous simulations as well as important simulation details are noted below.

The same thermal and hydrological properties in solid rock were used as previously with the Tptpll THC Model REV02 (BSC 2003 [162050], Table 6.8-4). Properties of the rubble zone

were the same as used in BSC 2003 ([165564], Section 6.4.3.4). The rock matrix blocks within the rubble zone were assigned the properties of the Tptpll matrix. The “void” (true void + 20% rock) continuum in the rubble zone was given an arbitrary high permeability (10^{-10} m²), zero specific heat, and thermal conductivity and tortuosity values as specified for the Tptpll fracture continuum (with applied modifications as described in BSC 2003 [162050], Section 6.4.6.1, Approximations 11 and 17). The bulk porosity of the rubble zone was set to 0.231 (Section 6.3.1).

The “void” continuum in the rubble zone was set with an arbitrary small initial liquid saturation (10^{-5}). Initial liquid saturations in the rubble matrix continuum were set to the same values as in adjacent solid rock matrix under ambient conditions.

Two simulations were run (Table 6.3-3). The first simulation considers only coupled thermal-hydrological effects (no chemical reaction) and provides a baseline for the second simulation considering coupled thermal, hydrological, and chemical effects. Only one input water composition was considered (Table 6.3-3). Also, the molecular diameter of CO₂ was taken as 2.5×10^{-10} m (see BSC 2003 [162050], Section 6.8.3), yielding a diffusion coefficient consistent for direct comparison with previous run thc6_w0b (Table 6.3-3) for the case of an intact drift.

Table 6.3-3. Drift-Scale Simulations Considering Drift Degradation

Input Water ^a	Infiltration Case (Table 6.3-2)	Equation of State (EOS) Module ^b	Simulation Type	Run ID (used in Output-DTN LB0311ABSTHCR2.001; also see Attachment II)	Directly Comparable Corresponding Run for Intact Drift Case ^c
None	Mean Infiltration	EOS4	TH (2-D)	th6_col	th6_1.45kw
W0	Mean Infiltration	EOS4	THC (2-D)	thc6_w0col	thc6_w0b

NOTE: a HD-PERM water composition as shown in Attachment III

b TOUGHREACT V3.0 (LBNL 2002 [161256]) flow modules: EOS4 takes into account the effect of vapor pressure lowering due to capillary pressure.

c Run ID of directly comparable simulations considering an intact drift, presented in BSC (2003 [162050], Table 6.8.4)

6.3.5 Simulation Results

The model results are presented below for the TH (base line) and THC simulations considering drift degradation. All model results were submitted to the technical database under DTNs as listed in Attachment I.2.

6.3.5.1 TH Results (No Chemical Reaction)

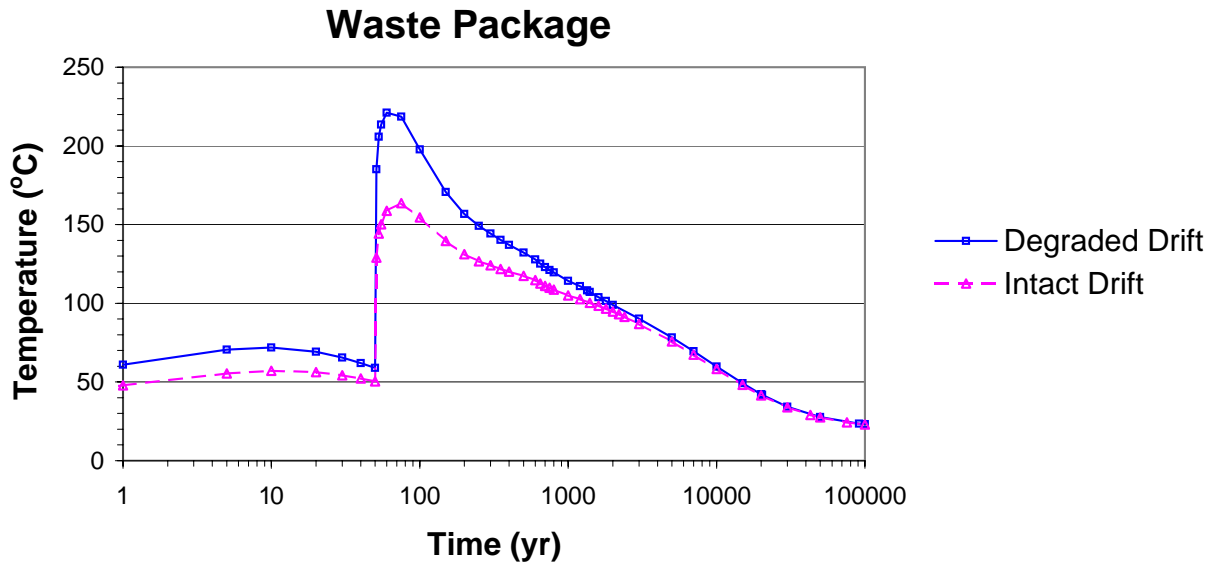
Detailed TH results for simulations considering drift degradation are presented in BSC 2003 ([165564], Section 6.4.3.4) for an essentially identical model setup. For this reason, TH results are only discussed briefly here. These results are compared below to results of intact-drift simulations presented in BSC 2003 ([162050], Section 6.8.5.2) and are consistent with those presented in BSC 2003 ([165564], Section 6.4.3.4).

The presence of rubble wallrock material directly above the drip shield causes the waste package temperature to increase by approximately 60°C (at peak temperatures at around 70 years)

compared to the intact-drift case (Figure 6.3-2). For both the intact- and degraded-drift cases, temperatures remain similar at locations corresponding to the crown and springline of the intact-drift wall (Figures 6.3-3a and 6.3-3b). At the base of the drift, however, the effect of drift degradation on temperature is most pronounced, with temperatures higher by approximately 32°C (at peak temperature at around 70 years) in the degraded-drift case because, in contrast with the intact-drift case, rubble rock fragments prevent radiative heat transport from taking place above the waste package. Correspondingly, the effect of degradation on the size of the dryout zone (Figures 6.3-4a and 6.3-4b) is visible essentially only below the drift. In matrix, the maximum extent of dryout is approximately 6 m below the original drift center (at 100–150 years), compared to approximately 4.5 m for the intact drift case. In fractures, the effect is more noticeable, with maximum dryout (at around 600 years) extending approximately 14 m below the drift compared to 10 m for the intact-drift case. The extent of dryout above the drift does not change significantly between the two cases (approximately 4.5 m in matrix and 7.5 m in fractures above drift center for both cases).

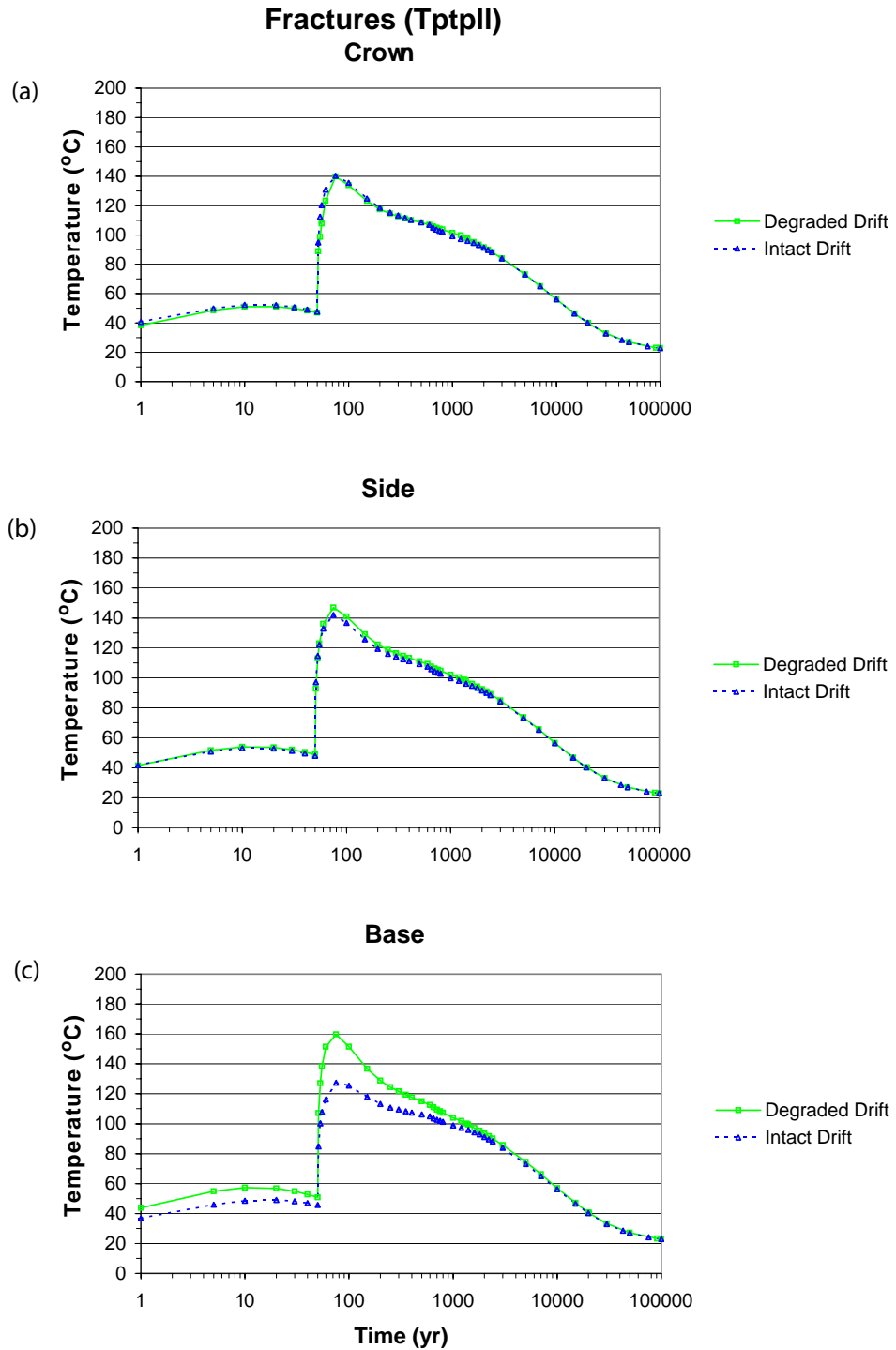
The most important difference between the intact- and degraded-drift cases, with respect to impact on water-rock interactions (Section 6.3.5.2), is that the contact between the intact rock and the rubble zone acts as a capillary barrier for water flowing into fractures. As a result, incoming fracture water is diverted around the rubble zone, from a point higher above the waste package than if diversion occurred directly around the intact drift wall. Furthermore, the boiling front is predicted to always remain below the contact between the rubble zone and intact rock. Consequently, fracture water above the location of the original drift wall never boils.

At the locations of the original drift crown, springline, and base, liquid saturations in the “void” medium of the rubble zone remain mostly nil (Figure 6.3-5). Small non-zero liquid saturations are predicted during the first 50 years at the base and crown locations and at the base at around 15,000 years as a result of condensation (Figures 6.3-5a and c). Liquid saturation profiles for the matrix (Figure 6.3-6) show that the drift base rewets at later times for the drift degradation case (at 600 versus 250 years). These profiles also show that the matrix rewets slower, and that the effect of infiltration increase imposed on the model at 2,000 years (from 16 to 25 mm/year) appears to be delayed. Predicted air mass fractions do not change significantly (Figures 6.3-7) between the intact- and degraded-drift cases, as would be expected. Because of the capillary barrier effect discussed earlier, there is no vertical liquid flux in fractures (“void” medium) at the location of the original drift crown during postclosure (Figure 6.3-8). The flux peak at 50 years is the result of condensation and is not very meaningful, because modeled conditions during the first 50 years (drift collapse with ventilation, see Section 6.3.1) cannot be expected to be very representative of real conditions.



Output-DTN: LB0311ABSTHCR2.003

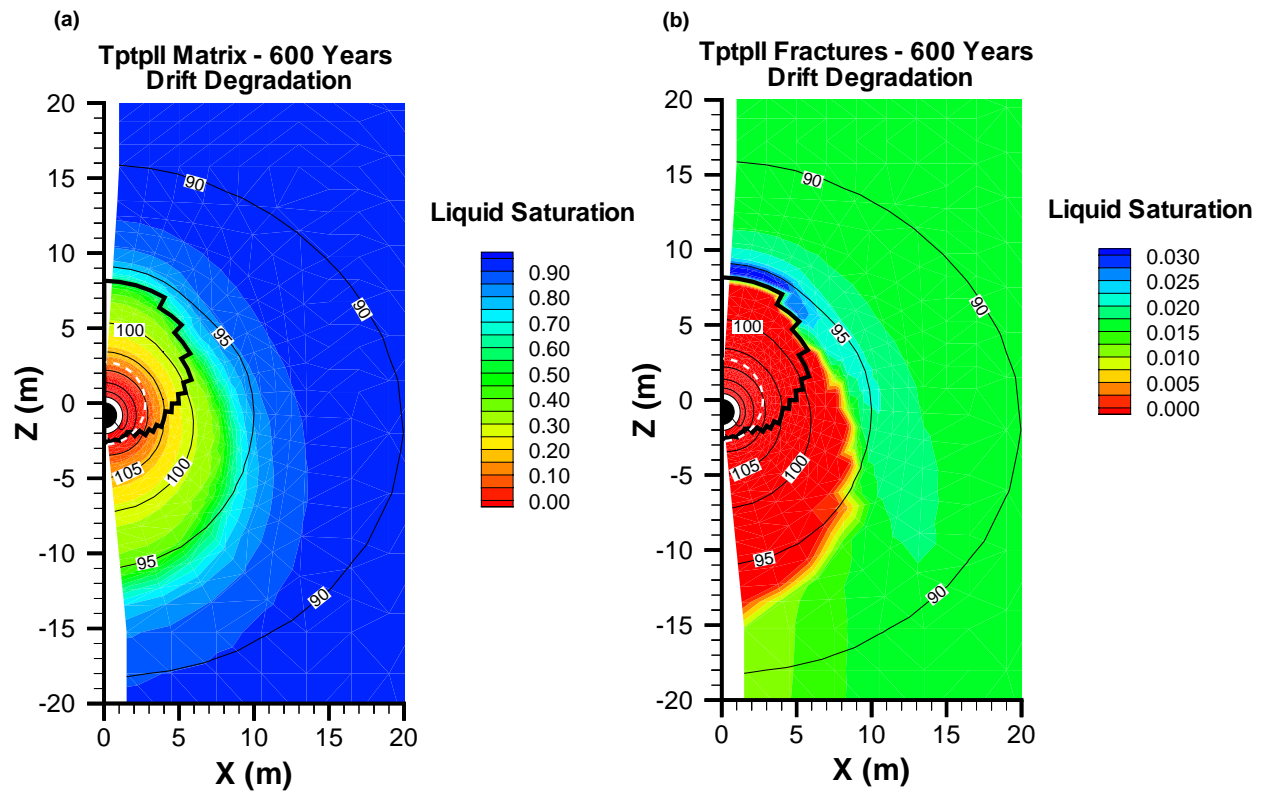
Figure 6.3-2. TH Simulation (Degraded vs. Intact Drift): Time Profiles of Modeled Waste Package Temperatures



Output-DTN: LB0311ABSTHCR2.003

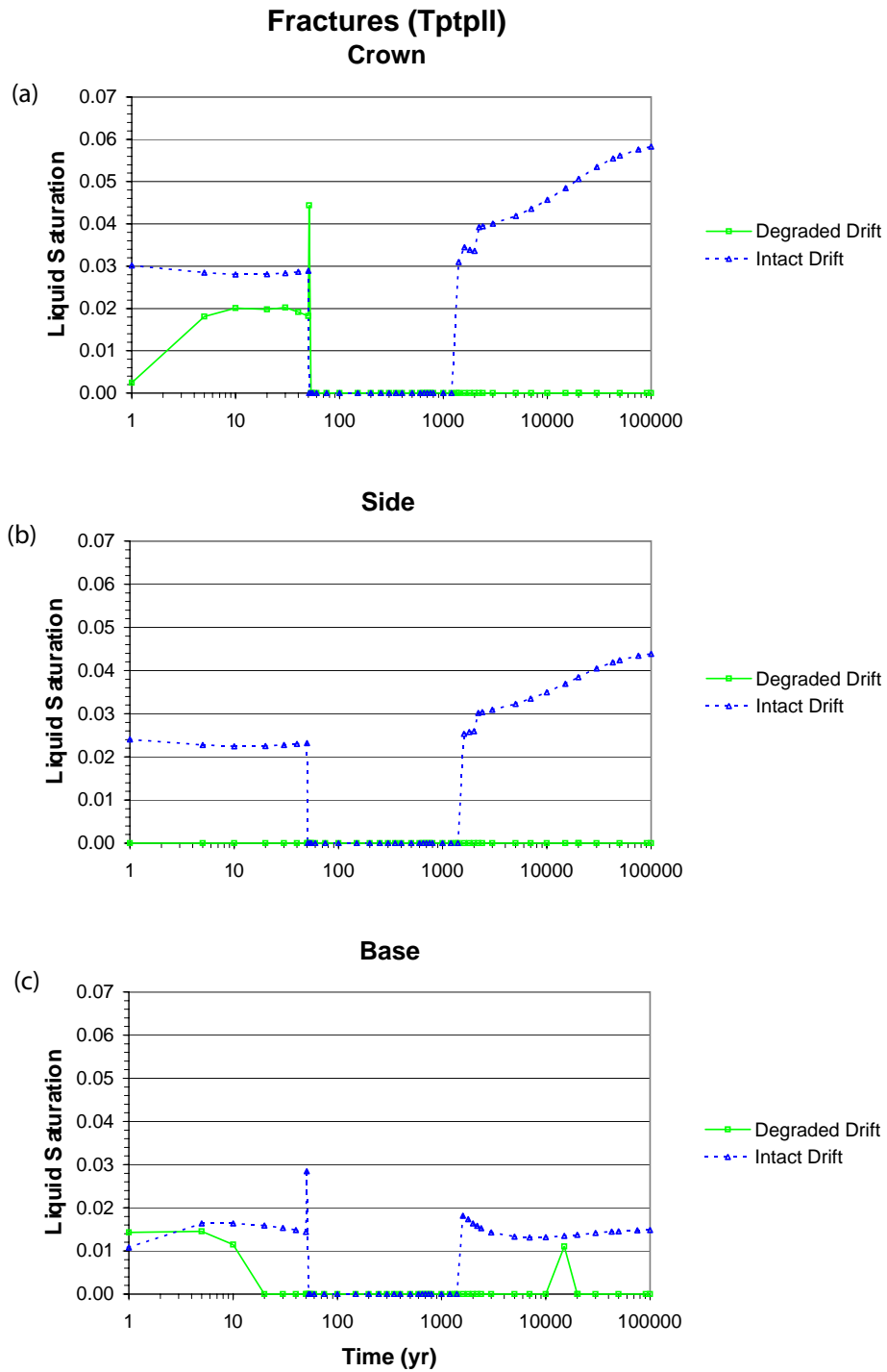
NOTE: For the degraded-drift case, the crown, side, and base locations refer to points located in the rubble zone at the location of the original crown, springline, and base of the intact drift; “fractures” in the rubble zone correspond to the void continuum in this zone.

Figure 6.3-3. TH Simulation (Degraded vs. Intact Drift): Time Profiles of Modeled Temperatures in Fractures at Three Drift-Wall Locations



NOTE: The white dashed line shows the trace of the original drift wall, and the thick solid line delineates the rubble zone.

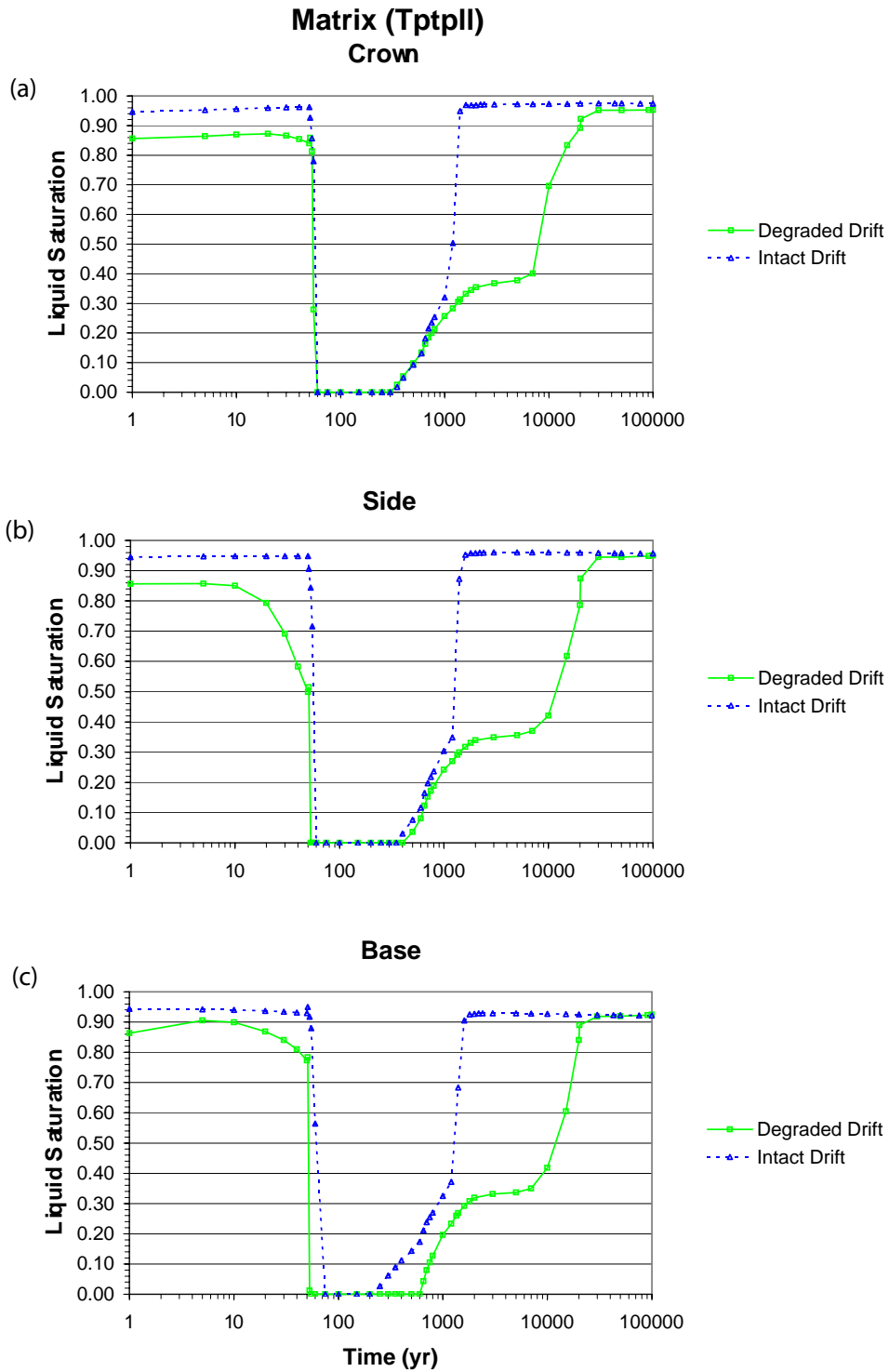
Figure 6.3-4. TH Simulation (Degraded Drift): Contour Plot of Modeled Temperatures (solid contour lines, in°C) and Liquid Saturations in the Matrix and Fractures at 600 Years (color scale) Near the Time of Maximum Dryout in Fractures



Output-DTN: LB0311ABSTHCR2.003

NOTE: For the degraded-drift case, the crown, side, and base locations refer to points located in the rubble zone at the location of the original crown, springline, and base of the intact drift; “fractures” in the rubble zone correspond to the void continuum in this zone.

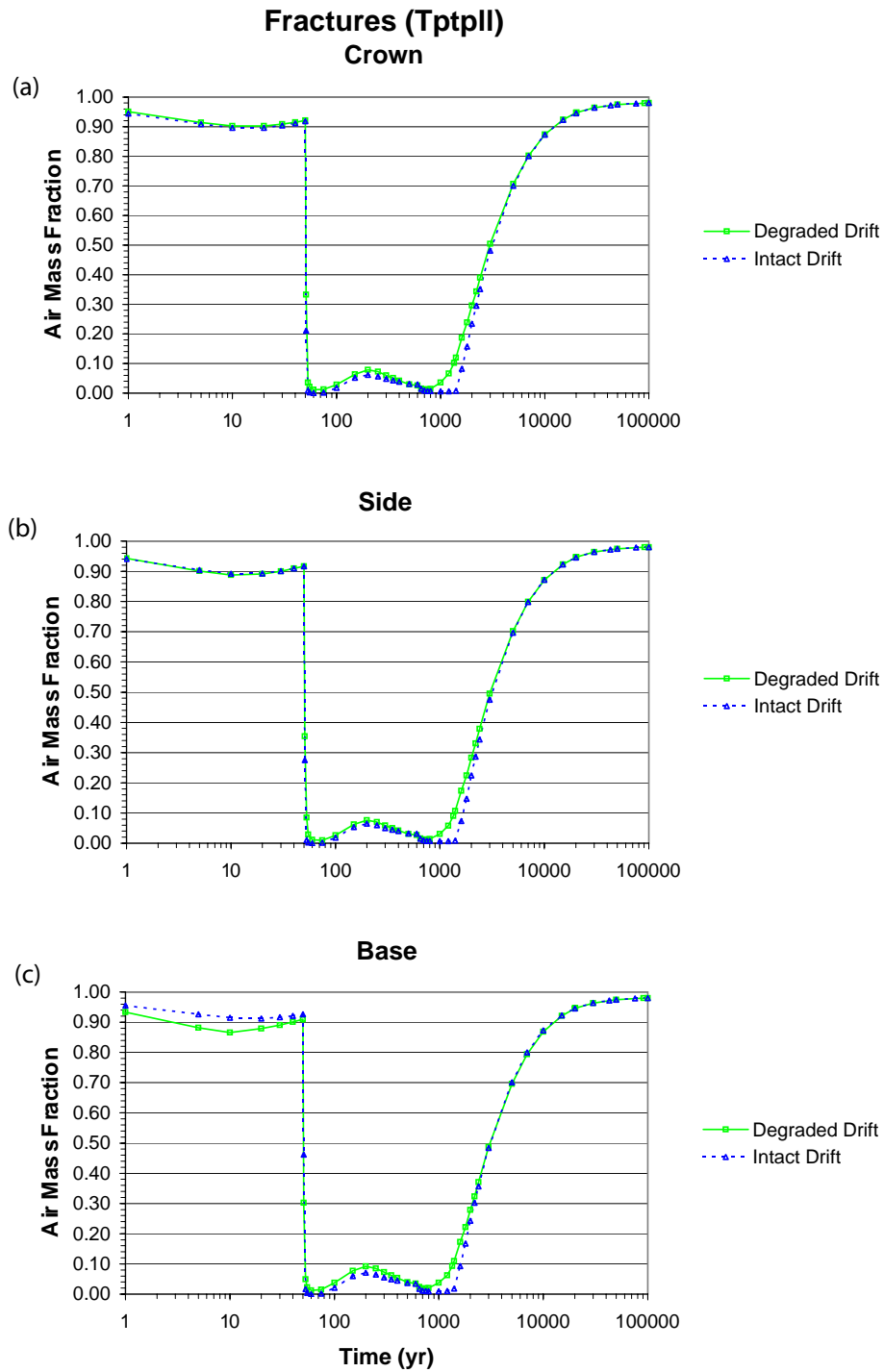
Figure 6.3-5. TH Simulation (Degraded vs. Intact Drift): Time Profiles of Modeled Liquid Saturations in Fractures at Three Drift-Wall Locations



Output-DTN: LB0311ABSTHCR2.003

NOTE: For the degraded-drift case, the crown, side, and base locations refer to points located in the rubble zone at the location of the original crown, springline, and base of the intact drift.

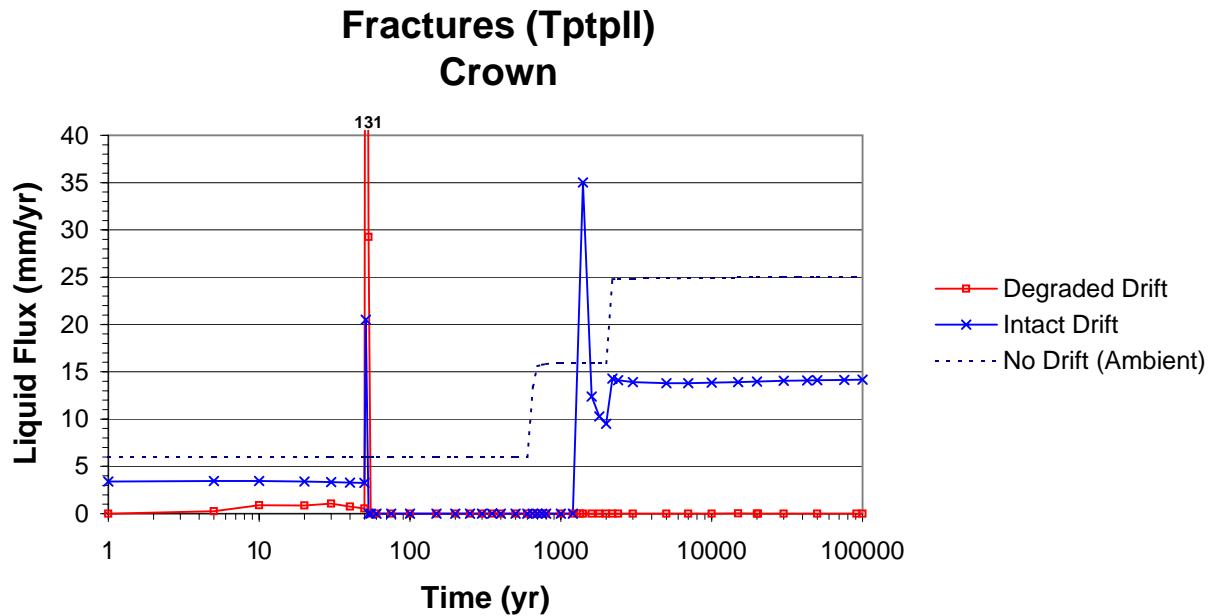
Figure 6.3-6. TH Simulation (Degraded vs. Intact Drift): Time Profiles of Modeled Liquid Saturations in Matrix at Three Drift-Wall Locations



Output-DTN: LB0311ABSTHCR2.003

NOTE: For the degraded-drift case, the crown, side, and base locations refer to points located in the rubble zone at the location of the original crown, springline, and base of the intact drift; “fractures” in the rubble zone correspond to the void continuum in this zone.

Figure 6.3-7. TH Simulation (Degraded vs. Intact Drift): Time Profiles of Modeled Air Mass Fractions in Fractures at Three Drift-Wall Locations



NOTE: For the degraded-drift case, the crown location refers to the point located in the rubble zone at the location of the original crown of the intact drift; “fractures” in the rubble zone correspond to the void continuum in this zone.

Figure 6.3-8. TH Simulation (Degraded vs. Intact Drift): Time Profiles of Modeled Vertical Water Flux in Fractures at the Drift Crown

6.3.5.2 THC Results

Results of THC simulations (predicted CO_2 and aqueous species concentrations) for the degraded-drift case were processed using the same spatial abstraction procedure as described previously in Section 6.2.1.1 for the intact-drift case, using waters selected using the same criteria to define potential seepage (Figure 6.2-3). Although the abstraction procedure and criteria are identical for both cases, the location of extracted data points for the degraded- and intact-drift cases are not necessarily the same (Figure 6.3-9). The diversion of fracture flow around the rubble zone causes FRONT-TOP, FRONT-BASE and HISAT-TOP waters in fractures generally to remain farther away from the original drift center than in the case of an intact drift (Figure 6.3-9a, b, and c). Before 50 years and after 2000 years, condensation in the rubble zone above the drift causes the wetting front to move into the rubble zone (Figure 6.3-9a). Note that the numerical mesh is not exactly the same in the intact- and degraded-drift cases, and thus abstracted locations could never match exactly. The changes in grid node coordinates, however, are much smaller than the changes in abstracted grid node locations resulting from differences in simulated TH behavior.

Predicted temperatures (Figure 6.3-10) and liquid saturations (Figure 6.3-11) in abstracted model gridblocks also show differences between the degraded- and intact-drift cases. Although the temperature profiles do not show large differences between the two cases (Figure 6.3-10), the

slightly lower temperatures of the FRONT-TOP and HISAT-TOP waters in the degraded-drift case (because temperatures are abstracted from grid nodes farther away from the waste package) are mostly below boiling. This has critical implications for the predicted water compositions and mineral precipitation patterns discussed below. This also affects liquid saturation profiles above the drift. Owing to the absence of boiling, liquid saturations remain larger during the evaporative concentration stage (defined previously for the intact drift case, from approximately 150 to 600 years; see Section 6.2.1.2) (Figures 6.3-11a and c). However, the absence of boiling results in smaller liquid saturations at later times because of decreased reflux (less water is mobilized by boiling and condensation), and because of water diversion around the rubble zone.

Predicted profiles of pH for the intact- and degraded-drift cases are similar (Figure 6.3-12), with somewhat lower values (by half a pH unit or so) for the intact-drift case from approximately 150 to 600 years (Figures 6.3-12a and c). The somewhat lower pH during this time period for the intact drift case is most likely related to the precipitation of calcite driven by evaporative concentration (BSC 2003 [162050], Figure 6.8-46). In the degraded-drift case, essentially no mineral precipitation driven by evaporative concentration takes place above the drift, as discussed subsequently.

CO₂ concentration profiles are similar in both cases (Figure 6.3-13), which would be expected because the rubble zone would affect gas flow less than liquid flow. Profiles of total aqueous carbonate concentrations (Figure 6.3-14) are also similar, consistent with the profiles of CO₂ and pH, which show little difference between the intact- and degraded-drift cases.

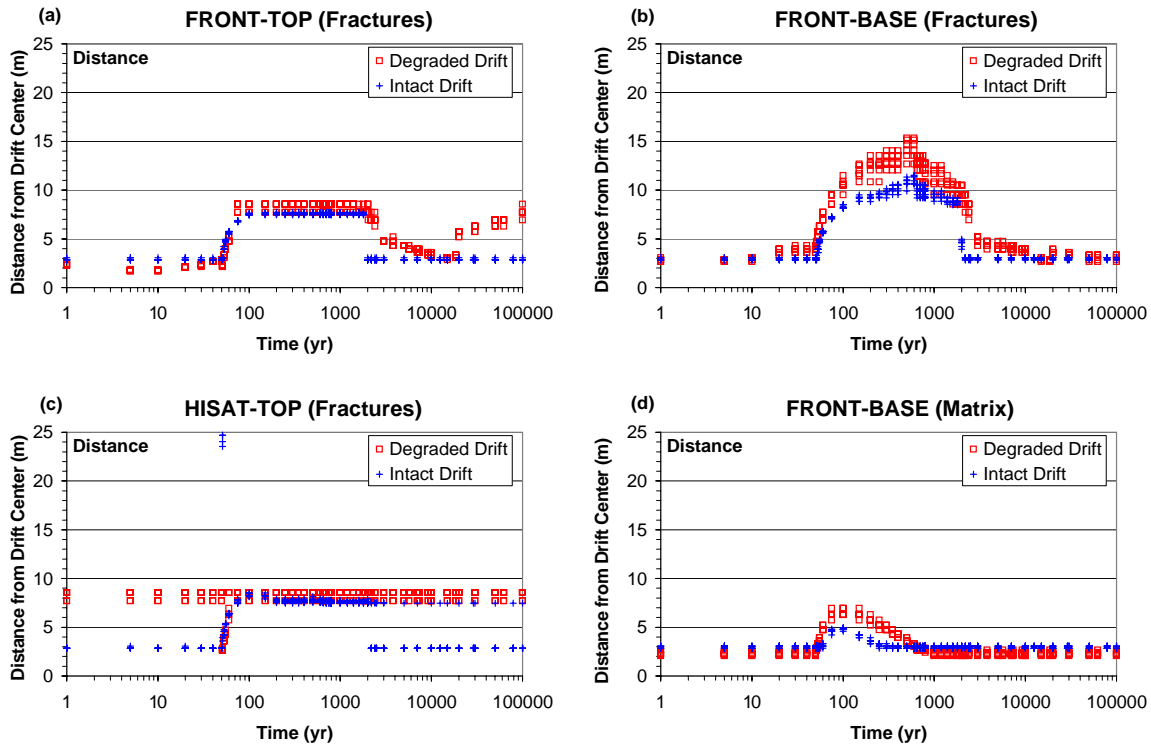
Profiles of predicted aqueous species concentrations (Figures 6.3-15 through 6.3-20) are mostly affected by differences in the degree of evaporative concentration calculated for the intact- and degraded-drift cases. The chloride profiles (Figure 6.3-15) are most indicative of these differences because this species exhibits a conservative behavior in the range of ionic strength (and liquid saturations) considered here. The lack of boiling and evaporative concentration in the degraded-drift case results in concentrations that remain at or below ambient for HISAT-TOP waters (Figure 6.3-15c) (dilution still occurs from condensation of evaporated matrix water in fractures or steam mobilization from other areas). Some evaporative concentration occurs in FRONT-TOP waters after 2,400 years (Figure 6.3-15a), when temperatures are well below boiling (Figure 6.3-10a). At that time, these waters occur below the capillary barrier defined by the edge of the rubble zone (i.e., below 8.25 m in Figure 6.3-9a) and at small liquid saturations (Figure 6.3-11a). This indicates an origin from *in situ* condensation impacted by diffusion from matrix water (calculated downward vertical liquid fluxes into the rubble zone are null). This condensation is temporary, and the long-term position of the wetting front eventually moves back to the edge of the rubble zone (Figure 6.3-9a). FRONT-BASE fracture waters show similar chloride concentration trends (Figure 6.3-15b), although the elevated concentrations from salt dissolution after rewetting in the intact-drift case are not observed in the degraded-drift case. This is not the case for FRONT-BASE matrix waters (Figure 6.3-15d), which exhibit a temporary increase in chloride concentrations after 600 years, caused by salt dissolution after rewetting of the matrix.

Sulfate and nitrate concentrations follow trends mimicking chloride, because these aqueous species are also essentially conservative for the cases investigated. For this reason, the concentration trends of these species are not shown.

Profiles of other aqueous species (Figures 6.3-16 through 6.3-20) can be analyzed in a similar fashion as done for chloride. In the case of fluoride (Figure 6.3-16), fast equilibration with the mineral fluorite reduces the differences between the intact- and degraded-drift cases. The lack of boiling for FRONT-TOP and HISAT-TOP waters and associated decreased evaporative concentration effect on predicted concentrations is quite noticeable for calcium and sodium (Figures 6.3-17a,c and 6.3-19a,c). The absence of boiling decreases both the magnitude and spatial variability of predicted concentrations for these waters. The FRONT-BASE matrix waters, however, exhibit generally higher and somewhat more spatially variable concentrations in the degraded-drift case compared to the intact-drift case (Figures 6.3-17d and 6.3-19d), as a result of significantly higher temperatures at the base of the drift (Figure 6.3-3). The impact of degradation on predicted total calcium to carbonate ratios is also noticeable (Figure 6.3-18).

The differences in predicted concentrations resulting from drift degradation appear comparable in magnitude to the spread in results presented in Section 6.2.4 for an intact drift, various input water compositions, and variations in other input parameters and model conceptualization. Further quantification of variability would require running simulations of the degraded-drift case for the same range of input parameters and conceptualizations as was considered for the intact-drift case. Nevertheless, the case of drift degradation simulated here would seem to indicate that drift degradation often results in lower predicted concentrations of aqueous species and Ca/CO₃ ratios in fracture FRONT-TOP and HISAT-TOP waters, and higher concentrations in FRONT-BASE waters, particularly in the rock matrix. The fracture FRONT-TOP and HISAT-TOP waters could be given more weight, in terms of their importance for in-drift seepage, than the FRONT-BASE waters.

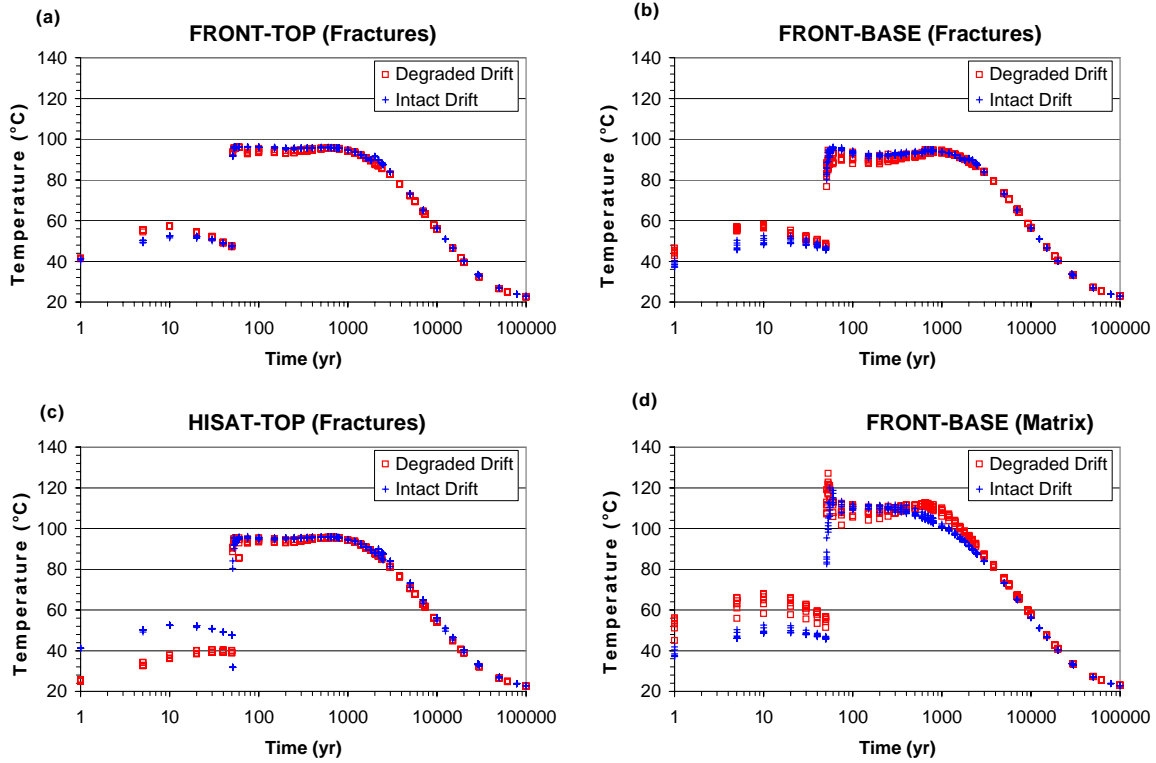
The effect of drift degradation on mineral precipitation was also examined, but is only briefly discussed here because of this report's focus on water and gas chemistry. As mentioned earlier, the edge of the rubble zone acts as a capillary barrier to downward percolation. Even after the end of the boiling period, all downward percolation in fractures is diverted around the rubble zone (Figure 6.3-21). Note that a small amount of water appears for some extent below the capillary barrier (Figure 6.3-21), but this amount represents *in situ* condensation and not actual flow into the rubble zone, as discussed previously. For the case of drift degradation considered here, with a rubble zone diameter twice the size of the original drift diameter, boiling does not extend past the edge of the rubble zone, and downward percolating fracture waters can never reach the boiling isotherm within the rubble zone directly above the drift (Figure 6.3-4b). These waters reach boiling temperatures on the side of the rubble zone (approximately between the 95 and 100°C isotherms on Figure 6.3-4b, to the outside of the rubble zone perimeter). As a result, mineral precipitation occurs primarily at this location and not directly above the drift (Figure 6.3-22). The maximum fracture porosity drop at this location is around 5% of the fracture continuum volume (10% of the fracture void volume) and is caused almost entirely by the precipitation of amorphous silica. The resulting fracture permeability drop is between one and two orders of magnitude (Figure 6.3-22).



Output-DTN: LB0311ABSTHCR2.003

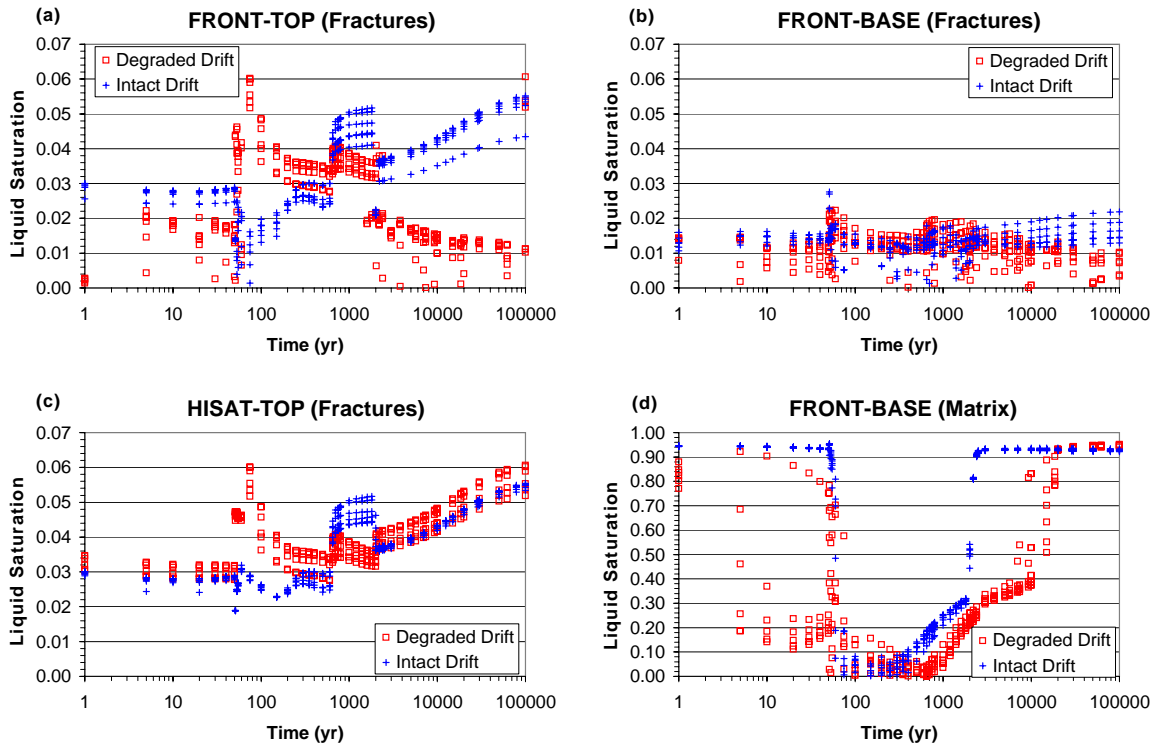
NOTE: Data shown on Figures 6.3-10–6.3-20 are for the same points as shown here. The top of the rubble zone is located at 8.25 m above drift center and the base at 2.75 m below drift center.

Figure 6.3-9. THC Simulation (Degraded vs. Intact Drift): Abstraction around the Modeled Drift as a Function of Time—Distance between Drift Center and Gridblocks Picked Up by the Abstraction Procedure



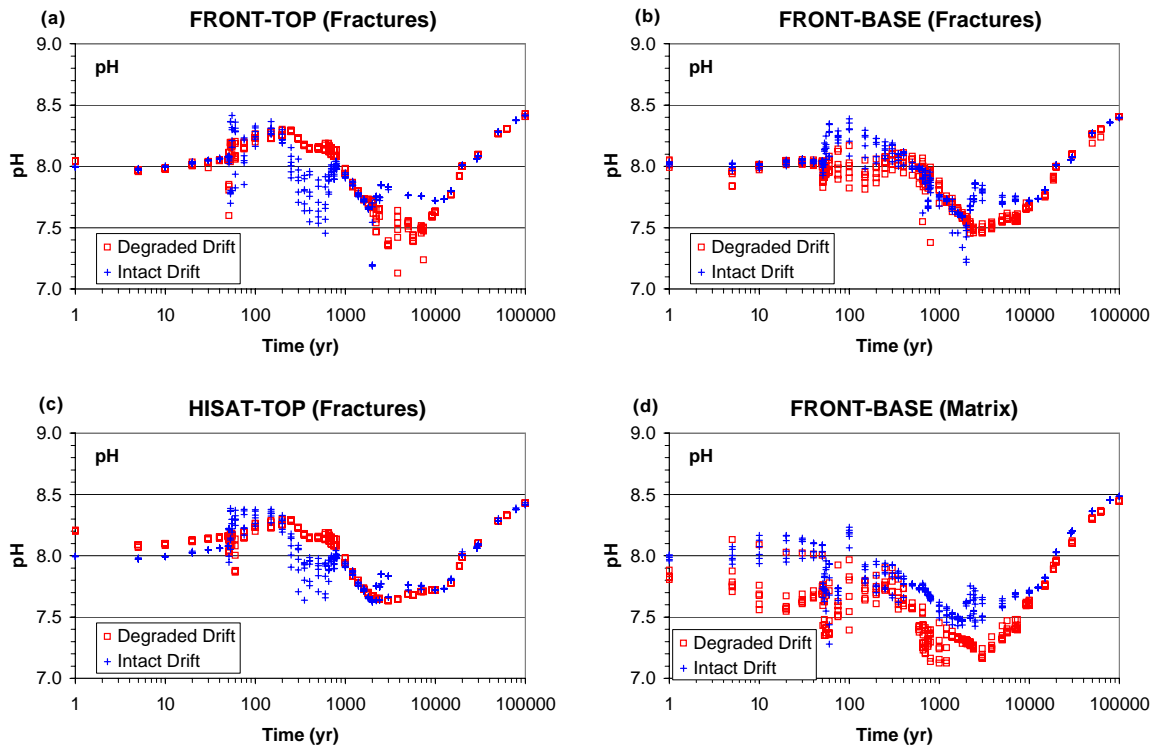
Output-DTN: LB0311ABSTHCR2.003

Figure 6.3-10. THC Simulation (Degraded vs. Intact Drift): Abstraction around the Modeled Drift as a Function of Time—Profiles of Modeled Temperatures



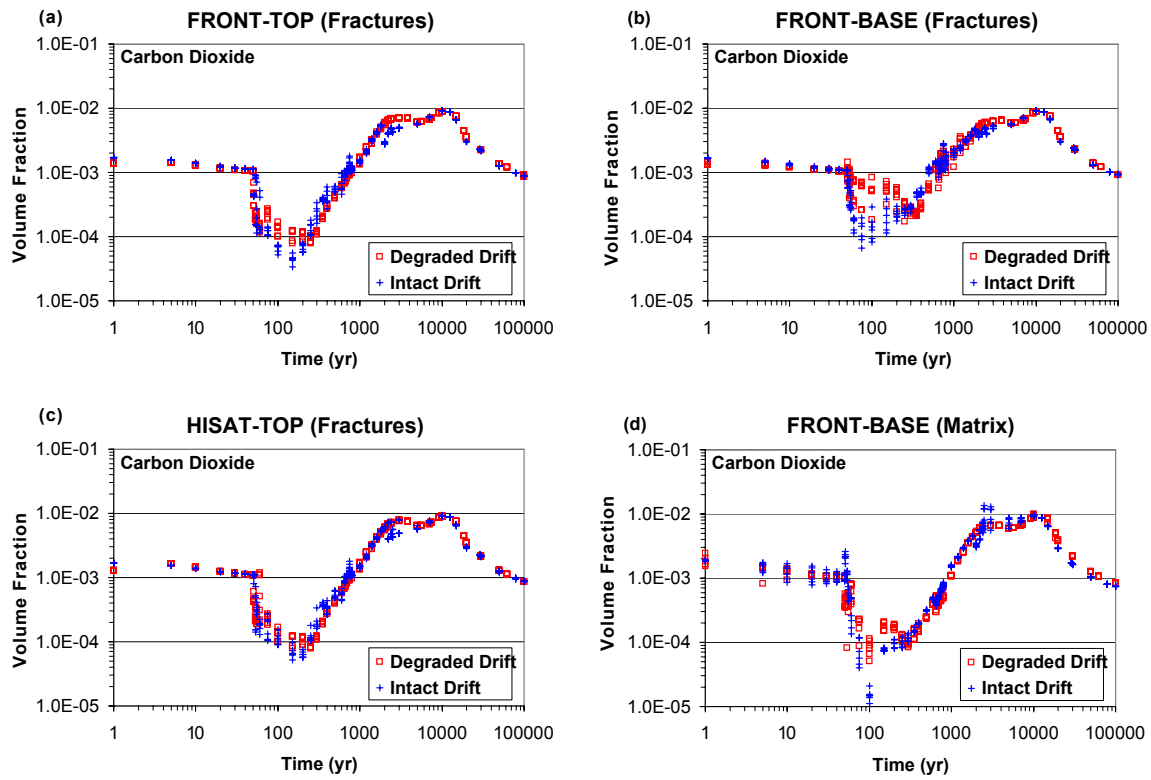
Output-DTN: LB0311ABSTHCR2.003

Figure 6.3-11. THC Simulation (Degraded vs. Intact Drift): Abstraction around the Modeled Drift as a Function of Time—Profiles of Modeled Liquid Saturations



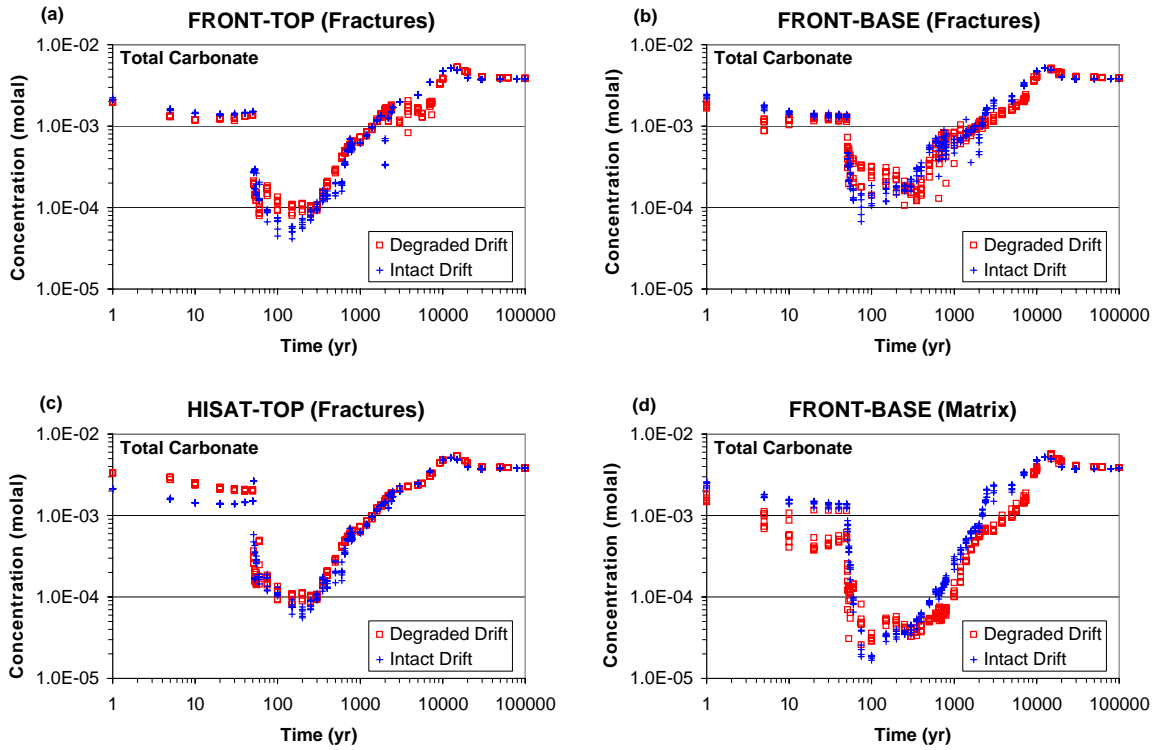
Output-DTN: LB0311ABSTHCR2.003

Figure 6.3-12. THC Simulation (Degraded vs. Intact Drift): Abstraction around the Modeled Drift as a Function of Time—Profiles of Modeled pH



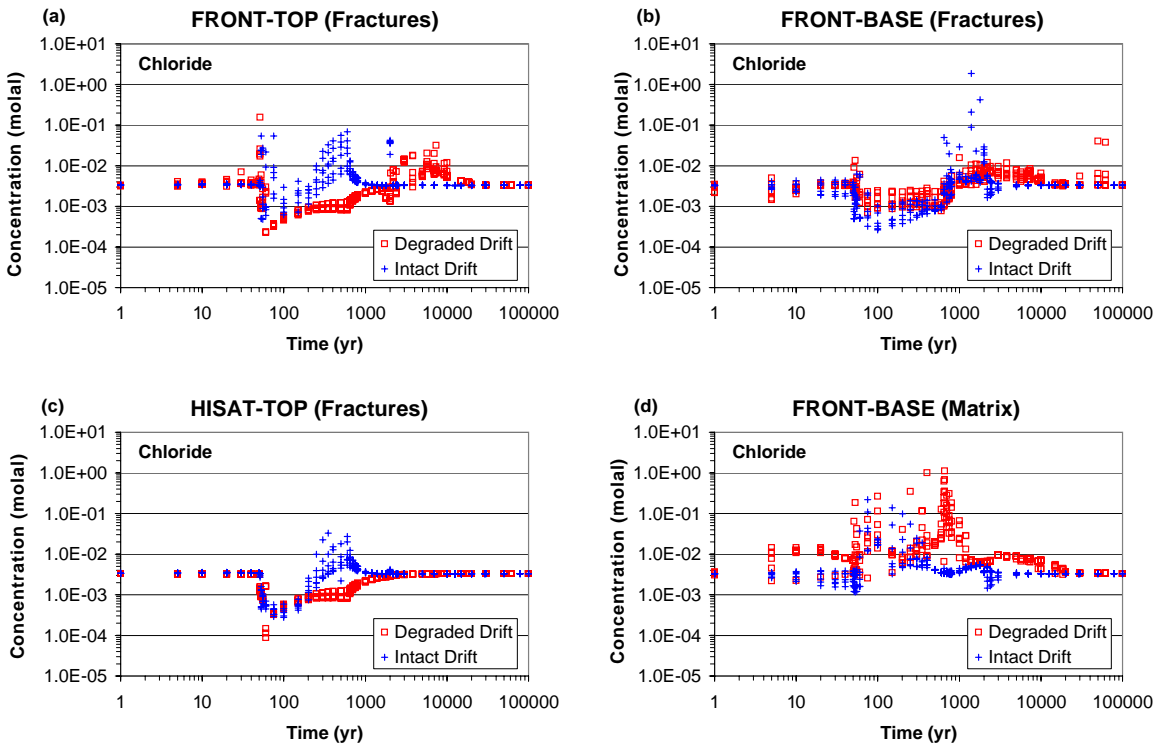
Output-DTN: LB0311ABSTHCR2.003

Figure 6.3-13. THC Simulation (Degraded vs. Intact Drift): Abstraction around the Modeled Drift as a Function of Time—Profiles of Modeled Carbon Dioxide Gas Concentrations



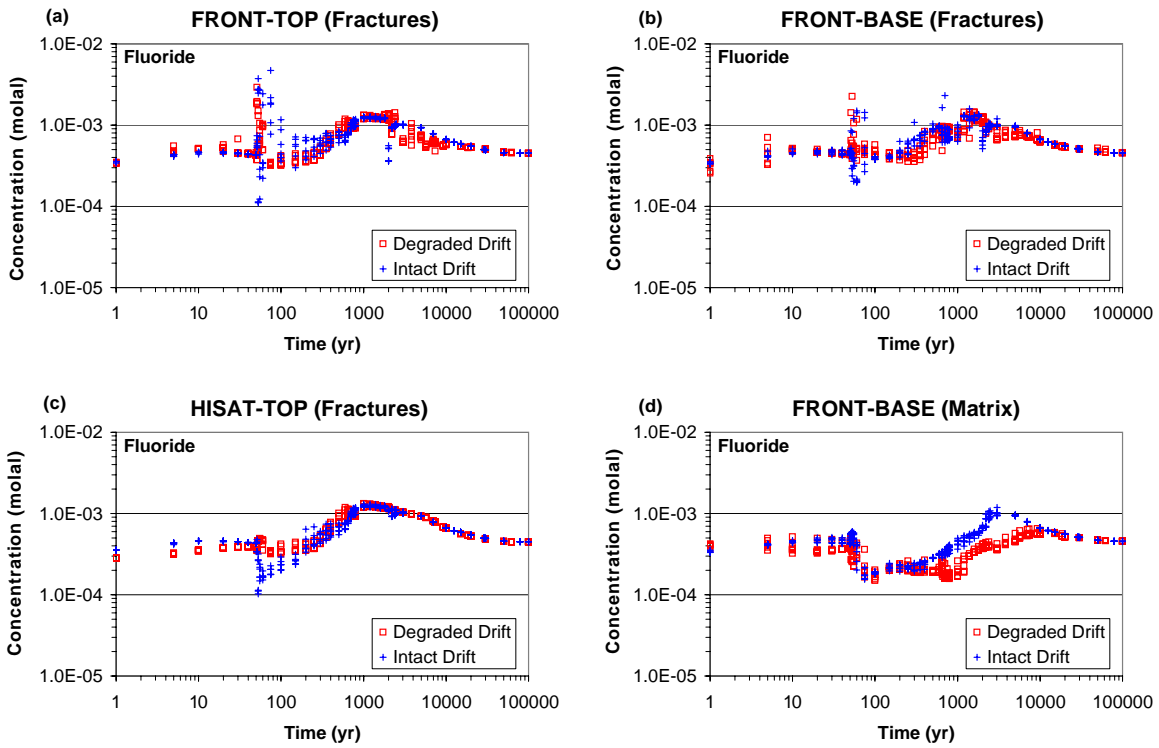
Output-DTN: LB0311ABSTHCR2.003

Figure 6.3-14. THC Simulation (Degraded vs. Intact Drift): Abstraction around the Modeled Drift as a Function of Time—Profiles of Total Aqueous Carbonate Concentrations



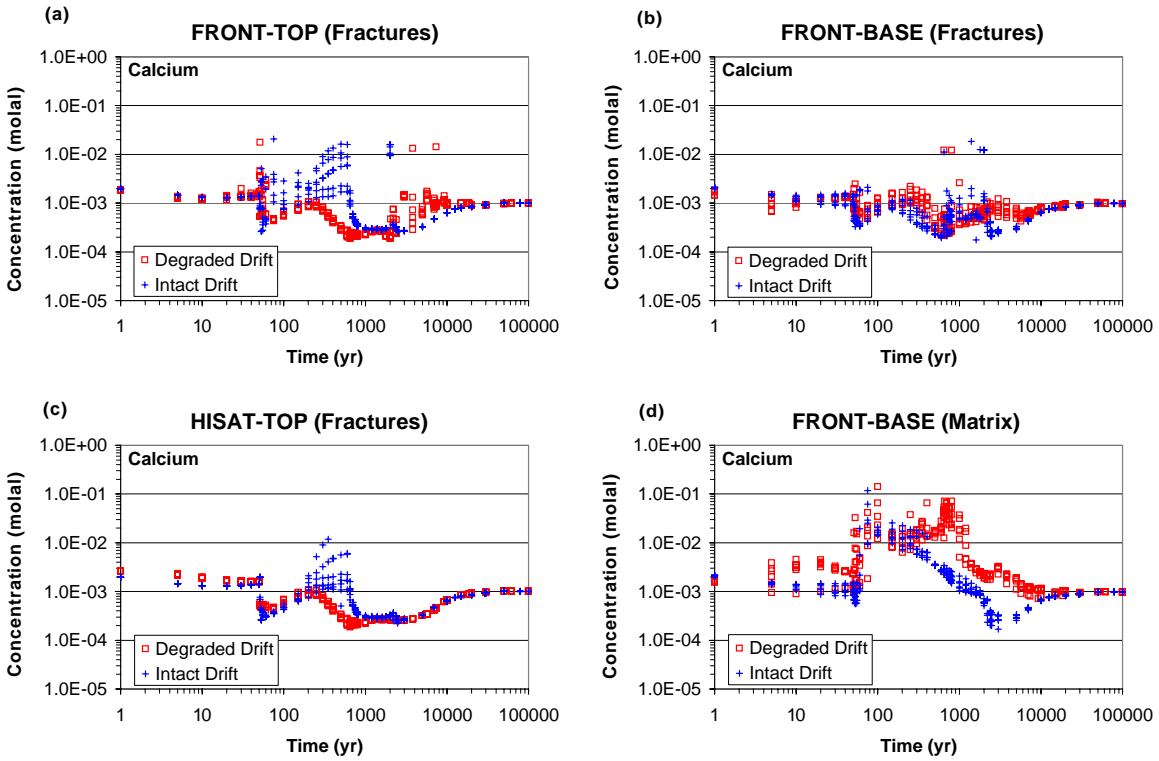
Output-DTN: LB0311ABSTHCR2.003

Figure 6.3-15. THC Simulation (Degraded vs. Intact Drift): Abstraction around the Modeled Drift as a Function of Time—Profiles of Total Aqueous Chloride Concentrations



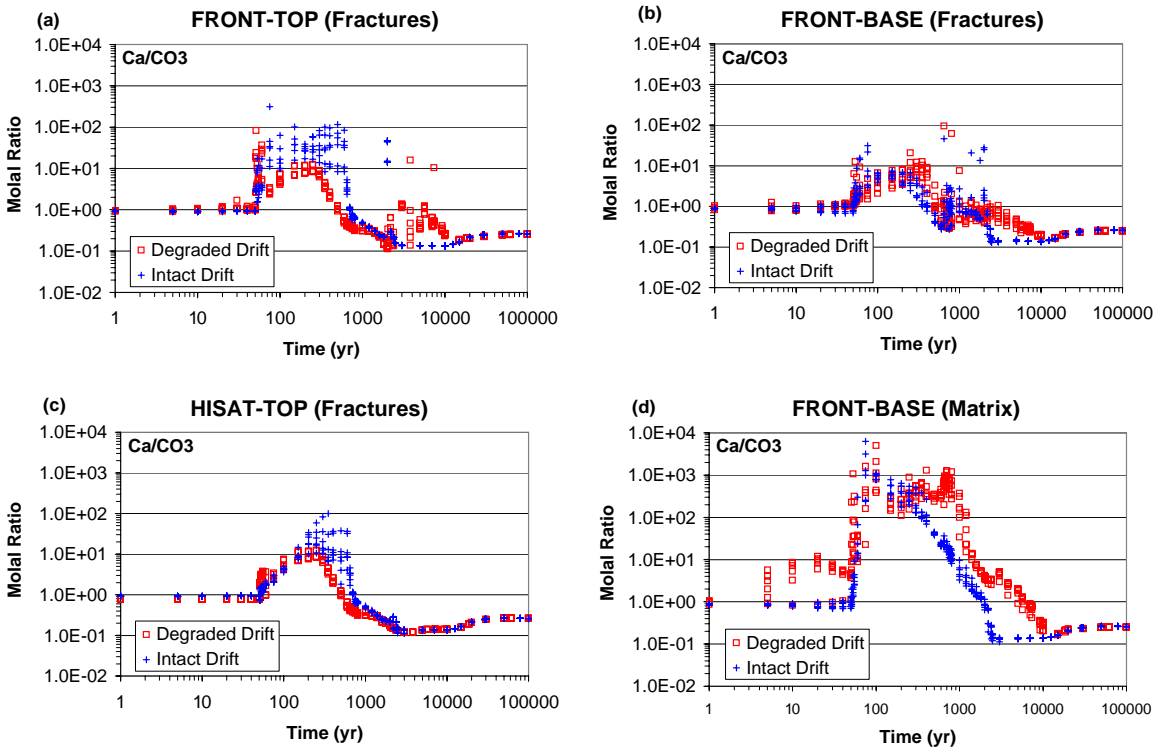
Output-DTN: LB0311ABSTHCR2.003

Figure 6.3-16. THC Simulation (Degraded vs. Intact Drift): Abstraction around the Modeled Drift as a Function of Time—Profiles of Total Aqueous Fluoride Concentrations



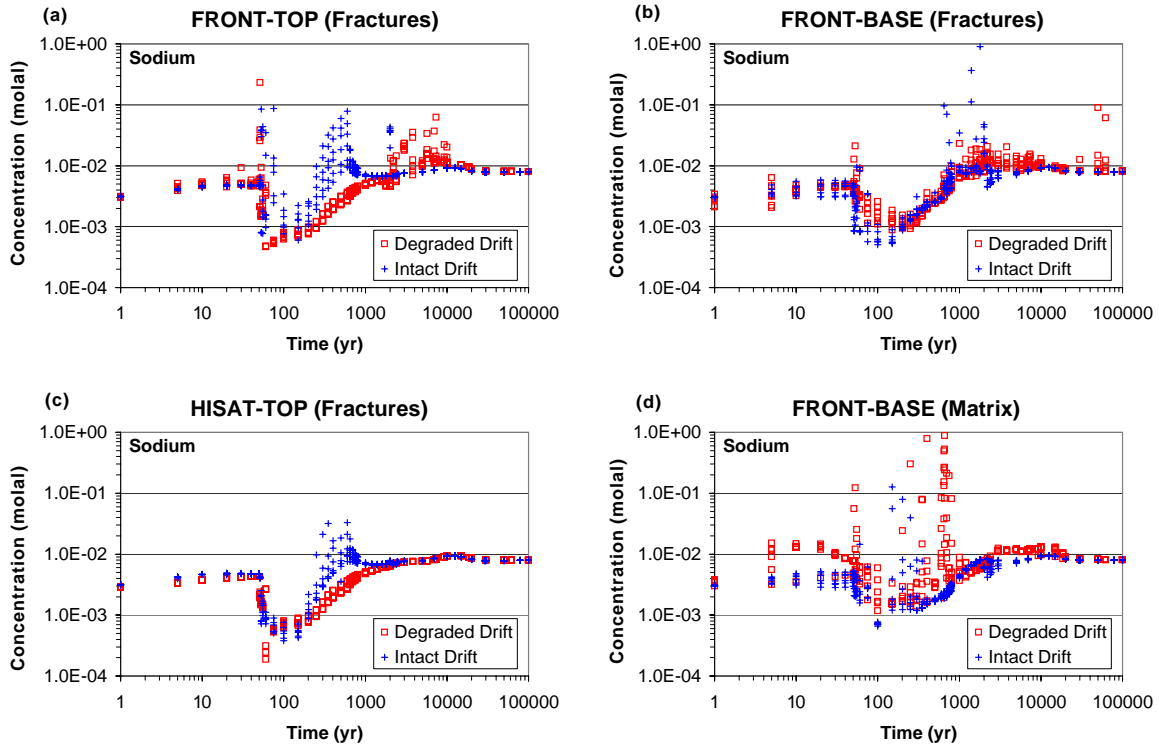
Output-DTN: LB0311ABSTHCR2.003

Figure 6.3-17. THC Simulation (Degraded vs. Intact Drift): Abstraction around the Modeled Drift as a Function of Time—Profiles of Total Aqueous Calcium Concentrations



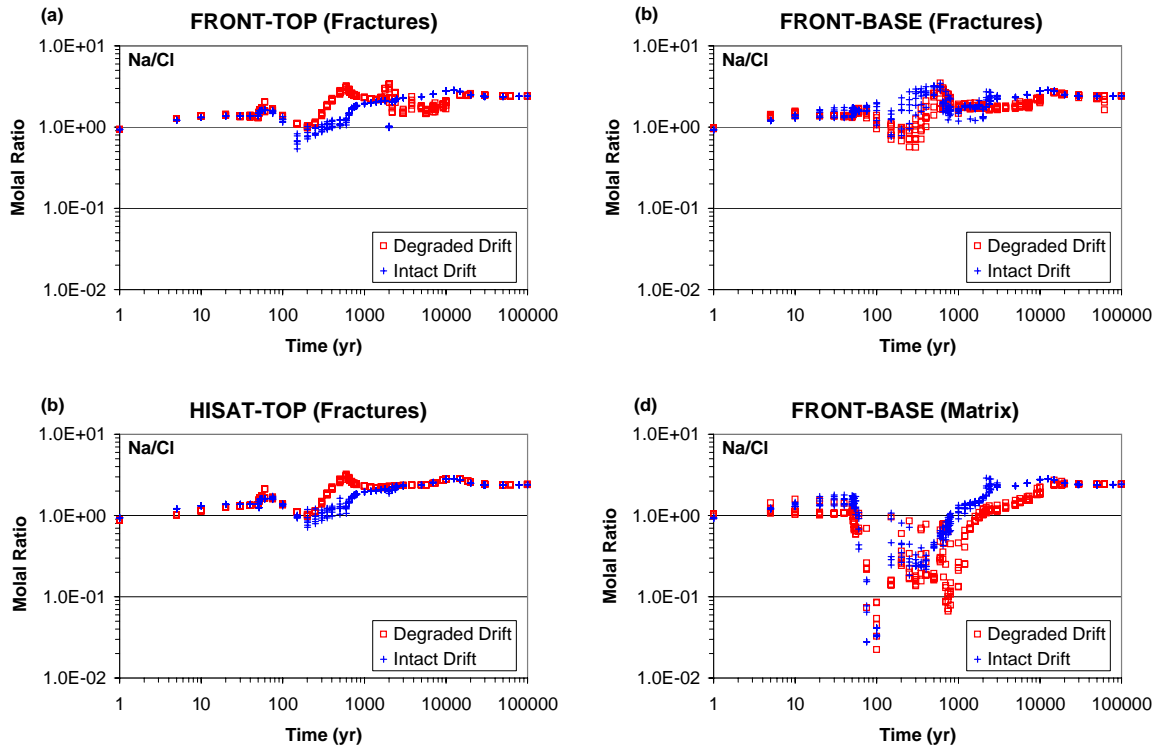
Output-DTN: LB0311ABSTHCR2.003

Figure 6.3-18. THC Simulation (Degraded vs. Intact Drift): Abstraction around the Modeled Drift as a Function of Time—Profiles of Total Aqueous Calcium and Total Aqueous Carbonate Concentrations



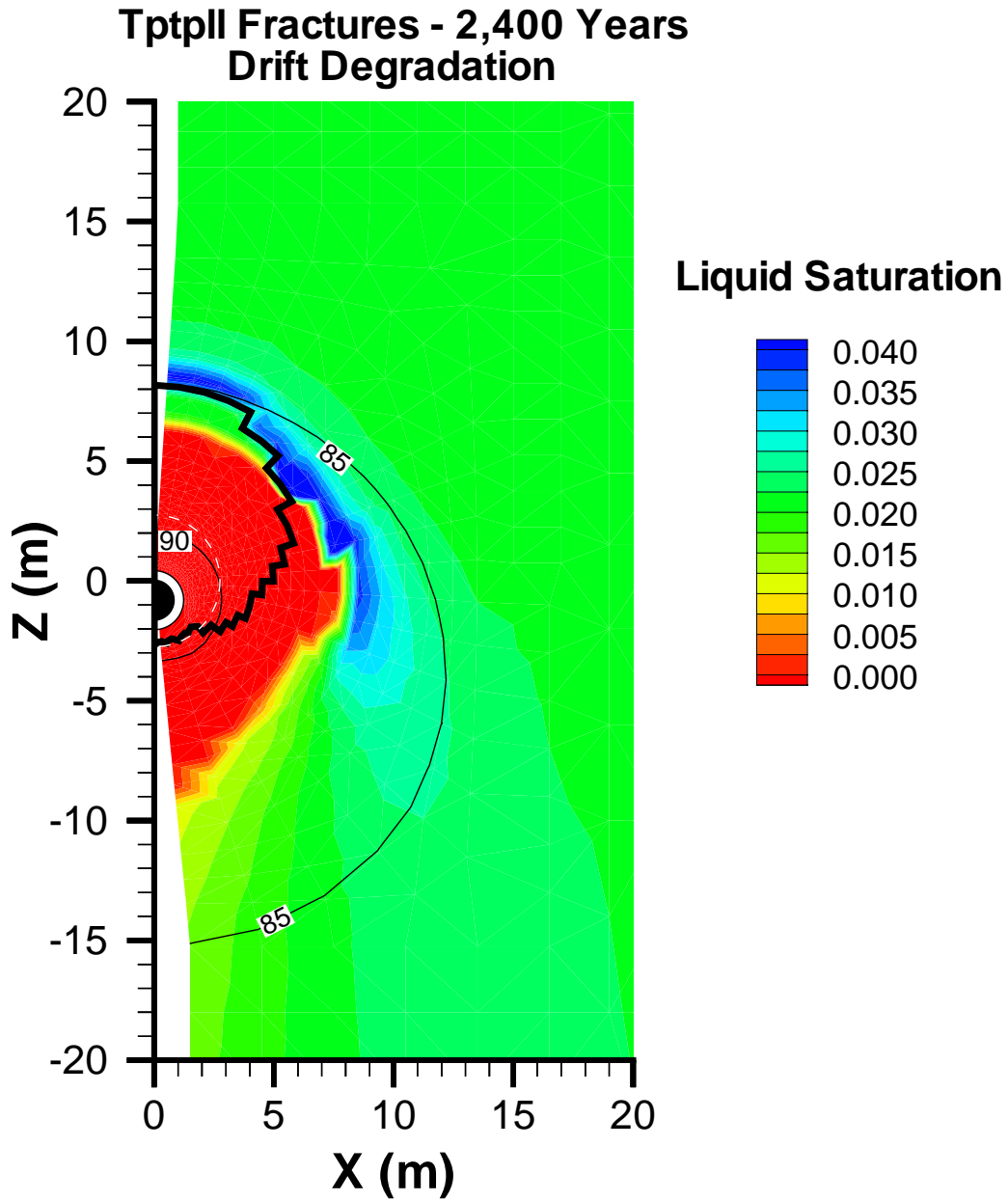
Output-DTN: LB0311ABSTHCR2.003

Figure 6.3-19. THC Simulation (Degraded vs. Intact Drift): Abstraction around the Modeled Drift as a Function of Time—Profiles of Total Aqueous Sodium Concentrations



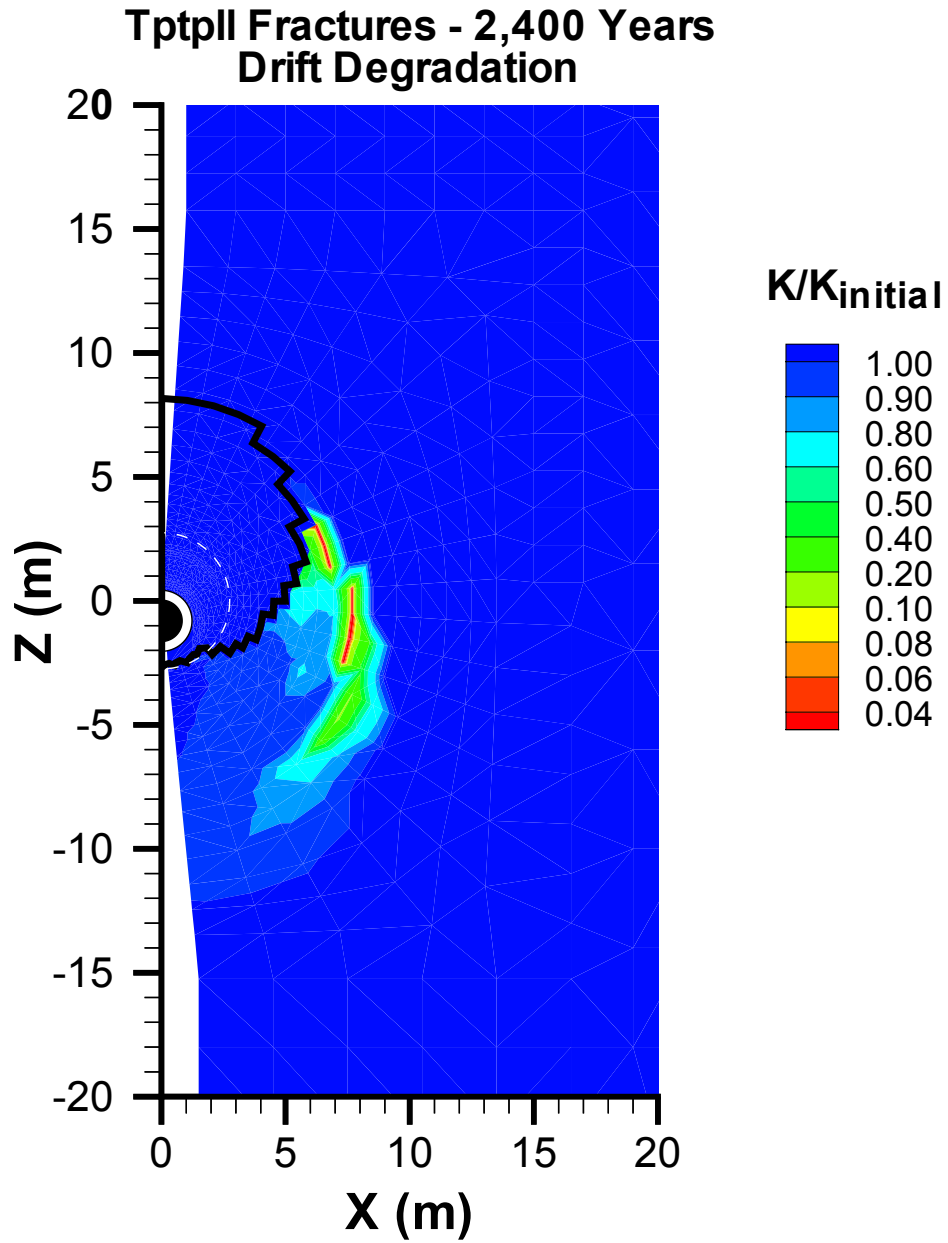
Output-DTN: LB0311ABSTHCR2.003

Figure 6.3-20. THC Simulation (Degraded vs. Intact Drift): Abstraction around the Modeled Drift as a Function of Time—Profiles of Total Aqueous Sodium and Total Aqueous Chloride Concentrations



Output-DTN: LB0311ABSTHCR2.002

Figure 6.3-21. THC Simulation (Degraded Drift): Contour Plot of Modeled Temperatures (solid lines in °C) and Liquid Saturations (color scale) in Fractures at 2,400 Years



Output-DTN: LB0311ABSTHCR2.002

Figure 6.3-22. THC Simulation (Degraded Drift): Contour Plot of Modeled Fracture Permeability Change at 2,400 Years

6.3.5.3 Guidance for Further Abstraction

As pointed out earlier, differences in predicted water and gas compositions between the results of the THC Seepage Model for cases of intact and degraded drifts are primarily related to the location of the boiling front relative to the roof of the rubble (collapsed) zone. For the drift degradation case investigated here, the boiling front always remains within the rubble zone (Section 6.3.5.1). The consequence is that percolating waters directly above the drift are diverted around the rubble zone before they can reach the boiling isotherm. As a result, these waters do not boil and are less concentrated than in the case of an intact drift (Section 6.3.5.2). If the rubble zone were smaller (i.e., less extensive roof collapse), the boiling front could penetrate into intact rock beyond the rubble zone. In such a case, it would be expected that predicted water compositions above the drift, during the boiling period, would be more similar to those predicted for the intact-drift case (thus more concentrated). Therefore, results for the intact-drift case can be regarded as providing more concentrated waters for locations above the drift (and therefore for locations where seepage is more likely) during the boiling period.

It should also be noted that the effect of drift degradation on in-drift seepage rates is investigated in another report (BSC 2003 [165564], Section 6.4.3.4). In that report, a recommendation is made to use ambient seepage rates for the entire TSPA period (BSC 2003 [165564], Section 6.5.3).

6.4 TEMPERATURE EFFECT ON RADIONUCLIDE SORPTION

Potential variations with temperature in the value of the sorption (distribution) coefficient, K_d , for a given radionuclide with respect to a host rock substrate could be important when modeling radionuclide transport in the near field of the nuclear waste repository at Yucca Mountain, Nevada. The near field is considered to be that region around the repository subject to temperature perturbations caused by radioactive decay of the waste. At Yucca Mountain, radionuclide transport in the unsaturated zone is restricted above about 95° C by the absence of a mobile liquid aqueous phase. Therefore, the temperature range of interest would normally range between approximately 0 and 100° C. Another potential reason for understanding variations in K_d with temperature would be the need for making precise corrections in K_d for temperature differences between laboratory experimental conditions and ambient conditions in the far field. However, as examined further below, such corrections would be small, and in any case, differences in physico-chemical conditions between laboratory and the field would probably introduce uncertainties larger than corrections for temperature.

6.4.1 Conceptual Model

Radionuclide sorption involves the uptake of ionic or molecular species of that radionuclide (associated in most cases with nonradioactive isotopes of the same element) from an aqueous solution onto a solid phase. Sorption, R_s , is usually presented as the ratio of the radionuclide partitioned between the aqueous and solid phases, expressed as the percentage sorbed, thus,

$$R_s = 100(A_i - A_f)/A_f \quad (\text{Eq. 1})$$

where A is measured in disintegration counts/second or Bq, and the subscripts, i and f , refer to the initial and final concentrations, respectively. Because a given concentration of a radioelement in solution is normally spiked with a known activity of one of its corresponding

radionuclides, the final concentration of the radioelement in solution can easily be calculated. Thus, $A_i \propto C_o$, where C_o is the initial concentration, usually given as the molarity, mol/mL, and $A_i - A_f \propto (C_o - C_f)$ equivalent to the moles sorbed on a given mass of solid. The ratio is then expressed as:

$$R_d = (C_o - C_f) / C_f \cdot V / m \text{ (mL/g)} \quad (\text{Eq. 2})$$

where V is the volume of solution in mL, and m is the mass of sorbent in g. Use of the term R_d implies that thermodynamic equilibrium has not necessarily been achieved. Upon achievement of equilibrium, R_d can be equated with K_d , the sorption (or distribution) coefficient, which is also expressed in units of mL/g.

If measurements to determine K_d are made at different temperatures, then the dependence of K_d on temperature can be evaluated. This dependence has a thermodynamic basis, which is defined further under Section 6.4.3.2.

Simple models incorporating the K_d term have the advantage of economical data acquisition and convenient incorporation in hydrological computer codes. However, their ability to replicate radionuclide transport in the near field of a nuclear waste repository is less than optimal. Experience with the environmental remediation of contaminated aquifers has demonstrated that transport models incorporating K_d seriously underestimate the length of time required for cleanup and grossly overestimate the maximum concentration at the time of breakthrough (Bethke and Brady 2000 [154437]). However, the objective of aquifer remediation is opposite to that of using a geologic formation as a natural barrier to radionuclide migration. In the former, the goal is to lower groundwater contamination permanently to some mandated standard acceptable for drinking water, whereas in the latter, the goal is to ensure that the radionuclide activity penetrating the barrier never rises above specified limits. The use of K_d formulations to predict radionuclide transport is therefore inherently conservative, because it tends to overpredict the maximum concentration in solution upon breakthrough to the so-called "accessible environment." Thus, such modeling would be consistent with regulatory guidelines requiring conservatism in predicting radionuclide release, i.e., at earlier times and at higher concentrations than would be predicted using more sophisticated site complexation models as illustrated by Bethke and Brady (2000 [154437]).

6.4.2 Alternative Conceptual Models

Models describing sorption range from the most primitive, such as that represented by the K_d term discussed above, to complex multisite surface complexation models. The choice of model for a particular application depends on the nature of the application and the degree of accuracy required. In the following paragraphs, some alternative models are briefly described that could be used, with potential improvements in the accuracy of predictive radionuclide transport simulations.

In Section 6.4.1, it is implicitly assumed that a single K_d value is constant for all radioelement concentrations at a given temperature. This assumption is based on an analysis of an isothermal series of measurements with differing initial aqueous concentrations of a given sorbent, sometimes over many decades of concentration. The resulting logarithms of the sorbed concentration can be plotted in relation to the corresponding logarithms of the equilibrium

concentration in solution. Various equations expressing this relationship have been developed, and are referred to as isotherms. The most commonly assumed relationship is the linear isotherm:

$$\text{Log } C_e = \text{Log}Q + k \quad (\text{Eq. 3})$$

where C_e is the equilibrium concentration of the sorbent in mol/L, usually equivalent to C_f , and Q is the amount adsorbed in mol/g. In rearranging Equation (3), we get $\text{Log } (C_e/Q) = k$ and $k = \log K_d$. This relationship is the basis for applications using K_d values in determinations of radionuclide transport at Yucca Mountain, as discussed above. In practice, experimentally determined isotherms are better fitted to more complex terms, the most common being the Freundlich isotherm (Freundlich 1926 [165848]):

$$\text{Log } C_e = n\text{Log}Q + k \quad (\text{Eq. 4})$$

where n and k are fitting parameters, and the Langmuir isotherm is (Langmuir 1918 [126305]):

$$C_e/Q = 1/(BC_m) + (1/C_m) \cdot C_e \quad (\text{Eq. 5})$$

C_m is the sorption capacity in mol/g, and B is a constant related to the heat of sorption. The applicability of each isotherm varies with the nature of the sorption process under investigation. It can be associated with specific sorption mechanisms, although model fitting is usually empirical. The nature of the sorption process, whether chemical or physical adsorption, ion exchange, or even precipitation, is commonly ignored. Thus, the term “sorption” is used in this Model Report rather than adsorption, unless the process has been specifically identified as the latter. The Freundlich isotherm, in particular, has enjoyed a large measure of success in fitting sorption data, and was long thought to have no theoretical basis. However, Sposito (1980 [127235]) determined that the Freundlich isotherm reflects the competitive adsorption of a tracer species in the presence of another species at much higher concentration. The theoretical basis for the Langmuir isotherm involves adsorption of a sorbent monolayer.

Other isotherms have also been formulated, particularly in relation to separation technology, e.g. the adsorption of gaseous and aqueous organic and inorganic species on activated carbon, or the adsorption of fatty acids on mineral surfaces for the purpose of selective flotation. These isotherms, such as the Flory-Huggins, Frumkin and Dubinin-Radushkevich (D-R) equations (Yehia et al. 1993 [164922]; Atun et al. 1996 [164865]; Sabah et al. 2002 [164909]; Kara et al. 2003 [164880]), could be potentially useful in describing radioelement adsorption on Yucca Mountain host rock minerals. Evaluation as to their suitability for that purpose is, however, beyond the scope of this Model Report. Finally, it should be noted that composite sorption models, invoking additive combinations of various sorption isotherms to describe sorption behavior, have been applied to describe adequately some experimental data, e.g., see Weber et al. (1992 [165228]).

The applicability of various isotherms is restricted to the experimental conditions under which they are tested. Models that permit predictions of sorptive behavior over a range of conditions, taking into account the effect of varying pH, competition between aqueous species, variations in ionic strength, and multiple adsorption sites, require much more sophisticated models. To address this problem, a variety of surface complexation models have been developed. These models require the precise measurement of more parameters and a more rigorous definition of

the conditions to be modeled than isotherm models. The basis for these models is recognition that mineral surfaces are invariably electrically charged, the charge arising from unsatisfied valences caused by the discontinuity in a crystal structure, or from polarization of molecules or atoms at the interface. Minerals in sediments and soils are usually negatively charged. The charge, which is intrinsic to the mineral, is referred to as a permanent structural charge. In the aqueous phase, this charge is partially satisfied by a tightly coordinated layer of so-called potential determining ions, which bind to the exposed functional groups on the mineral. The surface charge resulting from this coordinated layer of ions may be either negative or positive. To preserve electrical neutrality, a diffuse layer of counter-ions must accumulate in the aqueous phase adjacent to the surface. The resulting interfacial structure containing the surface layer with its attendant tightly coordinated ions and the diffuse layer of counter-ions is referred to as the electrical double layer (EDL). The thickness of the EDL varies with ionic strength of the aqueous phase. The distribution of ionic species in the coordinated and diffuse layers is some function of the surface properties of the mineral and the activities of competing solutes in the aqueous phase.

To predict quantitatively the adsorption of a given solute, an electrostatic model is required that reproduces the behavior of the electrical double layer in relation to the solute species. The history of the development of surface complexation models incorporating the EDL spans a period of more than 80 years. Bolt (1991 [165056]), Bolt and Van Riemsdijk (1991 [165188]), Sposito (1984 [127253]), Westall (1987 [127323]) and Davis and Kent (1990 [143280]) give historical reviews. Presently, three such surface complexation models have found widespread use, and are referred to respectively as the “constant capacitance,” “double layer,” and “triple layer” models. Detailed discussion of their formulation and theoretical basis can be found in the above-cited references.

Despite the promise of such models in predicting the adsorption behavior of aqueous species on mineral surfaces, they have serious limitations. The large majority of studies to quantify the surface complexation constants of aqueous species have been conducted on a limited set of substrates, such as “hydrrous ferric oxide,” α -alumina, aluminum hydroxide (usually gibbsite), and amorphous silica. Studies involving minerals of relevance to radioelement transport in soils and rocks have been undertaken only to a limited extent. Clays, zeolites, and carbonates, for example, have not been studied in relation to their surface complexation properties in any detail. Furthermore, even had the surface complexation properties of the mineral been investigated, it is not feasible to use measurements on individual minerals to predict the sorption behavior of mineral aggregates such as soils or rocks.

The formulation of a surface complexation model assumes experimental characterization of the adsorbent properties under conditions in which the substrate is a dilute suspension in the aqueous phase. However, with increasing concentration of the suspension, particles come into contact with each other and modify the apparent surface properties of the adsorbent. Still greater effects have been observed when two different adsorbents are mixed. It would have been advantageous if the sorption properties of an aggregate of different adsorbents had been additive, obeying the so called Linear Adsorptivity Model (LAM). However, experimental studies reported by Honeyman (1984 [164878]) reveal that major nonlinear effects on adsorption are sometimes observed with mixtures. The LAM may therefore be an exception rather than the rule.

To overcome the practical limitations of surface complexation models, Davis et al. (1998 [154436]) formulated a semi-empirical version of a site complexation model with limited parameterization, which represents a considerable advance over empirical isotherm formulations. Their approach could, with further refinement, finally realize a suitable model for predicting species adsorption under field conditions.

6.4.3 Mathematical Model

6.4.3.1 Approximations and Simplifications

The advantage in assuming a linear isotherm for a given radioelement lies in its simplicity of measurement, and in the ease with which the term can be incorporated into hydrological models, where it is assumed that all other geochemical parameters except the concentration of the sorbent remain invariant. Under these conditions, experimentally determined K_d values from the laboratory can be used for approximate predictions of radionuclide migration, provided that the host rocks have identical composition and properties per unit mass, and thus temperature and aqueous phase composition are identical and remain invariant. Without such constraints, predictions of radionuclide transport in the natural environment will be subject to large and unpredictable errors (Reardon 1981 [154434]). Table 6.4-1 modified after Apps et al. (1977 [164864]) and Apps (1992 [165225]), provides a very general estimate of potential uncertainties introduced through the application of experimental laboratory K_d values to radionuclide sorption in the field. The values given are only estimates, actual deviations being almost impossible to quantify.

Table 6.4-1. Factors Influencing K_d for an Adsorbent, Based on Conditions Expected in the Subsurface

Parameters	Principal Effect	Field Conditions	Potential Variation in K_d
1. Solution Chemistry			
a. Major components	Ionic strength, complexing	Determined by host rock chemistry and by other factors including the leaching chemistry of the waste product.	Difficult to predict, probably 10^{+3}
b. Minor components	Complexing	Same as above	Same as above
c. pH	Complexing, hydrolysis	5.0–8.5 Buffering by heterogeneous and homogeneous reactions keep the pH range within narrow limits.	Up to 10^{+4}
d. Eh	Change in redox state	Variable, over a narrow range, usually reducing.	Up to 10^{10} or even more. Effect likely to be small in Yucca Mountain UZ. Localized effects in the vicinity of the waste containers could be significant.
2. Radioelement Concentration	Supersaturation, polymerization, colloid formation, metastable equilibrium.	Very variable concentration. Could range from 0 to 10,000 mg/L	Difficult to estimate, but could be very large for inorganic amphoteric species near the isoelectric point (approx. 10^6).
3. Flow rate	Impact on transport rate; metastable equilibrium, colloid transport. Changes in apparent surface area contacted.	10^{-3} to 10^{-7} cm/s	Slow flow rates could lead to different rate controlling transport mechanisms (e.g. ionic or molecular diffusion) and lead to different thermodynamic controls (0 to 10^6)
4. Permeability	Flow rate (see above)	$1 - 10^{-5}$ millidarcy	Same as above
5. Surface area	Adsorption	Approx. 10^{-2} cm ² /g Fractures, microfractures, intergranular pores.	Approx. 10^3
6. Temperature	Complexing, solubility, adsorption	25 to 95 °C	Up to 10^1

Source: Modified after Apps et al. (1977 [164864]) and Apps (1992 [165225]).

The presumption is also made that the K_d measurements reflect a process that has achieved stable or metastable thermodynamic equilibrium. In many studies, scant consideration is given to the question of reversibility, although some measurements by Los Alamos National Laboratory (LANL) staff took into account both sorption and desorption (Daniels et al. 1982 [105803]; Thomas 1987 [101361]). If a temporal variation in K_d is observed, and no basis exists for temporal extrapolation to an equilibrium state, then no correlation between a K_d measurement and a thermodynamic model can be established. Nonattainment of equilibrium invalidates any true or quasi-thermodynamic treatment for the temperature dependence of K_d measurements given in Section 6.4.3.2 below.

The nonattainment of thermodynamic equilibrium can be attributed to many factors, depending on the nature of the sample and its preparation. Crushed tuff samples, for example, could be actively dissolving, with concurrent precipitation of secondary products that entrain and coprecipitate radionuclides. Diffusional processes could also be active, either through intergranular pores or through “volume” diffusion or ion exchange, including diffusion through altered surface layers. In the presence of organic matter, field evidence suggests that long-term structural reorganization can lead to so-called “irreversible” adsorption, indicating that kinetically controlled processes are at play.

Measurements are commonly made on materials where several sorption mechanisms might be operative, either concurrently or over different time domains. Because K_d determinations do not discriminate as to the mechanism of adsorption, ion-exchange processes in clays and zeolites can be confounded with adsorption on the exterior crystal faces. The thermodynamic treatment of ion exchange processes is entirely different from that of adsorption on surfaces. Many ion exchange models have been formulated and are described in the literature (Sposito 1981 [129861]). If a K_d determination has been conducted on a zeolitized vitroclastic tuff, such as one from the Calico Hills formation at Yucca Mountain, none of the foregoing arguments pertaining to corrections for surface area or the formulation of EDL models involving site surface complexation is relevant. With such measurements, both surface adsorption and ion exchange may be acting interdependently, requiring the formulation of mixed process models (Meyer et al. 1990 [165040]).

The surfaces of different minerals also have different adsorptive properties for different sorbents. Thus, for example, Np adsorbs weakly on silicate surfaces, but quite strongly on iron oxides and carbonates under field conditions. At Yucca Mountain, both iron oxides and carbonates are present in the silicic vitroclastics in only minor quantities. Yet they could have a significant impact on the sorptive properties of the rock as a whole¹. Although a doubling of the concentration of either mineral would have only a minor impact on the bulk mineralogy and composition of the host rock, the sorptivity of Np could increase substantially. In such situations, the representativeness of the sample chosen for experimental determination of Np K_d values becomes critical. However, the selection of isolated intervals of drill core for testing calls into question whether a representative sampling of rocks that could host potential transport paths at Yucca Mountain has been achieved.

¹ The evaluation in this model report of the temperature dependence of neptunium sorption on two samples of Yucca Mountain Tuff, and on natural calcite and synthetic hematite (Fig 6.4-1d) suggests that neptunium sorption behavior on tuffs is dominated by the presence of small quantities of hematite.

Another problem concerns the actual characterization of the mineral surface in relation to those surfaces encountered in the field. Both surface complexation and K_d characterization studies commonly are conducted on materials that have been synthesized, chemically treated, or subjected to grinding or comminution. Such preparatory work can result in exposed mineral surfaces that bear little relation to surfaces exposed under field conditions. Furthermore, it is well established that groundwaters exposed to rocks weathering under near-surface conditions tend to attain a quasi equilibrium state with a metastable hydrated alumino-silicate phase of uncertain composition and structure (Paces 1978 [164891]). The field evidence suggests that this phase coats aluminosilicate minerals.

Mineral surfaces in soils and shallow sediments also respond to adsorbents in quite different ways, depending on the presence of swelling clays (i.e., smectites) and the quantity of organic material present— e.g., see Karickhoff (1984 [164881]), regarding the sorption of biquinoline and pyrene. Soil scientists believe that the organic content of soils and sediments is present as a coating on mineral grains forming the matrix of the soil or sediment. The concentration of this organic coating is in direct proportion to the specific surface area of the soil and suggests the presence of a “biofilm.” There is circumstantial evidence that a biofilm may be present throughout the vadose zone at Yucca Mountain (Kieft et al. 1997 [100767]). However, the organic content is sufficiently low such that the mineral surfaces are probably exposed to the adsorbate with little hindrance from a biofilm.

The organic coating responds quite differently to sorbing species than does the uncoated mineral surface; consequently, a bimodal sorptive behavior is sometimes observed. It has become common practice among soil scientists, therefore, to consider sorption by soils and sediments to be a function of both the organic coating and the mineral surface. Neither surface complexation models nor laboratory K_d measurements would be relevant to soil and vadose zones unless the significance of these film coatings was evaluated.

6.4.3.2 Thermodynamic Basis for K_d Determinations

The gross feature of sorption, as reflected by empirical K_d determinations, can be treated thermodynamically, as with any other equilibrium process, provided that the limitations cited in Section 6.4.3.1 are recognized and taken into account. Consider any chemical reaction involving sorption:



Where $S(s)$ is the solid, $i(aq)$ is the sorbent, and $S-i(s)$ is the sorbed species. Here, $S(s)$ and $S-i(s)$ are expressed as mole fractions, normalized to that surface occupied by one mole of sorbent at full site occupancy, and $i(aq)$ is in mol/L. The Gibbs free energy of the reaction is

$$\Delta G_r = \Delta G_r^\circ + RT \ln K_r \quad (\text{Eq. 7})$$

At equilibrium, $\Delta G_r = 0$, and

$$\Delta G_r^\circ = -RT \ln K_r \quad (\text{Eq. 8})$$

where $K_r = [S-i(s)] / \{[S(s)][i(aq)]\}$, the [] representing the activities of the participating species.

K_r and the molal activities are all dimensionless. In terms of measurable concentrations:

$$K_r = \lambda_{S-i(s)} X_{S-i(s)} / \{ \lambda_{S-(s)} X_{S-(s)} \cdot \gamma_{i(aq)} m_{i(aq)} \} \quad (\text{Eq. 9})$$

where X stands for mole fraction, m for molality, and λ and γ are the activity coefficients of the solid and aqueous species, respectively. The relationship between the empirical K_d measurement and K_r is complex. It may be expressed as:

$$K_r = f(x_1, x_2, x_3, \dots, x_n) K_d \quad (\text{Eq. 10})$$

where $f(x_1, x_2, x_3, \dots, x_n)$ are correction functions required to reconcile the experimental K_d with the thermodynamic K_r . Thus, K_r is dimensionless, in contrast to the conventional K_d value, which has the dimensions of $[L]^3/[M]$, expressed as mL/g. K_d can be corrected to the dimensionless form by converting the measured aqueous concentration from molarity (mol/L) to molality (mol/kg), which involves the density term, $\rho(\text{aq})$, ($[M]/[L]^3$). Thus,

$$K_r \propto K_d \cdot \rho(\text{aq}) \quad (\text{Eq. 11a})$$

In making K_d determinations, the nature of the sorption reaction is normally ignored, and the specification of a reactive surface area is not considered. However, normalization of measurements to a fixed reactive surface area can be accomplished through incorporation of a dimensionless coefficient, σ , expressed as the ratio of the measured surface area per unit mass of sorbent, divided by a specified standard surface area per unit mass of sorbent. Taking this correction into account yields:

$$K_r \propto K_d \cdot \sigma \quad (\text{Eq. 11b})$$

σ is not easily defined, because it depends on the method of measuring surface area in relation to the adsorption of a given sorbent, which can vary with mineral substrate and other factors affecting its interaction with the liquid aqueous phase. A common method is the Brunauer, Emmett, Teller (B.E.T.) (Brunauer et al. 1938 [156646]) method in which a gaseous species, usually nitrogen, is allowed to adsorb on the sorbate under evacuated conditions. This method, however, does not replicate conditions in which the reactive surface area of a mineral is in contact with the aqueous phase. Nevertheless, Pabalan et al. (1998 [162987]) determined that quartz, alpha-alumina, clinoptilolite, montmorillonite, amorphous silica, kaolinite and hydrous titanium dioxide all adsorbed the uranyl ion, UO_2^{2+} to the same extent, when the K_d values for each mineral were corrected for their respective B.E.T. surface areas (Brunauer et al. 1938 [156646]). This observation suggests a consistency between B.E.T. determinations and adsorption by aqueous species (Brunauer et al. 1938 [156646]), which do not participate in ion-exchange processes in clays or zeolites.

Limited corrections for species activity, γ_i , in relation to total concentration of all i in aqueous solution, taking account of complexation, pH, oxidation state and ionic strength might be profitably undertaken to calculate the thermodynamic activity of the sorbent. However, this requires that sufficient characterization of the aqueous phase be made at the time of measurement. Computer codes such as EQ3/6 (Wolery 1983 [108808]; Wolery and Daveler 1992 [100097]), PHREEQC (Parkhurst and Appelo 1999 [159511]) or SOLVEQ/CHILLER

(Reed 1982 [117901]; Spycher and Reed 1992 [165846]) could be employed to address corrections for the listed parameters.

Correction for the surface activity coefficients, λ , is much more difficult and implies some knowledge of the thermodynamic behavior of the sorption sites in competition with other species, as well as the nature of the sorption process itself. Parks (1990 [165849]) points out that there are two broad classes of adsorbate, each distinguished by characteristic behavior.

1. Sorption is nonspecific: There is negligible adsorption at the point of zero net proton charge (PZNPC) and isoelectric point (IEP), and both are coincident, suggesting that adsorption occurs primarily through coulombic attraction to an oppositely charged surface. Adsorption is assumed to take place through weak interactions, and the adsorbed ions remain solvated. The surface structure also remains essentially unaltered. Because no true chemical bond is created, the term “physical adsorption” is sometimes applied.
2. Sorption is specific: This class of sorption is characterized by reversal of charge at the surface, and adsorption can occur even though the surface charge and adsorbate charge are of the same sign. Such adsorption must be non-coulombic in character, suggesting that chemical bonding takes place. Evidence indicates that the adsorbate bonds close to the surface as an inner sphere complex, with disruption of both the solvation sheath around the sorbing ion and the surface functional groups. The term “chemical bonding” is sometimes applied to this form of adsorption.

Carefully conducted adsorption experiments with well-defined adsorption mechanisms could be designed to quantify the extent of non-ideality in the adsorption process, and thus determine the impact of λ_i .

6.4.3.3 Representation of K_d Measurements as a Function of Temperature

The temperature dependence of K_r can be established by invoking the thermodynamic relation:

$$\Delta G_r(P, T) = \Delta H_r(P, T) - T\Delta S_r(P, T) \quad (\text{Eq. 12})$$

Assuming equilibrium, substituting Equation 8 into Equation 12, and converting to base 10 logarithms, yields:

$$\text{Log } K_r = \Delta S_r/2.303R - [\Delta H_r/2.303R](1/T) \quad (\text{Eq. 13a})$$

Over small temperature intervals, such as between 0 and 100°C, it can be assumed that the heat capacity of reaction, $\Delta C_{P,r} \approx 0$, which means that ΔH_r and ΔS_r are constant over the specified temperature interval. Thus, Equation 13a is a good approximation of the variation of $\log K_r$ with temperature². A plot of $\text{Log } K_r$ data versus $1/T$ would yield, upon linear regression, a slope of –

² In reality, measurement of the heat capacity of sorption would be difficult. Relevant experimental data for this parameter was searched for in the literature, but no useful information was located. Precise K_d measurements as a function of temperature so far examined in the published literature indicate that the assumption, $\Delta C_{P,r} \approx 0$, would be a valid approximation. The approximation is consistent with the small variations in ΔS_r for Co(II) sorption on sepiolite at different temperatures reported by Kara et al. (2003 [164880]), and similar data for Cs(I) on KCNF (Ishfaq et al. 1997 [164879]) and Ag(I) on bentonite (Zafar et al. 2002 [165052]). [See a summary of these data in Table 6.4-10]. In general, the quality of the data is insufficient to justify other than a linear approximation.

$\Delta H_r/2.303R$ and a value of $\Delta S_r/2.303R$ on the y-axis where $(1/T) = 0$. Depending on the nature of the sorption process, ΔH_r° can be either negative or positive, leading respectively to either decreasing or increasing sorption with temperature.

No attempt is made in this Model Report to consider either corrections to K_d measurements at ambient temperature or the effect of such corrections on ΔH_r° . While such corrections could be made, or at least estimated in some cases, the effort involved is scarcely commensurate with the resulting increase in purported accuracy, given the known degree of uncertainty in existing measurements. Instead, we will assume, as a working assumption, that corrections will have a small effect on ΔH_r and that corrections will predominantly affect $\log K_d$, and the apparent value of ΔS . Therefore, we can assume that, by substituting Equation 10 into Equation 13a, we get

$$\text{Log } K_d + k' = \Delta S_r/2.303R - [\Delta H_r/2.303R](1/T) \quad (\text{Eq. 13b})$$

where k' is $\log[f(x_1, x_2, x_3, \dots, x_n)]$. Included in these corrections is that for correcting K_d [mL/g] to K_r [-], the dimensionless form. The corrections embedded in this parameter would result in differing intercepts of the y axis for differing experimental conditions for a given aqueous species sorbing on a given solid phase. However, the slope of Equation 13b, $-\Delta H_r/2.303R$, will remain essentially unchanged. Because of the practical difficulty in calculating k' , it will be ignored, and the uncorrected K_d will be plotted versus $1/T$ [K^{-1}].

The temperature dependence of K_d is somewhat more difficult to evaluate accurately. If the K_d measurements have demonstrated reversibility, as is the case with some measurements conducted under the auspices of the DOE Yucca Mountain Project (YMP) at LANL (Daniels et al. 1982 [105803]; Thomas 1987 [101361]), a thermodynamic basis for the sorption process can be tentatively accepted, and the relationship between K_r and K_d accepted, as specified in Equation 10. The question as to how to treat $f(x_1, x_2, x_3, \dots, x_n)$ remains. Many of the corrections necessary to correlate differing K_d measurements would affect both the Gibbs free energy, ΔG_r° , and the enthalpy of sorption, ΔH_r° . However, if such corrections were to be temperature independent, they would merely change the y intercept of a $\text{Log } K_d$ versus $1/T$ plot without affecting the slope. Most of the cited parameters required to correlate K_d s are functionally dependent on temperature, and as a consequence, the enthalpy of sorption will vary depending on the sorption model used, the concentration of the sorbent in solution, the degree of complexation, oxidation state and so on. These variations are illustrated by data presented by Kara et al. (2003 [164880]) [Table 6.4-10], where Co(II) sorption on sepiolite at different temperatures is interpreted using four different isotherms, each yielding quite different values of ΔH_r . Similarly, Rauf and Tahir (2000 [164893]) (Table 6.4-10) show an aqueous concentration dependence of ΔH_r for both Fe(II) and Mn(II) sorption on bentonite. This functional dependence probably reflects uncorrected effects of λ_i and γ_i respectively. Because the temperature dependence of most K_d measurements is small in many cases, such corrections, if they could be applied, might easily result in a change from negative to positive temperature dependence or vice versa, as will be illustrated below with examples from the published literature.

6.4.4 Evaluation of the Temperature Dependence of Selected K_d Data

Temperature dependent K_d data evaluated in this section are derived from three sources. The first two sources represent “qualified” (Sections 4.1.3 and 6.4.4.1) and “unqualified” (Section 6.4.4.2) measurements, respectively, conducted by the staff of the Los Alamos National Laboratory (LANL) over the last twenty or more years. The third source consists of data from the refereed literature (Section 6.4.4.3). These three sources of data are evaluated below in three separate subsections. The sorption analyses are compiled in files in Attachment I.3.

The LANL measurements were conducted primarily on natural rock samples obtained from Yucca Mountain and its vicinity at the U.S. Nevada Test Site (NTS), and on various synthetic and natural mineral samples. The rock samples were taken from drill cores penetrating the volcanoclastic stratigraphy of Yucca Mountain, and almost all were tuffaceous, including vitrophyre, devitrified welded tuff, and altered nonwelded (zeolitized) tuff. Experiments conducted on these samples employed intact core, or crushed and sized material in batch or column percolation studies. The tests were conducted using radionuclide tracers of the elements Sr, Cs, Ba, Ce, Eu, Np(V), Am, U(VI), and Pu in J-13 well water. A listing of the rock samples used, and radioelements investigated for their sorption properties, are given in Table 6.4-2. The mineralogical composition of these rocks is presented in Table 6.4-3.

The literature data were obtained from six independent literature searches with SCIFINDER on Chemical Abstracts of the American Chemical Society, using various combinations of key words involving sorption of inorganic constituents, including radionuclides on natural mineral substrates in the aqueous phase. The results of these searches were further screened for relevance and a subset of abstracts was selected for printing. The abstracts were reviewed, and a final selection of papers was copied from locally available journals in libraries of the U.C. Berkeley Campus and LBNL, or downloaded electronically.

Table 6.4-2. Rock Samples Used for Radioelement Sorption and Radioelements Sorbed

Sorption Sample	Rock Type	Sr	Cs	Ba	Ce	Eu	Np	Am	Pu	U
J-13 (18) ^a	GLASS2	√	√	√						√
J-13 (32) ^a	DEVIT1	√	√	√	√	√		√		√
J-13 (37) ^a	CLAYS	√	√	√		√		√	√	√
USW-GU3 (0433 ft) ^b	DEVITRIFIED							√	√	
USW-GU3 (1203 ft) ^b	GLASS							√	√	
USW-GU3 (1301 ft) ^b	GLASS							√	√	
USW-GU3 (1407 ft) ^b	GLASS	√	√	√						
USW-G4 (0270 ft) ^b	ZEOLITIZED	√	√	√			√			
USW-G4 (1506 ft) ^b	ZEOLITIZED	√	√	√						
Nat. Calcite ^c							√			
Syn. Hematite ^c							√			

Source: From Thomas (1987 [101361], pp. 14–16).

NOTE: ^a Daniels et al. (1982 [105803])

^b Bish and Vaniman (1985 [101196], Appendix A)

^c DTN: LA0010JC831341.007 [153319]

Table 6.4-3. Mineralogical Composition of Rock Samples, by X-Ray Analysis

Sorption Sample	Hole depth, ft ^a	Mineral Composition, Wt. %										
		Calcite	Hematite	Smectite	Micas`	Clinoptilolite	Mordenite	Quartz	Cristobalite	Alkali feldspar	Tridymite	Glass
J-13 (18) ^b	1420			5	5	5-10			15-25	15-25		≈50
J-13 (32) ^b	2533			5	5-15			30-50		30-50		
J-13 (37) ^b	3497			20-40	5	≈5		30-60		15-30		
USW-GU3 (0433 ft) ^c	430.5				2-4				10-15	75-85	2-6	
USW-GU3 (1203 ft)	1195.7			4-6				2-4	25-30	30-40		20-40
USW-GU3 (1301 ft) ^c	1302.4			1-3				2-6	10-15	35-45		30-60
USW-GU3 (1407 ft) ^c	1415.5							2-8	2-10	30-40		40-70
USW-G4 (0270 ft) ^c	268				≈1				6±2	73±10	20±10	
USW-G4 (1506 ft) ^c	1470			3±2		77±10		6±2	14±4			
	1544			3±2		50±10	20±10	6±2	12±4			
Nat. Calcite ^d		100										
Syn. Hematite ^d			100									

NOTE: ^a Hole depth is the depth closest to the depth from which a sample was taken for which a mineralogical analysis is available.

^b Source of X-ray analyses: Daniels et al. (1982 [105803], Table XXIV)

^c Source of X-ray analyses: Bish and Vaniman (1985 [101196], Appendix A)

^d DTN: LA0010JC831341.007 [153319]

6.4.4.1 Qualified LANL Data

The qualified data were generated and compiled subsequent to 1987 and are recorded under DTNs shown in Table 4.1-3 (Section 4.1.3). These data contain K_d values for Cs, and Sr, collected at 20, 60 and 80°C, for Ba at 20 at 60°C and data for Np, collected at 20, 25, 60, 80, and 90°C (Table 6.4-4).

Table 6.4-4. Batch Sorption Ratios for Pulverized Tuff and Mineral Samples* from Sorption Experiments at Room Temperature (20 ± 4°C), 60°C, and 80 or 90°C with J-13 Well Water

MATERIAL	SAMPLE DESCRIPTION	T, °C	K_d , mL/g	1/T X1000, K ⁻¹	Log K_d
Strontium					
G4-270	J-13 G4-270-C.955-20	20	31.6	3.411	1.500
G4-270	J-13 G4-270-C.956-20	20	30.3	3.411	1.481
G4-270	J-13 G4-270-C.961-20	20	26.4	3.411	1.422
G4-270	J-13 G4-270-C.962-20	20	27.4	3.411	1.438
G4-270	J-13 G4-270-C.967-20	20	23.8	3.411	1.377
G4-270	J-13 G4-270-C.968-20	20	25.1	3.411	1.400
G4-270	J-13 G4-270-C.1021-60	60	32.5	3.002	1.512
G4-270	J-13 G4-270-C.1022-60	60	33.5	3.002	1.525
G4-270	J-13 G4-270-C.1029-80	80	40	2.832	1.602
G4-270	J-13 G4-270-C.1030-80	80	37.8	2.832	1.577
G4-1506	J-13 G4-1506-C.957-20	20	25615.4	3.411	4.409
G4-1506	J-13 G4-1506-C.958-20	20	12941.8	3.411	4.112
G4-1506	J-13 G4-1506-C.963-20	20	53434.8	3.411	4.728
G4-1506	J-13 G4-1506-C.964-20	20	38473.4	3.411	4.585
G4-1506	J-13 G4-1506-C.969-20	20	147540.9	3.411	5.169
G4-1506	J-13 G4-1506-C.970-20	20	142538.9	3.411	5.154
G4-1506	J-13 G4-1506-C.1019-60	60	75289	3.002	4.877
G4-1506	J-13 G4-1506-C.1020-60	60	207934.7	3.002	5.318
G4-1506	J-13 G4-1506-C.1027-80	80	151746.5	2.832	5.181
G4-1506	J-13 G4-1507-C.1028-80	80	245084.5	2.832	5.389
GU3-1407	J-13 GU3-1407-C.959-20	20	132.2	3.411	2.121
GU3-1407	J-13 GU3-1407-C.960-20	20	168.7	3.411	2.227
GU3-1407	J-13 GU3-1407-C.965-20	20	188.2	3.411	2.275
GU3-1407	J-13 GU3-1407-C.966-20	20	186.5	3.411	2.271
GU3-1407	J-13 GU3-1407-C.971-20	20	169.7	3.411	2.230
GU3-1407	J-13 GU3-1407-C.972-20	20	175.6	3.411	2.245
GU3-1407	J-13 GU3-1407-C.1023-60	60	183	3.002	2.262
GU3-1407	J-13 GU3-1407-C.1024-60	60	183.3	3.002	2.263
GU3-1407	J-13 GU3-1407-C.1031-80	80	175.5	2.832	2.244
GU3-1407	J-13 GU3-1407-C.1032-80	80	198.4	2.832	2.298

NOTE: *Fractions do not contain <75 µm diameter particles.

DTN: LA0010JC831341.003 [153322]

Table 6.4-4. Batch Sorption Ratios for Pulverized Tuff and Mineral Samples* from Sorption Experiments at Room Temperature ($20 \pm 4^\circ\text{C}$), 60°C , and 80 or 90°C with J-13 Well Water (Continued)

MATERIAL	SAMPLE DESCRIPTION	T, °C	K _d , mL/g	1/T X1000, K ⁻¹	Log K _d
Barium					
G4-270	J-13 G4 -270-C.955-20	20	384.2	3.411	2.585
G4-270	J-13 G4-270-C.956-20	20	349.7	3.411	2.544
G4-270	J-13 G4 -270-C.961-20	20	356	3.411	2.551
G4-270	J-13 G4-270-C.962-20	20	362.3	3.411	2.559
G4-270	J-13 G4 -270-C.967-20	20	324.8	3.411	2.512
G4-270	J-13 G4-270-C.968-20	20	322.7	3.411	2.509
G4-270	J-13 G4-270-C.1021-60	60	516.9	3.002	2.713
G4-270	J-13 G4-270-C.1022-60	60	517.7	3.002	2.714
G4-1506	J-13 G4-1506-C.957-20	20	30828.8	3.411	4.489
G4-1506	J-13 G4-1506-C.958-20	20	12959.9	3.411	4.113
G4-1506	J-13 G4-1506-C.963-20	20	100657.6	3.411	5.003
G4-1506	J-13 G4-1506-C.964-20	20	42781.2	3.411	4.631
G4-1506	J-13 G4-1506-C.1019-60	60	106252	3.002	5.026
GU3-1407	J-13 GU3-1407-C.959-20	20	2662.8	3.411	3.425
GU3-1407	J-13 GU3-1407-C.960-20	20	4187	3.411	3.622
GU3-1407	J-13 GU3-1407-C.965-20	20	3820.4	3.411	3.582
GU3-1407	J-13 GU3-1407-C.966-20	20	4144.8	3.411	3.618
GU3-1407	J-13 GU3-1407-C.971-20	20	4674.9	3.411	3.670
GU3-1407	J-13 GU3-1407-C.972-20	20	4739.8	3.411	3.676
GU3-1407	J-13 GU3-1407-C.1023-60	60	8177	3.002	3.913
GU3-1407	J-13 GU3-1407-C.1024-60	60	7366.2	3.002	3.867

NOTE: *Fractions do not contain $<75 \mu\text{m}$ diameter particles.

DTN: LA0010JC831341.001 [162476]

Table 6.4-4. Batch Sorption Ratios for Pulverized Tuff and Mineral Samples* from Sorption Experiments at Room Temperature ($20 \pm 4^\circ\text{C}$), 60°C , and 80 or 90°C with J-13 Well Water (Continued)

MATERIAL	SAMPLE DESCRIPTION	T, °C	K _d , mL/g	1/T X1000, K ⁻¹	Log K _d
Cesium					
G4-270	J-13 G4-270-C.955-20	20	220.3	3.411	2.343
G4-270	J-13 G4-270-C.956-20	20	212.8	3.411	2.328
G4-270	J-13 G4-270-C.961-20	20	218	3.411	2.338
G4-270	J-13 G4-270-C.962-20	20	126.4	3.411	2.102
G4-270	J-13 G4-270-C.967-20	20	123.7	3.411	2.092
G4-270	J-13 G4-270-C.968-20	20	125.06	3.411	2.097
G4-270	J-13 G4-270-C.1021-60	60	239.4	3.002	2.379
G4-270	J-13 G4-270-C.1022-60	60	244.6	3.002	2.388
G4-270	J-13 G4-270-C.1029-80	80	165.7	2.832	2.219
G4-270	J-13 G4-270-C.1030-80	80	170.9	2.832	2.233
G4-1506	J-13 G4-1506-C.957-20	20	7381.5	3.411	3.868
G4-1506	J-13 G4-1506-C.958-20	20	42321.6	3.411	4.627
G4-1506	J-13 G4-1506-C.963-20	20	10206.3	3.411	4.009
G4-1506	J-13 G4-1506-C.964-20	20	8271.6	3.411	3.918
G4-1506	J-13 G4-1506-C.969-20	20	36364.24	3.411	4.561
G4-1506	J-13 G4-1506-C.970-20	20	29730.22	3.411	4.473
G4-1506	J-13 G4-1506-C.1019-60	60	19553.2	3.002	4.291
G4-1506	J-13 G4-1506-C.1020-60	60	35154.3	3.002	4.546
G4-1506	J-13 G4-1506-C.1027-80	80	16468	2.832	4.217
G4-1506	J-13 G4-1507-C.1028-80	80	17518.1	2.832	4.243
GU3-1407	J-13 GU3-1407-C.959-20	20	767.4	3.411	2.885
GU3-1407	J-13 GU3-1407-C.960-20	20	950.2	3.411	2.978
GU3-1407	J-13 GU3-1407-C.965-20	20	525.8	3.411	2.721
GU3-1407	J-13 GU3-1407-C.966-20	20	516.7	3.411	2.713
GU3-1407	J-13 GU3-1407-C.971-20	20	1052	3.411	3.022
GU3-1407	J-13 GU3-1407-C.972-20	20	1041.13	3.411	3.018
GU3-1407	J-13 GU3-1407-C.1023-60	60	1061.4	3.002	3.026
GU3-1407	J-13 GU3-1407-C.1024-60	60	1026.7	3.002	3.011
GU3-1407	J-13 GU3-1407-C.1031-80	80	672.3	2.832	2.828
GU3-1407	J-13 GU3-1407-C.1032-80	80	767.9	2.832	2.885

NOTE: *Fractions do not contain <75 μm diameter particles.

DTN: LA0010JC831341.002 [153321]

Table 6.4-4. Batch Sorption Ratios for Pulverized Tuff and Mineral Samples* from Sorption Experiments at Room Temperature ($20 \pm 4^\circ\text{C}$), 60°C , and 80 or 90°C with J-13 Well Water (Continued)

MATERIAL	SAMPLE DESCRIPTION	T, °C	K _d , mL/g	1/T X1000, K ⁻¹	Log K _d
Neptunium					
G4-270	J-13-G-4 270-K-01-20	20	-0.5		
G4-270	J-13-G-4 270-K-02-20	20	0.2	3.411	-0.699
G4-270	J-13-G-4 270-K-01D-20	20	1.1	3.411	0.041
G4-270	J-13-G-4 270-K-02D-20	20	0.9	3.411	-0.046
G4-270	J-13-G-4 270-C.15-20	20	0.4	3.411	-0.398
G4-270	J-13-G-4 270-C.16-20	20	0.8	3.411	-0.097
G4-270	J-13-G-4 270-C.33-60	60	0.9	3.002	-0.046
G4-270	J-13-G-4 270-C.51-90	90	1	2.754	0.000
G4-270	J-13-G-4 270-C.52-90	90	1.1	2.754	0.041
G4-270	J-13-G-4 270-C.67-20	20	0.2	3.411	-0.699
G4-270	J-13-G-4 270-C.68-20	20	0.5	3.411	-0.301
G4-270	J-13-G-4 270-C.70-60	60	12.9	3.002	1.111
G4-270	J-13-G-4 270-C.171-20	20	1	3.411	0.000
G4-270	J-13-G-4 270-C.172-20	20	1.1	3.411	0.041
G4-270	J-13-G-4 270-C.189-60	60	1.1	3.002	0.041
G4-270	J-13-G-4 270-C.190-60	60	0.8	3.002	-0.097
G4-270	J-13-G-4 270-C.223-20	20	0.1	3.411	-1.000
G4-270	J-13-G-4 270-C.227-90	90	1.7	2.754	0.230
G4-270	J-13-G-4 270-C.228-90	90	2.7	2.754	0.431
G4-270	J-13-G4 270-C.341-20	20	0.7	3.411	-0.155
G4-270	J-13-G4 270-C.342-20	20	0.8	3.411	-0.097
G4-270	J-13-G4 270-C.395-20	20	0.1	3.411	-1.000
G4-270	J-13-G4 270-C.396-20	20	0.6	3.411	-0.222
G4-270	J13-G4-270-C.409-80	80	0.6	2.832	-0.222
G4-270	J13-G4-270-C.410-80	80	0.9	2.832	-0.046
G4-270	J-13 G4-270-C.437-20	20	0.1	3.411	-1.000
G4-270	J-13 G4-270-C.438-20	20	0.2	3.411	-0.699
G4-270	J-13 G4-270-C.459-60	60	0.7	3.002	-0.155
G4-270	J-13 G4-270-C.460-60	60	0.2	3.002	-0.699
G4-270	J-13 G4-270-C.973-20	20	0.4	3.411	-0.398
G4-270	J-13 SYN. G4-270-C.994-20	20	0.5	3.411	-0.301
G4-270	J-13 SYN. G4-270-C.2047-20	20	0.4	3.411	-0.398
G4-270	J-13 SYN. G4-270-C.2048-20	20	0.3	3.411	-0.523
G4-270	J-13 G4-270-C.2251-25	25	0.3	3.354	-0.523
G4-270	J-13-G4 270 C.2295-25	25	0.2	3.354	-0.699
G4-270	J-13-G4 270 C.2296-25	25	0.5	3.354	-0.301
G4-270	J-13 G4-270-C.6000-20	20	0.9	3.411	-0.046
G4-270	J-13 G4-270-C.6001-20	20	0.5	3.411	-0.301
G4-270	J-13 G4-270-C.6006-20	20	0.5	3.411	-0.301
G4-270	J-13 G4-270-C.6007-20	20	3.5	3.411	0.544

NOTE: *Fractions do not contain <75 μm diameter particles.

DTN: LA0010JC831341.007 [153319]

Table 6.4-4. Batch Sorption Ratios for Pulverized Tuff and Mineral Samples* from Sorption Experiments at Room Temperature ($20 \pm 4^\circ\text{C}$), 60°C , and 80 or 90°C with J-13 Well Water (Continued)

MATERIAL	SAMPLE DESCRIPTION	T, °C	K _d , mL/g	1/T X1000, K ⁻¹	Log K _d
Neptunium					
G4-1506	J-13-G-4 1506-K-03-20	20	3.7	3.411	0.568
G4-1506	J-13-G-4 1506-K-04-20	20	4.3	3.411	0.633
G4-1506	J-13-G-4 1506-C.17-20	20	4.4	3.411	0.643
G4-1506	J-13-G-4 1506-C.18-20	20	5.1	3.411	0.708
G4-1506	J-13-G-4 1506-C.35-60	60	6.8	3.002	0.833
G4-1506	J-13-G-4 1506-C.36-60	60	1.5	3.002	0.176
G4-1506	J-13-G-4 1506-C.53-90	90	5.4	2.754	0.732
G4-1506	J-13-G-4 1506-C.54-90	90	10	2.754	1.000
G4-1506	J-13-G-4 1506-C.73-20	20	2.9	3.411	0.462
G4-1506	J-13-G-4 1506-C.74-20	20	2.4	3.411	0.380
G4-1506	J-13-G-4 1506-C.76-60	60	3660.5	3.002	3.564
G4-1506	J-13-G-4 1506-C.173-20	20	6.1	3.411	0.785
G4-1506	J-13-G-4 1506-C.174-20	20	6.4	3.411	0.806
G4-1506	J-13-G-4 1506-C.191-60	60	8.5	3.002	0.929
G4-1506	J-13-G-4 1506-C.192-60	60	8.4	3.002	0.924
G4-1506	J-13-G-4 1506-C.229-20	20	4.1	3.411	0.613
G4-1506	J-13-G-4 1506-C.230-20	20	4	3.411	0.602
G4-1506	J-13-G-4 1506-C.233-90	90	1.9	2.754	0.279
G4-1506	J-13-G-4 1506-C.234-90	90	7.8	2.754	0.892
G4-1506	J-13-G4 1506-C.343-20	20	3.7	3.411	0.568
G4-1506	J-13-G4 1506-C.344-20	20	4	3.411	0.602
G4-1506	J-13-G4 1506-C.397-20	20	1.9	3.411	0.279
G4-1506	J-13-G4 1506-C.398-20	20	2.2	3.411	0.342
G4-1506	J-13 G4-1506-C.439-20	20	1.9	3.411	0.279
G4-1506	J-13 G4-1506-C.440-20	20	2	3.411	0.301
G4-1506	J-13 G4-1506-C.461-60	60	3.2	3.002	0.505
G4-1506	J-13 G4-1506-C.462-60	60	3.1	3.002	0.491
G4-1506	J-13 G4-1506-C.975-20	20	2.3	3.411	0.362
G4-1506	J-13 G4-1506-C.976-20	20	2.2	3.411	0.342
G4-1506	J-13 G4-1506-C.987-20	20	2.9	3.411	0.462
G4-1506	J-13 G4-1506-C.988-20	20	2.5	3.411	0.398
G4-1506	J-13 SYN. G4-1506-C.991-20	20	3.7	3.411	0.568
G4-1506	J-13 SYN. G4-1506-C.992-20	20	3.4	3.411	0.531
G4-1506	J-13 SYN. G4-1506-C.2045-20	20	5.2	3.411	0.716
G4-1506	J-13 SYN. G4-1506-C.2046-20	20	5.4	3.411	0.732
G4-1506	J-13-G-4 1506-C.209X-90	90	8.7	2.754	0.940
G4-1506	J-13-G-4 1506-C.210X-90	90	10.4	2.754	1.017
G4-1506	J-13-G-4 1506-C.231-60	60	5.7	3.002	0.756
G4-1506	J-13-G-4 1506-C.232-60	60	6.4	3.002	0.806
G4-1506	J-13 G4-1506-C.571-20	20	2.5	3.411	0.398
G4-1506	J-13 G4-1506-C.572-20	20	2.6	3.411	0.415
G4-1506	J-13 G4-1506-C.981-20	20	2.2	3.411	0.342
G4-1506	J-13 G4-1506-C.571-20	20	2.5	3.411	0.398
G4-1506	J-13 G4-1506-C.2002-20	20	3.5	3.411	0.544
G4-1506	J-13 G4-1506-C.2003-20	20	3.2	3.411	0.505

NOTE: *Fractions do not contain <75 μm diameter particles.

DTN: LA0010JC831341.007 [153319]

Table 6.4-4. Batch Sorption Ratios for Pulverized Tuff and Mineral Samples* from Sorption Experiments at Room Temperature ($20 \pm 4^\circ\text{C}$), 60°C , and 80 or 90°C with J-13 Well Water (Continued)

MATERIAL	SAMPLE DESCRIPTION	T, °C	K _d , mL/g	1/T X1000, K ⁻¹	Log K _d
Neptunium					
Natural Calcite	J-13-B-C.3-20	20	979.5	3.411	2.991
Natural Calcite	J-13-B-C.4-20	20	883.4	3.411	2.946
Natural Calcite	J-13-B-C.21-60	60	154.5	3.002	2.189
Natural Calcite	J-13-B-C.22-60	60	136.9	3.002	2.136
Natural Calcite	J-13-B-C.40-90	90	66.5	2.754	1.823
Natural Calcite	J-13-B-C.55-20	20	96.9	3.411	1.986
Natural Calcite	J-13-B-C.56-20	20	73.1	3.411	1.864
Natural Calcite	J-13-B-C.57-60	60	30	3.002	1.477
Natural Calcite	J-13-B-C.58-60	60	28.8	3.002	1.459
Natural Calcite	J-13-B-C.159-20	20	640.5	3.411	2.807
Natural Calcite	J-13-B-C.160-20	20	543.9	3.411	2.736
Natural Calcite	J-13-B-C.177-60	60	95.8	3.002	1.981
Natural Calcite	J-13-B-C.178-60	60	77.1	3.002	1.887
Natural Calcite	J-13-B-C.195-90	90	38.8	2.754	1.589
Natural Calcite	J-13-B-C.196-90	90	93.5	2.754	1.971
Natural Calcite	J-13-B-C.211-20	20	54.6	3.411	1.737
Natural Calcite	J-13-B-C.212-20	20	56.4	3.411	1.751
Natural Calcite	J-13-B-C.213-60	60	9	3.002	0.954
Natural Calcite	J-13-B-C.214-60	60	9	3.002	0.954
Natural Calcite	J-13-B-C.215-90	90	3.1	2.754	0.491
Natural Calcite	J-13-B-C.216-90	90	3.6	2.754	0.556
Natural Calcite	J-13-B-C.331-20	20	51.5	3.411	1.712
Natural Calcite	J-13-B-C.332-20	20	53	3.411	1.724
Natural Calcite	J-13 B-C.575-20	20	2.4	3.411	0.380
Natural Calcite	J-13 B-C.576-20	20	3.9	3.411	0.591
Natural Calcite	J-13 SYN. B-C.997-20	20	1.9	3.411	0.279
Natural Calcite	J-13 SYN. B-C.998-20	20	2.1	3.411	0.322
Natural Calcite	J-13 SYN. B-C.2051-20	20	4.3	3.411	0.633
Natural Calcite	J-13 SYN. B-C.2052-20	20	5	3.411	0.699
Natural Calcite	SYN.J13.B B-C.2127-20	20	36.1	3.411	1.558
Natural Calcite	SYN.J13.B B-C.2128-20	20	38.7	3.411	1.588
Natural Calcite	J-13 B-C.3882-20 (3 Days)	20	680.3	3.411	2.833
Natural Calcite	J-13 B-C.3883-20 (3 Days)	20	650.9	3.411	2.814
Natural Calcite	J-13 B-C.3886-20 (30 Days)	20	6492.9	3.411	3.812
Natural Calcite	J-13 B-C.3887-20 (30 Days)	20	7808.9	3.411	3.893

NOTE: *Fractions do not contain $<75 \mu\text{m}$ diameter particles.

DTN: LA0010JC831341.007 [153319]

Table 6.4-4. Batch Sorption Ratios for Pulverized Tuff and Mineral Samples* from Sorption Experiments at Room Temperature ($20 \pm 4^\circ\text{C}$), 60°C , and 80 or 90°C with J-13 Well Water (Continued)

MATERIAL	SAMPLE DESCRIPTION	T, °C	K _d , mL/g	1/T X1000, K ⁻¹	Log K _d
Neptunium					
Synthetic Hematite	J-13-C-C.42-90	90	2662.8	2.754	3.425
Synthetic Hematite	J-13-C-C.161-20	20	2003.7	3.411	3.302
Synthetic Hematite	J-13-C-C.162-20	20	1749.1	3.411	3.243
Synthetic Hematite	J-13-C-C.179-60	60	696.8	3.002	2.843
Synthetic Hematite	J-13-C-C.180-60	60	848.1	3.002	2.928
Synthetic Hematite	J-13-C-C.197-90	90	5898.5	2.754	3.771
Synthetic Hematite	J-13-C-C.198-90	90	18360.3	2.754	4.264
Synthetic Hematite	J-13-C-C.333-20	20	149.4	3.411	2.174
Synthetic Hematite	J-13-C-C.334-20	20	567.5	3.411	2.754
Synthetic Hematite	J-13-C-C.387-20	20	233.5	3.411	2.368
Synthetic Hematite	J-13-C-C.388-20	20	199.2	3.411	2.299
Synthetic Hematite	J13-C-C.403-80	80	561.5	2.832	2.749
Synthetic Hematite	J13-C-C.404-80	80	462.5	2.832	2.665
Synthetic Hematite	J-13-C-C.433-20	20	67.8	3.411	1.831
Synthetic Hematite	J-13-C-C.434-20	20	74.8	3.411	1.874
Synthetic Hematite	J-13-C-C.451-60	60	199.9	3.002	2.301
Synthetic Hematite	J-13-C-C.452-60	60	215.5	3.002	2.333
Synthetic Hematite	J-13 C-C.577-20	20	732.8	3.411	2.865
Synthetic Hematite	J-13 C-C.578-20	20	539.1	3.411	2.732
Synthetic Hematite	J-13 SYN. C-C.999-20	20	432	3.411	2.635
Synthetic Hematite	J-13 SYN. C-C.1000-20	20	330.6	3.411	2.519
Synthetic Hematite	J-13 SYN. C-C.2053-20	20	782.4	3.411	2.893
Synthetic Hematite	J-13 SYN. C-C.2054-20	20	1022.2	3.411	3.010
Synthetic Hematite	SYN.J13.B C-C.2129-20	20	1973.3	3.411	3.295
Synthetic Hematite	SYN.J13.B C-C.2130-20	20	2720.7	3.411	3.435

NOTE: *Fractions do not contain $<75 \mu\text{m}$ diameter particles.

DTN: LA0010JC831341.007 [153319]

These K_d measurements were plotted as $\text{Log } K_d$ versus $1/T$ [K^{-1}]. The plots are illustrated in Figures 6.4-1a–d. Data were regressed to obtain linear equations, and the slopes and calculated enthalpies of sorption were summarized in Table 6.4-5.

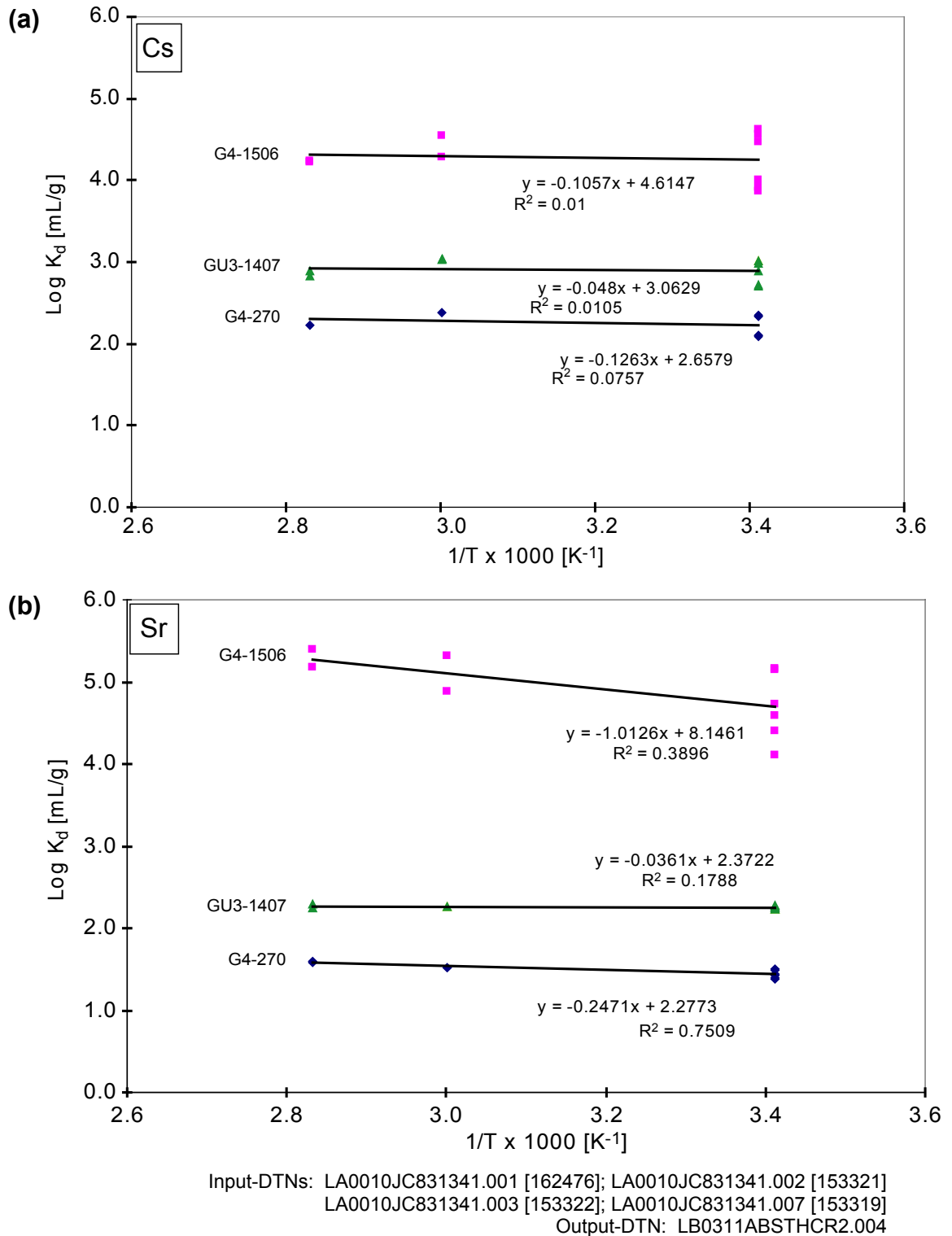
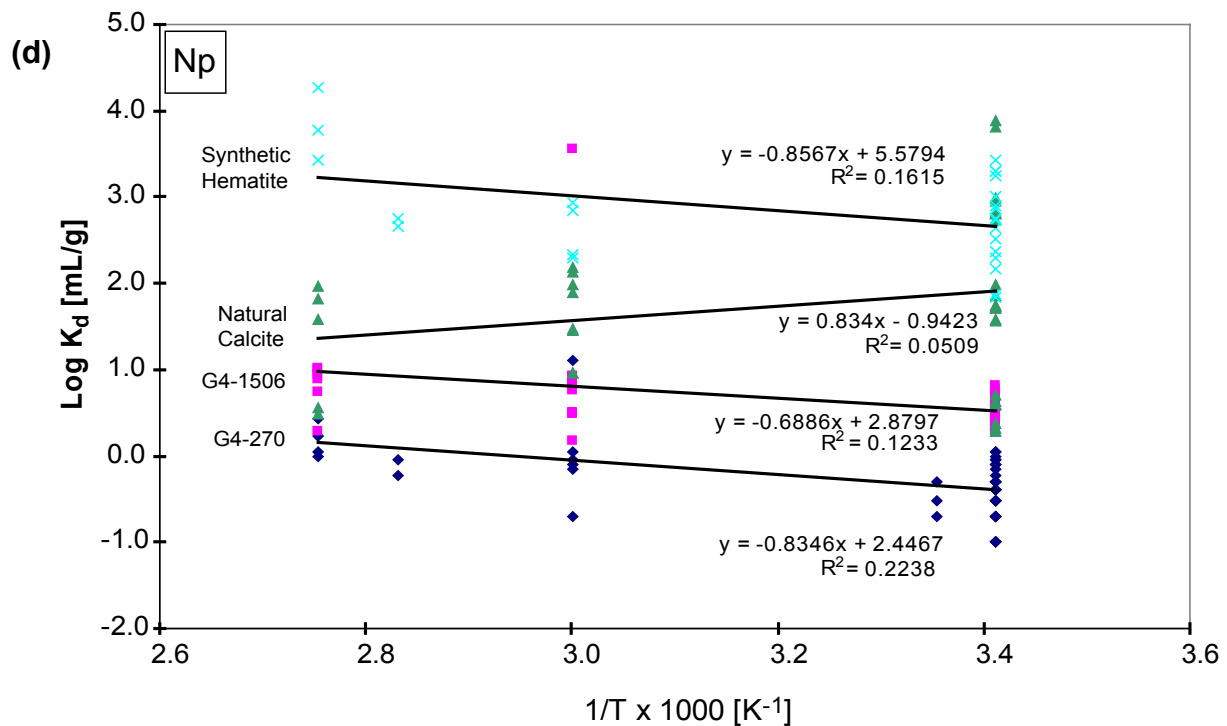
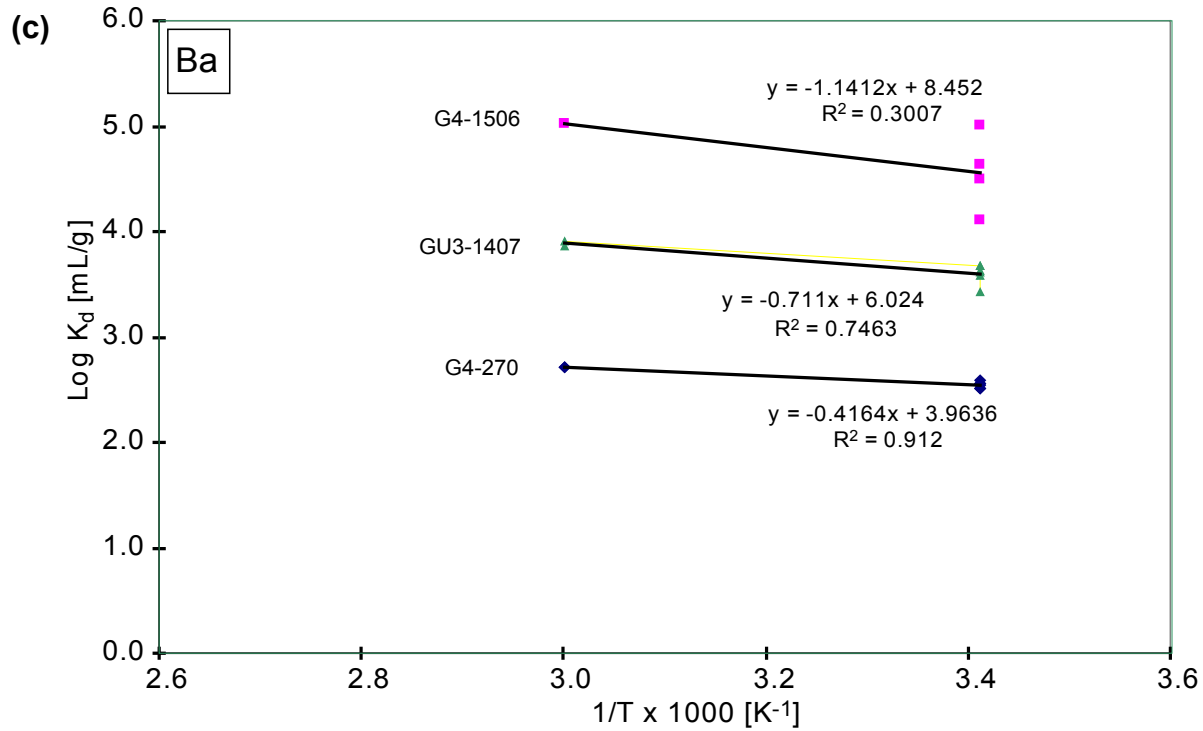


Figure 6.4-1. Calculated Values of log K_d as a Function of Reciprocal Absolute Temperature, Based on Batch Sorption of Specified Radioelements on Crushed Yucca Mountain Tuff and Mineral Samples



Input-DTNs: LA0010JC831341.001 [162476]; LA0010JC831341.002 [153321]
 LA0010JC831341.003 [153322]; LA0010JC831341.007 [153319]
 Output-DTN: LB0311ABSTHCR2.004

NOTE: The K_d measurements are listed in Table 6.4-4.

Figure 6.4-1. Calculated Values of log K_d as a Function of Reciprocal Absolute Temperature, Based on Batch Sorption of Specified Radioelements on Crushed Yucca Mountain Tuff and Mineral Samples (Continued)

Table 6.4-5. Calculation of the Enthalpy of Sorption of Aqueous Species on Various Sorbents^a

Aq. Species	Sorbent	Temperature Range, °C	Slope	R ²	ΔH _r , kcal/mol	Notes
Sr	G4-270	20, 60, 80	-0.2471	0.751	1.13	sorption
	G4-1506		-1.0126	0.390	4.63	
	GU3-1407		-0.0361	0.179	0.17	
Cs	G4-270	20, 60, 80	-0.1263	0.076	0.58	sorption
	G4-1506		-0.1057	0.010	0.48	
	GU3-1407		-0.0480	0.011	0.22	
Ba	G4-270	20, 60	-0.4164	0.912	1.91	sorption
	G4-1506		-1.1412	0.301	5.22	
	GU3-1407		-0.7110	0.746	3.25	
Np	G4-270	20, 25, 60, 80, 90	-0.8346	0.224	3.82	sorption
	G4-1506		-0.6886	0.123	3.15	
	Natural calcite		0.8340	0.051	-3.82	
	Synthetic hematite	20, 60, 80, 90	-0.8567	0.162	3.92	

Sources: DTN: LA0010JC831341.001 [162476]; LA0010JC831341.002 [153321]; LA0010JC831341.003 [153322]; LA0010JC831341.007 [153319]
Output-DTN: LB0311ABSTHCR2.004

NOTE: ^aSummarized from Table 6.4-4 and Figure 6.4-1.

6.4.4.2 Unqualified LANL Data

These data consist of K_d measurements made prior to 1987, compiled in LANL Report No. LA-10960-MS (Thomas 1987 [101361]) (Table 6.4-7) and those averaged at discrete temperatures summarized in LANL Report No. LA-9328-MS (Daniels et al. 1982 [105803]) (Table 6.4-6).

Table 6.4-6. Average Sorption and Desorption Ratios for Pulverized Tuff^a from Sorption and Desorption Experiments at Room Temperature (20 ± 4°C) and at 70°C with J-13 Well Water

Sample	Depth, ft	USW-G1 depth ^b , ft.	K _d , mL/g								
			Sr	Cs	Ba	Ce	Eu	Am	Pu	U	Np
Room Temperature (20 ± 4°C)											
Sorption											
JA-18	1420	1339	17000 (3000) ^c	16000 (1000)	38000 (18000)	2800 (1400)	1400 (200)	180 (30)	120 (20)	2.5 (0.4)	
JA-32	2533	2467	57 (3)	123 (4)	380 (30)	82 (14)	90 (20)	130 (30)	110	2.2 (0.9)	
JA-37	3497	3286	287 (14)	610 (40)	760 (150)		6000 (800)	28000 (10000)	400 (70)	4.6 (0.3)	28 (7)
Desorption											
JA-18	1420	1339	15000 (2000)	17500 (700)	280000 (50000)	1600 (500)	2400 (300)	1100 (300)	350 (140)	9.4 (1.4)	
JA-32	2533	2467	53 (3)	175 (11)	490 (40)	530 (120)	850 (130)	2200 (600)		8 (2)	
JA-37	3497	3286	312 (9)	850 (50)	920 (40)		11000 (2000)	32000 (10000)	1400 (300)	9.9 (0.4)	170 (50)

Source: Daniels et al. (1982 [105803], Tables XXI, XXII)

NOTE: ^a Fractions do not contain <75 μm diameter particles

^b Depth equivalent in drill hole USW-G1 according to position in geologic unit.

^c Values in parentheses are the absolute value standard deviations of the means.

Table 6.4-6. Average Sorption and Desorption Ratios for Pulverized Tuff^a from Sorption and Desorption Experiments at Room Temperature (20 ± 4 °C) and at 70°C with J-13 Well Water (Continued)

Sample	Depth, ft	USW-G1 depth ^b , ft.	K _d , mL/g								
			Sr	Cs	Ba	Ce	Eu	Am	Pu	U (VI)	Np
70 °C											
Sorption											
JA-18	1420	1339	18000 (2000) ^{c,d}	18000 (1000)	49000 (7000)					4.0 (0.2)	
JA-32	2533	2467	113 (9)	97 (6)	110 (120)	80 (20)	140 (30)	110 (20)		11.7 (1.7)	
JA-37	3497	3286	1050 (130)	1360 (85)	3670 (700)		4200 (400)	1000 (200)	240	16 (2)	
Desorption											
JA-18	1420	1339	21000 (2000)	19300 (1300)	108000 (13000)					14 (3)	
JA-32	2533	2467	100 (8)	108 (4)	1160 (100)	640 (8)	1800 (300)			21.1 (1)	
JA-37	3497	3286	1340 (110)	2700 (500)	5900 (900)		14000 (1000)			47 (6)	

Source: Daniels et al. (1982 [105803], Table XXVII)

NOTE: ^a Fractions do not contain <75 μm diameter particles^b Depth equivalent in drill hole USW-G1 according to position in geologic unit.^c Nonweighted average^d Values in parentheses are the absolute value standard deviations of the means.

Table 6.4-7. Sorption and Desorption Ratios for Plutonium and Americium on Tuffaceous Core from Sorption and Desorption Experiments at Room Temperature ($20 \pm 4^\circ\text{C}$) and at 85°C with J-13 Well Water

Core Sample	Approach to equilibrium	Temperature, $^\circ\text{C}$	Duration, day	Concentration of sorbent, mol/L	K_d , mL/g	$1/T \times 1000$, K^{-1}	Log K_d
Plutonium							
GU3-0433	Sorption	20	42	2.60×10^{-8}	340	3.411	2.531
		20			500	3.411	2.699
		20			240	3.411	2.380
		20			240	3.411	2.380
		85			1700	2.792	3.230
		85			1800	2.792	3.255
	Desorption	20	42	2.60×10^{-8}	960	3.411	2.982
		20			810	3.411	2.908
		20			100	3.411	2.000
		20			890	3.411	2.949
		85			4500	2.792	3.653
		85			7800	2.792	3.892
GU-1203	Sorption	20	42	2.40×10^{-8}	330	3.411	2.519
		20			480	3.411	2.681
		20			300	3.411	2.477
		20			340	3.411	2.531
		85			440	2.792	2.643
		85			940	2.792	2.973
	Desorption	20	42	2.40×10^{-8}	920	3.411	2.964
		20			880	3.411	2.944
		20			920	3.411	2.964
		20			950	3.411	2.978
		85			620	2.792	2.792
		85			830	2.792	2.919
GU3-1301	Sorption	20	42	4.60×10^{-8}	380	3.411	2.580
		20			330	3.411	2.519
		20			200	3.411	2.301
		20			250	3.411	2.398
		85			2500	2.792	3.398
		85			7600	2.792	3.881
	Desorption	20	42	4.60×10^{-8}	1800	3.411	3.255
		20			2400	3.411	3.380
		20			560	3.411	2.748
		20			600	3.411	2.778
		85			1300	2.792	3.114
		85			1600	2.792	3.204

NOTE: * Fractions do not contain $<75 \mu\text{m}$ diameter particles.
Unqualified data from Thomas (1987 [101361], pp. 58–62, Appendix)

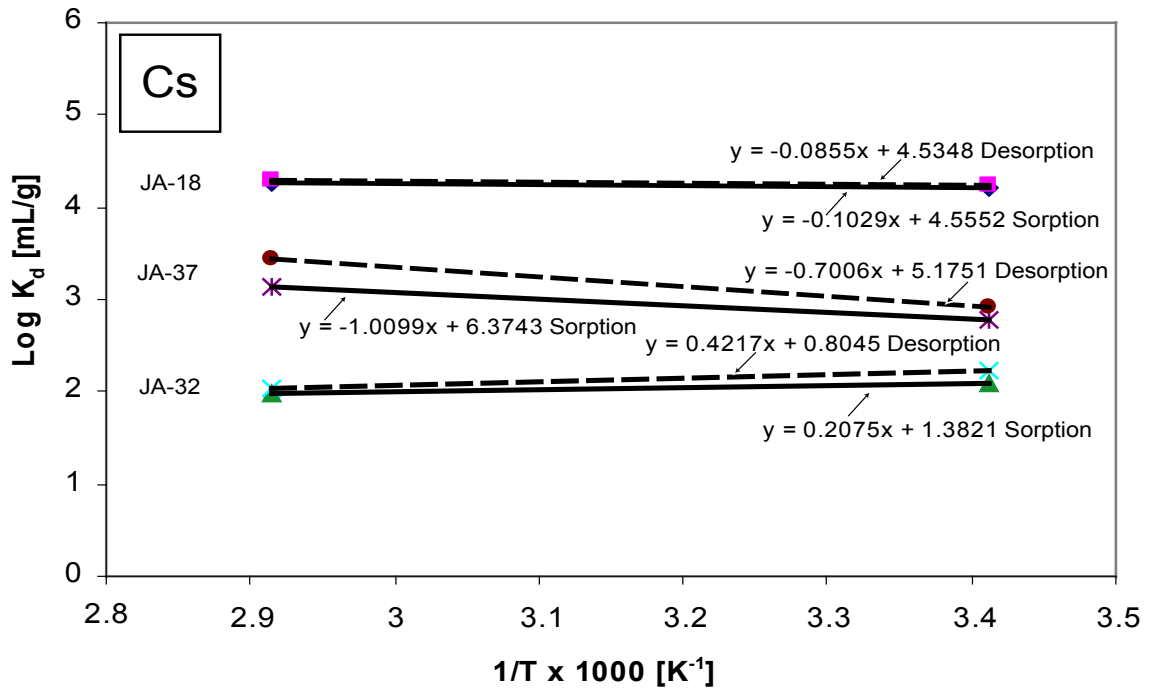
Table 6.4-7. Sorption and Desorption Ratios for Plutonium and Americium on Tuffaceous Core from Sorption and Desorption Experiments at Room Temperature ($20 \pm 4^\circ\text{C}$) and at 85°C with J-13 Well Water (Continued)

Core Sample	Approach to equilibrium	Temperature, $^\circ\text{C}$	Duration, day	Concentration of sorbent, mol/L	K_d , mL/g	$1/T \times 1000$, K^{-1}	Log K_d
Americium							
GU3-0433	Sorption	20	42	2.10×10^{-7}	3300	3.411	3.519
		20			2900	3.411	3.462
		20			3500	3.411	3.544
		20			3800	3.411	3.580
		85			2100	2.792	3.322
		85			4200	2.792	3.623
	Desorption	20	42	2.10×10^{-7}	9500	3.411	3.978
		20			6000	3.411	3.778
		20			7800	3.411	3.892
		20			14000	3.411	4.146
		85			6700	2.792	3.826
		85			3500	2.792	3.544
GU3-1203	Sorption	20	42	2.10×10^{-7}	1400	3.411	3.146
		20			1200	3.411	3.079
		20			860	3.411	2.934
		20			970	3.411	2.987
		85			4200	2.792	3.623
		85			4300	2.792	3.633
	Desorption	20	42	2.10×10^{-7}	900	3.411	2.954
		20			1800	3.411	3.255
		20			990	3.411	2.996
		20			1400	3.411	3.146
		85			7200	2.792	3.857
		85			10500	2.792	4.021
GU3-1301	Sorption	20	42	2.40×10^{-7}	1600	3.411	3.204
		20			1400	3.411	3.146
		20			2000	3.411	3.301
		20			2050	3.411	3.311
		85			8600	2.792	3.934
		85			11000	2.792	4.041
	Desorption	20	42	2.40×10^{-7}	3800	3.411	3.580
		20			3200	3.411	3.505
		20			1500	3.411	3.176
		20			1500	3.411	3.176
		85			23000	2.792	4.362
		85			19000	2.792	4.279

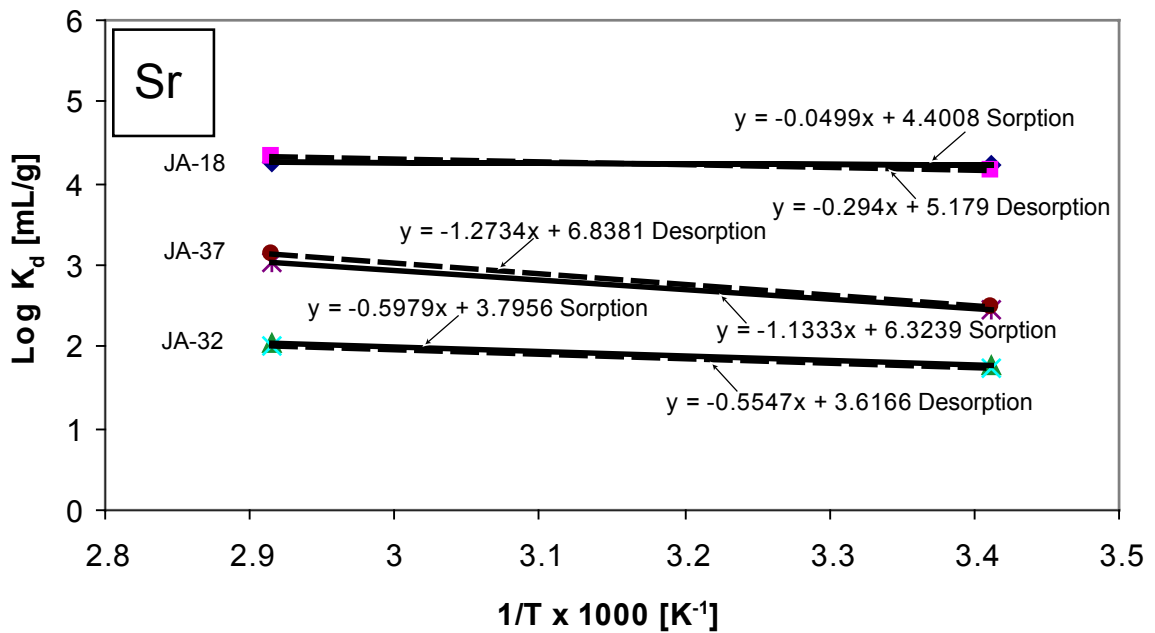
NOTE: * Fractions do not contain $<75 \mu\text{m}$ diameter particles.
Unqualified data from Thomas (1987 [101361], pp. 58–62, Appendix)

The data from Daniels et al. (1982 [105803]) are tabulated for each given radioelement averaged at “room temperature” (estimated at $20^{\circ}\text{C} \pm 4^{\circ}\text{C}$) and a smaller set of measurements averaged at 70°C in Tables XXI, XXII and XXVII, respectively, in the subject reference. These data are summarized in Table 6.4-6. The radioelements for which there are K_d data include Cs, Sr, Ba, Ce, Eu, Am, Pu and U(VI). Advantage was taken of this compilation and the data plotted as $\text{Log } K_d$ versus $1/T [\text{K}^{-1}]$, as illustrated in Figures 6.4-2a–h. Because averaged values were entered, no statistical fit is obtained. In addition, Thomas (1987 [101361]) also includes data on Pu and Am adsorption on core material at 20 and 85°C , which are summarized in Table 6.4-7. The corresponding $\text{Log } K_d$ values were plotted and regressed to obtain linear equations, as illustrated in Figures 6.4-3a–b. The calculated enthalpies of sorption are summarized in Table 6.4-8.

(a)



(b)



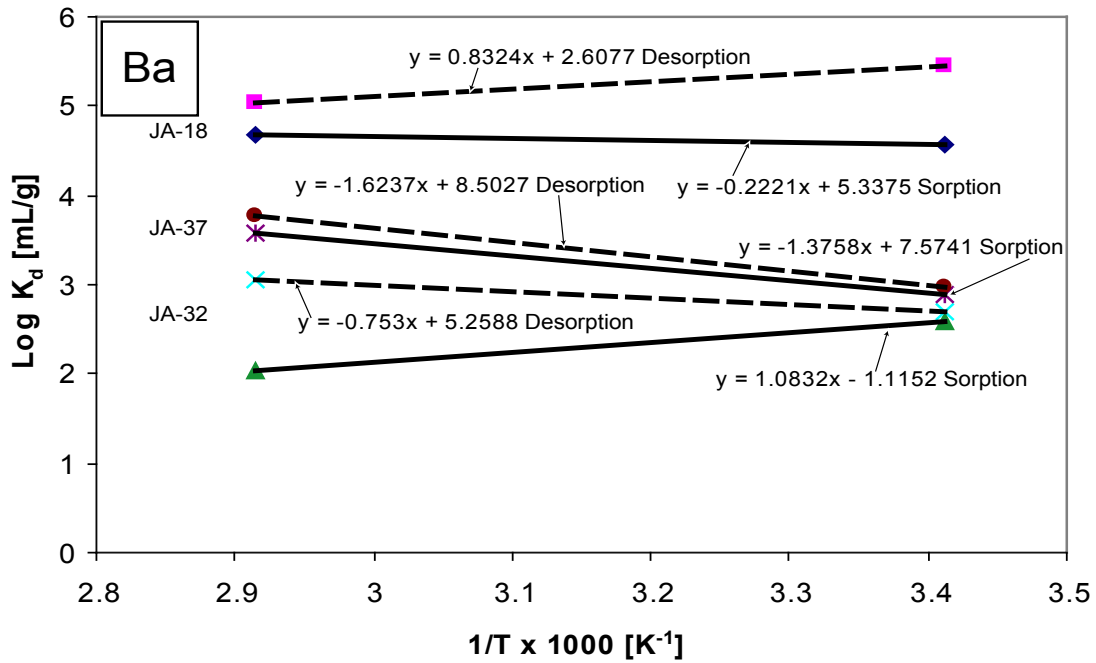
Output-DTN: LB0311ABSTHCR2.004

Source: Daniels et al. (1982 [105803], pp. 78–79, 111, Tables XXI, XXII, and XXVII).

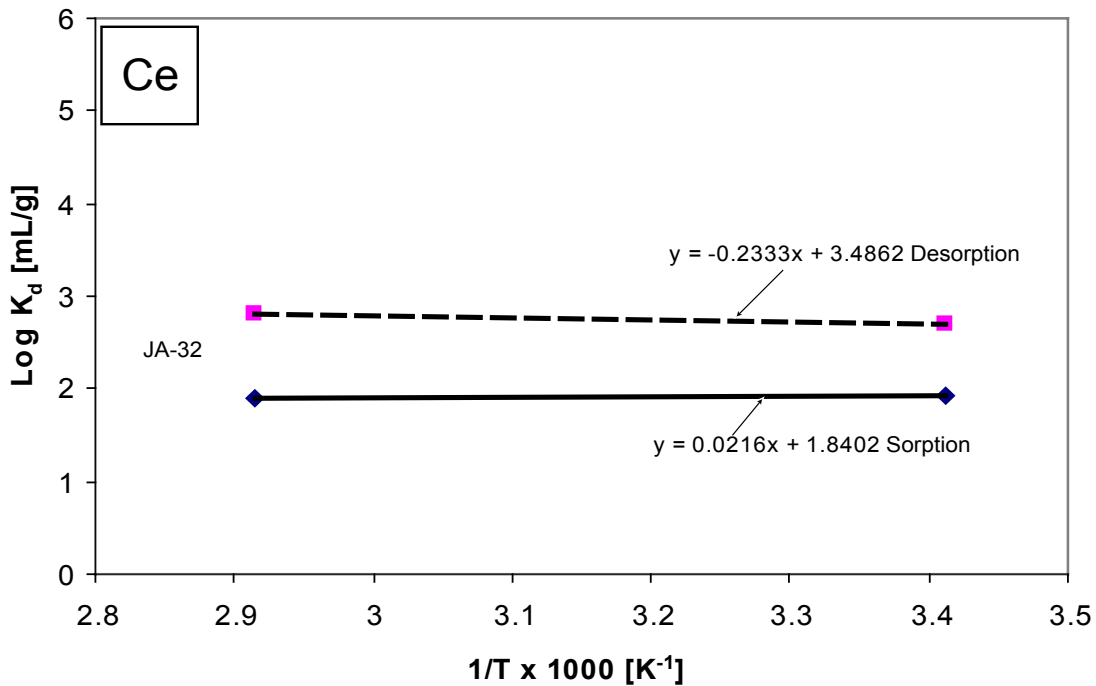
NOTE: Data listed in Table 6.4-6; data summarized in Table 6.4-8.

Figure 6.4-2. Calculated Values of log K_d as a Function of Reciprocal Absolute Temperature, Based on Both Sorption and Desorption Radioelements on Crushed Yucca Mountain Tuff

(c)



(d)



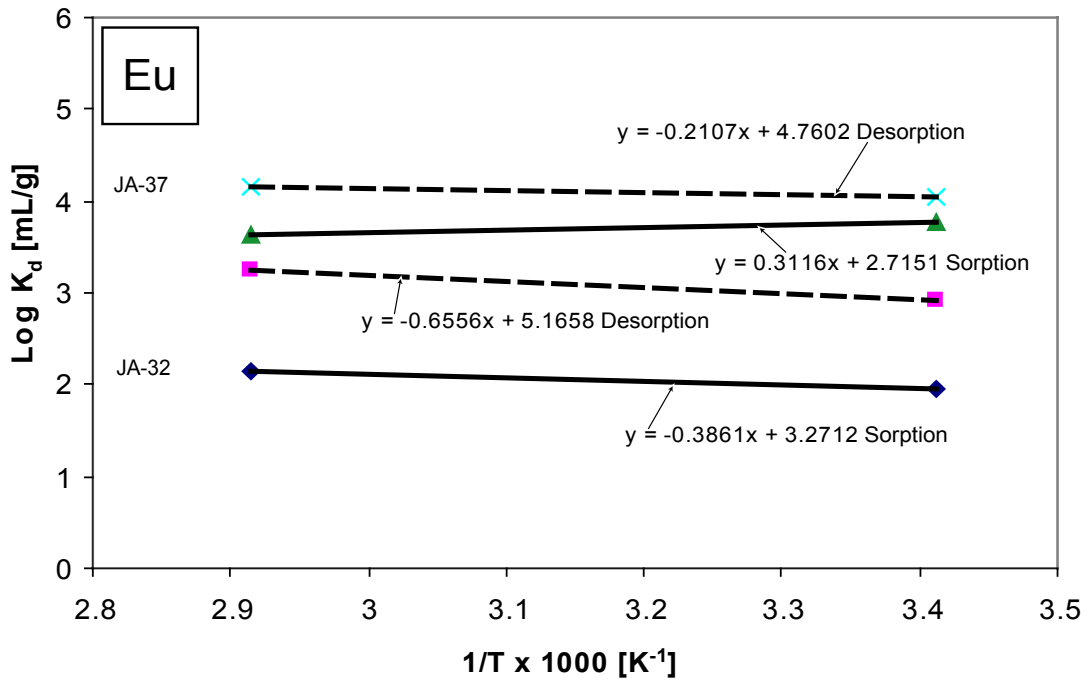
Output-DTN: LB0311ABSTHCR2.004

Source: Daniels et al. 1982 ([105803], pp. 78–79, 111, Tables XXI, XXII, and XXVII).

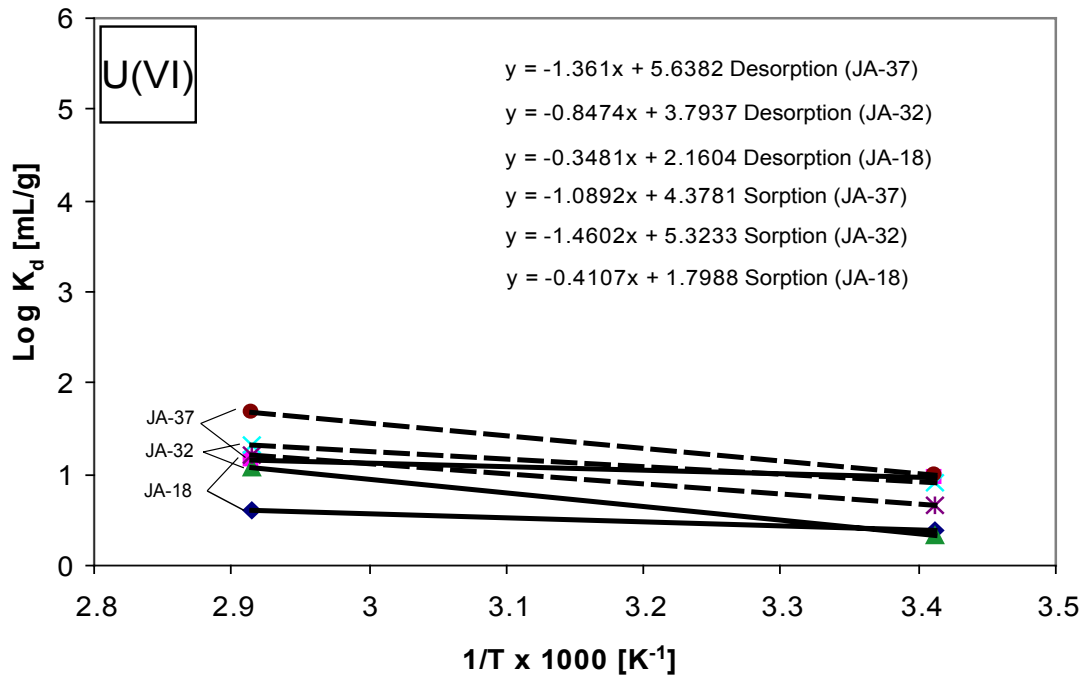
NOTE: Data listed in Table 6.4-6; data summarized in Table 6.4-8.

Figure 6.4-2. Calculated Values of log K_d as a Function of Reciprocal Absolute Temperature Based on Both Sorption and Desorption Radioelements on Crushed Yucca Mountain Tuff (Continued)

(e)



(f)



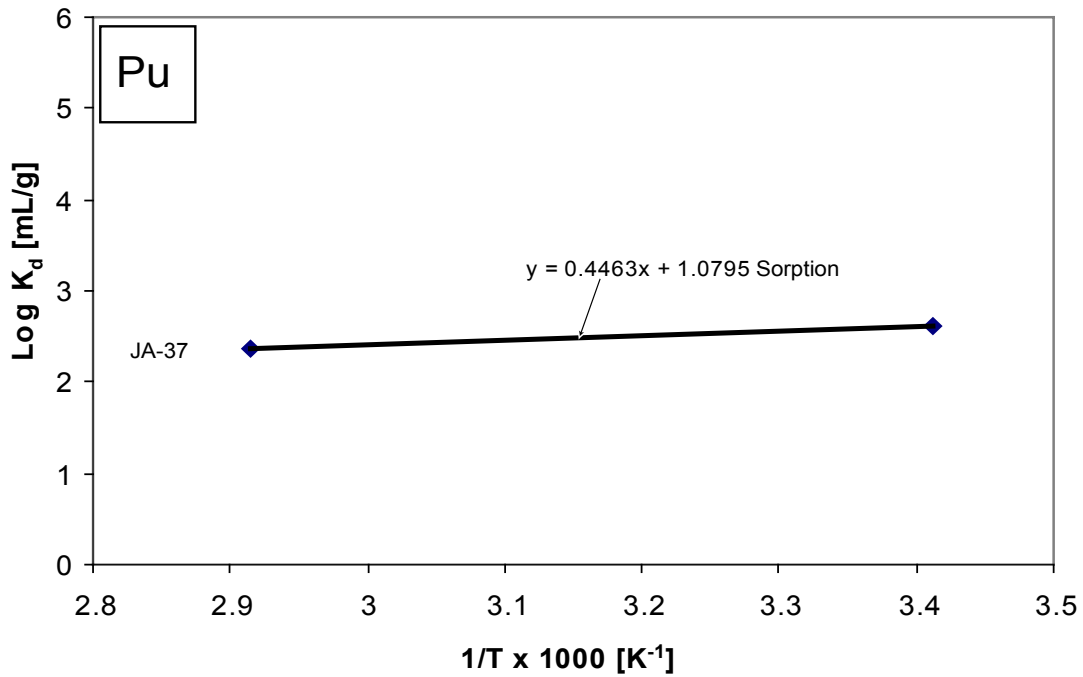
Output-DTN: LB0311ABSTHCR2.004

Source: Daniels et al. (1982 [105803], pp. 78–79, 111, Tables XXI, XXII, and XXVII).

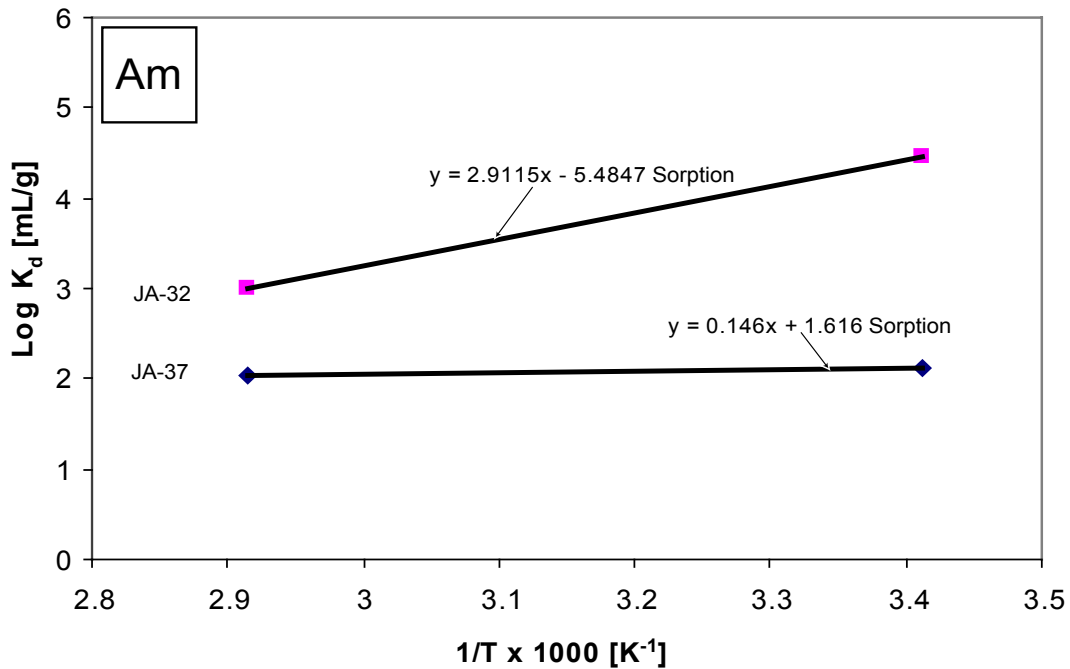
NOTE: Data listed in Table 6.4-6; data summarized in Table 6.4-8.

Figure 6.4-2. Calculated Values of log K_d as a Function of Reciprocal Absolute Temperature, Based on Both Sorption and Desorption Radioelements on Crushed Yucca Mountain Tuff (Continued)

(g)



(h)

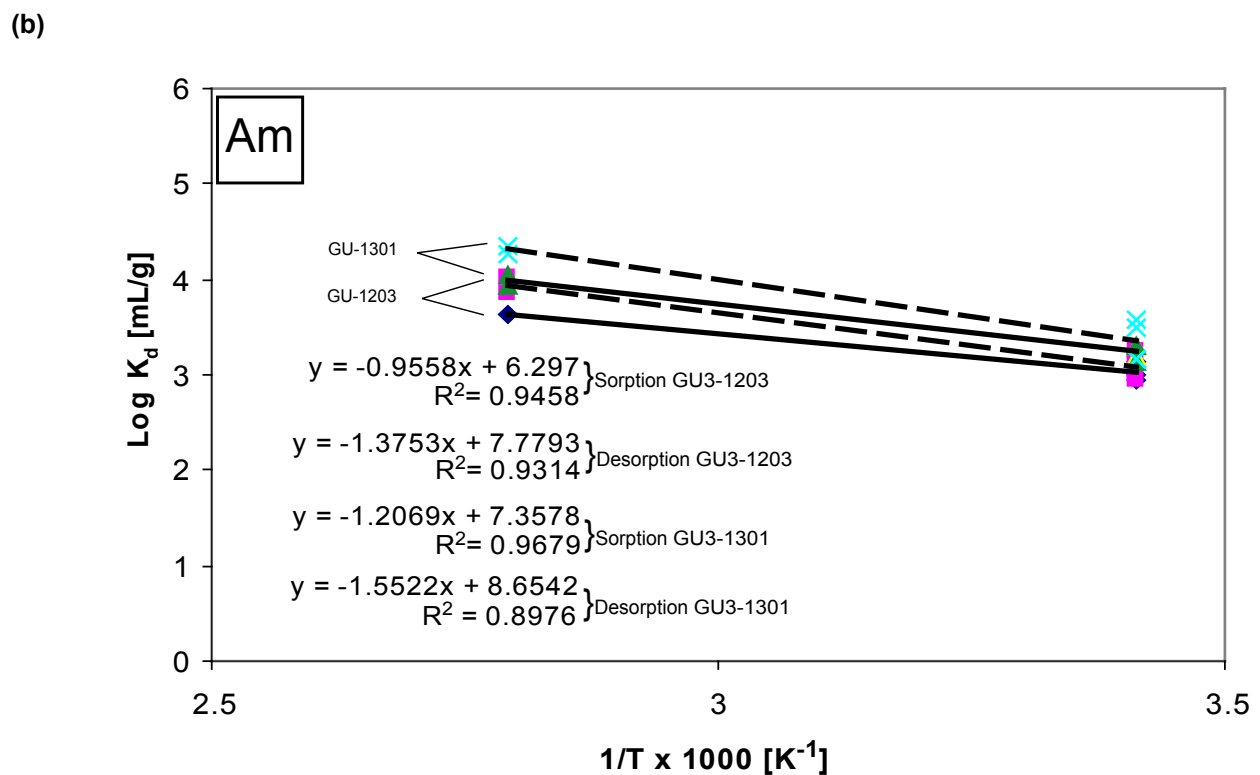
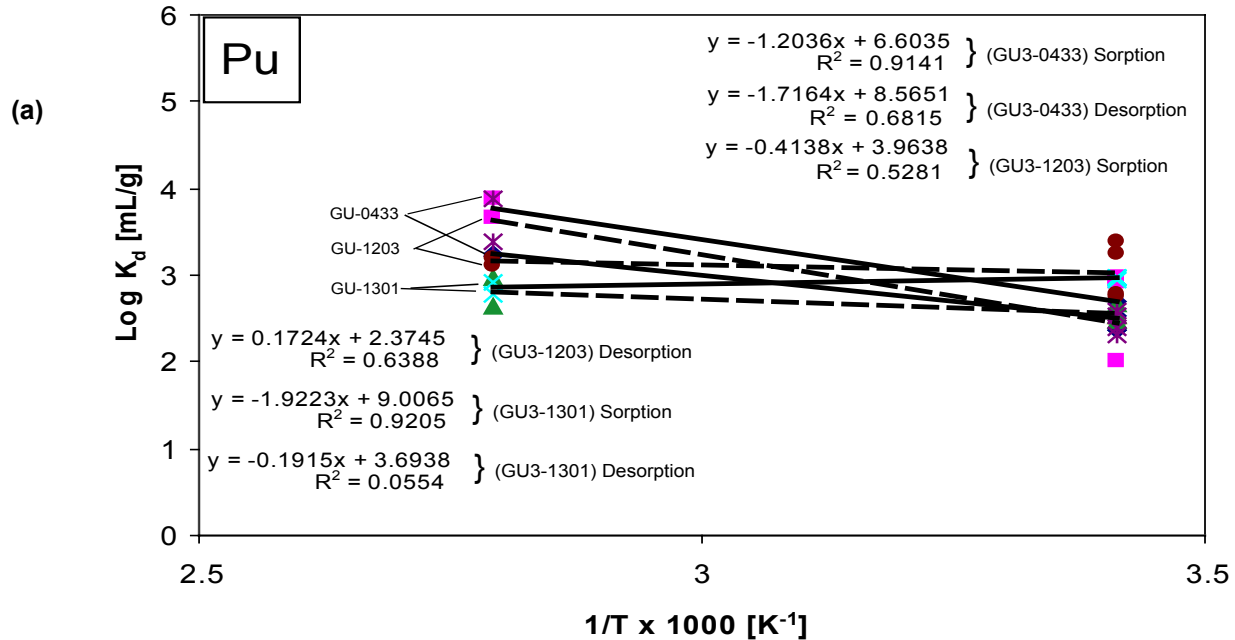


Output-DTN: LB0311ABSTHCR2.004

Source: Daniels et al. (1982 [105803], pp. 78–79, 111, Tables XXI, XXII, and XXVII).

NOTE: Data listed in Table 6.4-6; data summarized in Table 6.4-8.

Figure 6.4-2. Calculated Values of $\log K_d$ as a Function of Reciprocal Absolute Temperature, Based on Both Sorption and Desorption Radioelements on Crushed Yucca Mountain Tuff (Continued)



Output-DTN: LB0311ABSTHCR2.004

NOTE: Data source: Thomas 1987 (101361), pp. 58–62, Appendix), which are listed in Table 6.4-7. Data summarized in Table 6.4-8.

Figure 6.4-3a–b. Calculated Value of $\log K_d$ as a Function of Reciprocal Absolute Temperature, Based on Both Sorption and Desorption of Specified Radioelements on Tuff Core Samples from Yucca Mountain

Table 6.4-8. Calculation of the Enthalpy of Sorption of Aqueous Species on Various Sorbents^a

Aq. Species	Sorbent	Temperature Range °C	Slope	R ²	ΔH _r , kcal/mol	Notes
Sr	JA-18	20-70	-0.0499		+0.23	sorption
			-0.294		+1.35	desorption
	JA-32		-0.5979		+2.74	sorption
			-0.5547		+2.54	desorption
	JA-37		-1.1333		+5.19	sorption
			-1.2753		+5.83	desorption
Cs	JA-18		-0.1029		+0.47	sorption
			-0.0855		+0.39	desorption
	JA-32		+0.2075		-0.95	sorption
			+0.4217		-1.93	desorption
	JA-37		-0.7006		+3.21	sorption
			-1.0099		+4.62	desorption
Ba	JA-18		-0.2221		+1.02	sorption
			+0.8324		-3.81	desorption
	JA-32		+1.0832		-4.96	sorption
			-0.7530		+3.45	desorption
	JA-37		-1.3758		+6.30	sorption
			-1.6237		+7.43	desorption
Ce	JA-32		+0.0216		-0.10	sorption
			-0.2333		+1.07	desorption
Eu	JA-32		-0.3861		+1.77	sorption
			-0.6556		+3.00	desorption
	JA-37		+0.3116		-1.43	sorption
			-0.2107		+0.96	desorption
Am	JA-32		+0.146		-0.67	sorption
			JA-37		+2.9115	-13.32
Pu	JA-37		+0.4463		-2.04	sorption
U (VI)	JA-18		-0.4107		+1.88	sorption
			-0.3481		+1.59	desorption
	JA-32		-1.4602		+6.68	sorption
			-0.8474		+3.88	desorption
	JA-37		-1.0892		+4.98	sorption
			-1.3610		+6.23	desorption
Pu	GU3-0433	20-85	-1.2036	0.914	+5.51	sorption
			-1.7164	0.682	+7.85	desorption
	GU3-1203		-0.4138	0.528	+1.89	sorption
			0.1724	0.639	-0.79	desorption
	GU3-1301		-1.9223	0.921	+8.80	sorption
			-0.1915	0.055	+0.88	desorption
Am	GU3-1203		-0.9558	0.946	+4.37	sorption
			-1.3753	0.931	+6.29	desorption
	GU3-1301		-1.2069	0.968	+5.52	sorption
			-1.5522	0.898	+7.10	desorption

Output-DTN: LB0311ABSTHCR2.004

Source: Data from Daniels et al. (1982 [105803], Tables XXI, XXII, and XXVII), and Thomas (1987 [101361], pp. 58–62, Appendix).

NOTE: ^aSummarized from Figure 6.4-2, which plots data in Tables 6.4-6 and 6.4-7.

6.4.4.3 Data from the Refereed Literature

Only a few papers report on the temperature dependence of radionuclide sorption on natural substrates. Several other papers containing useful information in the general subject area were also reviewed and data extracted for comparative purposes. A summary of information contained in journal articles that are considered for further review is given in Tables 6.4-9 and 6.4-10. The refereed data fall into two classifications: (1) (Table 6.4-9), raw data, where K_d values at various temperatures are provided without further evaluation of sorption thermodynamic properties in relation to temperature; and (2) (Table 6.4-10), evaluated data, where $\Delta G_r(T)$, ΔH_r and ΔS_r of the sorption reaction under consideration have been determined. The latter data sources commonly omit tabulated sorption coefficient data, data instead being presented in graphical form. Note that the data summarized in these two tables were collected using various concentrations of sorbent and pH values, as well as using aqueous solutions containing differing supporting electrolytes at various specified concentrations. Details concerning these study conditions can be found in the cited sources. Direct intercomparison between data sets from these sources is therefore not feasible, as will be discussed further, below.

Table 6.4-9. Sorption Coefficients, K_d , for Various Metal Species, Reported in the Literature (Unqualified Data)

Sorbate and Sorbent	T, °C	K_d , mL/g	1/T x 1000, K ⁻¹	Log K_d
<u>van Geldermalsen and Duursma (1984 [165087])</u>				
Cd, Estuarine Sediments	4	1765	3.608	3.247
	20	1150	3.411	3.061
	37	941	3.224	2.974
	50	624	3.095	2.795
	75	246	2.872	2.391
	90	111	2.754	2.045
Cd, Marine Sediments	4	56	3.608	1.748
	37	45.9	3.224	1.662
	60	28.6	3.002	1.456
	90	17.6	2.754	1.246
Pu-239, Estuarine Sediments	4		3.608	5.945
	20		3.411	5.624
	80		2.832	5.038
Pu-239, Marine Sediments	4		3.608	6.360
	20		3.411	6.101
	80		2.832	5.904
	140		2.420	6.027
Eu-152, Estuarine Sediments	4		3.608	4.284
	80		2.832	4.277
Eu-152, Marine Sediments	4		3.608	4.678
	80		2.832	4.827
<u>Kenna (1981 [165049]) and Erickson (1979 [164876])</u>				
Cs, Seabed Smectite Clay	4	5012	3.608	3.700
	20	1180	3.411	3.072
	60	343	3.002	2.535
Sr, Seabed Smectite Clay	4	200	3.608	2.301
	20	126	3.411	2.100
	60	170	3.002	2.230
Eu, Seabed Smectite Clay	4	2500	3.608	3.398
	20	1.00E+07	3.411	7.000
	60	1.00E+07	3.002	7.000
Ba, Seabed Smectite Clay	4	1.12E+05	3.608	5.049
	20	9.30E+04	3.411	4.968
	60	5.50E+04	3.002	4.740

Table 6.4-9. Sorption Coefficients, K_d , for Various Metal Species, Reported in the Literature (Unqualified Data) (Continued)

Sorbate and Sorbent	T, °C	K_d , mL/g	1/T x 1000, K ⁻¹	Log K_d	
Aksyuk et al. (1995 [165054])					
Sr, porphyrite	20	308	3.411	2.489	
		280	3.411	2.447	
		60	3.411	1.778	
		33.2	3.411	1.521	
		852	3.411	2.930	
		25.2	3.411	1.401	
		368	3.411	2.566	
		1192	3.411	3.076	
		280	3.411	2.447	
		596	3.411	2.775	
		2548	3.411	3.406	
		1880	3.411	3.274	
		1824	3.411	3.261	
		138.4	3.411	2.141	
		38.4	3.411	1.584	
	118.4	3.411	2.073		
	86.4	3.411	1.937		
		100	11.96	2.680	1.078
			1.86	2.680	0.271
	5.86		2.680	0.768	
	4.03		2.680	0.606	
	17.87		2.680	1.252	
	18.82		2.680	1.275	
	200	38.63	2.113	1.587	
		17.76	2.113	1.249	
		29.32	2.113	1.467	
		4.53	2.113	0.656	
		16.66	2.113	1.222	
		16.36	2.113	1.214	
	250	8.89	1.911	0.949	
		13.95	1.911	1.145	
		1.37	1.911	0.137	
		13.05	1.911	1.116	
		6.00	1.911	0.778	
		2891.4	1.911	3.461	
		2916.1	1.911	3.465	

Table 6.4-10. Enthalpy, Entropy and Gibbs Free Energy of Adsorption of Aqueous Species on Various Sorbents (Unqualified Data from the Published Literature)

Sorbate	Sorbate Concentration, mmol/dm ³	Sorbent	Model	Temperature, °C	ΔH°_{ads} , kcal/mol	ΔS°_{ads} , cal/mol·K	ΔG°_{ads} , kcal/mol	Reference		
Cs(I)	3.7	KCNF	Assumed linear ¹	20	11.13	57.36	-6.01	Ishfaq et al. (1997 [164879])		
				30		56.88	-6.33			
				40		56.41	-6.51			
				50		56.41	-7.08			
				60		56.88	-7.82			
Co(II)	5 x 10 ⁻⁴ – 10.0	sepiolite	Frumkin	20	0.98	16.13	-3.75	Kara et al. (2003 [164880])		
				30		16.23	-3.93			
				40		16.13	-4.07			
			Modified Frumkin	20	0.89	15.82	-3.74			
				30		15.89	-3.92			
				40		15.82	-4.06			
			Langmuir	20	-1.37	8.91	-3.27			
				30		6.29	-3.28			
				40		6.48	-3.40			
			Flory-Higgins	20	0.22	12.52	-3.45			
				30		12.52	-3.58			
				40		11.76	-3.47			
Fe(II)	1.79	bentonite	Assumed linear ²	25	8.14	42.30	-5.52	Rauf and Tahir (2000 [164893])		
				30			-5.09			
				40			-4.67			
				50			-4.46			
				3.58	25	16.20	67.29		-5.54	
					30				-4.87	
	40					-4.19				
	5.37		25	16.03	67.29	-5.70				
			30			-5.03				
			40			-4.36				
					50			-4.02		

Table 6.4-10. Enthalpy, Entropy and Gibbs Free Energy of Adsorption of Aqueous Species on Various Sorbents (Unqualified Data from the Published Literature) (Continued)

Sorbate	Sorbate Concentration, mmol/dm ³	Sorbent	Model	Temperature, °C	ΔH°_{ads} , kJ/mol	ΔS°_{ads} , J/mol · K	ΔG°_{ads} , kJ/mol	Reference
Mn(II)	1.82			25	-3.13	0.12	-3.16	Rauf and Tahir (2000 [164893])
				30			-3.16	
				40			-3.16	
				50			-3.16	
	3.64			25	-2.32	0.63	-2.51	
				30			-2.51	
				40			-2.52	
				50			-2.52	
	5.46			25	-0.62	2.21	-2.29	
				30			-2.30	
				40			-2.32	
				50			-2.34	
Cu(II)	0.157	α -Al hydroxide	Calculation of the apparent stability constant, K_s , for the surface complexation reaction: $AlO^- + M^{2+} = AlOM^+$	20	6.87	27.96	-1.31	Mustafa et al. (1991 [165048])
				30			-1.59	
				40			-1.87	
				50			-2.15	
Zn(II)	0.153			20	14.97	53.54	-0.69	
				30			-1.22	
				40			-1.75	
				50			-2.29	
Co(II)	0.170			20	11.82	37.52	0.83	
				30			0.45	
				40			-0.08	
				50			-0.30	
Ni(II)	0.170			20	10.45	29.16	1.90	
				30			1.61	
				40			1.32	
				50			1.03	
Ag(I)	1 - 200	bentonite	Binding constant, K_L , for Langmuir isotherm ³	10	-0.87	5.74	0.78	Zafar et al. (2002 165052)]
				25		5.74	0.86	
				45		5.98	0.99	

Table 6.4-10. Enthalpy, Entropy and Gibbs Free Energy of Adsorption of Aqueous Species on Various Sorbents (Unqualified Data from the Published Literature) (Continued)

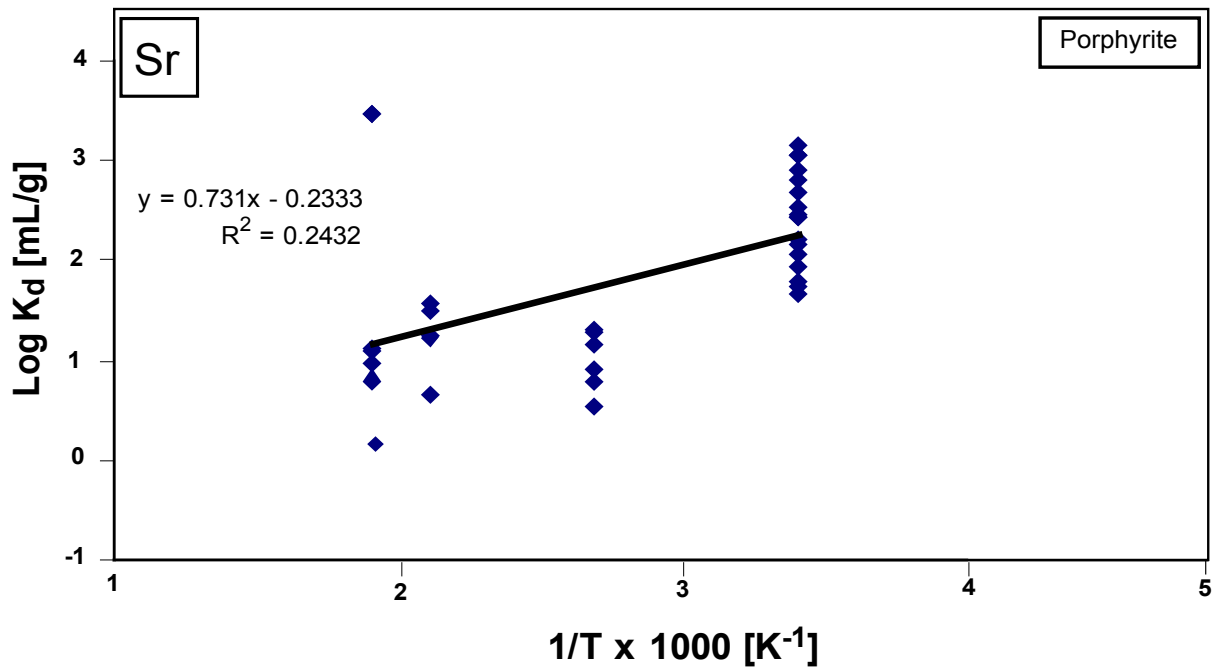
Sorbate	Sorbate Concentration, mmol/dm ³	Sorbent	Model	Temperature, °C	ΔH°_{ads} , kJ/mol	ΔS°_{ads} , J/mol·K	ΔG°_{ads} , kJ/mol	Reference
U(VI)	10 - 100	halloysite	Assumed linear ⁴	20	1.55	15.61	-3.02	Kilislioglu and Bilgin (2002 [165050])
				30			-3.18	
				40			-3.33	
				50			-3.49	
				60			-3.64	

NOTE: ¹ Freundlich, Langmuir and Dubinin-Radushkevich (D-R) isotherms tested.
² Freundlich and Langmuir isotherms tested.
³ Freundlich isotherm also tested.
⁴ Freundlich, Langmuir and Dubinin-Radushkevich (D-R) isotherms tested.

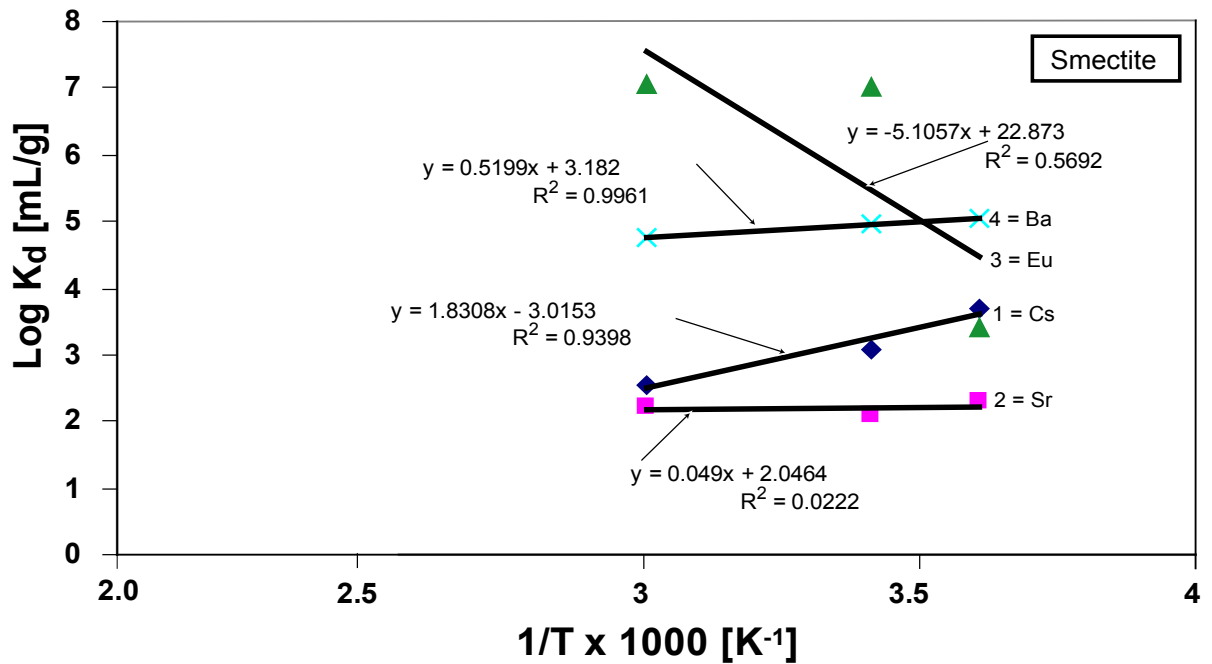
Note also that considerable study was devoted to the sorption behavior of radioelements (Tc, I, Np, Ra, Se, Pu, U, Cs, Am, and Sr) on basalt, secondary alteration minerals, and interbed materials under the former Basalt Waste Isolation Project (BWIP) at the Hanford Site, near Richland, Washington. A significant body of sorption measurements was conducted at elevated temperatures. Some of the data collected during the project were abstracted and summarized by Kelmers (1984 [165041]). However, the summary is too cursory for suitable analysis, and cited original sources were neither located nor consulted for this evaluation.

Data from Aksyuk et al. (1995 [165054]), Kenna (1981[165049]) and Van Geldermalsen and Duursma (1984 [165087]) were manipulated to obtain values of $\log K_d$ as a function of $1/T$ [K^{-1}], which were plotted graphically as illustrated in Figures 6.4-4a-c. The data were further subjected to linear regression analysis to obtain the calculated enthalpies of sorption summarized in Table 6.4-11.

(a)



(b)



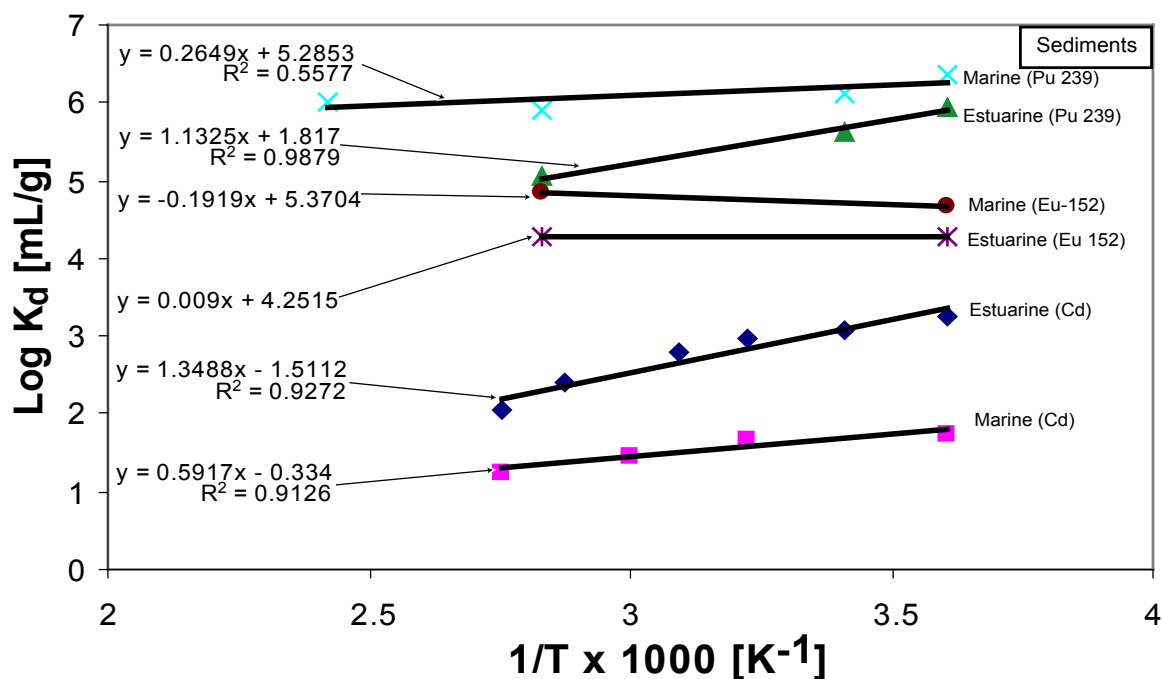
Output-DTN: LB0311ABSTHCR2.003

Source: (a) Aksyuk et al. 1995 [165054], (b) Kenna 1981 [165049], (c) van Geldermalsen and Duursma 1984 [165087]

NOTE: Data are listed in Table 6.4-9

Figure 6.4-4a-c. Log K_d Values as a Function of the Reciprocal Absolute Temperature for Specified Elements on Various Sorbents

(c)



Output-DTN: LB0311ABSTHCR23.004

Source: (a) Aksyuk et al. 1995 [165054], (b) Kenna 1981 [165049], (c) van Geldermalsen and Duursma 1984 [165087]

NOTE: Data are listed in Table 6.4-9

Figure 6.4-4a–c. Log K_d Values as a Function of the Reciprocal Absolute Temperature for Specified Elements on Various Sorbents (Continued)

Table 6.4-11. Calculated Enthalpy of Sorption of Aqueous Species on Various Sorbents (from the literature)

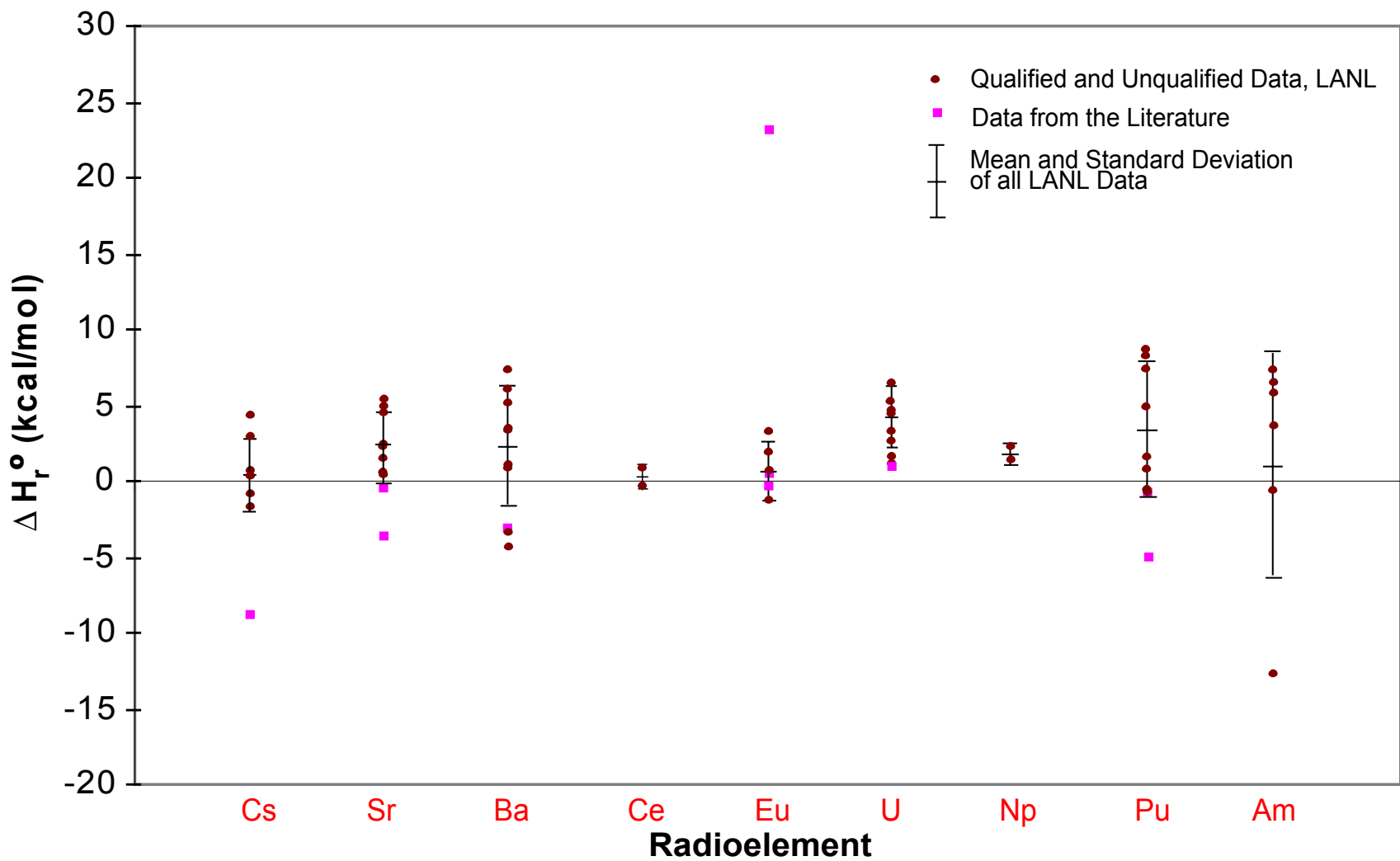
Aq. Species	Sorbent	Temperature Range, °C	Slope	R ²	ΔH _r (kcal/mol)	Source	Notes
Cs	Seabed smectite clay	4-60	+1.8308	0.940	-8.38	Kenna (1981 [165049]) and Erickson (1980 [164876])	
Sr			+0.0490	0.022	-0.22		
Ba			+0.5199	0.996	-2.38		
Eu			-5.1057	0.569	+23.4		
Sr	Porphyrite	20-250	+0.7310	0.243	-3.35	Aksyuk et al. (1995 [165054])	
Cd	Estuarine sediment	4-90	+1.3488	0.927	-6.17	van Geldermalsen and Duursma (1984 [165087])	In seawater
Cd	Marine sediment	4-90	+0.5917	0.913	-2.71		In seawater
Pu-239	Estuarine sediment	4-80	+1.1325	0.988	-5.18		In seawater
Pu-239	Marine sediment	4-140	+0.2649	0.558	-1.21		In seawater
Eu-152	Estuarine sediment	4, 80	+0.0090	-	-0.04		In seawater
Eu-152	Marine sediment	4, 80	-0.1919	-	+0.88		In seawater

Output-DTN: LB0311ABSTHCR2.004

NOTE: Data were illustrated in Figure 6.4-4a–c.

6.4.4.4 Evaluation of Results

The calculated enthalpies of sorption on Yucca Mountain tuffs, ΔH_r° , based on linear regression of the K_d data with respect to the reciprocal of absolute temperature, are plotted in Figure 6.4-5 for the radioelements Cs, Sr, Ba (a proxy for Ra), Ce, Eu (a proxy for trivalent actinides), U(VI), Np, Pu and Am, given in Tables 6.4-5, 6.4-8, 6.4-10, and 6.4-11. ΔH_r° values for Np adsorption on natural calcite and synthetic hematite are omitted from this analysis, because they are not necessarily representative of Np sorption on tuffaceous rocks. The mean value and standard deviation at the 95% confidence level for each radioelement is also included and summarized separately in Table 6.4-12. All radioelements are characterized by a positive mean ΔH_r° . The range for all but Sr, U(VI), and Np is sufficiently large that the assumption of a zero enthalpy of sorption might be conveniently assumed. Any variation in the sorption behavior of the radioelements with temperature can therefore be ignored in modeling radionuclide transport in the near field of the proposed Yucca Mountain geologic waste repository. A positive ΔH_r° for Sr, U(VI), and Np is indicative of increasing sorption with temperature. Thus, for the range of temperatures of interest to those modeling radionuclide release scenarios from the proposed repository at Yucca Mountain, i.e., $\sim 25^\circ\text{C}$ to 95°C , K_d increases by approximately 2.3, 3.9, and 2.3 times, respectively (Wang 2003 [165562], SN-LBNL-SCI-005-V1, p. 283).



Output-DTN: LB0311ABSTHCR2.004
 (See Wang 2003 [165562], SN-LBNL-SCI-005-V1, pp. 249–285 for analyses details.)

Figure 6.4-5. Range of ΔH_r° for the Sorption of Radioelements on Natural Substrates

Table 6.4-12. Radioelement Enthalpies of Sorption, ΔH_r , based on Qualified and Unqualified Data from LANL

Radioelement	Count	ΔH_r , kcal/mol	
		Mean value	Standard Deviation (95%)
Cs	9	+0.788	1.990
Sr	9	+2.646	2.136
Ba	9	+2.201	4.255
Ce	2	+0.485	0.827
Eu	4	+1.075	1.869
U(VI)	6	+4.207	2.153
Np	2	+2.640	0.721
Pu	7	+3.157	4.258
Am	6	+1.548	7.785

Output-DTN: LB0311ABSTHCR2.004

It should be noted that the analysis presented in this Model Report is superficial. A detailed evaluation was not made of the effects of various cited parameters on computed K_d values, and therefore a refinement that could result in a reduction in the uncertainty of ΔH_r for each radioelement was not accomplished. This includes consideration of the experimental conditions under which the sorption tests were conducted, e.g., whether any initial conditions would indicate supersaturation of the radioelement with respect to a solid phase. Given the difficulty in making such an evaluation, the writer believes that the present analysis should suffice. Any such analysis has the potential for creating far more complex and unwieldy equations relating radionuclide sorption to the rock physical, chemical, and spatial properties and to the ground water composition, pH, and redox state. Furthermore, considerable uncertainty would attend the outcome of such an endeavor.

INTENTIONALLY LEFT BLANK

7. VALIDATION

7.1 DRIFT-SCALE COUPLED PROCESSES ABSTRACTION MODEL

The results of abstraction analyses presented in this report are based directly on the results of the THC Seepage Model (the process model), which was previously validated against results from the Drift Scale Test and laboratory experiments (BSC 2003 [162050], Section 7). Validation of the abstraction itself (the DSCPA Model) is discussed here in accordance with the TWP (BSC 2002 [160819], Attachment I, Section I-3-5), and AP-SIII.10Q Sections 5.3.3(b) and 5.3.3(c), *Confidence Building during Model Development*, and *Post-Development Validation Activities*, respectively. Limitations are discussed in Section 1.3.

As already mentioned in Section 1.1, abstracted results using the DSCPA Model are not directly used in the TSPA Model. The results first feed models documented in *In-Drift Precipitates/Salts Model*, (BSC 2003 [162529]) and *Engineered Barrier System: Physical and Chemical Environment Model*, (BSC 2003 [161963]). Results of these two studies are then used in the TSPA Model, which directly supports LA.

7.1.1 Confidence Building During Model Development

This phase of validation is mostly relevant to the process model, although it also applies to the abstraction analyses presented in Section 6. As noted above, the development of the DSCPA model was documented in accordance with AP-SIII.10Q Section 5.3.3(b), and the TWP (BSC 2002 [160819], Attachment I, Section I-3-5) including:

- (a) Discussion and justification of input data: input parameters (in this case water and gas compositions predicted by the process model) were selected from certain zones within the process model domain with given rationale and justifications (Section 6.2.1).
- (b) Discussion and justification of initial conditions: this validation phase is applicable to the process model but not to abstraction analyses presented here.
- (c) Discussion of the impacts of input uncertainties: in Section 6.2.4.1, the spread of process model results was evaluated for simulations using five different input water compositions (Group 1 simulations), and simulations considering variations in conceptualization and certain input parameters other than input water composition (Group 2 simulations). Minimum, maximum, mean, and standard deviations of predicted concentrations of aqueous species and CO₂ gas were presented, including the aggregate uncertainty resulting from adding the spread of Group 1 and Group 2 simulation results.

7.1.2 Post-Development Validation Activities

Confidence in the DSCPA model was gained using validation Method 6, *Corroboration of Abstraction Models with Process Model* (BSC 2002 [160819], Attachment I, Section I-3-5) and AP-SIII.10Q Section 5.3.3(c). According to the TWP (BSC 2002 [160819], Attachment I, Section I-3-5), the main validation of an abstraction model is to show that it can provide results sufficiently close to the predictions of the supporting process model. The supporting process

model in turn is validated to ensure appropriate representation of the physical processes, as done in BSC 2003 ([162050], Section 7).

The validation criterion in the TWP stipulates that the DSCPA model is considered validated if predicted compositions fall within an order of magnitude from the process model predictions. The abstraction analyses presented in Section 6.2.4 do not result in modifications of predicted data from the process model, and therefore the validation criterion in the TWP is met. Figures 6.2-4 through 6.2-20 also demonstrate that abstracted data subsets that include only FRONT waters with INDX=4, and HISAT waters with INDX=5, are representative of the process model data as a whole. These subsets, at most points in time, have mean values similar to the mean of the full data set, and minimum/maximum values mostly encompassing the two-standard deviation spread calculated for the full data set. Therefore, it can be concluded that the DSCPA model results corroborate the results of the validated process model from which the abstraction was derived.

7.2 THC SIMULATIONS CONSIDERING DRIFT DEGRADATION

Results of new THC simulations using the THC Seepage Model were presented in Section 6.3 for a case of drift degradation. These simulations involved applying the same process model (i.e., the THC Seepage Model) as that previously validated in BSC (2003 [162050], Section 7). The results of these simulations were then abstracted using the same DSCPA model as that validated in Section 7.1. Therefore, no further validation is required for these new THC simulations.

7.3 TEMPERATURE EFFECT ON RADIONUCLIDE SORPTION

The evaluation of specific radioelement K_d values to determine their temperature dependence was conducted with the aid of standard thermodynamic relations that are well established and accepted in the refereed literature, and therefore require no further validation. See Mustafa et al. (1991 [165048]), Ishfaq et al. (1997 [164879]), Rauf and Tahir (2000 [164893]), Zafar et al. (2002 [165052]) and Kara et al. (2003 [164880]). These relations constitute the “model,” together with assumptions and approximations inherent in the use of experimentally determined laboratory sorption measurements to compute K_d values (see Section 6.4.3.1). The assumptions and approximations are implicit to the nature of the measurement technique and cannot be evaluated independently, unless other parameters are measured concurrently with the sorption measurement. Because no corrections can be made when relevant parameters remain indeterminate, intercomparison is not generally possible between differing sorbents, or similar sorbents where radioelement sorption takes place under differing conditions (e.g., with differing temperatures, aqueous solution compositions, or sorption mechanisms). Thus, it is to be expected that radioelement K_d values for Yucca Mountain substrates are poorly correlated with independent data from the literature (e.g., see Figure 6.4-5). Indeed, even the K_d data collected under the auspices of the YMP is so diverse that no consistent K_d temperature dependence can be discerned, with the possible exception of Sr and U(VI), (Figure 6.4-5). Because the scatter in the derived values of the apparent enthalpy of sorption for the studied radioelements is so large, the present evaluation of the temperature dependence of these radioelement K_d values is itself a validation of the arguments presented in Section 6.4.3.1.

8. CONCLUSIONS

Conclusions for each part of this study are presented in individual subsections below. Output data generated in this study were submitted to the TDMS as described in Attachment I.

8.1 DSCPA MODEL

An abstraction model was presented and implemented using water compositions and CO₂ gas concentrations predicted with the THC Seepage Model (the process model as reported in BSC 2003 [162050]). Results of this abstraction model were submitted to the TDMS under DTN: LB0311ABSTHCR2.001.

The goal of the THC Seepage Model is to analyze the effect of THC processes in the rock around waste emplacement drifts. This includes the predictions of aqueous species and CO₂ gas concentrations in fluids that could seep into drifts. However, the THC Seepage Model does not simulate actual seepage of water into a drift because the range of simulated infiltration rates, including high rates for future climate conditions, remains below the seepage threshold for rocks around the modeled drift (e.g., BSC 2003 [161530], Section 6.2.2.1.2). For this reason, abstraction analyses must first consider which locations (around the modeled drift) would be most likely to yield fluids that could seep into the drift.

Around a typical drift, under thermal loading conditions, the temperature gradients are quite steep and, correspondingly, predicted concentrations in space around the drift are quite variable. This local spatial variability is generally larger than the variability resulting from a change in drift location within the repository units (e.g., Tptpll versus Ttpmn, see BSC 2003 [162050], Sections 6.5 and 6.7), because these repository units have very similar bulk chemical compositions.

Taking into account the spatial variability of predicted water compositions around the modeled drift, the abstraction model considers the following waters as best candidates for in-drift seepage:

- Waters in zones of highest liquid saturations in fractures above the drift (HISAT-TOP designation in the DSCPA model)
- Waters at the boiling/wetting front in fractures both above and below the drift (FRONT-TOP and FRONT-BASE designation, respectively, in the DSCPA model)
- Waters at the boiling/wetting front in matrix at the base of the drift (also FRONT-BASE designation in the DSCPA model, but for matrix instead of fracture water).

The DSCPA model is then used to evaluate the spread in process model results caused by considering five different input water compositions (Group 1 simulations) representing natural variability. The spread resulting from specific uncertainties other than input water compositions (Group 2 simulations) is also evaluated (Section 6.2.4). The spread (as two standard deviations) for Group 1 is up to around one order of magnitude, and is at most times greater than for Group 2. The combined spread from both groups (estimated as two times the combined Group 1

and Group 2 standard deviations) remains also mostly within one order of magnitude, but is commonly much less (Section 6.2.4.1).

A large amount of data is generated by the extraction procedure implemented into the DSCPA model: for each chemical constituent, 30 data points are extracted at each point in time (five runs in each group of simulations, with six points indexed INDX=1 through 6) for each simulation and each constituent). Evaluations using the DSCPA model are used to show that subsets of data using only points with INDX=4 for waters at the boiling/wetting front (FRONT waters), and with INDX=5 in zones of higher liquid saturations above the drift (HISAT waters), provide reasonable representations of the full data sets for these waters.

The DSCPA model is not used for further abstraction of process model results in time, because such abstraction is carried out in another report (BSC 2003 [161963]). It is expected that at drift wall temperatures greater than 100°C the vaporization barrier would prevent seepage from entering the drift. Therefore, it is recommended that only those abstracted water compositions for conditions when the drift wall temperature is less than 100°C be used to represent seepage compositions entering emplacement drifts. In addition, these abstracted water compositions may be more concentrated than seepage water compositions that would evolve under thermal loading conditions lower than the one considered in BSC 2003 [162050]. However, some results of abstraction as a function of drift-wall temperature and liquid saturation are presented. These analyses show that the spread in process-model results typically increases with increasing temperature and decreasing liquid saturation. The abstracted data and its spread could be narrowed by discarding points at temperatures above ~ 95°C in fractures and ~110°C in the matrix (i.e., above the water boiling point in these media), because a vaporization barrier at these temperatures would be expected to form and prevent seepage of liquid water into drifts. Discarding data at liquid saturations below residual (on the basis that no movement could occur below residual saturation) would further reduce the number of abstracted data and its spread. However, residual saturations in fractures, unlike boiling temperatures, are quite uncertain.

In the DSCPA model, a set of criteria must be applied to determine which model area is to be abstracted to obtain water and gas compositions representative of potential in-drift seepage. These criteria represent the main limitation of the DSCPA model itself (Section 6.2.1). The limitations and uncertainties of the process model have been discussed in detail in BSC (2003 [162050], Sections 1.3, 6.9 and 8.4). These limitations obviously also apply to the DSCPA model. Downstream users of data generated by this model must therefore be familiar with the process-model limitations, and with other details of the process model as well.

8.2 THC SIMULATIONS CONSIDERING DRIFT DEGRADATION

The THC Seepage Model, as presented in BSC 2003 ([162050], Section 6.8), was used to predict the composition of waters around a typical waste emplacement drift. The results of these simulations were abstracted in the present report (Section 6.2) and summarized above (Section 8.1). These simulations considered an intact drift (no drift wall collapse). To evaluate the effect of drift degradation on the chemistry of potential in-drift seepage, the same THC model and abstraction methods were applied here to a case of drift degradation (Section 6.3). Results of these analyses were submitted to the TDMS under DTNs: LB0311ABSTHCR2.002 and LB0311ABSTHCR2.003.

The case of drift degradation considered here is identical to one of the cases evaluated in BSC 2003 ([165564], Section 6.4.3.4). This case considered the collapse of wallrock on top of the drip shield, forming a more-or-less circular rubble zone with a base coinciding with the base of the original drift, and a diameter (11 m) equal to twice the original drift diameter. The rubble zone was modeled as two continua consisting of rock matrix and voids (23% by volume), in full contact with intact wallrock. The conclusions reached here regarding the impact of such drift degradation on thermal-hydrological behavior are consistent with the findings reported in BSC 2003 ([165564], Section 6.4.3.4). The rubble zone is predicted to act as a capillary barrier to fracture flow, and the presence of rubble directly above the drip shield is predicted to cause a significant increase in temperatures and dryout below the drift (Section 6.3.5.1).

For the drift degradation case considered, the boiling front was found to always remain within the rubble zone. As a result, fracture waters percolating downwards above the waste package are predicted to be diverted around the rubble zone before they can reach boiling temperatures. Therefore, waters directly above the location of the original drift do not boil and, as a result, chemical constituents are less concentrated than if drift degradation did not occur. Below the drift, higher temperatures, and reduced fluxes caused by the increased “shadow” zone effect of the rubble zone, generally result in more concentrated waters. Fracture waters originating from zones above the drift may be given more weight, in terms of their importance for in-drift seepage, than waters at the base of the drift. In such cases, drift degradation could be viewed as a less conservative scenario, when evaluating the chemistry of potential in-drift seepage, than if degradation did not take place. It could be argued that the composition of matrix water above the drip shield (in rubble fragments) should also be considered. This was not done here on the basis that these waters would not seep onto a waste package because of the high matrix capillarity. These waters have similar compositions to matrix water below the drift, which were considered here on the basis that the invert could potentially imbibe these waters. In any case, it would appear that the differences in predicted concentrations resulting from drift degradation are comparable in magnitude to the spread in model results evaluated for various ranges of input parameters and water compositions for an intact drift (Section 6.2.4).

8.3 TEMPERATURE EFFECT ON RADIONUCLIDE SORPTION

An evaluation was made of the temperature dependence of K_d for the following radioelements: Cs, Sr, Ba (a proxy for Ra), Ce, Eu, U(VI), Np, Pu, and Am when sorbed on various tuffaceous rocks from Yucca Mountain, Nevada, and selectively on individual minerals. The sources of the K_d data were reports issued by LANL or from the DTN computer database maintained by the DOE Yucca Mountain Project Office (YMPO). A comparison was also made of the sorption of various dissolved elemental species on various natural substrates as reported in the literature. Results of these analyses were submitted to the TDMS under DTN: LB0311ABSTHCR2.004.

The evaluation indicates that the enthalpy of sorption, ΔH_r , is positive for all radioelements examined. The mean value of ΔH_r for all radioelements is small, i.e., $< \pm 5$ kcal/mol, but the standard deviation (95% confidence level) is so large that ΔH_r can be assumed to be zero for all but Sr, U(VI), and Np where ΔH_r are 2.65 ± 2.14 , 4.21 ± 2.15 , and 2.64 ± 0.72 , respectively (Table 6.4-12). These values are equivalent to respective increases in K_d of 2.3, 3.9, and 2.3 times for an increase in temperature from 25°C to 95°C, the range of temperature expected within the near field when a liquid aqueous phase is present in fractures.

When modeling solute radionuclide transport in the near field, it can be assumed within experimental error that the K_{ds} of all cited radioelements except for Sr, U(VI), and Np are not temperature dependent. This assumption is conservative for all species, because the mean values of the respective ΔH_r are positive. With respect to Sr, U(VI), and Np, temperature corrections only for K_{ds} for U(VI) should be considered. However, even in this case, a conservative assumption that K_d is independent of temperature would simplify model computations.

9. INPUTS AND REFERENCES

The following is a list of the references cited in this document. Column 1 represents the unique six-digit numerical identifier (the Document Input Reference System [DIRS] number), which is placed in the text following the reference callout (e.g., BSC 2002 [160819]). The purpose of these numbers is to assist the reader in locating a specific reference. Within the reference list, multiple sources by the same author (e.g., BSC 2002) are sorted alphabetically by title.

9.1 DOCUMENTS CITED

- 165054 Aksyuk, A.M.; Zhukovskaya, T.N.; and Tikhomirova, V.I. 1995. "Sorption of Strontium on Porphyrite at Room and Enhanced Temperature (Experimental Data)." *[Proceedings of the Fifth International Conference on Radioactive Waste Management and Environmental Remediation, ICM '95, held in Berlin, Germany, September 3-7, 1995]*. [Slate, S.; Baker, R.; Benda, G.; Creer, J. and Feizollahi, F., eds.]. Pages 691-694. [New York, New York]: American Society of Mechanical Engineers. TIC: 254875.
- 165225 Apps, J.A. 1992. *Current Geochemical Models to Predict the Fate of Hazardous Wastes in the Injection Zones of Deep Disposal Wells*. LBL-26007. Berkeley, California: Lawrence Berkeley Laboratory, Earth Sciences Division. ACC: MOL.20030919.0119.
- 164864 Apps, J.A.; Lucas, J.; Mathur, A.K.; and Tsao, L. 1977. *Theoretical and Experimental Evaluation of Waste Transport in Selected Rocks: 1977 Annual Report of LBL Contract No. 45901AK*. Waste Isolation Safety Assessment Program—Collection and Generation of Transport Data. LBL-7022. Berkeley, California: Lawrence Berkeley Laboratory. TIC: 210918.
- 164865 Atun, G.; Bilgin, B.; and Mardinli, A. 1996. "Sorption of Cesium on Montmorillonite and Effects of Salt Concentration." *Journal of Radioanalytical and Nuclear Chemistry, 211*, (2), 435-442. [New York, New York]: Elsevier. TIC: 255302.
- 154437 Bethke, C.M. and Brady, P.V. 2000. "How the Kd Approach Undermines Ground Water Cleanup." *Ground Water, 38*, (3), 435-443. Westerville, Ohio: National Ground Water Association. TIC: 249781.
- 101196 Bish, D.L. and Vaniman, D.T. 1985. *Mineralogic Summary of Yucca Mountain, Nevada*. LA-10543-MS. Los Alamos, New Mexico: Los Alamos National Laboratory. ACC: MOL.19950412.0041.
- 165056 Bolt, G.H. 1991. "The Ionic Distribution in the Diffuse Double Layer." Chapter 1 of *Soil Chemistry*. Bolt, G.H., ed. B. Physico-Chemical Models. New York, New York: Elsevier. TIC: 254878.

- 165188 Bolt, G.H. and Van Riemsdijk, W.H. 1991. "Ion Adsorption on Inorganic Variable Charge Constituents." Chapter 13 of *Soil Chemistry*. Bolt, G.H., ed. B. Physico-Chemical Models. New York, New York: Elsevier. TIC: 254878.
- 156646 Brunauer, S.; Emmett, P.H.; and Teller, E. 1938. "Adsorption of Gases in Multimolecular Layers." [*Journal of American Chemical Society*, 60], 309-319. [Washington, D.C.: American Chemical Society]. TIC: 224534.
- 154826 BSC (Bechtel SAIC Company) 2001. *Features, Events, and Processes in UZ Flow and Transport*. ANL-NBS-MD-000001 REV 01. Las Vegas, Nevada: Bechtel SAIC Company. ACC: MOL.20010423.0321.
- 160819 BSC (Bechtel SAIC Company) 2002. *Technical Work Plan for: Performance Assessment Unsaturated Zone*. TWP-NBS-HS-000003 REV 02. Las Vegas, Nevada: Bechtel SAIC Company. ACC: MOL.20030102.0108.
- 160146 BSC (Bechtel SAIC Company) 2002. *Total System Performance Assessment-License Application Methods and Approach*. TDR-WIS-PA-000006 REV 00. Las Vegas, Nevada: Bechtel SAIC Company. ACC: MOL.20020923.0175.
- 165564 BSC (Bechtel SAIC Company) 2003. *Abstraction of Drift Seepage*. MDL-NBS-HS-000019 REV 00 ICN 01. Las Vegas, Nevada: Bechtel SAIC Company. ACC: DOC.20031112.0002.
- 161773 BSC (Bechtel SAIC Company) 2003. *Analysis of Hydrologic Properties Data*. MDL-NBS-HS-000014 REV 00. Las Vegas, Nevada: Bechtel SAIC Company. ACC: DOC.20030404.0004.
- 160240 BSC (Bechtel SAIC Company) 2003. *Calibrated Properties Model*. MDL-NBS-HS-000003 REV 01. Las Vegas, Nevada: Bechtel SAIC Company. ACC: DOC.20030219.0001.
- 160109 BSC (Bechtel SAIC Company) 2003. *Development of Numerical Grids for UZ Flow and Transport Modeling*. ANL-NBS-HS-000015 REV 01. Las Vegas, Nevada: Bechtel SAIC Company. ACC: DOC.20030404.0005.
- 162711 BSC (Bechtel SAIC Company) 2003. *Drift Degradation Analysis*. ANL-EBS-MD-000027 REV 02. Las Vegas, Nevada: Bechtel SAIC Company. ACC: DOC.20030709.0003.
- 161530 BSC (Bechtel SAIC Company) 2003. *Drift-Scale Coupled Processes (DST and TH Seepage) Models*. MDL-NBS-HS-000015 REV 00. Las Vegas, Nevada: Bechtel SAIC Company. ACC: MOL.20030910.0160.
- 162050 BSC (Bechtel SAIC Company) 2003. *Drift-Scale Coupled Processes (DST and THC Seepage) Models*. MDL-NBS-HS-000001 REV 02. Las Vegas, Nevada: Bechtel SAIC Company. ACC: DOC.20030804.0004.

- 164889 BSC (Bechtel SAIC Company) 2003. *Drift-Scale Radionuclide Transport*. MDL-NBS-HS-000016 REV 00. Las Vegas, Nevada: Bechtel SAIC Company. ACC: DOC.20030902.0009.
- 161963 BSC (Bechtel SAIC Company) 2003. *Engineered Barrier System: Physical and Chemical Environment Model, Review Copy*. ANL-EBS-MD-000033 REV 02D. Las Vegas, Nevada: Bechtel SAIC Company. ACC: MOL.20031209.0346.
- 162529 BSC (Bechtel SAIC Company) 2003. *In-Drift Precipitates/Salts Model*. ANL-EBS-MD-000045 REV 01. Las Vegas, Nevada: Bechtel SAIC Company. ACC: DOC.20031028.0003.
- 165692 BSC (Bechtel SAIC Company) 2003. *Multiscale Thermohydrologic Model Report*. ANL-EBS-MD-000049 REV 01E. Las Vegas, Nevada: Bechtel SAIC Company. ACC: MOL.20031009.0227.
- 163933 BSC (Bechtel SAIC Company) 2003. *Particle Tracking Model and Abstraction of Transport Processes*. MDL-NBS-HS-000020 REV 00A. Las Vegas, Nevada: Bechtel SAIC Company. ACC: MOL.20030611.0040.
- 165179 BSC (Bechtel SAIC Company) 2003. *Q-List*. TDR-MGR-RL-000005 REV 00. Las Vegas, Nevada: Bechtel SAIC Company. ACC: DOC.20030930.0002.
- 163228 BSC (Bechtel SAIC Company) 2003. *Radionuclide Transport Models Under Ambient Conditions*. MDL-NBS-HS-000008 REV 01. Las Vegas, Nevada: Bechtel SAIC Company. ACC: DOC.20031201.0002.
- 164069 BSC (Bechtel SAIC Company) 2003. *Repository Design Project, Repository/PA IED Emplacement Drift Configuration 1 of 2*. 800-IED-EBS0-00201-000-00A. Las Vegas, Nevada: Bechtel SAIC Company. ACC: ENG.20030630.0002.
- 163045 BSC (Bechtel SAIC Company) 2003. *UZ Flow Models and Submodels*. MDL-NBS-HS-000006 REV 01. Las Vegas, Nevada: Bechtel SAIC Company. ACC: DOC.20030818.0002.
- 161770 Canori, G.F. and Leitner, M.M. 2003. *Project Requirements Document*. TER-MGR-MD-000001 REV 01. Las Vegas, Nevada: Bechtel SAIC Company. ACC: DOC.20030404.0003.
- 123916 CRWMS M&O (Civilian Radioactive Waste Management System Management and Operating Contractor) 2000. *Abstraction of Drift-Scale Coupled Processes*. ANL-NBS-HS-000029 REV 00. Las Vegas, Nevada: CRWMS M&O. ACC: MOL.20000525.0371.
- 122799 CRWMS M&O 2000. *UZ Colloid Transport Model*. ANL-NBS-HS-000028 REV 00. Las Vegas, Nevada: CRWMS M&O. ACC: MOL.20000822.0005.

- 105803 Daniels, W.R.; Wolfsberg, K.; Rundberg, R.S.; Ogard, A.E.; Kerrisk, J.F.; Duffy, C.J.; Newton, T.W.; Thompson, J.L.; Bayhurst, B.P.; Bish, D.L.; Blacic, J.D.; Crowe, B.M.; Erdal, B.R.; Griffith, J.F.; Knight, S.D.; Lawrence, F.O.; Rundberg, V.L.; Skyes, M.L.; Thompson, G.M.; Travis, B.J.; Treher, E.N.; Vidale, R.J.; Walter, G.R.; Aguilar, R.D.; Cisneros, M.R.; Maestas, S.; Mitchell, A.J.; Oliver, P.Q.; Raybold, N.A.; and Wanek, P.L. 1982. *Summary Report on the Geochemistry of Yucca Mountain and Environs*. LA-9328-MS. Los Alamos, New Mexico: Los Alamos National Laboratory. ACC: NNA.19870406.0243.
- 143280 Davis, J.A. and Kent, D.B. 1990. "Surface Complexation Modeling in Aqueous Geochemistry." *Mineral-Water Interface Geochemistry*. Hochella, M.F., Jr. and White, A.F., eds. Reviews in Mineralogy Volume 23. Pages 177-260. Washington, D.C.: Mineralogical Society of America. TIC: 224085.
- 154436 Davis, J.A.; Coston, J.A.; Kent, D.B.; and Fuller, C.C. 1998. "Application of the Surface Complexation Concept to Complex Mineral Assemblages." *Environmental Science & Technology*, 32, (19), 2820-2828. Washington, D.C.: American Chemical Society. TIC: 249656.
- 164876 Erickson, K.L. 1979. "Radionuclide Adsorption Studies on Abyssal Red Clays." Chapter 15 of *Radioactive Waste in Geologic Storage, Symposium Sponsored by the Division of Nuclear Chemistry and Technology at the 176th Meeting of the American Chemical Society, Miami Beach, Florida, September 11-15, 1978*. Fried, S.; ed. ASC Symposium Series 100. Washington, D.C.: American Chemical Society. TIC: 213890.
- 165848 Freundlich, H. 1926. *Colloid & Capillary Chemistry*. London, England: Methuen & Company. TIC: 244810.
- 164878 Honeyman, B.D. 1984. *Cation and Anion Adsorption at the Oxide/Solution Interface in Systems Containing Binary Mixtures of Adsorbents: An Investigation of the Concept of Adsorptive Additivity*. Ph.D. dissertation. Stanford, California: Stanford University, Department of Civil Engineering. TIC: 245390.
- 164879 Ishfaq, M.M.; Karim, H.M.A.; and Khan, M.A. 1997. "A Radiochemical Study on the Thermodynamics of Cesium Adsorption on Potassium Copper Nickel Hexacyanoferrate(II) from Aqueous Solutions." *Journal of Radioanalytical and Nuclear Chemistry*, 222, (1-2), 177-181. Amsterdam, The Netherlands: Elsevier. TIC: 255231.
- 164880 Kara, M.; Yuzer, H.; Sabah, E.; and Celik, M.S. 2003. "Adsorption of Cobalt from Aqueous Solutions onto Sepiolite." *Water Research*, 37, ([1]), 224-232. [New York, New York]: Pergamon. TIC: 254847.
- 164881 Karickhoff, S.W. 1984. "Organic Pollutant Sorption in Aquatic Systems." *Journal of Hydraulic Engineering*, 110, (6), 707-735. [New York, New York]: American Society of Civil Engineers.. TIC: 255122.

- 165041 Kelmers, A.D. 1984. *Review and Assessment of Radionuclide Sorption Information for the Basalt Waste Isolation Project Site (1979 through May, 1983)*. NUREG/CR-3763. Washington, D.C.: U.S. Nuclear Regulatory Commission. TIC: 228866.
- 165049 Kenna, B.T. 1981. "Temperature and pH Effects on Sorption Properties of Subseabed Clay." *Scientific Basis for Nuclear Waste Management, Proceedings of the Third International Symposium, Boston, Massachusetts, November 17-20, 1980*. Moore, J.G., ed. 3, 491-498. New York, New York: Plenum Press. TIC: 204407.
- 100767 Kieft, T.L.; Kovacic, W.P., Jr.; Ringelberg, D.B.; White, D.C.; Haldeman, D.L.; Amy, P.S.; and Hersman, L.E. 1997. "Factors Limiting Microbial Growth and Activity at a Proposed High-Level Nuclear Repository, Yucca Mountain, Nevada." *Applied and Environmental Microbiology*, 63, (8), 3128-3133. [Washington, D.C.]: American Society for Microbiology. TIC: 236444.
- 165050 Kilislioglu, A. and Bilgin, B. 2002. "Adsorption of Uranium on Halloysite." *Radiochimica Acta*, 90, ([3]), 155-160. München, Germany: R. Oldenbourg Verlag. TIC: 254872.
- 126305 Langmuir, I. [1918]. "The Adsorption of Gases on Plane Surfaces of Glass, Mica and Platinum." [*Journal of the American Chemical Society*, 40], 1361-1403. [Washington, D.C.: American Chemical Society]. TIC: 223181.
- 165040 Meyer, R.E.; Arnold, W.D.; Case, F.I.; O'Kelley, G.D.; and Land, J.F. 1990. *Effects of Mineralogy on Sorption of Strontium and Cesium Onto Calico Hills Tuff*. NUREG/CR-5463. Washington, D.C.: U.S. Nuclear Regulatory Commission. TIC: 254856.
- 165048 Mustafa, S.; Safdar, M.; and Hussain, S.Y. 1991. "Temperature Effect on Heavy Metal Adsorption by (alpha)-Aluminium Hydroxide." *Journal of Surface Science Technology*, 7, (3), 273-281. [Calcutta, India: Indian Society for Surface Science & Technology]. TIC: 254869.
- 163274 NRC (U.S. Nuclear Regulatory Commission) 2003. *Yucca Mountain Review Plan, Final Report*. NUREG-1804, Rev. 2. Washington, D.C.: U.S. Nuclear Regulatory Commission, Office of Nuclear Material Safety and Safeguards. TIC: 254568.
- 162987 Pabalan, R.T.; Turner, D.R.; Bertetti, F.P.; and Prikryl, J.D. 1998. "Uranium^{VI} Sorption onto Selected Mineral Surfaces, Key Geochemical Parameters." *Adsorption of Metals by Geomedia*. [Jenne, E.A., ed]. Pages 99-130. New York, New York: Academic Press. TIC: 239504.
- 164891 Paces, T. 1978. "Reversible Control of Aqueous Aluminum and Silica during the Irreversible Evolution of Natural Waters." *Geochimica et Cosmochimica Acta*, 42, ([10]), 1487-1493. [New York, New York]: Pergamon. TIC: 235309.

- 159511 Parkhurst, D.L. and Appelo, C.A.J. 1999. *User's Guide to PHREEQC (Version 2)—A Computer Program for Speciation, Batch-Reaction, One-Dimensional Transport, and Inverse Geochemical Calculations*. Water-Resources Investigations Report 99-4259. Denver, Colorado: U.S. Geological Survey. TIC: 253046.
- 165849 Parks, G.A. 1990. "Surface Energy and Adsorption at Mineral-Water Interfaces: An Introduction." Chapter 4 of *Mineral-Water Interface Geochemistry*. Hochella, M.F., Jr. and White, A.F., eds. Reviews in Mineralogy Volume 23. Washington, D.C.: Mineralogical Society of America. TIC: 240202.
- 164893 Rauf, N. and Tahir, S.S. 2000. "Thermodynamics of Fe(II) and Mn(II) Adsorption onto Bentonite from Aqueous Solutions." *Journal of Chemical Thermodynamics*, 32, ([5]), 651-658. [New York, New York]: Academic Press. TIC: 254910.
- 154434 Reardon, E.J. 1981. "Kd's — Can They be Used to Describe Reversible Ion Sorption Reactions in Contaminant Migration?" *Ground Water*, 19, (3), 279-286. Worthington, Ohio: Water Well Journal Publishing Company. TIC: 249726.
- 117901 Reed, M.H. 1982. "Calculation of Multicomponent Chemical Equilibria and Reaction Processes in Systems Involving Minerals, Gases and an Aqueous Phase." *Geochimica et Cosmochimica Acta*, 46, (4), 513-528. New York, New York: Pergamon Press. TIC: 224159.
- 164909 Sabah, E.; Turan, M.; and Celik, M.S. 2002. "Adsorption Mechanism of Cationic Surfactants onto Acid- and Heat-Activated Sepiolites." *Water Research*, 36, ([16]), 3957-3964. [New York, New York]: Pergamon. TIC: 254848.
- 127235 Sposito, G. 1980. "Derivation of the Freundlich Equation for Ion Exchange Reactions in Soils." *Soil Science Society of America Journal*, 44, (3), 652-654. Madison, Wisconsin: Soil Science Society of America. TIC: 223199.
- 129861 Sposito, G. 1981. "Single-Particle Motions in Liquid Water. II. The Hydrodynamic Model." *Journal of Chemical Physics*, 74, (12), 6943-6949. New York, New York: American Institute of Physics. TIC: 246772.
- 127253 Sposito, G. 1984. *The Surface Chemistry of Soils*. New York, New York: Oxford University Press. TIC: 217687.
- 165846 Spycher, N.F. and Reed, M.H. 1992. "Microcomputer-Based Modeling of Speciation and Water-Mineral-Gas Reactions Using Programs SOLVEQ and CHILLER." *Water-Rock Interaction, Proceedings of the 7th International Symposium on Water-Rock Interaction, WRI-7, Park City, Utah, USA, 13-18 July 1992*. Kharaka, Y.K. and Maest, A.S., eds. 2, 1087-1090. Brookfield, Vermont: A.A. Balkema. TIC: 208527.

- 101361 Thomas, K.W. 1987. *Summary of Sorption Measurements Performed with Yucca Mountain, Nevada, Tuff Samples and Water from Well J-13*. LA-10960-MS. Los Alamos, New Mexico: Los Alamos National Laboratory. ACC: NNA.19900604.0045.
- 158378 USGS (U.S. Geological Survey) 2001. *Future Climate Analysis*. ANL-NBS-GS-000008 REV 00 ICN 01. Denver, Colorado: U.S. Geological Survey. ACC: MOL.20011107.0004.
- 160355 USGS (U.S. Geological Survey) 2001. *Simulation of Net Infiltration for Modern and Potential Future Climates*. ANL-NBS-HS-000032 REV 00 ICN 02. Denver, Colorado: U.S. Geological Survey. ACC: MOL.20011119.0334.
- 165087 van Geldermalsen, L.A. and Duursma, E.K. 1984. "Temperature Effects on Sorption of Cd, Eu, Pu and Am onto Estuarine and Marine Sediments." *Proceedings of an International Symposium on the Behavior of Long-Lived Radionuclides in a Marine Environment, 1984*. EUR 9214, Pages 83-95. Vienna, Austria: International Atomic Energy Agency.
- 165562 Wang, J.S. 2003. "Scientific Notebooks Referenced in Model Report N0125, Abstraction of Drift-Scale Coupled Processes, MDL-NBS-HS-000018 REV 00." Correspondence from J.S. Wang (BSC) to File, December 15, 2003, with attachments. ACC: MOL.20031217.0389.
- 165228 Weber Jr., W.J.; McGinley, P.M.; and Katz, L.E. 1992. "A Distributed Reactivity Model for Sorption by Soils and Sediments. 1. Conceptual Basis and Equilibrium Assessments." *Environmental Science & Technology*, 26, (10), 1955-1962. Washington, DC: American Chemical Society.
- 127323 Westall, J.C. 1987. "Adsorption Mechanisms in Aquatic Surface Chemistry." Chapter 1 of *Aquatic Surface Chemistry: Chemical Processes at the Particle-Water Interface*. A Volume in Environmental Science and Technology, A Wiley-Interscience Publication. Stumm, W., ed. New York, New York: John Wiley & Sons. TIC: 217674.
- 108808 Wolery, T.J. 1983. *EQ3NR, A Computer Program for Geochemical Aqueous Speciation-Solubility Calculations: User's Guide and Documentation*. UCRL-53414. Livermore, California: Lawrence Livermore National Laboratory. TIC: 1148.
- 100097 Wolery, T.J. and Daveler, S.A. 1992. *EQ6, A Computer Program for Reaction Path Modeling of Aqueous Geochemical Systems: Theoretical Manual, User's Guide, and Related Documentation (Version 7.0)*. UCRL-MA-110662 PT IV. Livermore, California: Lawrence Livermore National Laboratory. ACC: MOL.19980701.0459.
- 164922 Yehia, A.; Miller, J.D.; and Ateya, B.G. 1993. "Analysis of the Adsorption Behaviour of Oleate on Some Synthetic Apatites." *Minerals Engineering*, 6, (1), 79-86. [New York, New York]: Pergamon. TIC: 255300.

- 165052 Zafar, U.; Khan, I.; Jamshaid, F.; and Naeem, S. 2002. "Adsorption Studies of Silver (+1) on Bentonite." *Journal of the Chemical Society of Pakistan*, 24, (2), 92-97. Karachi, Pakistan: Chemical Society of Pakistan.

Software Cited

- 153217 LBNL (Lawrence Berkeley National Laboratory) 1999. *Software Code: SOLVEQ/CHILLER*. V1.0. PC w/Windows OS. 10057-1.0-00.
- 161127 LBNL (Lawrence Berkeley National Laboratory) 2002. *Software Code: CUTCHEM*. V1.0. DEC ALPHA/OSF1 V5.1, PC /WINDOWS 2000/NT 4.0/98. 10898-1.0-00.
- 161256 LBNL (Lawrence Berkeley National Laboratory) 2002. *Software Code: TOUGHREACT*. V3.0. DEC-Alpha with Unix OSF1 V5.1 and OSF1 V5.0, Sun UltraSparc w/Solaris 5.5.1, PC with Linux Redhat 7.2. 10396-3.0-00.

9.2 CODES, STANDARDS, REGULATIONS, AND PROCEDURES

- 156671 66 FR 55732. Disposal of High-Level Radioactive Wastes in a Proposed Geologic Repository at Yucca Mountain, NV. Final Rule 10 CFR Part 63. Readily available.

AP-2.22Q, Rev. 1, ICN 0. *Classification Analyses and Maintenance of the Q-List*. Washington, D.C.: U.S. Department of Energy, Office of Civilian Radioactive Waste Management. ACC: DOC.20030807.0002.

AP-SI.1Q, Rev. 5, ICN 2. *Software Management*. Washington, D.C.: U.S. Department of Energy, Office of Civilian Radioactive Waste Management. ACC: DOC.20030902.0003.

AP-SIII.10Q, Rev. 2, ICN 1. *Models*. Washington, D.C.: U.S. Department of Energy, Office of Civilian Radioactive Waste Management. ACC: DOC.20031126.0002.

9.3 SOURCE DATA, LISTED BY DATA TRACKING NUMBER

- 160899 GS020408312272.003. Collection and Analysis of Pore Water Samples for the Period from April 2001 to February 2002. Submittal date: 04/24/2002.
- 162476 LA0010JC831341.001. Radionuclide Retardation Measurements of Sorption Distribution Coefficients for Barium. Submittal date: 10/19/2000.
- 153321 LA0010JC831341.002. Radionuclide Retardation Measurements of Sorption Distribution Coefficients for Cesium. Submittal date: 10/19/2000.
- 153322 LA0010JC831341.003. Radionuclide Retardation Measurements of Sorption Distribution Coefficients for Strontium. Submittal date: 10/19/2000.
- 153319 LA0010JC831341.007. Radionuclide Retardation Measurements of Sorption Distribution Coefficients for Neptunium. Submittal date: 10/19/2000.

- 161282 LB0011DSTTHCR1.002. Model Input and Output Files, Excel Spreadsheets and Resultant Figures which are Presented in AMR U0110/N0120, "Drift-Scale Coupled Processes (DST and THC Seepage) Models REV 01". Submittal date: 12/19/2000.
- 161277 LB0101DSTTHCR1.002. Attachment II - Mineral Initial Volume Fractions for TPTPLL THC Model for AMR N0120/U0110 REV01, "Drift-Scale Coupled Processes (Drift-Scale Test and THC Seepage) Models.". Submittal date: 01/26/2001.
- 159525 LB0205REVUZPRP.001. Fracture Properties for UZ Model Layers Developed from Field Data. Submittal date: 05/14/2002.
- 159672 LB0207REVUZPRP.002. Matrix Properties for UZ Model Layers Developed from Field and Laboratory Data. Submittal date: 07/15/2002.
- 161243 LB0208UZDSCPMI.002. Drift-Scale Calibrated Property Sets: Mean Infiltration Data Summary. Submittal date: 08/26/2002.
- 160799 LB0210THRMLPRP.001. Thermal Properties of UZ Model Layers: Data Summary. Submittal date: 10/25/2002.
- 164744 LB0302DSCPTHCS.001. Drift-Scale Coupled Processes (THC Seepage) Model: Simulations. Submittal date: 02/11/2003.
- 161976 LB0302DSCPTHCS.002. Drift-Scale Coupled Processes (THC Seepage) Model: Data Summary. Submittal date: 02/11/2003.
- 162277 LB0302PTNTSW9I.001. PTN/TSW Interface Percolation Flux Maps for 9 Infiltration Scenarios. Submittal date: 02/28/2003.
- 163688 LB0303DSCPTHSM.001. Drift-Scale Coupled Process Model for Thermohydrologic Seepage: Simulation Files. Submittal date: 03/20/2003.
- 163690 LB0305PTNTSW9I.001. PTN/TSW Interface Percolation Flux Maps for 9 Alternative Infiltration Scenarios. Submittal date: 05/12/2003.
- 166054 LB0307DSTTHCR2.001. Drift-Scale Coupled Processes (DST Seepage) Model: Simulations. Submittal date: 07/24/2003.
- 165541 LB0307DSTTHCR2.002. Drift-Scale Coupled Processes (DST Seepage) Model: Data Summary. Submittal date: 07/24/2003.
- 111475 LB990501233129.004. 3-D UZ Model Calibration Grids for AMR U0000, "Development of Numerical Grids of UZ Flow and Transport Modeling". Submittal date: 09/24/1999.

- 111480 LB991091233129.006. Thermal Properties and Tortuosity Factor for the UZ Model Layers for AMR U0090, "Analysis of Hydrologic Properties Data". Submittal date: 10/15/1999.
- 150930 MO0005PORWATER.000. Perm-Sample Pore Water Data. Submittal date: 05/04/2000.
- 164527 MO0307SEPFEPS4.000. LA FEP List. Submittal date: 07/31/2003.

9.4 OUTPUT DATA, LISTED BY DATA TRACKING NUMBER

LB0311ABSTHCR2.001. Drift Scale Coupled Process Abstraction Model (for Intact-Drift Case). Submittal date: 11/07/2003.

LB0311ABSTHCR2.002. THC Simulations Considering Drift Degradation: Input and Output Files of Model Runs. Submittal date: 11/07/2003.

LB0311ABSTHCR2.003. THC Simulations Considering Drift Degradation: Summary/Abstraction Data Files. Submittal date: 11/07/2003.

LB0311ABSTHCR2.004. Radionuclide Sorption Analyses. Submittal: 11/24/2003.

ATTACHMENT I—LIST OF MODEL INPUT AND OUTPUT FILES

I.1. DSCPA MODEL (FOR INTACT-DRIFT CASE)

These files were submitted to the TDMS under DTN: LB0311ABSTHCR2.001.

These files consist of MS Excel97 spreadsheets used to calculate summary statistics (Attachment II) presented in Tables 6.2-2 and 6.2-3 and Figures 6.2-4 through 6.2-20 for predicted aqueous species and CO₂ gas concentrations. Original data sets are also included, and were compiled from data already submitted to the TDMS under DTNs LB0302DSCPTHCS.002 [161976] and LB0307DSTTHCR2.002 [165541].

top-front_f1.xls – Data for FRONT waters in TOP quadrant in fractures, Group-1 simulations

top-hisat_f1.xls – Data for HISAT waters in TOP quadrant in fractures, Group-1 simulations

base-front_f1.xls – Data for FRONT waters in BASE quadrant in fractures, Group-1 simulations

base-front_m1.xls – Data for FRONT waters in BASE quadrant in matrix, Group-1 simulations

top_front_f2.xls – Data for FRONT waters in TOP quadrant in fractures, Group-2 simulations

top-hisat_f2.xls – Data for HISAT waters in TOP quadrant in fractures, Group-2 simulations

w04567_f.xls – Complete original data set for fracture water, Group-1 simulations

w04567_m.xls – Complete original data set for matrix water, Group-1 simulations

w0sensi_f.xls – Complete original data set for fracture water, Group-2 simulations

Note: input to the DSCPA model for intact-drift simulations consists of process model output already submitted to the TDMS under DTNs: LB0302DSCPTHCS.001 [164744], LB0307DSTTHCR2.001 [166504].

I.2. THC SIMULATIONS CONSIDERING DRIFT DEGRADATION

I.2.1 Input and Output Files of Model Runs

I/O files for these simulations were submitted to the TDMS under DTN: LB0311ABSTHCR2.002.

For each simulation, I/O files were concatenated into one file using the Unix *tar* utility then compressed using the Unix *gzip* utility. Resulting concatenated/compressed files have the extension *.tar.gz*.

TH simulation: Run ID th6_col

th6_col_.tar.gz I/O files for time 0 to 50 years
th6_col_a.tar.gz I/O files for time 50 to 600 years
th6_col_b.tar.gz I/O files for time 600 to 2000 years
th6_col_bb.tar.gz I/O files for time 2000 to 2400 years
th6_col_c.tar.gz I/O files for time 2400 to 20000 years
th6_col_d.tar.gz I/O files for time 20000 to 100000 years

THC simulation: Run ID thc6_w0col

thc6_w0col_.tar.gz I/O files for time 0 to 50 years
thc6_w0col_a.tar.gz I/O files for time 50 to 600 years
thc6_w0col_b.tar.gz I/O files for time 600 to 2000 years
thc6_w0col_bb.tar.gz I/O files for time 2000 to 2400 years
thc6_w0col_c.tar.gz I/O files for time 2400 to 20000 years
thc6_w0col_d.tar.gz I/O files for time 20000 to 100000 years

Each of the above concatenated/compiled files contain the following specific I/O run files:

flow.inp	Rock thermal and hydrological properties, run flags and other specifications (input)
flow.out	Thermal and hydrological results (gas/liquid saturation, T, P, air mass fraction, etc.) (output)
GENER	Infiltration rates, heat load, and effective thermal conductivity (input)
INCON	Initial thermal and hydrological conditions (T, P, liquid saturation, etc.) (input)
MESH	Input numerical mesh (input)
SAVE	Thermal and hydrological conditions (T, P, liquid saturation, etc.) to use for restarting a run (output, same format as INCON file)
TABLE	Miscellaneous output data
VERS	Miscellaneous output data
LINEQ	Miscellaneous output data (sometimes erased because very large and not useful)
CHEMICAL.INP	Water chemistry, mineralogy, and CO ₂ partial pressure data (input)
CHEMICAL.OUT	Echo of data read in CHEMICAL.INP
SOLUTE.INP	Run flags and other data relating to reactive transport (input)
SOLUTE.OUT	Echo of data read in SOLUTE.INP
thermk1.01.dat	Thermodynamic database for REV02 (input). Note: The solid KNO ₃ in this file is actually NaNO ₃ .
TEC_CONC.DAT	Calculated concentrations of aqueous species (moles/liter) at each grid node (two records for each node - first record for fractures and second record for matrix) (output)

TEC_MIN.DAT	Calculated volume fraction change for minerals at each grid node (two records for each node - first record for fractures and second record for matrix) (output)
TEC_GAS.DAT	Calculated CO ₂ volume fraction at each grid node (two records for each node - first record for fractures and second record for matrix) (output)
TIME.DAT	Chemical data at selected grid nodes (output)
chdump.dat	Chemical speciation of initial water (output) and nodes with convergence problems
inchem	Chemistry data at all grid nodes to use for restarting a run (input)
savechem	Chemistry data at all grid nodes to use for restarting a run (output, same format as INCHEM file)
ITER.DAT	Iteration information (output)
runlog.dat (run_log.dat)	Miscellaneous run-time information. Note: mass balances may not be printed out correctly in this file for runs that have been restarted (i.e., starting at times different than zero).
mbalance.out	Mass balance information for chemical species Note: mass balances may not be accurate for runs that have been restarted (i.e., starting at times different than zero). Also, mass balances do not reflect mass loss by transport into large boundary grid blocks.
GASOBS.DAT	optional tabular flow output for individual grid blocks

I.2.2 Summary/Abstraction Data Files

These files were submitted to the TDMS under DTN: LB0311ABSTHCR2.003.

These files consist of MS Excel97 spreadsheets summarizing data at the location of the original drift wall, and abstracted data in and around the rubble zone. These data were used to generate time profiles shown in figures in Section 6.3 for predicted TH parameters, and aqueous species and CO₂ gas concentrations:

<i>th6_col.xls</i>	Summary of predicted TH parameters at the location of the original drift crown, springline, and base (TH simulation, no reaction)
<i>thc6_w0col_drift.xls</i>	Summary of predicted aqueous species and CO ₂ gas concentrations, as well as TH parameters, at the location of the original drift crown, springline, and base (THC simulation, including reaction)
<i>thc6_w0col.xls</i>	Summary of predicted aqueous species and CO ₂ gas concentrations, as well as TH parameters, abstracted within and around the rubble zone

I.3. RADIONUCLIDE SORPTION ANALYSES

These files were submitted to the TDMS under DTN: LB0311ABSTHCR2.004.

<i>Kd.xls</i>	Regression of $\log(K_d)$ as a function of (1/Temperature) for unqualified LANL data (Section 6.4.4.2, Tables 6.4-6, 6.4-7 and 6.4-8)
<i>Lit.KdData.xls</i>	Regression of $\log(K_d)$ as a function of (1/Temperature) for unqualified data obtained from the literature (Section 6.4.4.3, Tables 6.4-9, 6.4-10 and 6.4-11)
<i>Cesium.xls</i>	Regression of $\log(K_d)$ as a function of (1/Temperature) for the cesium qualified LANL data (Section 6.4.4.1, Tables 6.4-4 and 6.4-5) (Source data from DTN: LA0010JC831341.002 [153321])
<i>Strontium.xls</i>	Regression of $\log(K_d)$ as a function of (1/Temperature) for the strontium qualified LANL data (Section 6.4.4.1, Tables 6.4-4 and 6.4-5) (Source data from DTN: LA0010JC831341.003 [153322])
<i>Barium.xls</i>	Regression of $\log(K_d)$ as a function of (1/Temperature) for the barium qualified LANL data (Section 6.4.4.1, Tables 6.4-4 and 6.4-5) (Source data from DTN: LA0010JC831341.001 [162476])
<i>Neptunium.xls</i>	Regression of $\log(K_d)$ as a function of (1/Temperature) for the neptunium qualified LANL data (Section 6.4.4.1, Tables 6.4-4 and 6.4-5) (Source data from DTN: LA0010JC831341.007 [153319])
<i>Del H Scatter.xls</i>	Mean ΔH_f for various elements (qualified and unqualified LANL data) (Section 6.4.4.5, Table 6.4-12)

ATTACHMENT II—ABSTRACTED DATA STATISTICAL CALCULATIONS

Minimum, maximum, average and standard deviations of abstracted concentrations of aqueous species and CO₂ gas were calculated using standard MS Excel97 functions as described in the scientific notebook by Wang (2003 [165562], SN-LBNL-SCI-141-V2 pp. 202-204), and summarized below. These calculations refer to materials discussed in Section 6.2.3 of this report.

Outputs

The calculations were implemented and output in the following spreadsheets, submitted to the TDMS under DTN: LB0311ABSTHCR2.001:

top-front_f.xls – Data for FRONT waters in TOP quadrant in fractures, Group-1 runs
top-hisat_f.xls – Data for HISAT waters in TOP quadrant in fractures, Group-1 runs
base-front_f.xls – Data for FRONT waters in BASE quadrant in fractures, Group-1 runs
base-front_m.xls – Data for FRONT waters in BASE quadrant in matrix, Group-1 runs

top_fr_f.xls – Data for FRONT waters in TOP quadrant in fractures, Group-2 runs
top_hi_f.xls – Data for HISAT waters in TOP quadrant in fractures, Group-2 runs

Inputs

Inputs to the above spreadsheets consisted of records from the following data files, also submitted to the TDMS under DTN: LB0311ABSTHCR2.001:

w04567_f.xls – Complete original data set for fracture water, Group-1 simulations
w04567_m.xls – Complete original data set for matrix water, Group-1 simulations
wsensi_f.xls – Complete original data set for fracture water, Group-2 simulations

Records from these files were filtered for the desired specific attributes (FRONT, HISAT, TOP, BASE, and INDX values) using the MS Excel97 menu “Data/Auto Filter”, then cut and pasted into the calculation (and output) spreadsheets listed earlier.

Functions

The function LOG10() was used to log the input data

The following array functions were used to calculate summary statistics:

Mean:	{ =AVERAGE (IF (time_range = time, data_range)) }
Maximum:	{ =MAX (IF (time_range = time, data_range)) }
Minimum:	{ =MIN (IF (time_range = time, data_range)) }
Std. Deviation:	{ =STDEV (IF (time_range = time, data_range)) }
Count (for info only):	{ =COUNT (IF (time_range = time, data_range)) }

with arguments defined as

ATTACHMENT III—INPUT WATER COMPOSITIONS

This attachment summarizes pore-water compositions (Table III-1 and Figure III-1) used as input to the THC Seepage Model simulations presented in BSC (2003 [162050], Section 6.8). Results of these simulations are abstracted in the present report (Section 6.2.4).

Table III-1. Input Pore-Water Compositions for the THC Seepage Model (BSC 2003 [162050], Table 6.2-1)

Sample ID:		HD-PERM ¹ (Alcove 5)		ECRB-SYS- CS1000/7.3-7.7/UC ²		ECRB-SYS- CS2000/16.5-21.1/UC ²		SD-9/990.4-991.7/UC ²		ECRB-SYS- CS500/12.0-16.7/UC ²	
Lithostratigraphic Unit:		Ttpmn		Ttpul (base)		TtpII		TtpII		Ttpul	
Simulation Water ID:		W0		W5		W4		W6		W7	
Water Input Type:		Fract/Matrix	Boundary	Fract/Matrix	Boundary	Fract/Matrix	Boundary	Fract/Matrix	Boundary	Fract/Matrix	Boundary
	Units										
Temperature	°C	25	17	25	17	25	17	25	17	25	17
pH (measured)	pH	8.31	-	7.6	-	7.4	-	7.9	-	8.0	-
pH (calc) ³	pH	-	7.750	8.062	8.026	8.175	8.140	8.001	7.964	8.073	8.038
Na ⁺	mg/L	61.5	61.5	39	39	130	130	84	84	57	57
K ⁺	mg/L	8	8	7.6	7.6	10.6	10.6	7.9	7.9	10.3	10.3
Ca ⁺²	mg/L	101	101	94	94	82	82	56	56	120	120
Mg ⁺²	mg/L	17	17	18.1	18.1	5.3	5.3	0.9	0.9	19.3	19.3
SiO ₂	mg/L	70.5	70.5	42.0	42.0	48	48	50	50	49	49
Cl ⁻	mg/L	117	117	21	21	26	26	23	23	54	54
SO ₄ ⁻²	mg/L	116	116	36	36	39	39	10	10	78	78
HCO ₃ ⁻ (measured)	mg/L	-	-	333	-	382	382	313	-	286	-
HCO ₃ ⁻ (calc) ⁴	mg/L	200	216	395	400	515	515	335	338	412	417
NO ₃ ⁻	mg/L	6.5	6.5	2.6	2.6	4.2	4.2	17	17	6.1	6.1
F ⁻	mg/L	0.86	0.86	3.4	3.4	6.01 ⁹ (11)	5.52	2.5	2.5	4.8	4.8
Al ⁺³ (calc) ⁵	molal	6.173E-10	9.775E-11	1.112E-09	3.415E-10	1.082E-09	3.305E-10	1.00E-09	3.08E-10	8.061E-10	2.477E-10
Fe ⁺³ (calc) ⁶	molal	1.155E-12	5.162E-13	1.138E-12	5.000E-13	1.143E-12	4.984E-13	1.14E-12	5.02E-13	1.138E-12	5.006E-13
log(PCO ₂) ⁷	bar	-3.1	-2.5	-2.5	-2.5	-2.5	-2.5	-2.5	-2.5	-2.5	-2.5
CO ₂ (approx) ⁸	ppmv	900	3100	3100	3100	3100	3100	3100	3100	3100	3100

NOTES: Compositions shown are those used for initial fracture and matrix water (column labeled "Fract/Matrix") and infiltration water at the model top boundary (column labeled "Boundary")

- (1) Average of Ttpmn porewater analyses ESF-HD-PERM-2 (30.1'-30.5') and ESF HD-PERM-3 (34.8'-35.1'), DTN: MO0005PORWATER.000 [150930]
- (2) Pore water analyses from the ECRB cross-drift and borehole SD-9 reported with DTN: GS020408312272.003 [160899]
- (3) pH calculated by speciation at the temperature and log(P_{CO2}) shown (using SOLVEQ/CHILLER V1.0 LBNL 1999 [153217]).
- (4) Total aqueous carbonate as HCO₃⁻, calculated from charge balance computed by speciation at the temperature and pH shown (at measured pH for HD-PERM sample; at calculated pH for other samples) (using SOLVEQ/CHILLER V1.0 LBNL 1999 [153217]). Note: these are slightly different values than values calculated from charge balance reported in DTN: GS020408312272.003 [160899] because the latter do not include the effect of speciation.
- (5) Calculated by equilibrating with illite at the temperature and calculated pH shown (using SOLVEQ/CHILLER V1.0 LBNL 1999 [153217]) (Section 6.2.2.1).
- (6) Calculated by equilibrating with hematite at the temperature and calculated pH shown (using SOLVEQ/CHILLER V1.0 LBNL 1999 [153217]) (Section 6.2.2.1).
- (7) Set at values shown except for HD-PERM sample at 25°C (calculated in this case) (Section 6.2.2.1).
- (8) Approximate conversion assuming 1 bar total pressure.
- (9) Value shown is calculated at equilibrium with fluorite at 25°C. Value in parentheses is measured value.

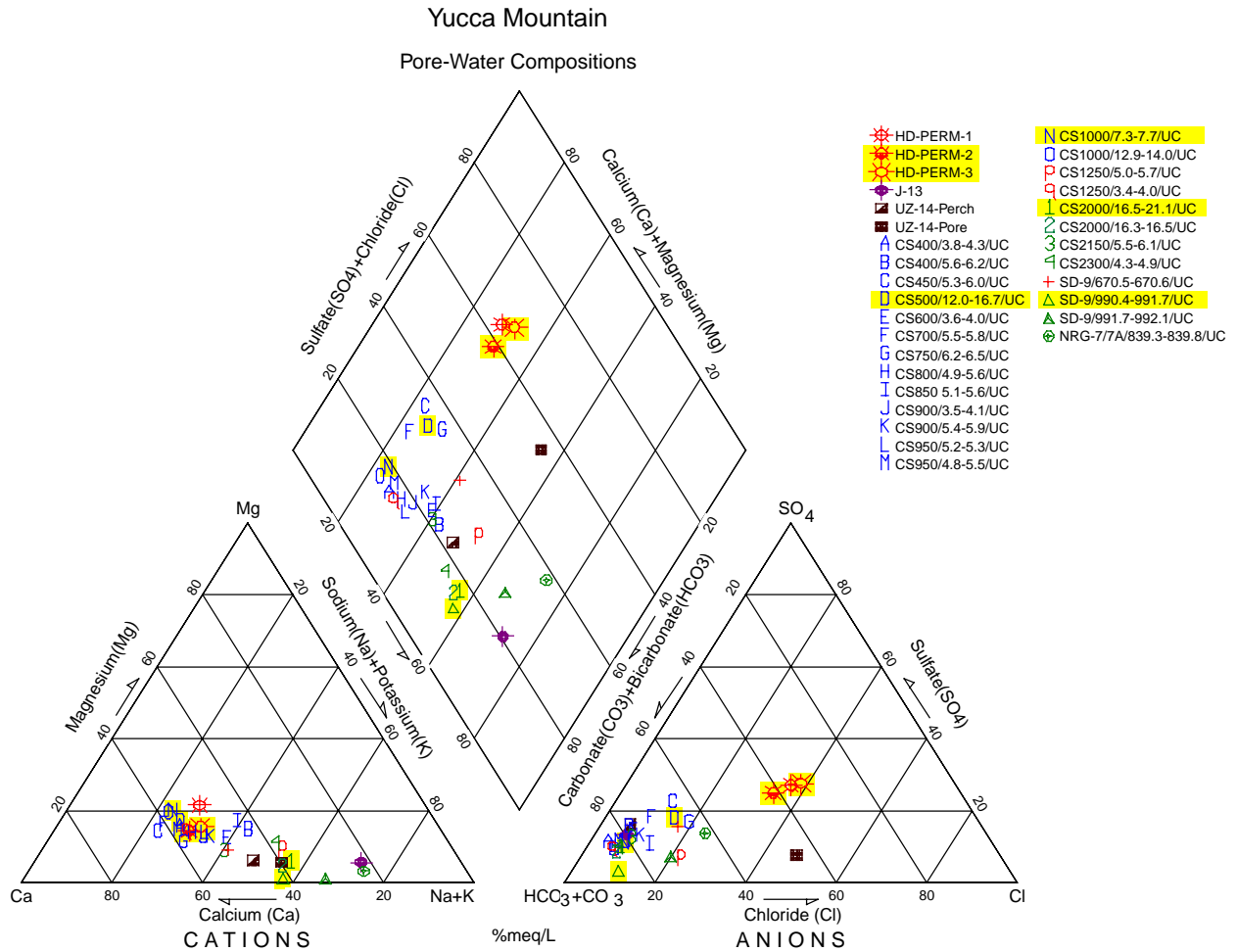


Figure III-1. Piper Plot of Water Compositions (meq/L) from Repository Units (BSC 2003 [162050], Figure 6.2-4)

INTENTIONALLY LEFT BLANK